INVESTIGATIONS INTO COSMOLOGY AND ASTRONOMY

by

Andrew David Payne

A thesis submitted in fulfilment of the

requirements for the Degree of

Doctor of Philosophy

in the

UNIVERSITY OF TASMANIA

HOBART

October, 1969

PREFACE

This thesis contains no material which has been submitted or accepted for the award of any degree or diploma in any University.

To the best of my knowledge and belief the thesis contains no material previously published or written by another person, except where due acknowledgement is made in the text.

A. D. Payne

ACKNOWLEDGEMENTS

I am indebted to Mr. P. A. Hamilton for his invaluable advice on the many problems in numerical analysis which arose during the course of this project.

My sincere thanks are extended to my wife for her moral support and assistance in preparation of the manuscript.

The financial assistance of a Commonwealth Post-graduate Scholarship is gratefully acknowledged.

CONTENTS

CHAPTER I	SUMMARY	1
CHAPTER II	A THEORETICAL BASIS FOR COSMOLOGY	
2.1	Introduction	4
2.2	The Principles of General Relativity	4
2.3	Riemannian Spaces and Geodesics	5
2.4	Formation of Tensors by Differentiation	9
2.5	The Riemann-Christoffel Tensor	11
2.6	The Energy-Momentum Tensor	15
2.7	Einstein's Equations	16
2.8	Spherical Symmetry	18
2.9	Summary	23
CHAPTER III	THEORY OF ISOTROPIC AND HOMOGENEOUS WORLD-MODELS	
3.1	The Robertson-Walker Metric	24
3.2	Properties of the Metric	26
3.3	Summary	29
CHAPTER IV	GEOMETRICAL PROPERTIES OF WORLD-MODELS	
4.1	Model Classification	30
4.2	Variation of q and σ	46
4.3	Expansion Parameter as a Function of Epoch	52
4.4	Age of Model Universes	59
4.5	Light Travel Time	65

4.6	Horizons	66
4.7	Event Horizons	67
4.8	Particle Horizons	74
4.9	The Small Redshift Approximation	83
4.10	Conclusions	86
CHAPTER V	RADIO SOURCE PARAMETERS	
5.1	The Angular Distribution of Radio Sources	87
5.2	The Luminosity Distribution	97
5.3	Luminosity Distance and Flux Density	107
5.4	Angular Diameters	110
5.5	Radio Source Spectra	122
5.6	Number Flux Relations	151
5.7	The Log N - Log S Relation	157
5.8	Conclusions	174
CHAPTER VI	RADIO WAVES IN THE INTERGALACTIC MEDIUM	
6.1	The Universal Plasma	176
6.2	Low Frequency Absorption in Isotropic World-Models	179
6.3	Conclusions	190
CHAPTER VII	THE BACKGROUND RADIATION IN ISOTROPIC WORLD-MODELS	
7.1	Equation for the Background Radiation	191
7.2	The Emission Coefficient	195
7.3	The Observed Background Intensity	198

7.4	Steady-State Models	201
7.5	Constant Temperature Model	205
7.6	The Thermal History of the Intergalactic Gas	208
7.7	Adiabatic Cooling	214
7.8	Black-Body Radiation	218
7.9	The Background Spectrum	225
7.10	The Soft X-ray Background Flux	229
7.11	Conclusions	232
CHAPTER VIII	THE X-RAY BACKGROUND IN ISOTROPIC WORLD-MODELS	
8.1	Introduction	234
8.2	Electron Energy Losses in Metagalactic Space	239
8.3	The Electron Energy Spectrum	244
8.4	Equation for the X-ray Background Intensity	247
8.5	Theoretical X-ray Spectra	255
8.6	Conclusions	264
CHAPTER IX	GENERAL VECTOR-FIELD COSMOLOGIES	
9.1	Introduction	265
9.2	Theory for Universes of Arbitrary Curvature	266
9.3	A Conjectural Model	270
9.4	Conclusions	273

CHAPTER X CONCLUSIONS 275

REFERENCES 278

CHAPTER I

SUMMARY

The thesis begins with a short review of tensor analysis and general relativity. Only those equations which have direct application to cosmology are considered in any detail. The analyses throughout this thesis are based on the metric for homogeneous and isotropic space-times, defined by the Robertson-Walker line element.

The classification of relativistic world-models containing both matter and radiation is considered in some detail. The properties of some model parameters are determined as a function of the temperature of the radiation field which is assumed to be Planckian. Some attention is also given to the problems of event and particle horizons in uniform world-models.

Data derived from radio source observations are used extensively in an attempt to solve the cosmological problem. The distribution of source angular diameters with redshift and the variation of source average spectral index with redshift (or luminosity) both provide useful information on the evolutionary properties of the universe. The radio source counts of the recent 5C survey are examined for their cosmological implications. The analysis provides important evidence on the epoch corresponding to galaxy formation and the variation with time (or more directly with expansion parameter) of source luminosity or density in co-ordinate volume. Arguments are given supporting a

rapidly expanding evolutionary universe in which the matter density is somewhat greater than usually accepted values.

The effect of free-free absorption by intergalactic ionized hydrogen on the low frequency spectra of radio galaxies is examined for the steady-state, adiabatic and constant temperature universes.

Using thermodynamic principles, a differential equation is derived which determines the temperature path of the intergalactic gas in evolutionary universes. The gas is assumed to be heated by cosmic rays and plasma waves, and cooled by radiative losses and expansion of co-ordinates.

An integral equation is obtained for the extragalactic background intensity when intergalactic absorption is present. The radio background spectrum is determined for the steady-state, "adiabatic" and constant temperature models of the universe. In each case the theoretical spectrum is compared with the observed background spectrum.

The extragalactic component of the sky brightness is calculated by using the differential equation describing the thermal history of the intergalactic gas and the cosmological parameters derived from the source counts. The calculations include the separate cases of source luminosity evolution and source density evolution.

The diffuse X-ray flux is described in terms of Compton radiation from cosmic ray electrons in intergalactic space. The electrons are assumed to be ejected from radio galaxies in a time which is small compared with the characteristic time of evolution of the universe. Normalisation of the derived X-ray spectra yield estimates for the intergalactic cosmic ray energy density.

Finally a mathematical treatment is given which describes the consequences of the introduction of a general vector field into Einstein's field equations. The theory is applicable to universes of arbitrary intrinsic curvature. Some tentative conclusions are drawn concerning possible annihilation of matter.

CHAPTER II

A THEORETICAL BASIS FOR COSMOLOGY

2.1 Introduction

The concepts which form the fundamental basis of cosmology are those of general relativity. The redshift of spectral lines of remote cosmic objects ~~and the approximate isotropy and uniformity of the universe~~ find ~~an explanation and~~ description in terms of Einstein's general theory of relativity. A brief review of the constructs of this theory is provided here for completeness and for future reference. The theory has been well documented by several authors (e.g. Einstein, 1916, 1917; Weyl, 1918; Tolman, 1934; Fock, 1959; Synge, 1960; McVittie, 1965), but, in this thesis, only features of the theory important for the elucidation of the cosmological problem will be described in any detail.

2.2 The Principles of General Relativity

The theory of relativity as proposed by Einstein may be regarded as based on the fundamental idea of the relativity of motion. In accordance with this idea, only the motions of bodies relative to one another have an objective meaning. The special theory of relativity is based on the Lorentz transformations in Galilean spaces. Of course, universal gravitation does not fit into the framework of these inertial frames, and it proved possible to provide a theory of gravitation only by abandoning the concept of uniformity of space-time

as a whole. This meant the introduction of Riemann geometry in place of the Euclidean geometry applicable to the special theory.

The ideas of general relativity require that physical laws be independent of the particular space-time coordinates. This is a general statement of the principle of covariance. If equations involving functions of independent variables are of the same form (subject to suitable transformations) in different coordinate systems, then the equations are said to be covariant. A satisfactory way of ensuring covariant relations is to use tensors and tensor analysis. The important functions in Riemannian geometry are the coefficients $g_{\mu\nu}$ of the quadratic form for the squared infinitessimal "distance". The introduction of these functions allows the formation of equations that are covariant with respect to arbitrary coordinate transformations. In Riemannian geometry, transformations of coordinates are accompanied by a transformation of the $g_{\mu\nu}$, but, as pointed out by Fock (1959), neither such a combined transformation nor covariance with respect to it has any relation to the uniformity or otherwise of space-time. It follows that "general relativity" has in fact nothing to do with "relativity" as such. Einstein's theory is essentially a theory of space-time and (consequently) gravitation.

2.3 Riemannian Spaces and Geodesics

The general theory of relativity is based on the properties of n-dimensional manifolds of points or Riemannian spaces. In such

spaces, the interval between two events whose coordinates are x^μ and $x^\mu + dx^\mu$ respectively is an invariant quantity ds, defined by the Riemannian metric

$$ds^2 = g_{\mu\nu}\, dx^\mu dx^\nu \tag{2.1}$$

The functions $g_{\mu\nu}$ are the components of a covariant tensor of rank two called the metrical tensor which can be assumed, without loss of generality, to be symmetrical in their indices. The corresponding contravariant metrical tensor is simply defined by

$$g^{\mu\nu} = (\text{co-factor of } g_{\mu\nu} \text{ in } g)/g \tag{2.2}$$

where g is the determinant of the metric assumed to be not identically equal to zero. It follows immediately from the law of multiplication of determinants that

$$g^{\lambda\mu} g_{\lambda\nu} = \delta^\mu_\nu \tag{2.3}$$

where δ^μ_ν is the Kronecker delta.

Applications of Riemannian spaces to general relativity and cosmology are usually restricted to orthogonal spaces in which $g_{\mu\nu} = 0$ for $\mu \neq \nu$. In particular, the solution to the cosmological problem involves the use of orthogonal space-times, and this will be considered in detail in the next chapter.

The fundamental paths of Riemannian spaces are called geodesics. As the interval ds is defined independently of the system of co-ordinates, the line drawn between two points P and P' of the n-dimensional manifold in such a way that the $\int ds$ is stationary - a geodetic line - has a meaning which is also independent of the choice of co-ordinates. Its equation is

$$\delta \int_{P}^{P'} ds = 0 \tag{2.4}$$

which states that the total interval along a geodesic shall be an extremum for small variations which vanish at the two limits of integration. Substitution for ds from equation (2.1) yields (e.g. Einstein, 1916) a set of n differential equations for the geodesic

$$\frac{d}{ds}\left(g_{\sigma\nu}\frac{dx^{\nu}}{ds}\right) - \frac{1}{2}\frac{\partial g_{\mu\nu}}{\partial x^{\sigma}}\frac{dx^{\mu}}{ds}\frac{dx^{\nu}}{ds} = 0 \qquad \sigma = 1,2,..n \tag{2.5}$$

It is convenient to introduce here the three-index Christoffel symbols of the first and second kind. These are defined respectively as follows:

$$\Gamma_{\sigma,\mu\nu} = \Gamma_{\sigma,\nu\mu} = \frac{1}{2}\left(\frac{\partial g_{\mu\sigma}}{\partial x^{\nu}} + \frac{\partial g_{\nu\sigma}}{\partial x^{\mu}} - \frac{\partial g_{\mu\nu}}{\partial x^{\sigma}}\right) \tag{2.6}$$

$$\Gamma^{\sigma}_{\mu\nu} = \Gamma^{\sigma}_{\nu\mu} = \frac{1}{2}\left(\frac{\partial g_{\mu\lambda}}{\partial x^{\nu}} + \frac{\partial g_{\nu\lambda}}{\partial x^{\mu}} - \frac{\partial g_{\mu\nu}}{\partial x^{\lambda}}\right)g^{\sigma\lambda} \tag{2.7}$$

These symbols are symmetrical with respect to the two indices that are written together, but neither quantities are components of tensors. It should be noted that the two kinds of Christoffel symbols are related

by the equations

$$\Gamma^{\sigma}_{\mu\nu} = g^{\sigma\tau}\Gamma_{\tau,\mu\nu}, \qquad \Gamma_{\sigma,\mu\nu} = g_{\sigma\tau}\Gamma^{\tau}_{\mu\nu} \tag{2.8}$$

Equation (2.5) may now be written in terms of the new notation, and the resulting equations are

$$\frac{d^2x^{\sigma}}{ds^2} + \Gamma^{\sigma}_{\mu\nu}\frac{dx^{\mu}}{ds}\frac{dx^{\nu}}{ds} = 0 \qquad (\sigma = 1,2,\ldots n) \tag{2.9}$$

which are the standard forms of the equations to the geodesics in Riemannian spaces provided, of course, that the interval ds along the curve is not identically equal to zero.

The null-geodesic is obtained by assuming that the interval between any two points on the curve is zero. If $\eta(x)$ is a non-zero scalar which is a function of position along the null-geodesic, then a curve of this kind will be characterised by possessing an integral of its defining equations expressed by

$$\xi \equiv g_{\mu\nu}\frac{dx^{\mu}}{d\eta}\frac{dx^{\nu}}{d\eta} = 0 \tag{2.10}$$

It follows that if P and P' are two points on the null-geodesic, then

$$\int_{P}^{P'} \xi \, d\eta = 0 \tag{2.11}$$

along the curve. The calculus of variations then yields the set of

n differential equations

$$\frac{d^2x^\sigma}{d\eta^2} + \Gamma^\sigma_{\mu\nu} \frac{dx^\mu}{d\eta} \frac{dx^\nu}{d\eta} = 0 \tag{2.12}$$

which define a null-geodesic in a Riemannian space.

2.4 Formation of Tensors by Differentiation

The geodesics as defined by the equations (2.9) constitute a set of paths, in Riemannian spaces, which are invariant under coordinate transformations. This is simply due to the stationary property of the scalar interval as measured along any one of them. Geodesics are therefore useful in describing the way in which vectors or tensors vary from one point of the space to another. With the aid of the equation for the geodetic line and the rules of tensor analysis, it is easy to deduce the laws by which new tensors can be formed from old by differentiation.

The covariant derivative of the contravariant vector A^μ is

$$\nabla_\nu A^\mu \equiv A^\mu_\nu = \frac{\partial A^\mu}{\partial x^\nu} + \Gamma^\mu_{\nu\tau} A^\tau \tag{2.13}$$

Alternatively, an extension of this analysis yields a definition for the covariant derivative of the covariant vector B_μ. The result is

$$\nabla_\nu B_\mu \equiv B_{\mu\nu} = \frac{\partial B_\mu}{\partial x^\nu} - \Gamma^\tau_{\mu\nu} B_\tau \tag{2.14}$$

which is a covariant tensor of the second rank.

It is possible to extend the analysis further and obtain for the covariant derivative of the tensor $T_{\mu\nu}$:

$$\nabla_\sigma T_{\mu\nu} \equiv T_{\mu\nu,\sigma} = \frac{\partial T_{\mu\nu}}{\partial x^\sigma} - \Gamma^\tau_{\sigma\mu} T_{\tau\nu} - \Gamma^\tau_{\sigma\nu} T_{\mu\tau} \tag{2.15}$$

which are components of a covariant tensor of rank three. Similarly, ~~it may be proved that~~

$$\nabla_\sigma T^{\mu\nu} \equiv T^{\mu\nu}_{\ ,\sigma} = \frac{\partial T^{\mu\nu}}{\partial x^\sigma} + \Gamma^\mu_{\tau\sigma} T^{\tau\nu} + \Gamma^\nu_{\tau\sigma} T^{\mu\tau} \tag{2.16}$$

is the covariant derivative of the contravariant tensor $T^{\mu\nu}$. Contraction with respect to μ and ν in equation (2.13) gives a unique scalar:

$$\Phi = \nabla_\nu A^\nu = \frac{\partial A^\nu}{\partial x^\nu} + \Gamma^\nu_{\nu\tau} A^\tau \tag{2.17}$$

which is the divergence of the contravariant vector A^μ. This equation can be easily simplified by application of the definitions (2.6) and (2.7) for the Christoffel symbols and the rules of differentiation of determinants to yield

$$\Phi = \frac{1}{\sqrt{(-g)}} \frac{\partial}{\partial x^\nu} \{\sqrt{(-g)}\, A^\nu\} \tag{2.18}$$

$$= \frac{1}{\sqrt{(-g)}} \frac{\partial \sqrt{(-g)}}{\partial x^\nu} A^\nu + \frac{\partial A^\nu}{\partial x^\nu} \tag{2.19}$$

It is therefore apparent that the divergence Φ is analogous to the ordinary scalar divergence in Euclidean space when the determinant of the metrical tensor is independent of position.

2.5 The Riemann-Christoffel Tensor

In this section, we turn to the problem of deriving a new tensor from the metrical tensor alone. If the tensor difference $(\nabla_\sigma\nabla_\tau - \nabla_\tau\nabla_\sigma)A_\mu$ is formed with the aid of equation (2.15), then some terms cancel and the end result is

$$(\nabla_\sigma\nabla_\tau - \nabla_\tau\nabla_\sigma)A_\mu = G^\lambda_{\mu,\sigma\tau}A_\lambda \tag{2.20}$$

where

$$G^\lambda_{\mu,\sigma\tau} = \frac{\partial}{\partial x^\sigma}\Gamma^\lambda_{\mu\tau} - \frac{\partial}{\partial x^\tau}\Gamma^\lambda_{\mu\sigma} + \Gamma^\kappa_{\mu\tau}\Gamma^\kappa_{\sigma\kappa} - \Gamma^\kappa_{\mu\sigma}\Gamma^\lambda_{\kappa\tau} \tag{2.21}$$

The important feature of the result (2.20) is that, on the right hand side of the equation, A_λ occurs alone without any derivatives. Since $(\nabla_\sigma\nabla_\tau - \nabla_\tau\nabla_\sigma)A_\mu$ is a tensor and A_λ is an arbitrary vector, it follows immediately that the $G^\lambda_{\mu,\sigma\tau}$ must be components of a mixed tensor of rank four. This tensor is usually referred to as the Riemann-Christoffel tensor and is constructed entirely out of components of the metrical tensor $g_{\mu\nu}$ and their first and second derivatives. The vanishing of the Riemann-Christoffel tensor is a necessary condition for the existence of at least one coordinate system in which the $g_{\mu\nu}$ are constants. For suppose that, when referred to a particular coordinate system, the $g_{\mu\nu}$ are indeed

constants with all the $G^{\lambda}_{\mu,\sigma\tau}$ vanishing as a consequence of equation (2.21). If a new coordinate system is set up relative to which the $g_{\mu\nu}$ are not constants, then it follows from the laws of transformations of tensors that the components of $G^{\lambda}_{\mu,\sigma\tau}$ are identically zero.

The covariant form of the Riemann-Christoffel tensor is derived easily from the inner product

$$G_{\kappa\mu,\sigma\tau} = g_{\lambda\kappa}G^{\lambda}_{\mu,\sigma\tau}$$

$$= \frac{\partial}{\partial x^{\sigma}}\Gamma_{\kappa,\mu\tau} - \frac{\partial}{\partial x^{\tau}}\Gamma_{\kappa,\mu\sigma} + g^{\alpha\beta}\{\Gamma_{\alpha,\mu\sigma}\Gamma_{\beta,\kappa\tau} - \Gamma_{\alpha,\mu\tau}\Gamma_{\beta,\sigma\kappa}\} \qquad (2.22)$$

In the theory of space-time and gravitation, a very important role is played by a symmetrical tensor of rank two which is derived by a contraction of the Riemann-Christoffel tensor. Contracting in (2.21) with respect to the indices λ and τ, we obtain the quantities

$$G_{\mu\nu} = \frac{\partial}{\partial x^{\nu}}\Gamma^{\sigma}_{\mu\sigma} - \frac{\partial}{\partial x^{\sigma}}\Gamma^{\sigma}_{\mu\nu} + \Gamma^{\tau}_{\mu\sigma}\Gamma^{\sigma}_{\nu\tau} - \Gamma^{\tau}_{\mu\nu}\Gamma^{\sigma}_{\tau\sigma} \qquad (2.23)$$

which are components of a covariant tensor of the second rank. Clearly, the mixed form of this tensor is $G^{\nu}_{\mu} = g^{\nu\sigma}G_{\sigma\mu}$, from which a scalar called the scalar curvature may be obtained by contraction:

$$G = G^{\nu}_{\nu} = g^{\nu\sigma}G_{\sigma\nu} \qquad (2.24)$$

Consideration of spherical surfaces shows how the Riemann-Christoffel tensor measures a property in Riemannian spaces which is analogous to the curvature of a two-dimensional surface. When the space is of more than three dimensions, the concept of curvature is rather remote, but it is apparent from the preceeding remarks that the Riemann-Christoffel tensor is a measure of the flatness or otherwise of a particular space. The problems associated with space curvature will be examined more fully in a later section and it is sufficient to remark here that a space is flat if the Riemann-Christoffel tensor vanishes at ~~any~~ every point of a Riemannian space. If the components $G^{\lambda}_{\mu,\sigma\tau} \neq 0$ at ~~all~~ some set of points of the space, then the space is said to be curved.

The expression (2.22) yields the following symmetry properties:

$$G_{\kappa\mu\sigma\tau} = - G_{\mu\kappa\sigma\tau} = - G_{\kappa\mu\tau\sigma} = G_{\sigma\tau\kappa\mu} \tag{2.25}$$

$$G_{\kappa\mu\sigma\tau} + G_{\kappa\tau\mu\sigma} + G_{\kappa\sigma\tau\mu} = 0 \tag{2.26}$$

Using these relations and equation (2.24), the scalar curvature is found to be defined by one component only of the Riemann-Christoffel tensor, in two-dimensional space, by ~~three~~ six components in three dimensions and by ~~fourteen~~ twenty independent components in four-dimensional space.

Introducing a locally geodesic coordinate system in which covariant derivatives reduce to ordinary partial derivatives, it is

possible to prove that the Riemann-Christoffel tensor satisfies the set of differential equations

$$\nabla_\nu G^\lambda_{\mu,\sigma\tau} + \nabla_\sigma G^\lambda_{\mu,\tau\nu} + \nabla_\tau G^\lambda_{\mu,\nu\sigma} = 0 \tag{2.27}$$

called the Bianchi identities. Contracting this equation with respect to the indices λ and τ, multiplying by $g^{\mu\rho}$ and using the symmetry rules of (2.25) and (2.26), we find

$$\nabla_\nu G^\rho_\sigma = \nabla_\sigma G^\rho_\nu + \nabla_\tau (g^{\tau\kappa} G^\rho_{\kappa\sigma\nu}) = 0$$

Contracting with respect to ρ and ν, and changing the summation index τ in the last term to ρ, the last equation becomes

$$2\nabla_\rho G^\rho_\sigma - \nabla_\sigma G = 0 \tag{2.28}$$

and if Λ is an arbitrary constant, then this equation may be written in the form

$$\nabla_\lambda \left[G^\lambda_\sigma - \frac{1}{2} \delta^\lambda_\sigma (G - 2\Lambda) \right] = 0 \tag{2.29}$$

Hence the divergence of the tensor

$$E^\mu_\nu = G^\mu_\nu - \frac{1}{2} \delta^\mu_\nu (G - 2\Lambda) \tag{2.30}$$

vanishes identically. Raising and lowering indices in (2.30), we obtain the following contravariant and covariant tensors

$$E^{\mu\nu} = G^{\mu\nu} - \frac{1}{2} g^{\mu\nu}(G - 2\Lambda) \tag{2.31}$$

$$E_{\mu\nu} = G_{\mu\nu} - \frac{1}{2} g_{\mu\nu}(G - 2\Lambda) \tag{2.32}$$

which are obviously symmetric. These tensors will be found to have fundamental application in the subsequent work.

2.6 The Energy-Momentum Tensor

The non-relativistic equations of motion in the mechanics of continuous media have the form

$$\frac{\partial v_i}{\partial t} + \sum_{k=1}^{3} v_k \frac{\partial v_i}{\partial x_k} = F_i + \frac{1}{\rho} \sum_{i=1}^{3} \frac{\partial p_{ik}}{\partial x_k} \quad (i=1,2,3) \tag{2.33}$$

and

$$\frac{\partial \rho}{\partial t} + \sum_{i=1}^{3} \frac{\partial (\rho v_i)}{\partial x_i} = 0 \tag{2.34}$$

where the symbols have their usual meanings with p_{ik} being the stress tensor, and F_i the components of the external force acting on unit mass. Using the equation (2.34) of continuity in the equation (2.33) of motion, we find

$$\frac{\partial \rho v_i}{\partial t} + \sum_{k=1}^{3} \frac{\partial}{\partial x_k} (\rho v_i v_k - p_{ik}) = \rho F_i \tag{2.35}$$

which expresses the law of conservation of momentum. The generalisation of equations (2.34) and (2.35) to covariant tensor equations is more easily solved if the only force acting on the fluid is its pressure-gradient ($F_i = 0$, $p_{ik} = -p\delta_{ik}$). In this case, ~~and in~~

~~general~~, we write for the energy-momentum tensor:

$$T^{\mu\nu} = (\rho + p/c^2)u^\mu u^\nu - g^{\mu\nu}\frac{p}{c^2} \tag{2.36}$$

where u^μ is the velocity 4-vector of the fluid which satisfies the relation

$$1 = g_{\mu\nu}u^\mu u^\nu \tag{2.37}$$

Equation (2.36) must also satisfy

$$\nabla_\nu T^{\mu\nu} = 0 \tag{2.38}$$

so that the vectorial divergence of the energy tensor vanishes identically.

2.7 Einstein's Equations

In the general theory of relativity, Riemannian spaces of four dimensions are employed. The metrics of these spaces are therefore written

$$ds^2 = g_{\mu\nu}dx^\mu dx^\nu \qquad \mu,\nu = 1,2,3,4 \tag{2.39}$$

The fact that line elements of the second order are sufficient to describe the space-time metric, only indicates a property of reality. Equation (2.39) also implies that measuring instruments

obey the laws of Euclidean geometry in infinitessimal regions of the space-time.

Guided by the analogy of Poisson's equations for the gravitational potential,

$$\nabla^2\phi = -4\pi G\rho$$

to the problem of gravitation and space-times, Einstein (1916) asserted that the vectorial divergence of the energy-momentum tensor and the tensors defined in equations (2.30) to (2.32) were directly proportional to each other (both divergences being equal to zero). Hence from (2.31) and (2.36)

$$\nabla_\nu(-\kappa c^2 T^{\mu\nu}) = \nabla_\nu E^{\mu\nu}$$

where $-\kappa c^2$ is a constant of proportionality. Integrating the last equation, we obtain the ten basic equations

$$-\kappa c^2 T^{\mu\nu} = G^{\mu\nu} - \frac{1}{2} g^{\mu\nu}(G - 2\Lambda) \tag{2.40}$$

which are known as Einstein's equations. Also consideration of the Newtonian approximation to (2.40) yields

$$\kappa = \frac{8\pi G}{c^2} \tag{2.41}$$

where G is the gravitational constant.

Einstein's equations relate the metrical tensor (geometry) which represents the distribution of mass-energy to the energy-momentum tensor of the distribution. The constant Λ was introduced by Einstein when considering the cosmological problem and is therefore referred to as the cosmological constant.

It should be noted that the equations (2.40) may be derived in a straightforward manner (Landau and Lifshitz, 1961) by the application of the action principle to the gravitational field and matter.

The principle of least action requires that

$$\delta(\delta m + \delta g) = \delta\left[\Sigma m \int ds - \frac{1}{\kappa c^2} \int G \sqrt{-g}\, d^4x\right]$$

$$= \int T^{\mu\nu} \delta g_{\mu\nu} \sqrt{-g}\, d^4x + \frac{1}{\kappa c^2} \int (G^{\mu\nu} - \frac{1}{2} g^{\mu\nu} G)\, \delta g_{\mu\nu} \sqrt{-g}\, d^4x \tag{2.42}$$

must vanish identically. Equations (2.40) follow immediately because of the arbitrary nature of the $\delta g_{\mu\nu}$.

2.8 Spherical Symmetry

The investigations in this thesis will all be restricted to situations involving spherical distributions of matter. In these cases, if the distribution is symmetrical about a particular point in space then the metric (2.39) must also exhibit symmetry about that point.

The most general centrally symmetric expression for the interval ds in terms of space coordinates (r,θ,ϕ) must be

$$ds^2 = \alpha(r,t)dr^2 + \beta(r,t)(d\theta^2+\sin^2\theta d\phi^2) + \gamma(r,t)dt^2 + \varepsilon(r,t)drdt \qquad (2.43)$$

However, by an arbitrary transformation of the coordinates $r = r(r',t')$, $t = t(r',t')$, the coefficient $\varepsilon(r',t')$ can be made to vanishes while the coefficient $\beta(r',t')$ is simply equal to $-r'^2/c^2$. Also it will be found convenient to write α and γ in exponential form as $e^{\bar{\mu}}/c^2$ and $e^{\bar{\nu}}$ respectively. Thus the metric of an orthogonal space-time symmetric about the point $r = 0$ is

$$ds^2 = e^{\bar{\nu}}dt^2 - \frac{1}{c^2}[e^{\bar{\mu}}dr^2 + r^2(d\theta^2+\sin^2\theta d\phi^2)] \qquad (2.44)$$

where $\bar{\nu},\bar{\mu}$ are arbitrary functions of r and t. The isotropic form of the metric will be

$$ds^2 = e^{\nu}dt^2 - \frac{e^{\mu}}{c^2}[dr^2 + r^2(d\theta^2+\sin^2\theta d\phi^2)] \qquad (2.45)$$

It has been proved by Kustaanheimo (1953) that the metrics (2.44) and (2.45) are convertible into one another. Because of the particular importance of the isotropic form of the metric, a variety of formulae are developed here. Firstly, from equation (2.45) we may write for the components of the metrical tensor

$$g_{11} = -\frac{e^{\mu}}{c^2}, \quad g_{22} = -\frac{e^{\mu}}{c^2} r^2, \quad g_{33} = -\frac{e^{\mu}}{c^2} r^2 \sin^2\theta,$$

$$g_{44} = e^{\nu} \tag{2.46}$$

and using the formula (2.2), we obtain for the contravariant components of the metrical tensor

$$g^{11} = -c^2 e^{-\mu}, \quad g^{22} = -c^2 e^{-\mu} r^{-2}, \quad g^{33} = -c^2 e^{-\mu} r^{-2} \sin^{-2}\theta$$

$$g^{44} = e^{-\nu} \tag{2.47}$$

The surviving non-zero Christoffel symbols are according to (2.7)

$$\Gamma^1_{11} = \frac{1}{2}\mu' \qquad \Gamma^4_{11} = \frac{1}{2c^2}\dot{\mu} e^{\mu - \nu}$$

$$\Gamma^1_{22} = -(r + \frac{1}{2} r^2 \mu') \qquad \Gamma^4_{22} = \frac{1}{2c^2} e^{\mu-\nu} r^2 \dot{\mu}$$

$$\Gamma^2_{12} = \Gamma^3_{13} = \Gamma^2_{21} = r^{-1} + \frac{1}{2}\mu'$$

$$\Gamma^3_{32} = \Gamma^3_{23} = \Gamma^2_{24} = (\tan\theta)^{-1} \tag{2.49}$$

$$\Gamma^2_{42} = \Gamma^1_{14} = \Gamma^2_{24} = \Gamma^3_{34} = \frac{1}{2}\dot{\mu}$$

$$\Gamma^1_{33} = -r \sin\theta(\frac{\mu' r}{2} + 1), \quad \Gamma^2_{33} = -\sin\theta\cos\theta$$

$$\Gamma^4_{33} = \frac{1}{2} e^{\mu-\nu} \dot{\mu} r^2 c^{-2} \sin^2\theta$$

$$\Gamma^1_{44} = \frac{1}{2} e^{\nu-\mu} \nu' c^2, \quad \Gamma^4_{14} = \frac{1}{2}\nu', \quad \Gamma^4_{44} = \frac{1}{2}\dot{\nu}$$

In these equations, the prime denotes differentiation with respect to r, while a dot denotes differentiation with respect to t. The

Christoffel symbols of the first kind, $\Gamma_{\sigma,\mu\nu}$, can be easily derived from equations (2.44) and (2.8).

Direct calculation from equation (2.22) yields, for the surviving components of the Riemann-Christoffel tensor,

$$G_{1212} = \frac{e^{\mu}}{c^2}\left[\frac{5}{2} r\mu' + \frac{1}{2} r^2\mu'^2 + r^2\mu'' - \frac{1}{4}\frac{\dot{\mu}^2 r^2}{c^2} e^{\mu-\nu} + 1\right]$$

$$G_{2323} = \frac{e^{\mu} r^2 \sin^2\theta}{c^2}\left[\left(1 + \frac{r\mu'}{2}\right)^2 - \frac{1}{4}\frac{\dot{\mu}^2}{c^2} e^{\mu-\nu} r^2 - \tan^{-2}\theta\right]$$

$$G_{3131} = \sin^2\theta\, G_{1212}$$

$$G_{1224} = \frac{e^{\mu} r^2}{2c^2}\left[\dot{\mu}\left(\frac{1}{2}\nu' - r^{-1} - \frac{3}{2}\mu'\right) + \dot{\mu}' + \dot{\mu}\left(r^{-1} + \frac{1}{2}\mu'\right)\right] \qquad (2.50)$$

$$G_{3134} = -\sin^2\theta\, G_{1224}$$

$$G_{1414} = \frac{e^{\mu}}{c^2}\left[4\ddot{\mu} + 3\dot{\mu}^2 - \dot{\mu}\dot{\nu} - \dot{\mu}^2\right] + \frac{e^{\nu}}{4}\left[\mu'\nu' - 2\nu'' - \nu'^2\right]$$

$$G_{2424} = \frac{e^{\mu} r^2}{c^2}\left[\ddot{\mu} + \frac{3}{4}\dot{\mu}^2 - \frac{1}{4}\dot{\mu}\dot{\nu}\right] - \frac{e^{\nu}}{2}\nu'\left[r + \frac{1}{2} r^2\mu'\right]$$

$$G_{3434} = \sin^2\theta\, G_{2424}$$

The non-vanishing components of the curvature tensor are from equation (2.23)

$$G_{11} = \frac{e^{\mu-\nu}}{4c^2}\left[\dot{\mu}\dot{\nu} - 3\dot{\mu}^2 - 2\ddot{\mu}\right] + \frac{1}{4}\left[\nu'^2 - \mu'\nu' + \mu'^2\right] + \mu'' + r^{-1}\mu' + \frac{1}{2}\nu'$$

$$G_{22} = \frac{v^2 e^{\mu-\nu}}{4c^2}\left[\dot{\mu}\dot{\nu} - 3\dot{\mu}^2 - 2\ddot{\mu}\right] + \frac{r}{2}\left[\nu' + \frac{1}{2}r\mu'\nu' + r\mu''\right] + r\mu' + 2\sin^{-2}\theta$$

$$G_{33} = \sin^2\theta\, G_{22}$$

$$G_{44} = \frac{c^2 e^{\nu-\mu}}{4}\left[\mu'\nu' - 2\nu'' - \nu'^2 - 4\nu' r^{-1}\right] - \frac{3}{4}\dot{\mu}\dot{\nu} + \frac{3}{4}\dot{\mu}^2 + \frac{3}{2}\ddot{\mu}$$

$$G_{14} = G_{41} = \dot{\mu}' - \frac{1}{2}\nu'\dot{\mu} \qquad (2.51)$$

It is now possible to write down the set of Einstein's equations for the case of isotropic space-times. Inspection of equations (2.40), (2.50) and (2.51) indicate that the components T^{ij} of the energy-momentum tensor are identically zero for $i \neq j$. The velocity 4-vector in view of (2.37) must therefore satisfy

$$1 = e^{\nu}(u^4)^2 - \frac{e^{\mu}(u')^2}{c^2} \qquad (2.52)$$

Hence, by equations (2.36), (2.48), (2.50), (2.51) and (2.52), the set of Einstein's equations (2.40) become

$$\kappa\left[\left(\rho + \frac{p}{c^2}\right)(u')^2 + e^{-\mu}p\right]e^{\mu} = c^2 e^{-\mu}\left[\frac{1}{r}\left[\frac{1}{r}(\mu'+\nu') + \frac{1}{4}\mu'^2 + \frac{1}{2}\mu'\nu'\right]\right.$$

$$\left. -e^{-\nu}\left[\ddot{\mu} + \frac{3}{4}\dot{\mu}^2 - \frac{1}{2}\dot{\mu}\dot{\nu}\right]\right] + \Lambda \qquad (2.53)$$

$$\kappa p = \frac{c^2 e^{-\mu}}{2}\left[(\mu'' + \nu'') + \frac{1}{r}(\mu' + \nu') + \frac{1}{2}\nu'^2\right] - e^{-\nu}\left[\ddot{\mu} + \frac{3}{4}\dot{\mu}^2 - \frac{1}{2}\dot{\mu}\dot{\nu}\right] + \Lambda \qquad (2.54)$$

$$\kappa(\rho + p/c^2)u^4u' = e^{-(\mu+\nu)}(\dot{\mu}' - \frac{1}{2}\dot{\mu}\nu') \tag{2.55}$$

$$\kappa[(\rho + p/c^2)(u^4)^2 + e^{-\nu}\frac{p}{c^2}]e^{\nu} = -e^{-\mu}[\mu'' + \frac{1}{4}\mu'^2 + \frac{2}{r}\mu'] + \frac{3}{4}\frac{e^{-\nu}}{c^2}\dot{\mu}^2 - \frac{\Lambda}{c^2} \tag{2.56}$$

2.9 Summary

The general theory of relativity is developed by employing tensor calculus to describe the properties of Riemannian spaces. The metric of a Riemannian space is defined by the functions $g_{\mu\nu}$ which are components of the metrical tensor. Differentiation of the metric coefficients yields further fundamental tensors including the Riemann-Christoffel tensor, which measures a quantity analogous to curvature, and another tensor which has zero vectorial divergence. Einstein's equations may be obtained either by equating this latter tensor to the energy-momentum tensor of a 4-dimensional space-time or by the application of the action principle to the gravitational field and matter.

The set of Einstein's field equations are of basic importance to the development of cosmological theories and will be used throughout the following work. In the next chapter the equations will be used to derive a space-time metric for universes which have a uniform mass-energy distribution.

CHAPTER III

THEORY OF ISOTROPIC AND HOMOGENEOUS WORLD-MODELS

3.1 The Roberston-Walker Metric

The universe may be regarded as a collection of discrete masses (galaxies) together with a more or less uniform distribution of matter and radiation. In order to obtain a simplified mathematical description, this mass-energy distribution is idealised as a perfect fluid. In this situation, the most convenient coordinate system is one which is moving at each point of space, along with the matter located at that point. This is an intrinsic or co-moving coordinate system and by definition the velocity of matter is everywhere zero. The velocity 4-vector of the fluid therefore reduces to

$$u^4 \neq 0, \qquad u^i = 0, \qquad i = 1,2,3$$

If co-moving coordinates are present, then the left-hand side of equation (2.55) is zero and ~~then equating the right-hand side to zero~~ we obtain the partial differential equation

$$\dot{\mu}' = \frac{1}{2}\,\dot{\mu}\nu' \tag{3.1}$$

Selecting the time coordinate so that $g_{44} = 1$ $(\nu = 0)$ in the metric (2.45) and integrating (3.1) with respect to t and r, it is found (McVittie,1965) that

$$\mu = F(r) + \log R^2(t) \tag{3.2}$$

where $F(r)$ is an arbitrary function of r and $R(t)$ is an arbitrary function of t.

Introducing the condition $u^1 = 0$ into equations (2.53) and (2.54), two expressions for P are derived which are identical only if

$$\mu'' - \frac{\mu'}{r} - \frac{\mu'^2}{2} = 0 \tag{3.3}$$

Solving (3.2) and (3.3), we find

$$F(r) = - \log (1+ kr^2/4)^{-2}$$

where the factor k is of the nature of a scale factor. Substituting the last equation together with (2.2) into the equation (2.45), the metric for isotropic space times may be written in the form

$$ds^2 = dt^2 - \frac{R^2(t)}{c^2} \left\{ \frac{dr^2 + r^2 d\theta^2 + \sin^2\theta d\phi^2}{(1+ kr^2/4)^2} \right\} \tag{3.4}$$

This equation is of fundamental importance to cosmology and will be used extensively in the following work. The expression (3.4) was first derived by Robertson (1935) and derived independently by Walker (1936). Equations for the density and pressure of the mass-energy distribution are obtained from equations (2.54) and (2.56) by putting

$$\nu = 0, \qquad \mu = \log[R^2(1+ kr^2/4)^{-2}], \qquad u^4 = 1$$

and the results are

$$8\pi G\rho = -\frac{3}{R^2}(kc^2 + \dot{R}^2) - \Lambda \tag{3.5}$$

$$\frac{8\pi GP}{c^2} = -\frac{2\ddot{R}}{R} - \frac{\dot{R}^2}{R^2} - \frac{kc^2}{R^2} + \Lambda \tag{3.6}$$

since $\kappa = 8\pi G/c^2$. Clearly, the density and pressure are independent of any spatial coordinates and are functions of the time (epoch) t alone.

3.2 Properties of the Metric

It easily follows from equations (3.5) and (3.6) that

$$\frac{d\rho R^3}{dt^2} + \frac{P}{c^2}\frac{dR^3}{dt} = 0 \tag{3.7}$$

which is seen to be analogous to the first law of thermodynamics for an adiabatic expansion.

A suitable adjustment of the unit in which the radial coordinate r is measured can produce values of the space-curvature constant k equal to $+1$, 0, -1 depending on whether the space is closed, flat or open. From the set of equations (2.50), we see that the components of the Riemann-Christoffel tensor, $G_{\kappa\mu\sigma\tau}$, for the 3-geometry (a hypersurface in space-time with t = const) all vanish for $k = 0$. Of course, in this case the curvature of the 4-geometry is non-zero since some of the $G_{\kappa\mu\sigma\tau} \neq 0$ for values of the indices equal to four and non-constant $R(t)$.

Some useful equations are obtained by introducing in place of the coordinate r the "angle" ω defined by

$$\omega = \int \frac{dr}{1 + \frac{kr^2}{4}} \tag{3.8}$$

Furthermore we define a quantity

$$T_k(\omega) = \frac{r}{1 + kr^2/4} \tag{3.9}$$

so that the metric (3.4) becomes

$$ds^2 = dt^2 - \frac{R^2(t)}{c^2} (d\omega^2 + T_k{}^2 d\Omega^2) \tag{3.10}$$

where $d\Omega^2 = d\theta^2 + \sin^2\theta d\phi^2$.

According to (3.8) and (3.9),

$r = 2 \tan(\omega/2)$	$T_{+1}(\omega) = \sin(\omega)$	for $k = +1$
$r = \omega$	$T_0(\omega) = \omega$	" $k = 0$
$r = 2 \tanh(\omega/2)$	$T_{-1}(\omega) = \sinh(\omega)$	" $k = -1$

(3.11)

The equation to the null-geodesic (light path) in the space-time defined by the metric (3.4) is obtained by simply putting $ds = 0$, and the result is

$$\frac{dr}{dt} = - \frac{c}{R(t)} (1 + kr^2/4) \tag{3.12}$$

for signals travelling towards the origin of coordinates. The

formula for the redshift of radiation emitted at time t and received at time t_o follows easily (e.g. McVittie,1965) from (3.12). The redshift, z, written in terms of the scale factor $R(t)$ is

$$z = \frac{d\lambda}{\lambda} = \frac{R(t_o)}{R(t)} - 1 \tag{3.13}$$

or alternatively we write

$$z = y^{-1} - 1 \tag{3.14}$$

where $y = R/R_o$

At the epoch $t = t_o$, equations (3.5) and (3.6) may be written in the form

$$8\pi G\rho_o = 3H_o^2 + \frac{3kc^2}{R_o^2} - \Lambda \tag{3.15}$$

$$\frac{8\pi GP_o}{c^2} = (2q_o - 1)H_o^2 - \frac{kc^2}{R_o^2} + \Lambda \tag{3.16}$$

where the Hubble parameter is

$$H_o = \dot{R}_o/R_o \tag{3.17}$$

and the deceleration parameter is

$$q_o = -\ddot{R}_o/R_oH_o^2 \tag{3.18}$$

Introducing the density parameter, σ_o, and pressure parameter, ε_o, by

$$\sigma_o = \frac{4\pi G\rho_o}{3H_o^2} \quad , \qquad \varepsilon_o = \frac{P_o/c^2}{\rho_o} \tag{3.19}$$

then we obtain two fundamental equations

$$\lambda = \frac{\Lambda}{3H_o^2} = (1 + 3\varepsilon_o)\sigma_o - q_o \tag{3.20}$$

$$\frac{kc^2}{R_o^2 H_o^2} = 3(1 + \varepsilon_o)\sigma_o - q_o - 1 \tag{3.21}$$

which determine the cosmological constant and the curvature constant, respectively.

3.3 Summary

Einstein's equations may be solved for a homogeneous and isotropic mass-energy distribution. In this case the metrical tensor is given by the coefficients in the Robertson-Walker metric. The density and pressure of the mass-energy distribution are found to be functions of the cosmic time only. Other equations, which will have constant application throughout this thesis, are derived from the expression for the Robertson-Walker line element.

CHAPTER IV

GEOMETRICAL PROPERTIES OF WORLD-MODELS

In this chapter the theory of homogeneous and isotropic universes is further advanced by elucidation of the geometrical properties of world-models. These are the properties of model universes which are directly dependent on the equations derived from the space-time metric (3.4).

4.1 Model Classification

Some preliminary work has been done on the subject of model classification by Robertson (1933) and Bondi (1961). More recently Stabell and Refsdal (1966) have examined this problem on the basis of diagrams in which the cosmological constant, λ, is plotted against R (the radius of curvature) for $\dot{R} = 0$. However, this analysis is somewhat misleading since the (λ, R) plots imply that, for a particular λ, $\dot{R} = 0$ at the present epoch and this is clearly impossible for finite non-zero values of the Hubble constant H_o. The mistake lies in the fact that the curve $\dot{R} = 0$, in the (λ, R) plane, is a function not only of R, but also of λ.

Previous analyses of model classification have been restricted to universes filled with ordinary matter only. In this analysis, relativistic world-models containing both matter and radiation are classified by means of the cosmological constant, λ, and the density parameter σ_o.

The existence of a universal black-body radiation would introduce special conditions into the Einstein field equations. Some analytical solutions to these equations have been obtained for a universe containing non-interacting matter and radiation. Alpher and Herman (1949) have integrated Einstein's equations for the special case when the cosmological constant $\Lambda = 0$, while a solution has been derived by Jacobs (1967) for space-times of zero intrinsic curvature. Conversion of radiation into matter has been considered by McIntosh (1967) and Davidson (1962), and for this purpose they define, ad hoc, particular functions of the radius of curvature R(t). In this analysis, we consider the universe to be filled with non-interacting matter and radiation, and a world-model is defined in a most general way by its density parameter σ_o and the constant $\lambda(=\Lambda/3H_o^2)$. Earlier measurements (e.g. Penzias and Wilson, 1965) have indicated a black-body temperature close to 3°K but more recent measurements (e.g. Shivanandan et. al., 1968) imply a dilute spectrum with a temperature of 3n°K, where the dilution factor $n > 3$. It therefore seems appropriate, in view of this possibility of a relatively high temperature, T_o, for the universal radiation field, to examine the properties of relativistic world-models for general $T_o > 0$. The thermal radiation spectrum is assumed to be Planckian throughout this analysis. It should be mentioned here that the consequences of cosmic black-body radiation will be discussed more fully in subsequent chapters.

Observational evidence indicates that the contribution to the isotropic pressure, p_o, from the random motions of galaxies and interstellar matter is negligibly small. Therefore, in accordance with the radiation laws we may write

$$p_o = \frac{\sigma' T_o^4}{3} \tag{4.1}$$

where T_o is the radiation temperature at the present time, and σ' is the Stefan-Boltzmann constant. Furthermore, Tolman (1934) has shown that as the universe expands the cosmological redshift serves to adiabatically cool the radiation while preserving its thermal character. The radiation temperature, T, will therefore vary inversely as the expansion parameter, y, and consequently

$$E_r = \sigma' T^4 = \sigma' T_o^4 y^{-4} \tag{4.2}$$

where E_r is the radiation energy density.

Thus, if radiation and matter are both conserved then

$$\rho = \rho_m + \rho_r = \rho_{mo} y^{-3} + \rho_{ro} y^{-4} \tag{4.3}$$

where ρ_{mo} is the present value of the matter density and $\rho_{ro} = E_{ro}/c^2$. We now define a function of the expansion parameter by

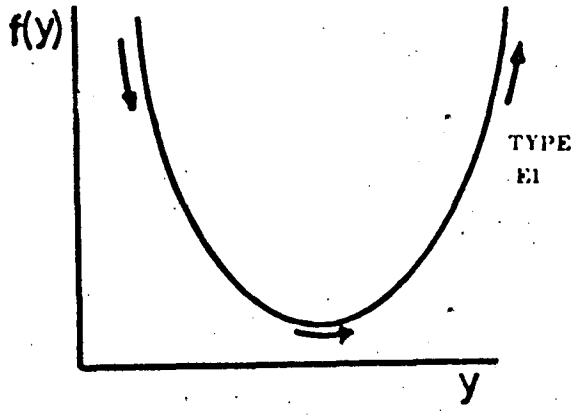

(a)

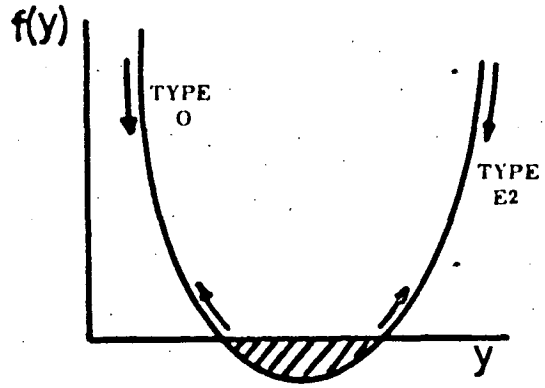

(b)

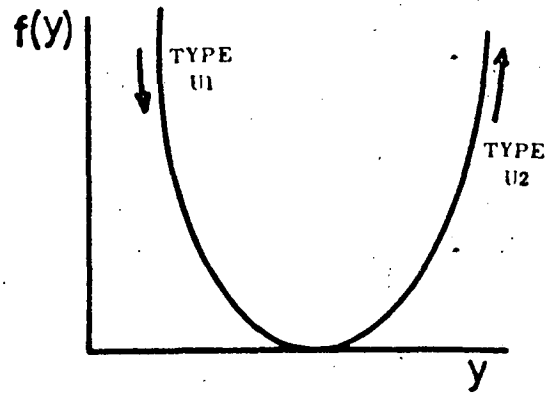

(c)

Figure 4.1 - Classification of relativistic world-models based on the form of the expansion function f(y).

$$f(y) \equiv \frac{1}{H_o^2}\left(\frac{dy}{dt}\right)^2 \tag{4.4}$$

Now solving equation (3.5) with the aid of (3.6), (3.19), (3.20) and (4.3) it is found that

$$\begin{aligned} f(y) &= 2\sigma_m y^{-1}(1 + \alpha y^{-1}) + q_o + 1 - 3(1 + \varepsilon_o)\sigma_o \\ &\qquad + [(1 + 3\varepsilon_o)\sigma_o - q_o]y^2 \\ &= 2\sigma_m y^{-1}(1 + \alpha y^{-1}) + 1 - 2\sigma_o - \lambda(1 - y^2) \end{aligned} \tag{4.5}$$

where $\alpha = \rho_{ro}/\rho_{mo}$ and the density parameter for matter is

$$\sigma_m = \sigma_o - \sigma_r = \sigma_o - \frac{4\pi G}{3H_o^2}\rho_{ro} \tag{4.6}$$

Consider the expression (4.5) for the function f(y) or indeed any arbitrary continuous function f(y) of the expansion parameter y. It is apparent that f(y) can never become negative ~~else~~ otherwise the universe as time derivative of y will be unreal. Several possible cases present themselves for the minimum (or minima) of the function f(y) and these are examined in turn:

(1) if $f(y) > 0$ for all $df(y)/dy \equiv f'(y) = 0$ then the universe must be in a state of continuous expansion since the first integral (with respect to t) of f(y) will be a continuously increasing function. This situation is indicated schematically in figure 4.1(a).

(2) if, for some value of $y = y_m$, $f'(y) = 0$ when $f(y) < 0$ then there are two alternative cases:

(a) if $f'(y) = 0$ at $y_m > 1$ (the value of y at the present epoch) then the universe expands from a singular state ($f(y) = \infty$) to a value of $y = y_{max} < y_m$ when contraction follows.

(b) if $f'(y) = 0$ at $y_m < 1$ then the universe must contract from arbitrarily large values of y to $y_{min} > y_m$ after which the universe rebounds into an expansive stage. Both of these cases are presented schematically in figure 4.1(b).

(3) if $f'(y) = 0$ when $f(y) = 0$ and $y = y_m$ then three possible situations arise. These are:

(a) $y_m = 1$: the universe is stationary corresponding to the Einstein world-model.

(b) $y_m < 1$: the universe can be considered as expanding from the static Einstein condition in the infinite past.

(c) $y_m > 1$: this corresponds to the universe expanding from a singular state with a value of $y < 1$ and approaching the Einstein universe asymptotically.

The last three models are illustrated in figure 4.1(c).

The properties of relativistic world-models with black-body radiation may now be represented by a diagram in which the constant

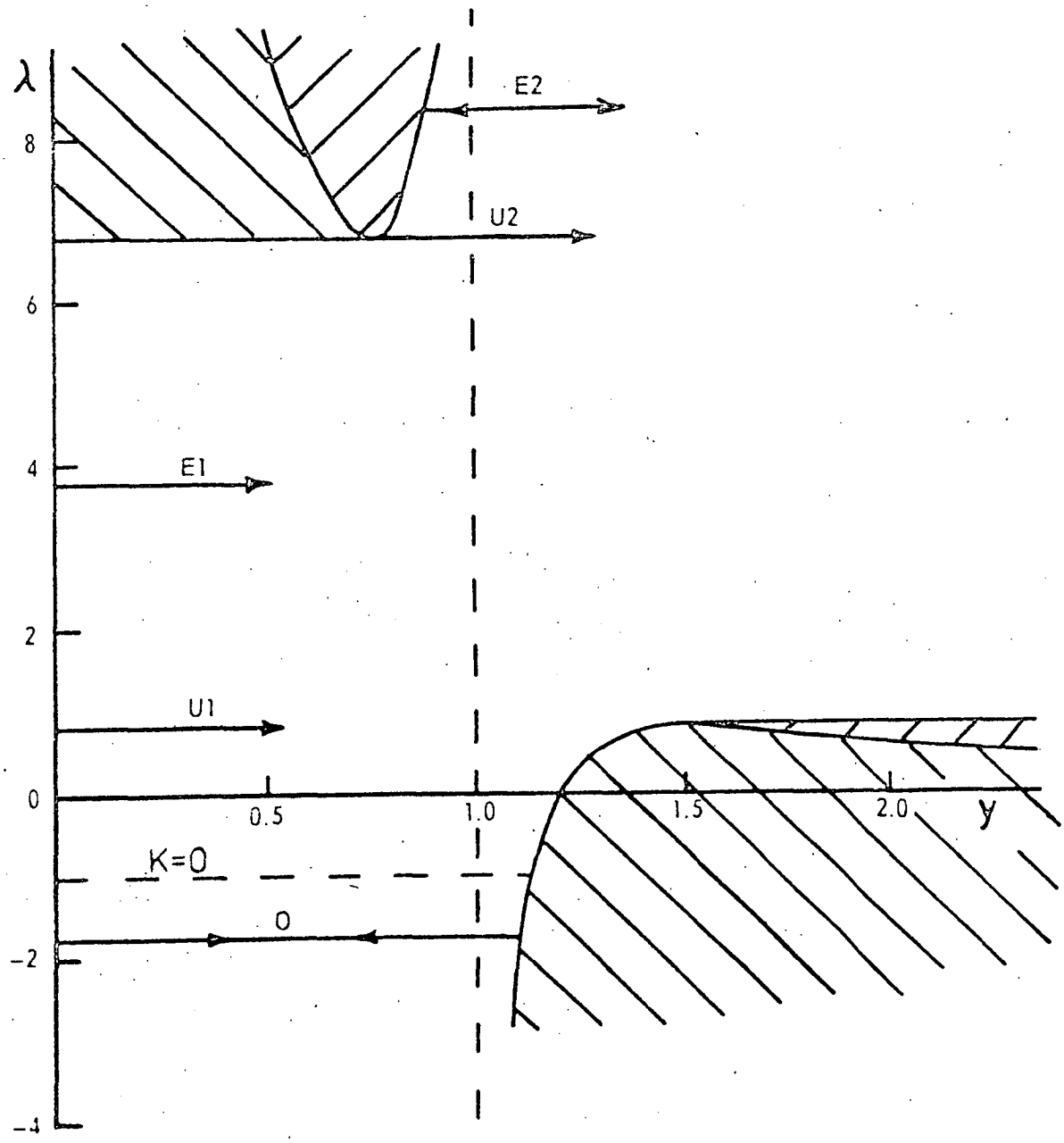

Figure 4.2 - Possible world-models having density parameter $\sigma_o = 1.0$ and black-body radiation temperature $T_o = 3°K$.

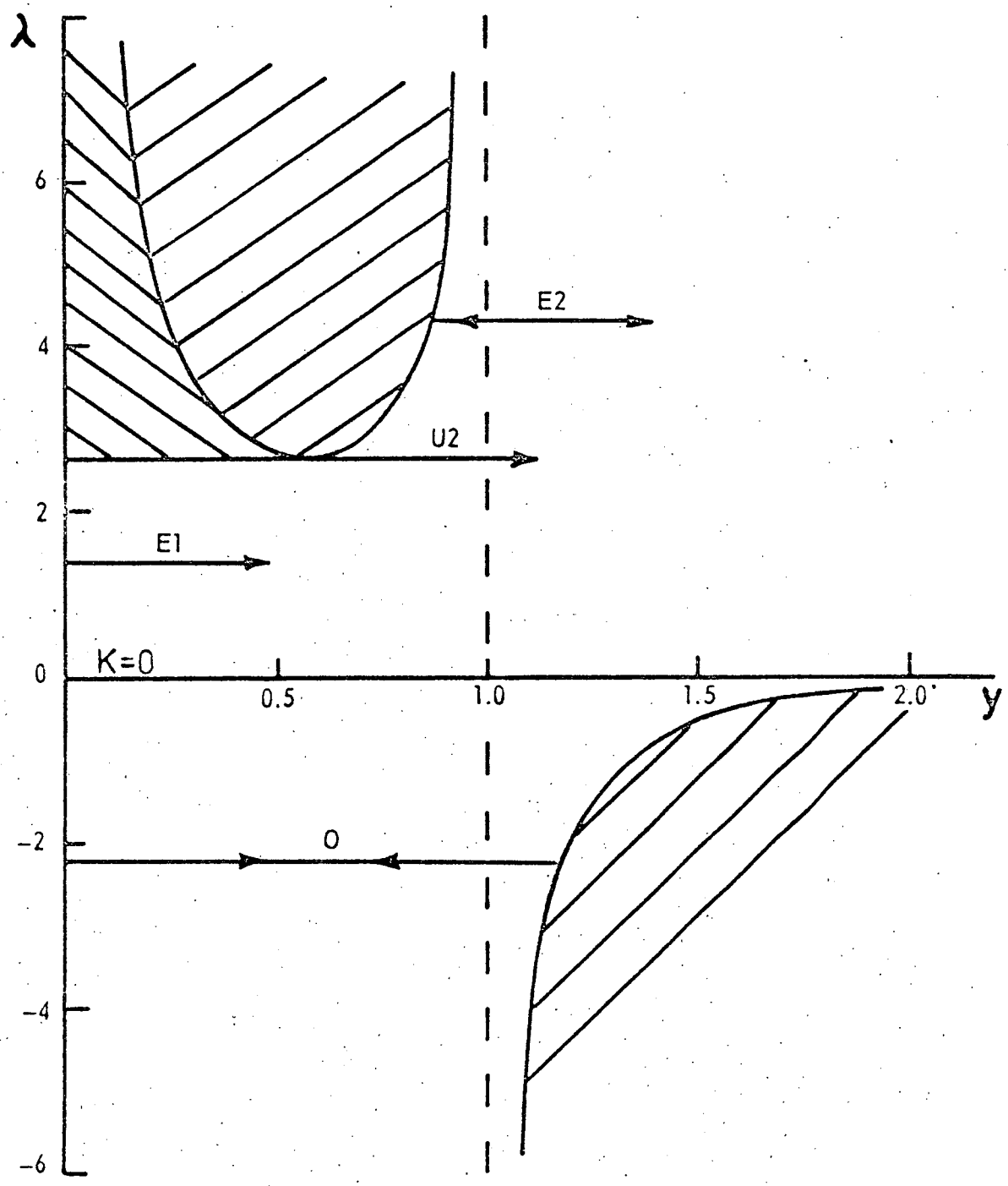

Figure 4.3 - Possible world-models with $\sigma_o = 0.5$, $T_o = 3°K$.

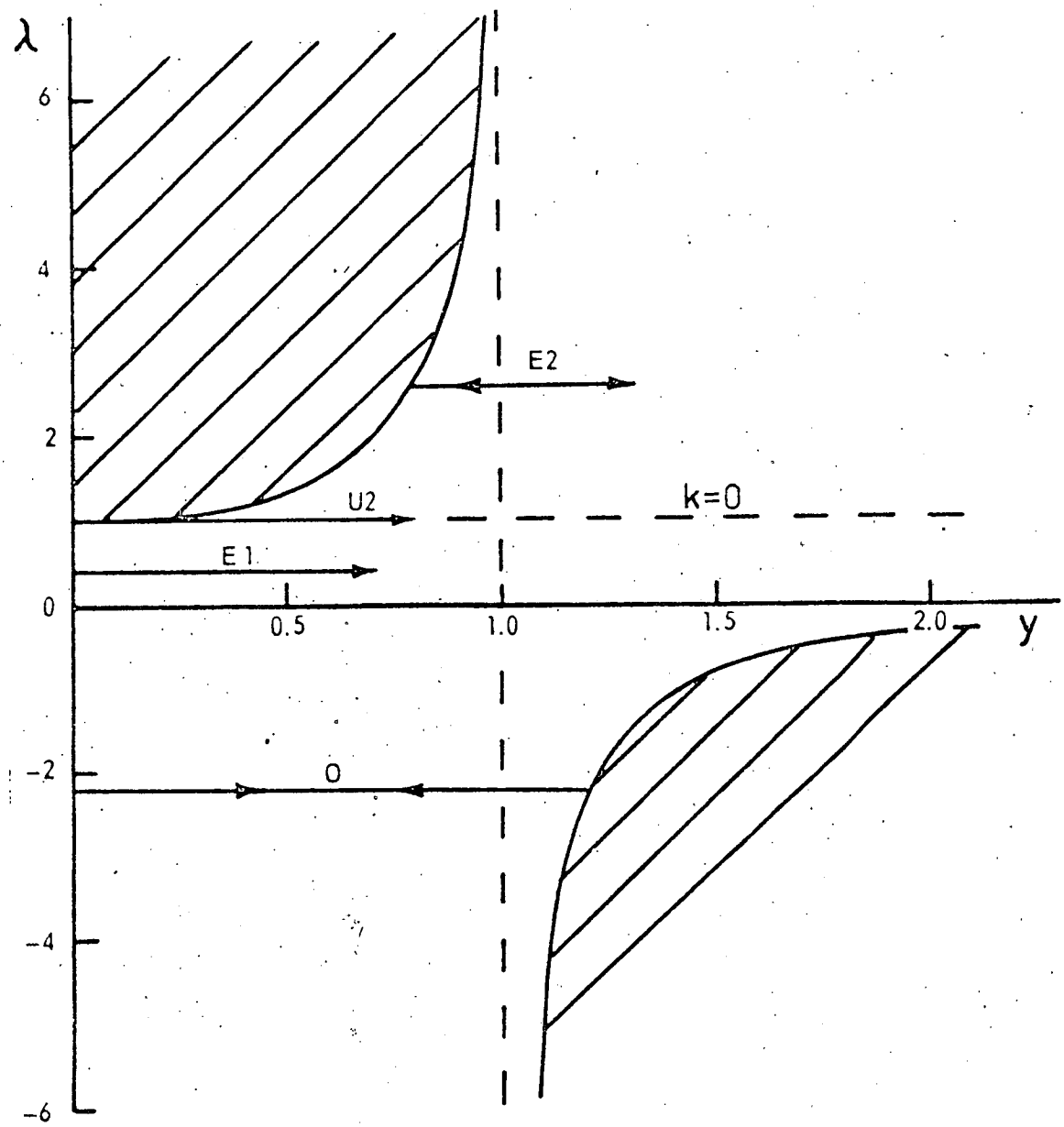

Figure 4.4 - Possible world-models with $\sigma_o = 0$.

λ is plotted against the expansion parameter y for the special condition $f(y) = 0$. It follows from equation (4.5) that the curve $f(y) = 0$ in the (λ, y) plane has the equation

$$\lambda = (1 - y^2)^{-1} [2\sigma_m y^{-1}(1 + \alpha y^{-1}) + 1 - 2\sigma_o] \qquad (4.7)$$

and differentiating, this curve has extremum values when

$$(1 - 2\sigma_o)y^3 + 3\sigma_m y^2 + 4\sigma_m \alpha y - \sigma_m(1 + 2\alpha y^{-1}) = 0 \qquad (4.8)$$

There are three separate classes of solutions to equations (4.7) and (4.8) according as $\sigma_o > 0.5$, $0 < \sigma_o \leq 0.5$ or $\sigma_o = 0$. Each of these cases is considered separately.

$\underline{\sigma_o > 0.5}$ This case is typified by the world-model with defining parameters $\sigma_o = 1.0$, $T_o = 3$. The curve $f(y) = 0$ for this model is shown in figure 4.2. A minimum value occurs at (λ_{min}, y_{min}) where $\lambda_{min} > 0$ and $0 < y_{min} < 1$, while a maximum value exists at the point (λ_{max}, y_{max}) where $\lambda_{max} > 0$ and $y_{max} > 1$. Recalling that Λ is a constant of integration, it follows that the evolution of the universe may be represented in the (λ, y) plane by a straight line parallel to the y-axis. In order that $(dy/dt)^2$ does not attain negative values, the regions above the curve in the interval $0 < y < 1$, and below the curve for $y > 1$ must be inaccessible. Further, the definition $y = R/R_o$ implies that the universe must evolve up to or

through the value of y = 1 at the present epoch. Thus all the areas in figure 4.2 covered by hatched lines are inaccessible to any relativistic world-model. The line k = 0 in the diagram is given by $\lambda = 1 - 2\sigma_o$, which is independent of ε_o (or T_o). This line separates the possible models into two classes - those which have a 3-geometry of positive curvature and those with negative intrinsic curvature. For the particular case $T_o = 0$ ($\sigma_m = \sigma_o$), the solution to equation (4.8) is, for positive y_m,

$$y_m = \frac{\sigma_o}{1 - 2\sigma_o} \left\{ 2 \cos\left[\frac{1}{3} \cos^{-} \left(\frac{1}{2} \frac{(1 - 2\sigma_o)^2}{\sigma_o^2} - 1 \right) + \frac{2n\pi}{3} \right] - 1 \right\} \qquad (4.9)$$

where n = -1 provides a minimum value for λ and n = +1 provides a maximum value. The corresponding extremum values of λ are given by

$$\lambda_m = \sigma_o / y_m^2$$

However for general T_o it is not possible to obtain analytical solutions to equations (4.8) and the general properties of this class of solution can be described by the following permissible world-models.

(1) $\lambda_{max} < \lambda < \lambda_{min}$: the universe must expand continuously from a singular state at y = 0 (infinite curvature) to an infinitely rarefied state in the infinite future. These models are denoted as type E1.

(2) $\lambda = \lambda_{max}$: as before, the universe has a singularity at $y = 0$, but expands monotonically into the static Einstein model ($y = 0$) at an infinite time in the future. These models are denoted as type U1.

(3) $\lambda = \lambda_{min}$: the universe expands continuously from the condition of an Einstein universe at $y_{min} < 1$ in the infinite past to an empty state at $y = \infty$. These models are denoted as type U2.

(4) $\lambda > \lambda_{min}$: universes of this type contract from an empty state in the infinite past until the expansion parameter y satisfies the equation $f(y) = 0$. The universe then reverses its motion and expands at an increasing speed into an empty state in the infinite future. These universes are type E2.

(5) $\lambda < \lambda_{max}$: the universe is in a state of continuous oscillation - expanding and contracting between the two extreme values of $y = 0$ and the value of $y > 1$ corresponding to $f(y) = 0$. These models are denoted as type O.

$0 < \sigma_o \leq 0.5$ This type of solution is shown in figure 4.3, where $\sigma_o = 0.5$, $T_o = 3$. In this case, there is only one extremum value of the curve $f(y) = 0$, and this occurs at (λ_{min}, y_{min}) where $y_{min} < 1$. The different possible world-models are labelled according to the classification described above. Universes of type U1 are not

obtainable for this range of the density parameter. If $T_o = 0$ then the extremum value occurs at

$$y_m = u + \frac{\sigma_o}{1 - 2\sigma_o}\left[\frac{\sigma_o}{(1 - 2\sigma_o)u} - 1\right] \qquad (4.10)$$

provided $\sigma_o \neq 0.5$ and u is the positive real root of

$$u^3 = -b \pm \sqrt{b^2 - 1}$$

with $b = (1 - 2\sigma_o)^3(2\sigma_o^2 - 4\sigma_o + 1)/2\sigma_o^5$

$\underline{\sigma_o = 0}$ In this case, both the matter and radiation energy densities are zero and the equation of the curve $f(y) = 0$ reduces to $\lambda = (1 - y^2)^{-1}$. This curve clearly has only one real minimum at $y_{min} = 0$, $\lambda_{min} = 1$, which corresponds to the static Einstein model. The radiation temperature must be zero for these empty models. This class of solution is shown in figure 4.4.

The results of these three separate classes of solution to equation (4.8) may now be combined in one single diagram in which the extrema values of $\lambda = \lambda_m$ are plotted against σ_o. A particular type of world-model is now specified by the co-ordinates (λ, σ_o) in figure 4.5. On the basis of the previous discussion, the different regions in figure 4.5 may be labelled as shown. Relatively large values of T_o have been assumed in order to clearly indicate, in the (λ, σ_o) plane,

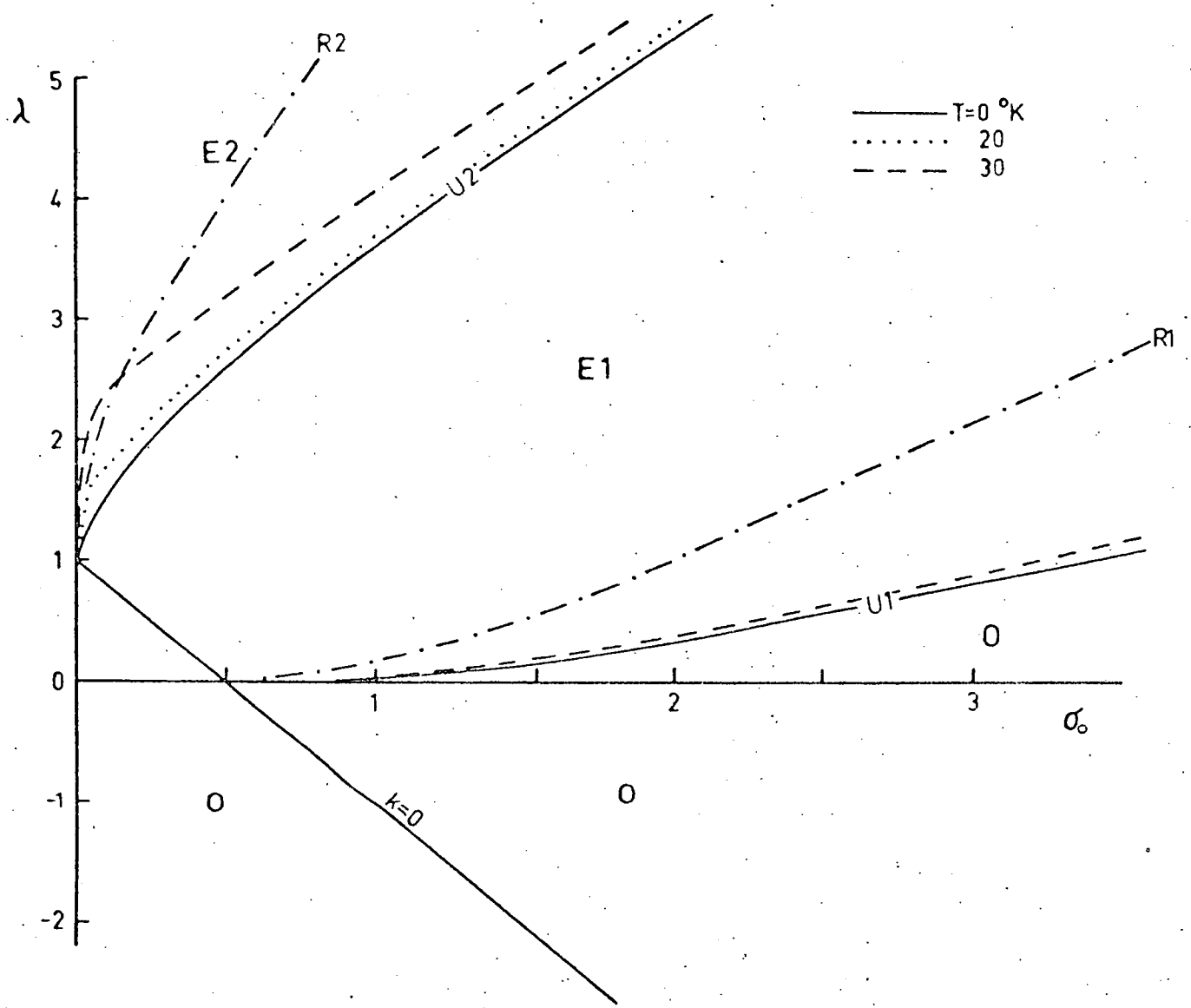

Figure 4.5 - Classification of relativistic world-models in the (λ, σ) plane. The full lines correspond to models containing matter only.

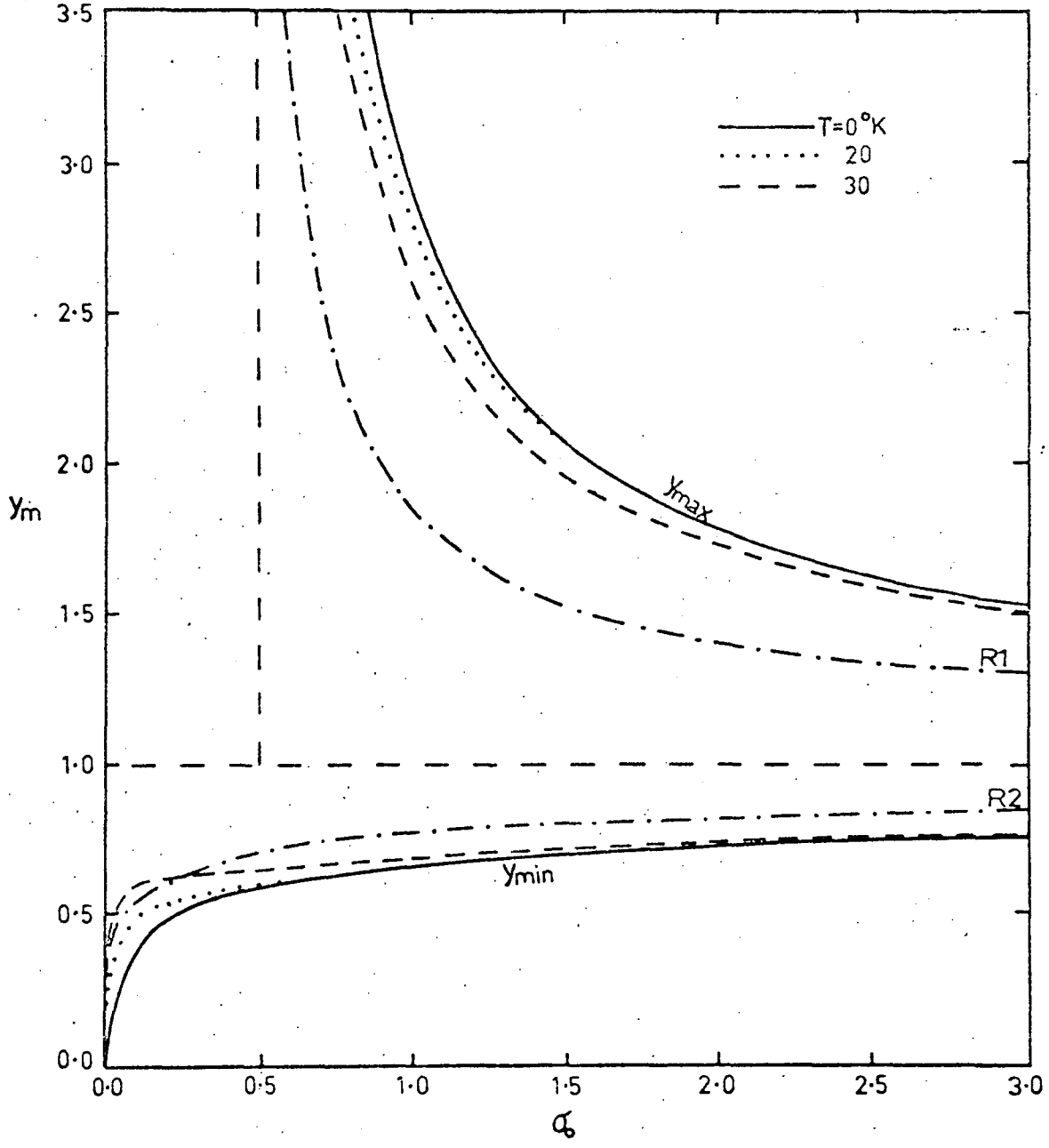

Figure 4.6 - Maximum and minimum values of the expansion parameter when the universe enters (y_{max}) and leaves (y_{min}) the static Einstein condition.
The curves R1 and R2 correspond to universes containing radiation only.

the effects of a radiation field on model classification. The effect is seen to be an expansion of the regions for model types E1 and 0 and a restriction of the area available to type E2 models. Since, in any real situation, $\sigma_m \geq 0$, there must be a region in the (λ, σ_o) plane inaccessible to all models and the boundary of this region will have the equation $\sigma_o = \sigma_r$.

The values of the expansion parameter y_m on the curves U1 and U2 in figure 4.5, are plotted as a function of σ_o in figure 4.6. At $\sigma_o = \infty(H_o = 0)$, the universe is, for all time, in the equilibrium configuration of an Einstein universe with $y_m = 1$. The consequences of an increment in the radiation temperature T_o are (a) a decrease in the value of y_{max} at which the universe enters the Einstein state, and (b) an increase in the value of y_{min} at which the universe leaves the Einstein state.

It should be noted that, for the universes containing radiation only, equation (4.5) becomes

$$f(y) = 2\sigma_o y^{-2} + q_o + 1 - 4\sigma_o + (2\sigma_o - q_o)y^2 \qquad (4.11)$$

$$= 2\sigma_o y^{-2} + 1 - 2\sigma_o + \lambda(1 - y^2)$$

where $\varepsilon_o = 1/3$ and $\sigma_o = \sigma_r$. It follows immediately that the curve $f(y) = 0$ in the (λ, y) plane must have the equation

$$\lambda = (1 - y^2)^{-1}(2\sigma_o y^{-2} + 1 - 2\sigma_o) \tag{4.12}$$

with extremum values occurring when

$$(1 - 2\sigma_o)y^3 + 4\sigma_o y - 2\sigma_o y^{-1} = 0 \tag{4.13}$$

The solutions to the last two equations are represented by the lines labelled R1 and R2 in figures 4.5 and 4.6.

4.2 Variation of q and σ

In this section, the variation of the deceleration parameter q and the density parameter σ is examined for universes filled with isotropic black-body radiation.

It follows from equation (4.4) and the general definition of the Hubble parameter at an arbitrary epoch that

$$H = \frac{\dot{y}}{y} = H_o \sqrt{f(y)}/y \tag{4.14}$$

where H_0 is the present value of H. The general density parameter is

$$\sigma = \frac{4\pi G\rho}{3H^2} = \frac{\sigma_m(1 + \alpha y^{-1})}{yf(y)} \tag{4.15}$$

while the deceleration parameter is

$$q = \frac{-\ddot{y}}{yH^2} = \frac{y^2}{f(y)} [\sigma_m y^{-3}(1 + 2\alpha y^{-1}) - \lambda] \qquad (4.16)$$

Clearly, from the last two equations

$$\sigma \to 0.5 \text{ and } q \to 1.0 \text{ as } y \to 0$$

for all models apart from the type E2 models which do not admit indefinitely small values of y. This result should be compared with the analogous equations (e.g. Stabell and Refsdal, 1966) derived for universes containing matter only, i.e. $\alpha = 0$. The significantly different result here is that q approaches unity near the singularity at $y = 0$, whereas q tends to 0.5 in the radiation free case. Curves of q versus σ are drawn in figure 4.7 for $\alpha = 0$ and are similar to the curves given by Stabell and Refsdal. The diagram is self-explanatory and does not require further explanation.

Except for the type 0 world-models, equations (4.15) and (4.16) yield

$$\sigma \to 0 \text{ and } q \to -1 \text{ as } y \to \infty$$

independent of any finite value for α. This is, of course, as expected, since according to the equations derived above all the terms containing α become insignificant at large y.

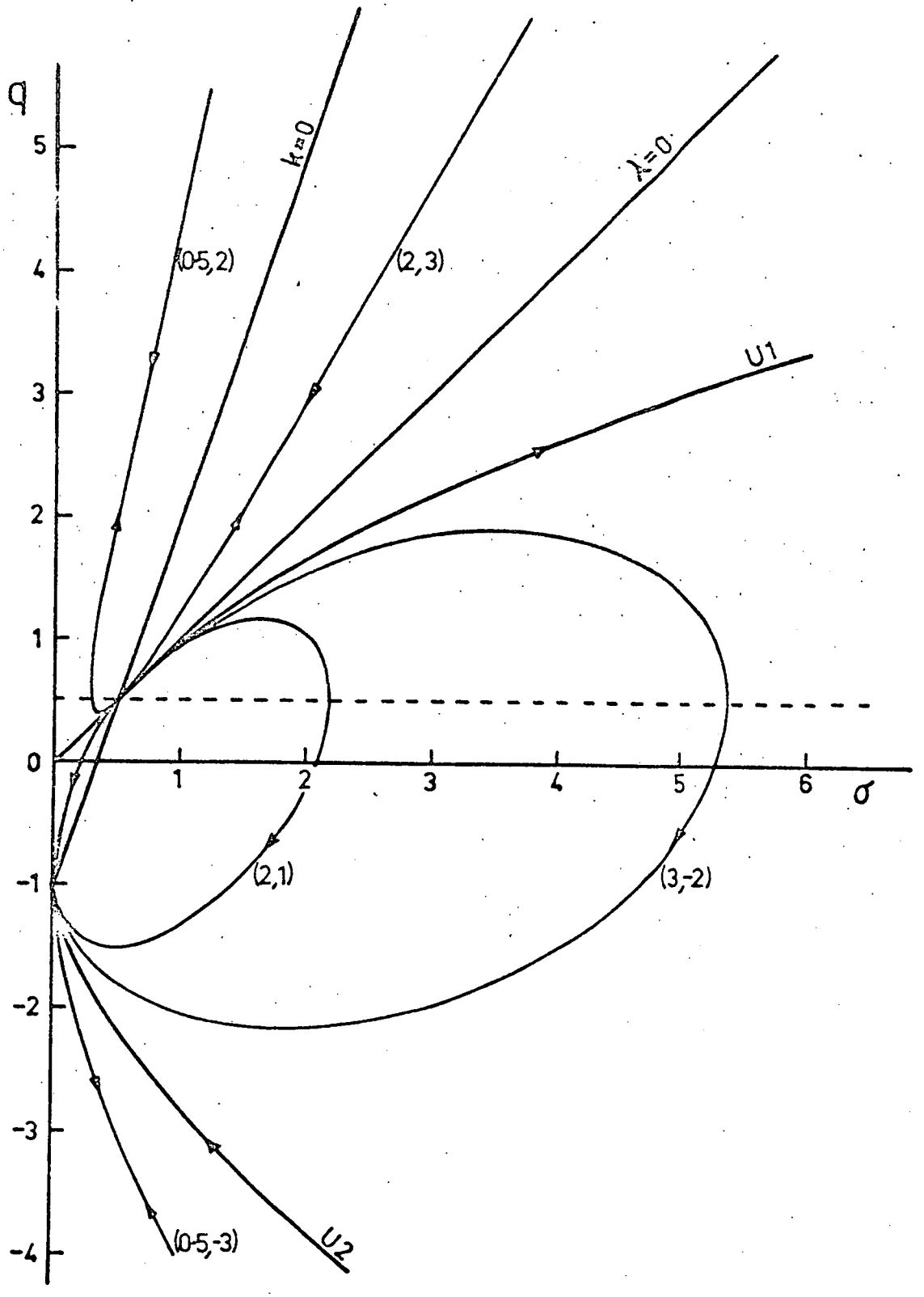

Figure 4.7 - The variation of deceleration parameter q with the density parameter σ for universes containing matter only.

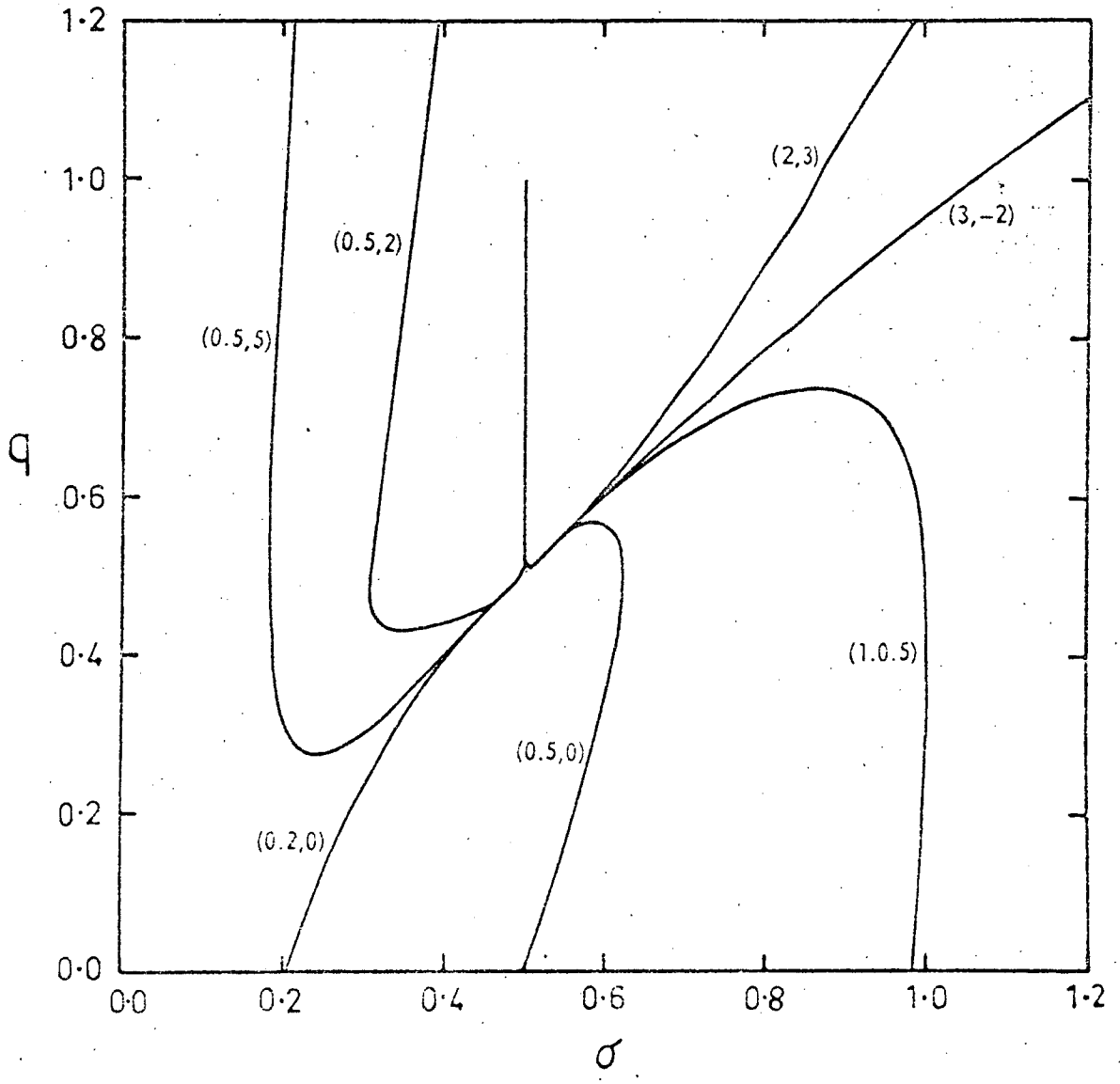

Figure 4.8 - Variation of the deceleration parameter q with the density parameter σ if the present black-body temperature is 3°K.

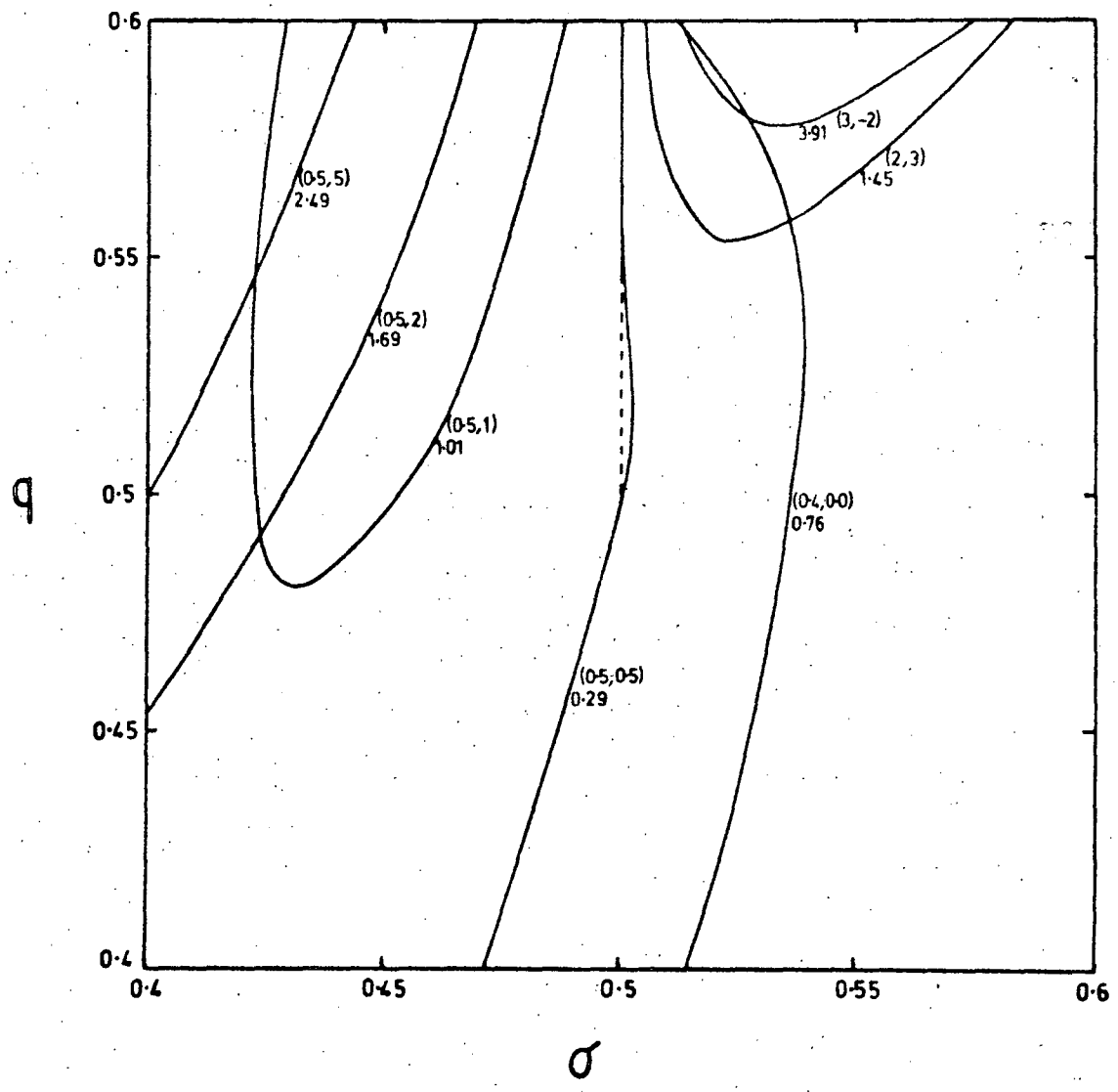

Figure 4.9 - Plots of q vs. σ for a radiation temperature T_o = 15°K.

In the radiation-free universe, it is possible to define (Stabell and Refsdal) two unique lines $k = 0$ and $\lambda = 0$ in the (σ, q) plane. However, when a non-zero pressure term is introduced, the equations for these lines become respectively

$$3(1 + \epsilon)\sigma - q - 1 = 0$$

$$(1 + 3\epsilon)\sigma - q = 0$$

and these equations are not unique since $\epsilon \equiv \epsilon(y, \sigma_0)$ for a particular T_Q. Solving the last two equations, we find that the intersection of the lines $k = 0$, $\lambda = 0$ in the (σ, q) plane has the equation $\sigma = 0.5$.

The functional relationship between σ and q is shown in figure 4.8. The diagram does not indicate the complete curves for types E1 and 0, but is restricted to relatively small values of y where the effects of a radiation field are greatest. For large y, the curves are the same as those given by Stabell and Refsdal for $\alpha = 0$.

Differentiating equation (4.15) and using (4.3), we obtain

$$\dot{\sigma} = \frac{\sigma_m \dot{y}}{y^2 f(y)} [2(1 + \alpha y^{-1})q - 2\alpha y^{-1} - 1] \qquad (4.17)$$

from which it follows immediately that $\dot{\sigma} = 0$ when

$$q = \frac{1 + 2\alpha y^{-1}}{2(1+\alpha y^{-1})} \tag{4.18}$$

Hence for small α, the density parameter σ attains an extremum value when $q \simeq 0.5$.

Plots of q versus σ in the neighbourhood of the point (0.5, 0.5) for $T_o = 15$ are shown in figure 4.9. The numbers attached to the curves define the particle horizon for the world model defined by (σ_o, q_o). Clearly, if $T_o > 0$, a point in the (σ, q) plane cannot uniquely define a world-model as is the case for $T_o = 0$. Of particular interest is the Einstein-de Sitter model which is radiation-free and defined by the parameters $\sigma_o = 0.5$, $q_o = 0.5$. The model is represented by a single point in the (σ, q) plane, but the introduction of a non-zero pressure term due to a Planckian radiation field produces an evolutionary curve of the type shown in figure 4.9.

4.3 Expansion Parameter as a Function of Epoch

According to equations (4.4) and (4.5)

$$\frac{dy}{dt} = H_o \sqrt{f(y)} \tag{4.19}$$

where

$$f(y) = 2\sigma_o/y + q_o + 1 - 3\sigma_o + (\sigma_o - q_o)y^2 \tag{4.20}$$

for zero-pressure world-models. Equation (4.19) can therefore be numerically integrated for a series of values of σ_o and q_o. The results are shown in figures 4.10-4.14 in which the expansion parameter $y = R/R_o$ is plotted against the epoch t as a fraction of the characteristic time of evolution of the universe H_o^{-1}. The values of q_o which separate the different model regions are marked as broken lines in the diagrams. The line separating the type E1 and type E2 regions corresponds to the curve U1 of figure 4.6 while the line separating the type 0 and type E1 regions corresponds to the curve U2.

The expansion parameter for type 0 models varies continuously between $y = 0$ and some upper limit $y = y_{max} > 1$ but the curves in figures 4.10-4.14 are drawn for only one cycle of the oscillation. Other features of model evolution are evident from these diagrams and will not be commented on.

The effects of an isotropic radiation field on model evolutions may be accounted for by substituting in equation (4.19) the expression for f(y) derived in equation (4.5). The changes are not great for small values of T_o and the effect will be measured in terms of the changes in the age of the universe.

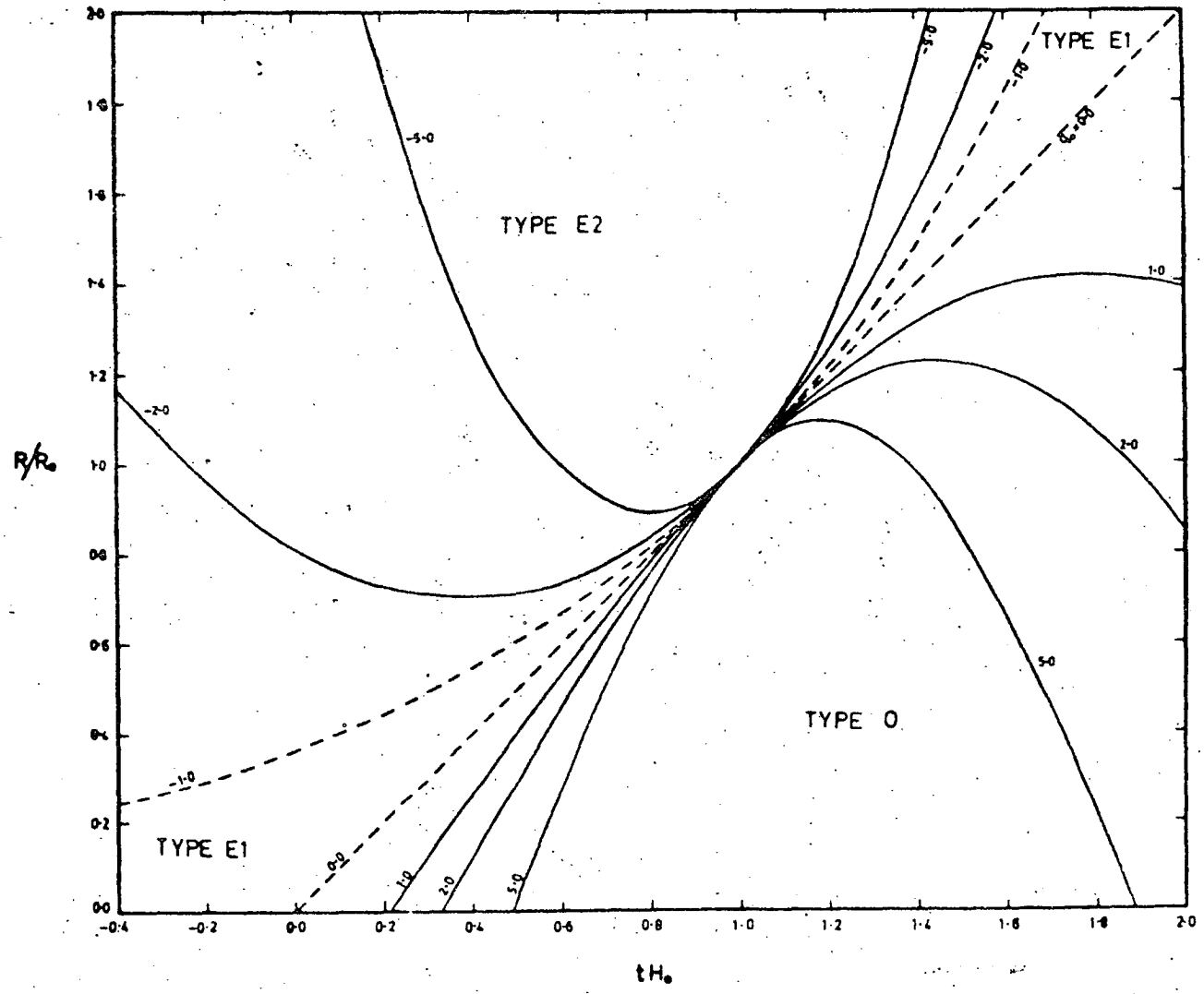

Figure 4.10 - Variation of the expansion parameter $y = R/R_0$ with epoch for $\sigma_0 = 0$.

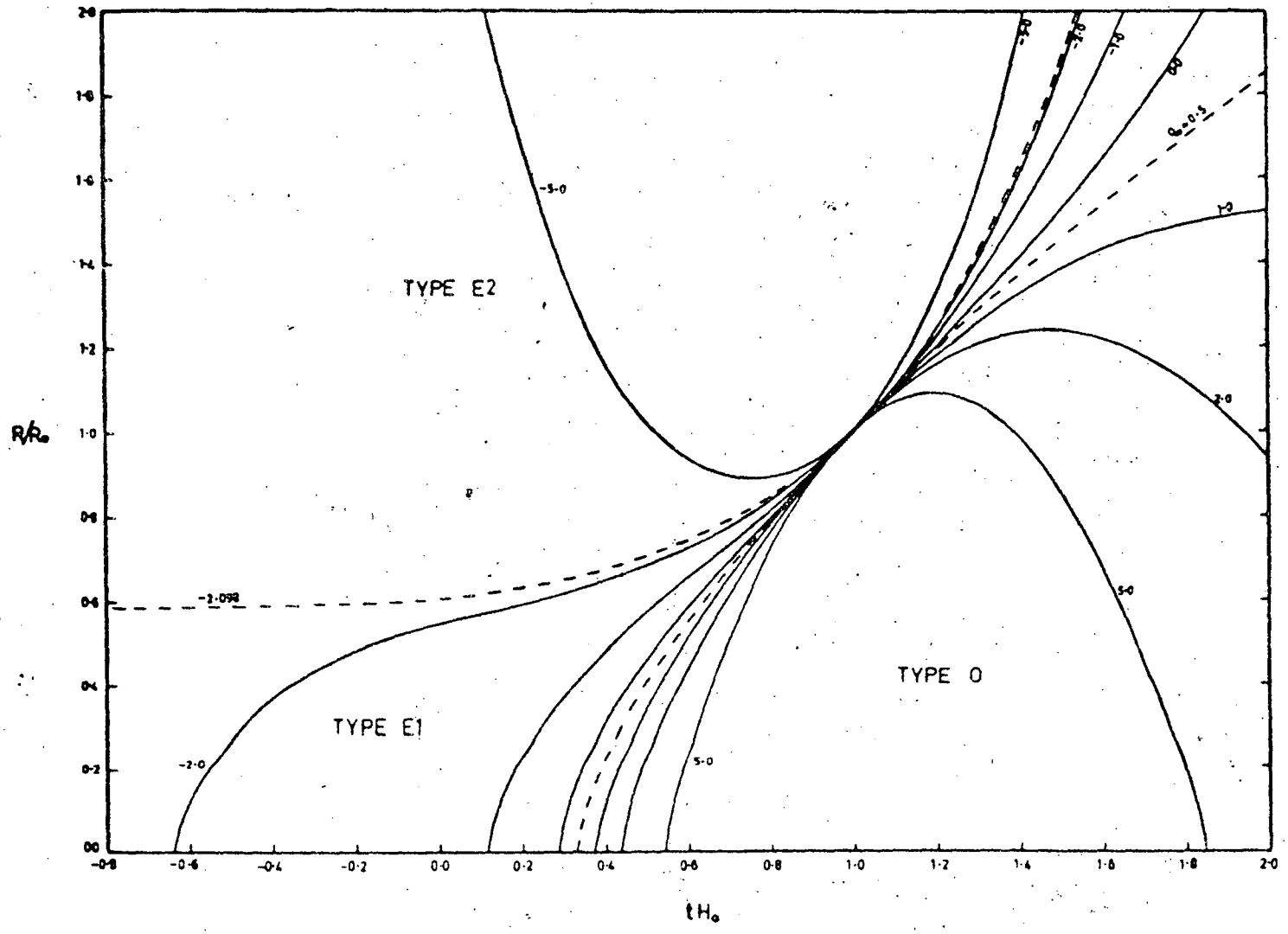

Figure 4.11 - Variation of the expansion parameter $y = R/R_O$ with epoch for $\sigma_o = 0.5$.

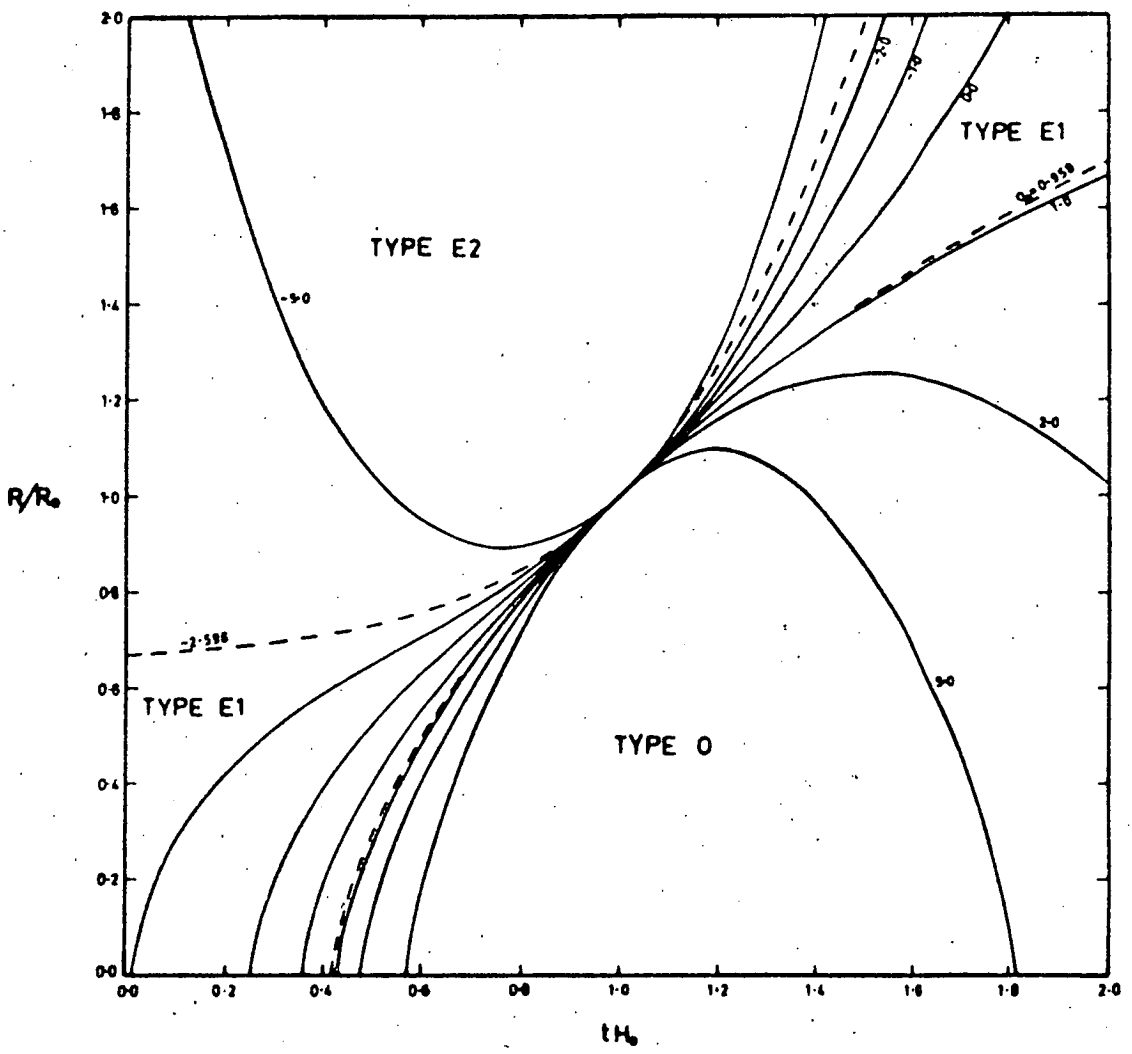

Figure 4.12 - Variation of the expansion parameter $y = R/R_0$ with epoch for $\sigma_0 = 1.0$.

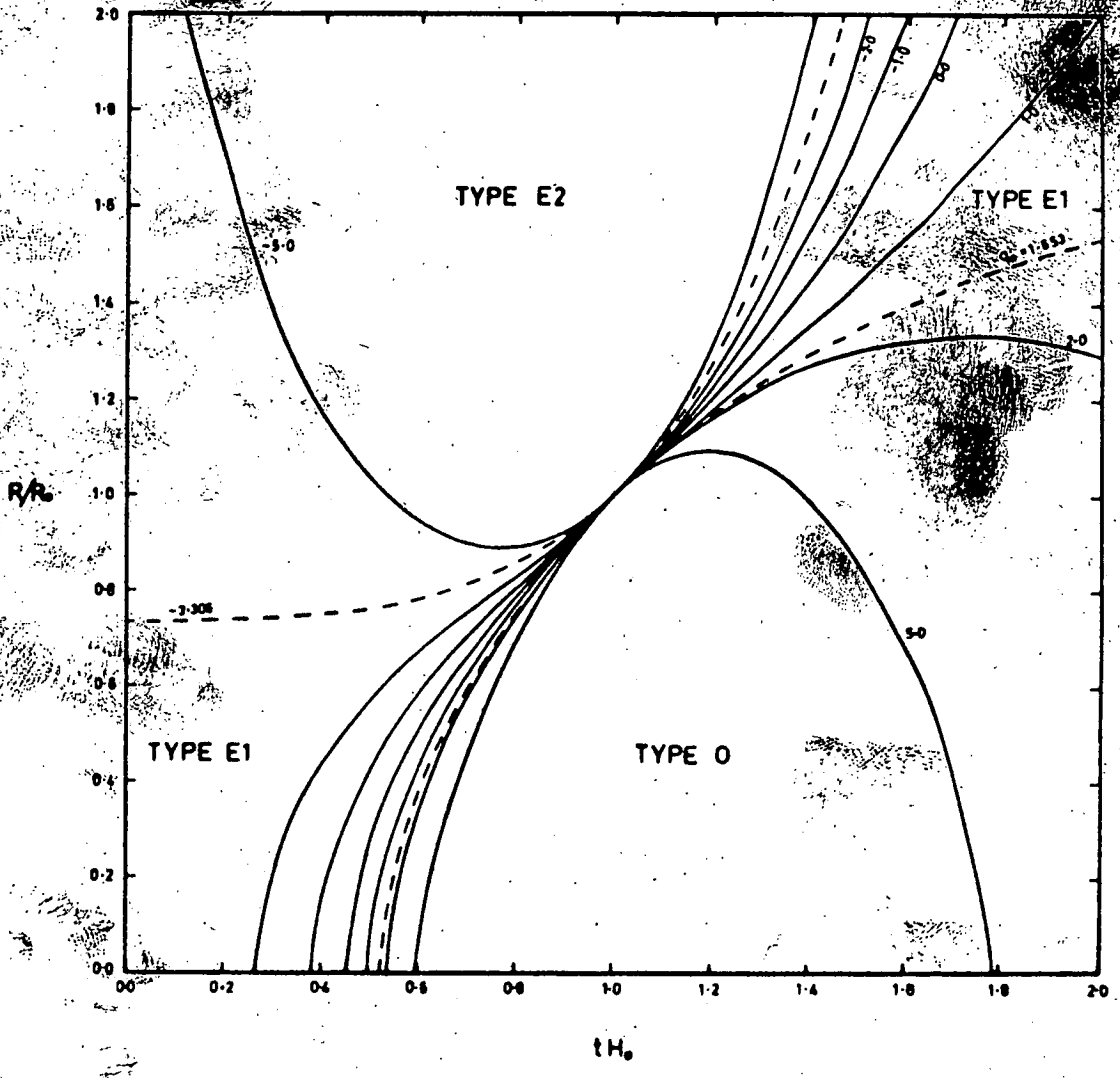

Figure 4.13 - Variation of the expansion parameter $y = R/R_0$ with epoch for $\sigma_0 = 2.0$.

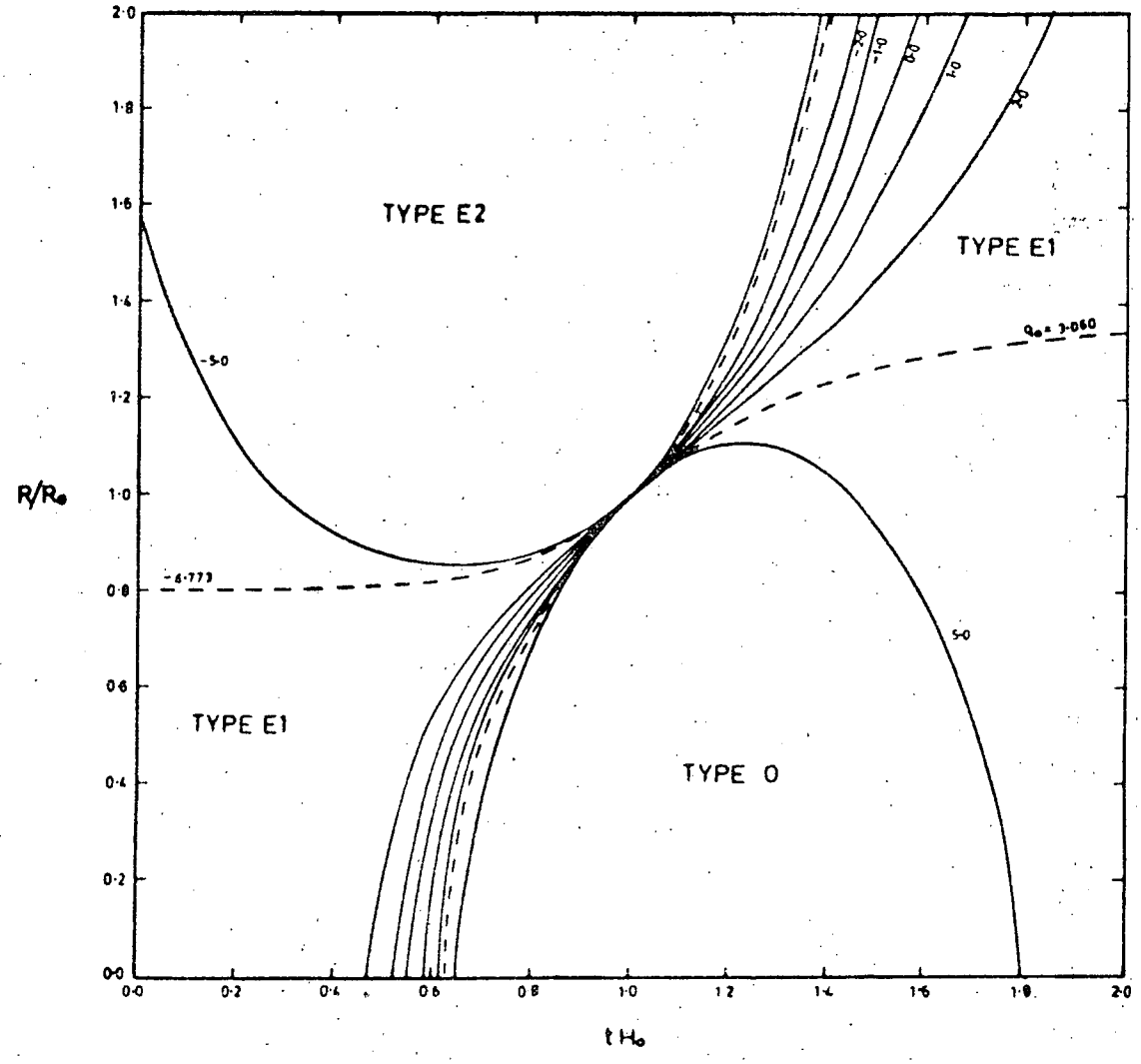

Figure 4.14 - Variation of the expansion parameter $y = R/R_0$ with epoch for $\sigma_0 = 5.0$.

4.4 Age of Model Universes

Integrating equation (4.5), it follows that the age of the universe (in units of H_o^{-1}) is given by

$$t = \int_0^1 \frac{dy}{\sqrt{f(y)}} \qquad (4.21)$$

for model types E1 and 0. The models oscillating between singular states are considered as existing for a finite time (the time of one oscillation). The results of the numerical integration of equation (4.21) are shown in figure 4.15 where curves of t versus σ_o are drawn for $T_o = 0$ and for different values of q_o. It is apparent that, for a particular σ_o, the age of a model increases as q_o decreases. The curves in figure 4.15 in effect summarise the information in figures 4.10-4.14. For values of $q_o < 0$ the age of the universe goes to infinity where the value of σ_o corresponds to the model type U1.

The results of the integration of (4.21) for $T_o > 0$ are shown in figure 4.16 where curves of constant t are drawn for different T_o. The general effect of increasing T_o is seen to be a decrease in the age of the universe. The results are also presented in Table I, where t is listed for a range of temperatures and density parameters with cosmological constant equal to zero.

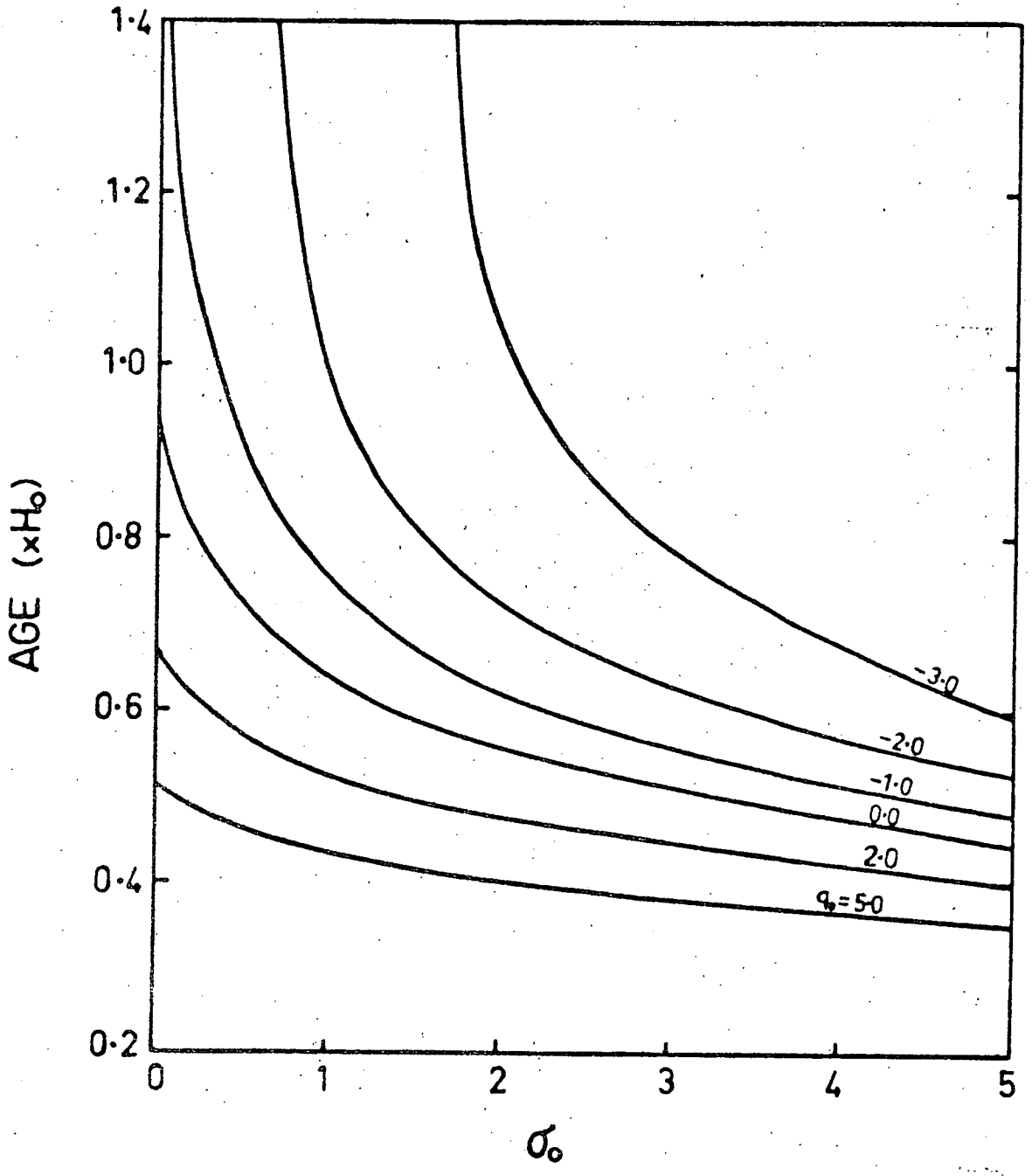

Figure 4.15 - The age of matter filled universes as a function of the density parameter σ_o.

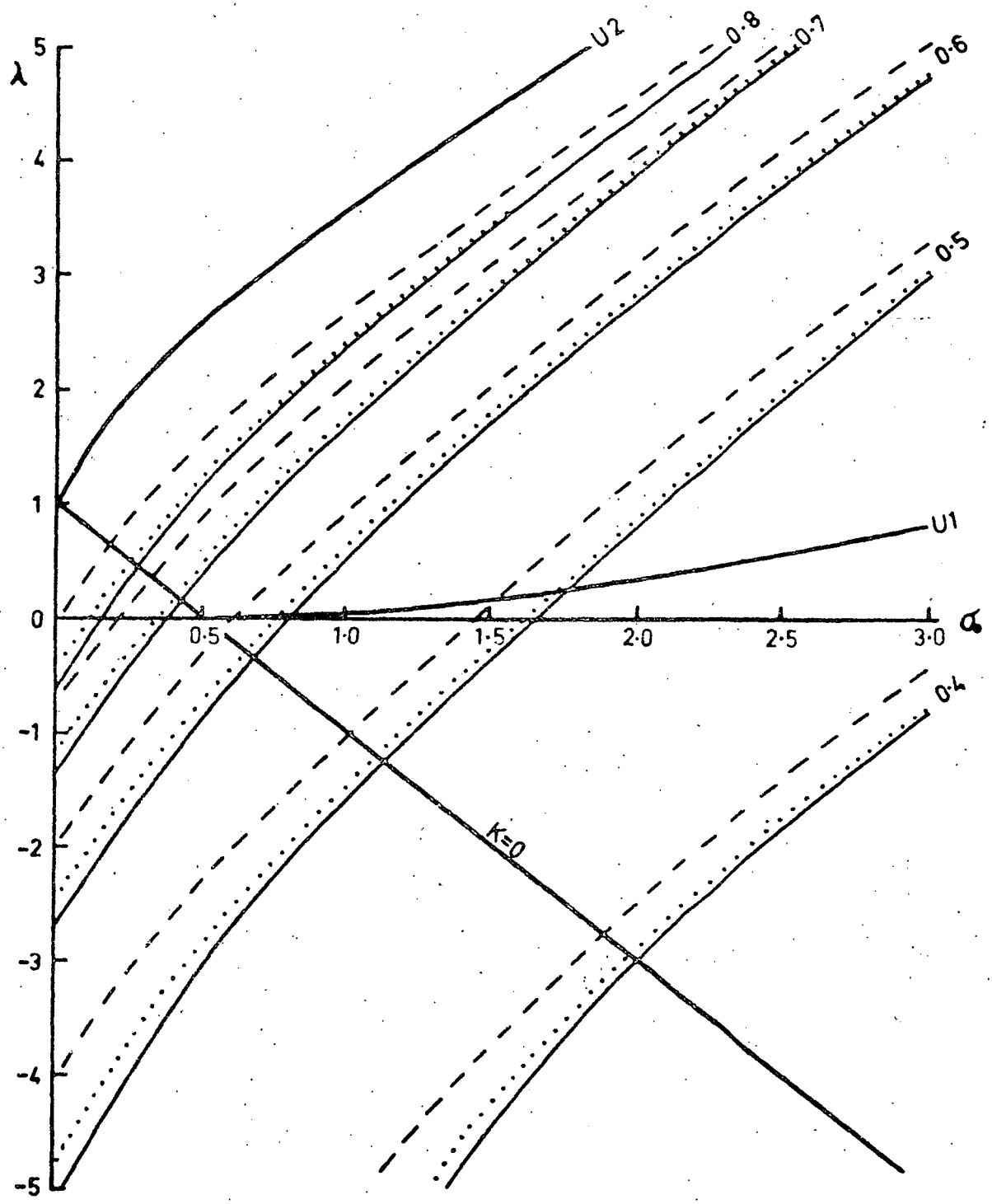

Figure 4.16 - The ages of universes containing matter and radiation illustrated by curves of $t \times H_0$ equal to a constant. The full lines correspond to $T_0 = 0°K$, the dotted lines to $T_0 = 15°K$, and the broken lines to $T_0 = 20°K$.

TABLE I

Age of the universe (in units of H_o^{-1}) for $\lambda = 0$

σ_o \ T_o	0	5	10	15	20	t_r
0.05	0.8981	0.8961	0.8782	0.8417	0.7818	0.7594
0.1	0.8465	0.8455	0.8343	0.8046	0.7582	0.6910
0.5	0.6667	0.6665	0.6641	0.6553	0.6371	0.5000
1.0	0.5708	0.5707	0.5694	0.5654	0.5557	0.4142
2.0	0.4728	0.4728	0.4723	0.4704	0.4658	0.3333
5.0	0.3515	0.3515	0.3513	0.3508	0.3492	0.2403

The effects of a radiation field are obviously greatest for small values of σ_o when $\rho_r >> \rho_m$ and $\alpha >> 1$. For $T_o = 20°K$, the radiation density parameter is $\sigma_r = 3.5 \times 10^{-2}$, so that the ages listed in Table I correspond to universes in which the matter density is a positive quantity.

The age of universes containing radiation only may be obtained by substituting for f(y) from equation (4.11) into (4.21). The results are

$$t_r = \frac{1}{2\sqrt{\lambda}} \log \frac{2\sqrt{\lambda} + 2 + C}{2\sqrt{2\sigma_o\lambda} + C} \qquad \text{for } \lambda > 0,$$

$$t_r = \frac{1}{\sqrt{-\lambda}} \left[\sin^{-1} \frac{-2\lambda - C}{\sqrt{C^2 - 8\sigma_o\lambda}} - \sin^{-1} \frac{C}{\sqrt{C^2 - 8\sigma_o\lambda}}\right] \qquad \text{for } \lambda < 0,$$

where $C = 1 - 2\sigma_o - \lambda$ for both equations and

$$t_r = \left| \frac{1 - \sqrt{2\sigma_o}}{1 - 2\sigma_o} \right| \qquad \text{for } \lambda = 0$$

The values for t_r are listed in Table I for each σ_o. The change in the age of the universe is greatest for large positive values of λ (large negative q_o) and this situation is shown in figure 4.17. The full lines refer to universes containing matter only and the dotted curves correspond to universes filled with radiation only. At a value of $\sigma_o = 2.0$, the ratio t_r/t is approximately 0.4 for $\lambda = 5.0$ while the ratio is about 0.8 for $\lambda = -5.0$.

Now according to equation (4.3) the mass density of radiation, ρ_r, exceeds the matter density, ρ_m, for $y < \alpha$. It is of some interest to determine the epoch at which $\rho_m = \rho_r$. This occurs when $y = y_c = \alpha$ and using this value of y as the upper limit of integration in equation (4.21) the epoch t may be computed for different σ_o. In figure 4.17 curves of log t (in seconds) are plotted against σ_o for $\lambda = 0$ and a series of temperatures for the radiation field. The epoch corresponding to $\rho_m = \rho_r$ is seen to be a fairly strong function of T_o but is practically independent of σ_o for $\sigma_o > 1$. Deviations from the curves in figure 4.17 are found to be small for $|\lambda| \leq 5$.

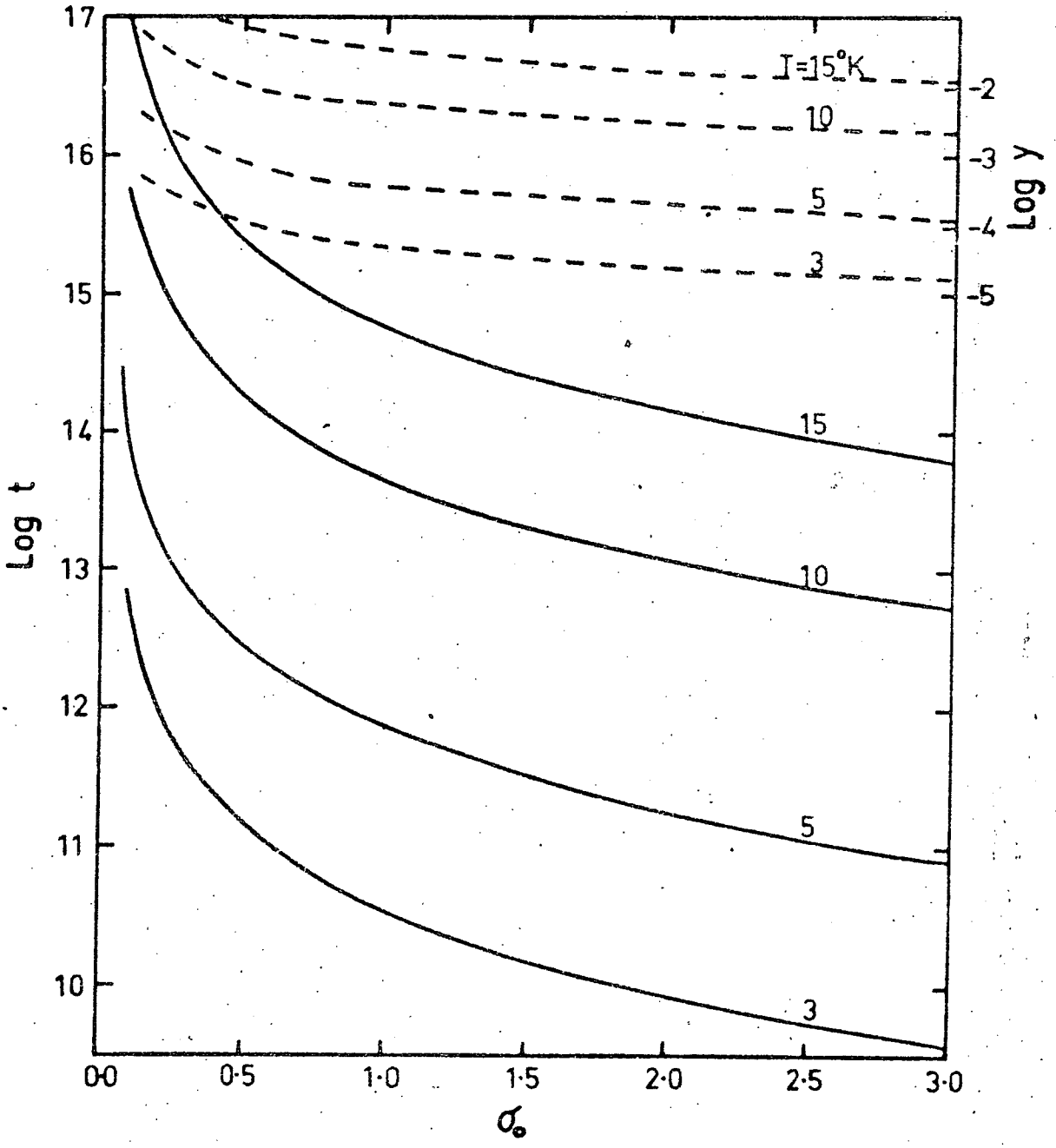

Figure 4.17 - The epoch t (in seconds) when the ordinary matter density ρ_m is equal to the mass density of radiation ρ_r for different radiation temperatures T_o.

4.5 Light Travel Time

Suppose a light quantum is emitted from a source at an epoch t corresponding to an expansion parameter y. If this quantum is received by the origin observer at time t_o and y = 1, then the light travel time will be

$$\tau = \int_t^{t_o} dt = \int_y^1 = H_o^{-1} \int_y^1 \frac{1}{\sqrt{f(y)}}\, dy \qquad (4.22)$$

The lower limit for this integral may be determined from the measured redshift of the source since $y = (1 + z)^{-1}$. The results of the integration of (4.22) are shown in figure 4.18 for $T_o = 0$. The light travel time in type E1 and type 0 models converges to a limit equal to the age of the particular model. The curves in figure 4.16 which are limited to a maximum value of z are the type E2 models. The properties of these models are indicated most clearly in figures 4.10-4.14. A source which emits a light quantum in the infinite past will have a redshift of z = -1 and the light travel time will be $\tau = \infty$.

The subject of light travel time suggests an investigation into the special conditions which might apply before a source can be "seen" by an origin observer. Furthermore the question arises as to when a source will be "seen". These problems are examined in the next section.

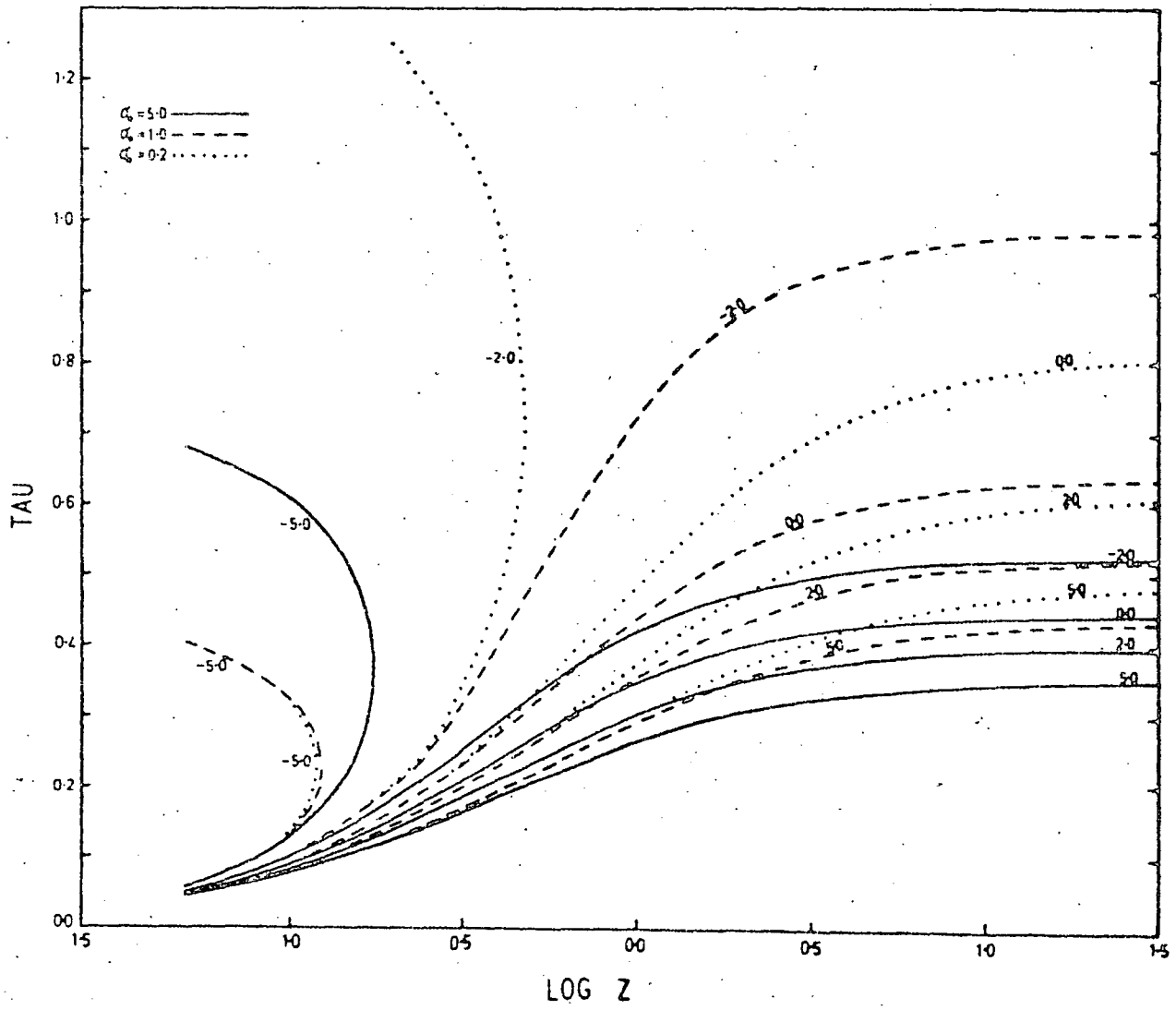

Figure 4.18 - The light travel time (in units of H_0^{-1}) as a function of the source redshift.

4.6 Horizons

The problem of horizons in relativistic world-models has been treated in some detail by Rindler (1957) but mainly in qualitative terms.

If we consider a source (fundamental particle) at epoch t_p and with co-moving radial co-ordinate, r_p, then the proper distance, U_p, between the origin and the source is

$$U_p = R(t_p) \int \frac{dr}{1 + kr^2/4}$$

$$= R(t_p)\omega(r_p) \qquad (4.23)$$

Now, integrating equation (3.12), it is clear that a photon emitted at the source will, at epoch t, have a co-ordinate

$$\omega(r) = \omega(r_p) - \int_{t_p}^{t} \frac{cdt}{R(t)} \qquad (4.24)$$

Using equations (4.4) and (4.23) the proper distance of the light quantum is therefore

$$U(y) = R_o y[\omega(r_p) - \frac{c}{R_o H_o} \int_{y_p}^{y} \frac{dy'}{y'\sqrt{f(y')}}] \qquad (4.25)$$

at the epoch corresponding to an expansion parameter of y.

Equations (3.11) indicate quite clearly that $\omega(r)$ can take all positive values if $k = 0$ or -1. However when $k = +1$ it appears that ω is restricted to values less than π and there is an apparent boundary at $U = R_o\pi$ for fundamental particles. Rindler (1957) asserts that this situation is due only to the peculiarities of the definition of the radial co-ordinate, r, which in this case makes $r = \infty$ correspond to the antipole of the origin of the spherical 3-space at epoch t_o. It follows from the definition of proper distance that the co-ordinate ω must be additive and the definition of ω is extended beyond the antipole by construction of an auxiliary origin of co-ordinates at the pole and computing ω relative to this new origin and adding π. Hence, for each fundamental particle, there are an infinity of ω co-ordinates all differing by multiples of 2π. The properties of the two different visual horizons are now examined.

4.7 Event Horizons

The necessary and sufficient condition for an event horizon to exist (Rindler, 1957) is the convergence of the integral

$$I = \int_{t_o}^{\infty} \frac{cdt}{R(t)} \qquad (4.26)$$

From equation (4.25), a photon emitted at time t_o with a radial co-ordinate

$$\omega = \omega_{EH} = \frac{c}{R_o H_o} \int_1^\infty \frac{dy'}{y'\sqrt{f(y')}} \tag{4.27}$$

will arrive at the origin in the infinite future. Replacing the lower limit of integration in (4.27) by y and multiplying by R(t) we have the equation of motion for a point on the event horizon

$$U(y) = \frac{cy}{H_o} \int_y^\infty \frac{dy'}{y'\sqrt{f(y')}} \tag{4.28}$$

Suppose a photon is emitted at time t_o, corresponding to y = 1, from a particle at the event horizon. Rewriting equation (4.25), the equation of motion of this photon is

$$U^*(y) = R_o y[\omega_{EH} - \frac{c}{R_o H_o} \int_1^y \frac{dy'}{y'\sqrt{f(y')}}]$$

$$= \frac{cy}{H_o} [\int_1^\infty + \int_y^1]$$

$$= U(y)$$

Hence the event horizon is associated with a particular set of photons travelling towards the origin at a proper distance given by equation (4.28). It is now evident that all events which lie beyond the event horizon ($\omega > \omega_{EH}$) remain forever undetectable by an origin observer attached to a fundamental particle. Also, the relative velocity, v, between a particle with radial co-ordinate r_o and the event horizon will be

$$|v| = \frac{\partial}{\partial t}\left[R(t)\left(|\omega(r_o) - \int_t^{\infty} \frac{cdt'}{R(t')}|\right)\right]$$

$$= \left| \frac{\partial R(t)}{\partial t}\left[\omega(r_o) - \int_t^{\infty} \frac{cdt'}{R(t')}\right] - c \right|$$

and with the aid of equation (4.27), the term in brackets must be zero when the particle crosses the horizon. The local relative velocity of the particle will be equal to the speed of light.

An event horizon exists only for the type E1 and type E2 models since the integral (4.27) must diverge for the type 0 models. In figure 4.19, the proper distance, divided by R_o, of the observer's event horizon in a type E1 is plotted against both the expansion parameter y and the epoch, tH_o. Curves for two fundamental particles A and B, together with A's event horizon, are also shown. The particle A has an angle co-ordinate $\omega_A = 0.5$ while $\omega_B = 1.0$. The broken lines correspond to light quanta which have been emitted by the particle A and are travelling towards the origin observer. Events occurring at the particle A once it has crossed the observer's horizon are completely undetectable. It is also apparent that once the particle B has crossed A's event horizon light quanta emitted at B (represented by dotted lines) cannot reach A or the origin of co-ordinates within the infinite future.

Similar curves are drawn in figure 4.20 for a type E2 model which has defining parameters $\sigma_o = 0.5$, $q_o = -5.0$. The model has a

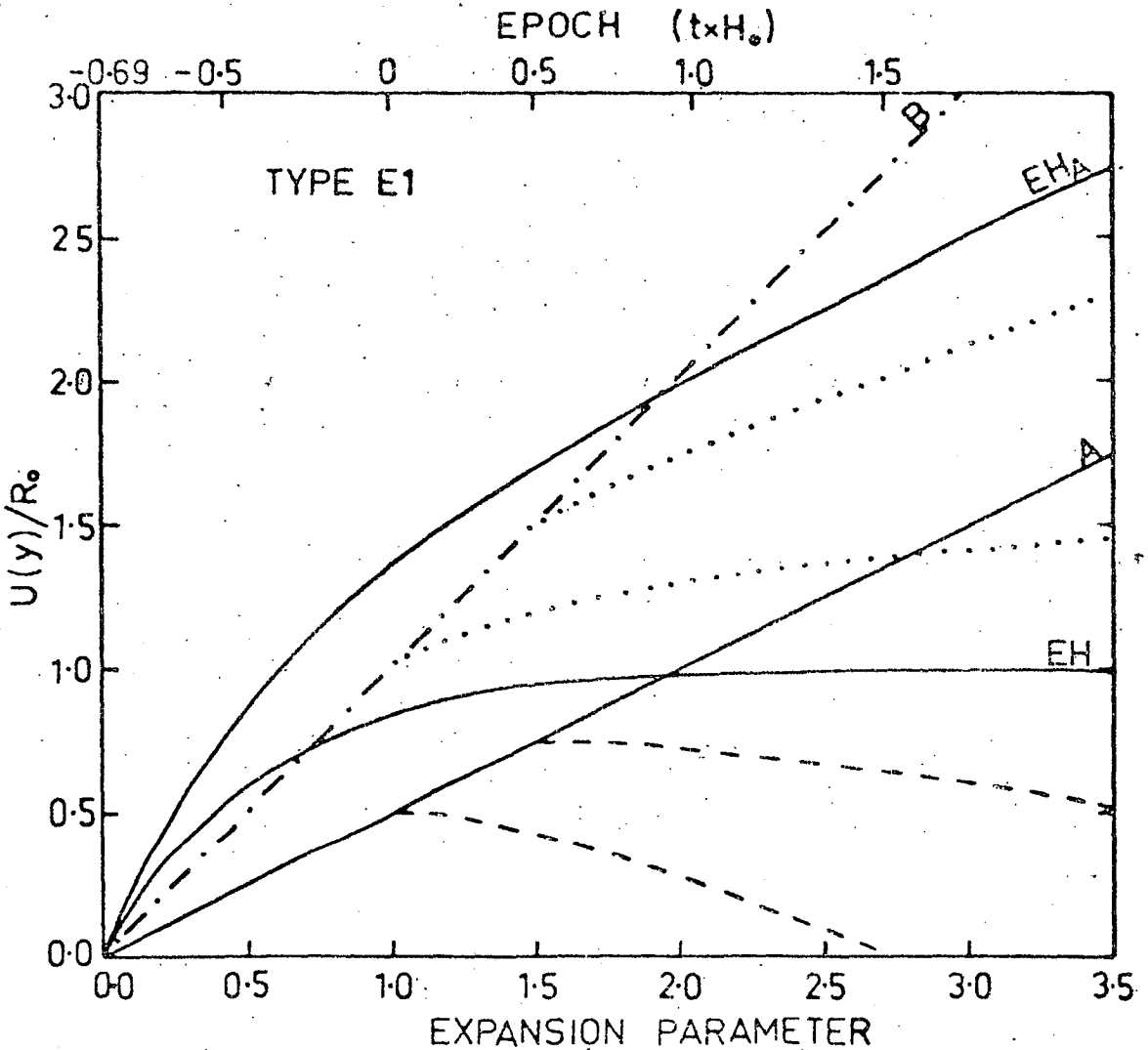

Figure 4.19 - Proper distances (divided by R_0) of event horizons, fundamental particles and light fronts in a type E1 model defined by $\sigma_0 = 0.5$, $q_0 = 0.2$.

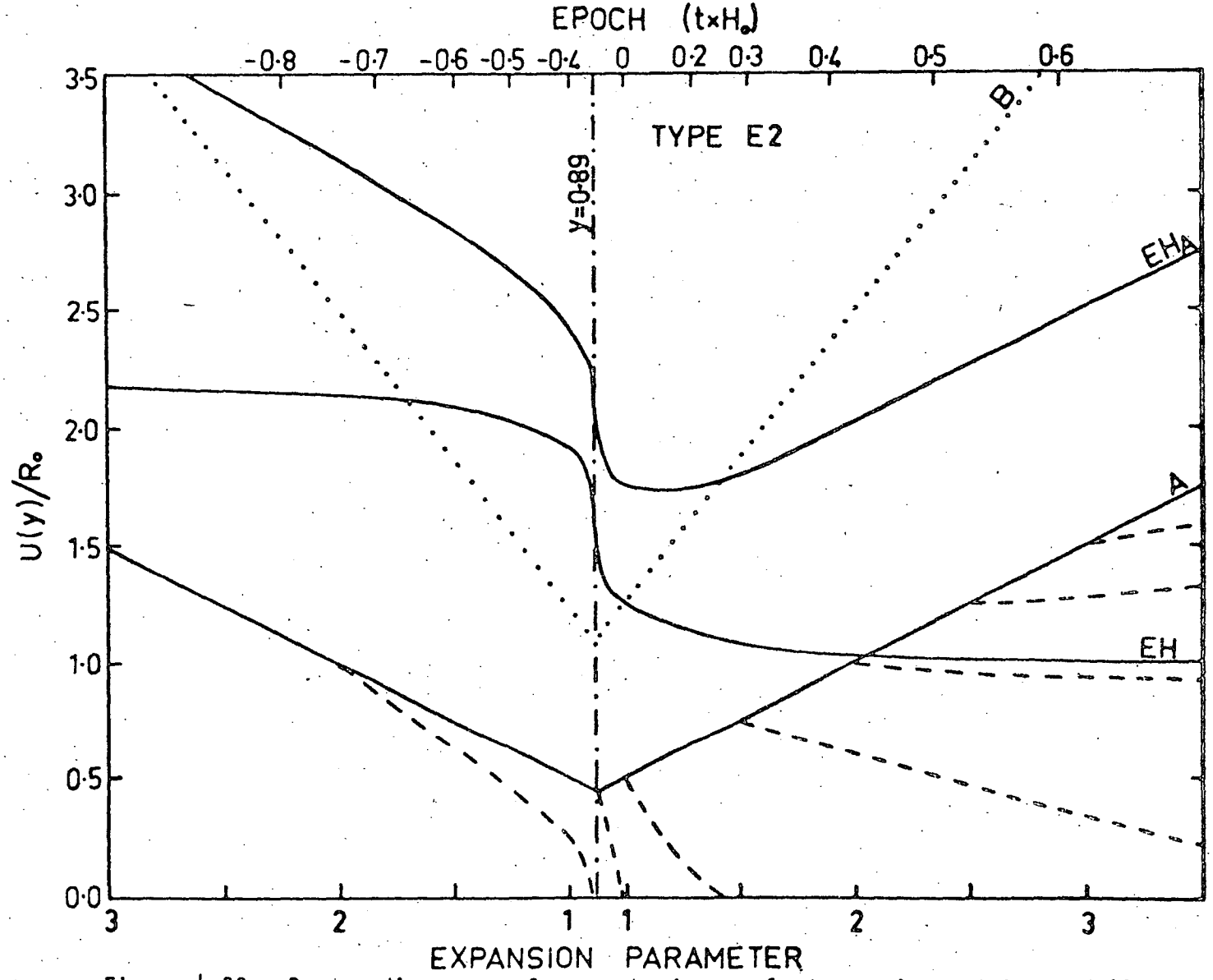

Figure 4.20 - Proper distances of event horizons, fundamental particles and light fronts in a type E2 model defined by $\sigma_0 = 0.5$, $q_0 = -5.0$.

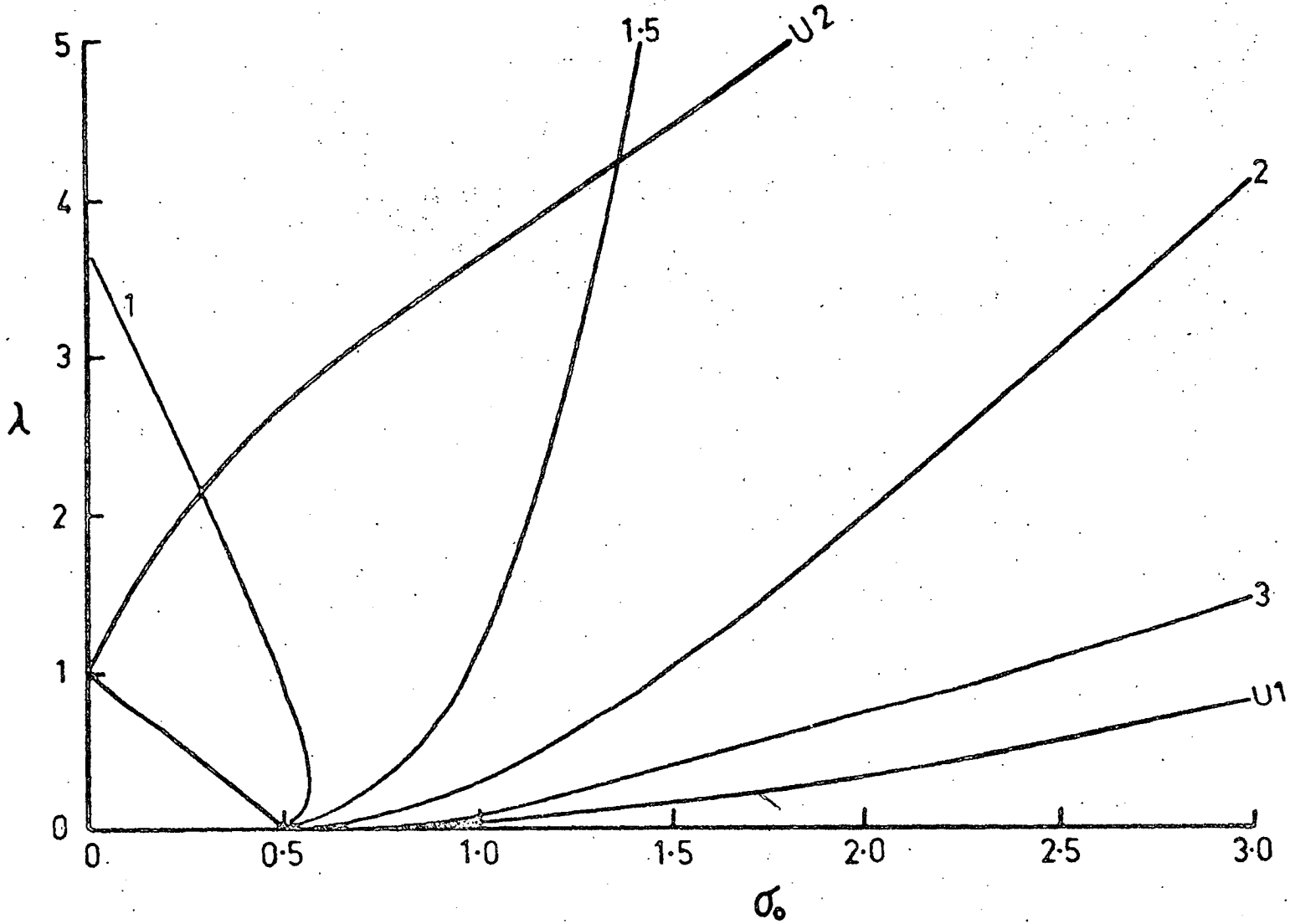

Figure 4.21 - Event horizons, in the (λ, σ) plane, represent by curves of constant ω_{EH}.

minimum value of y = 0.89. In this case it is possible for a fundamental particle to cross the observer's event horizon twice and this is indicated for the particle B which crosses the horizon at the present epoch.

The event horizons for different world-models are summarised in figure 4.21 where curves of constant ω_{EH} are drawn in the (λ, σ_o) plane. The value of ω_{EH} tends to infinity for models near to the curve U1.

4.8 Particle Horizons

Rindler defines the necessary and sufficient condition for the existence of a particle horizon to be the convergence of the integral

$$I = \int_0^{t_o} \frac{c\,dt}{R(t)} \qquad (4.29)$$

if the universe expands from a singular state at t = 0 or

$$I = \int_{-\infty}^{t_o} \frac{c\,dt}{R(t)} \qquad (4.30)$$

if the definition of t extends to negatively unbounded values (as in type E2 models). Substituting equation (4.4) into the first integral, it is clear that the surface (called the particle horizon) defined by

$$\omega_{PH} = \frac{c}{R_o H_o} \int_0^1 \frac{dy}{y\sqrt{f(y)}} \tag{4.31}$$

divides all fundamental particles into two classes: those that have been observed by the origin observer at or before the present epoch and those that have not. In the case of type E2 models we must have

$$\omega_{PH} = \frac{c}{R_o H_o} \left[\int_{\infty}^{y_{min}} \frac{dy}{y\sqrt{f(y)}} + \int_{y_{min}}^1 \frac{dy}{y\sqrt{f(y)}} \right] \tag{4.32}$$

Also, consider the replacement of the upper limit of integration (unity) in the last two integrations by a variable y_o. If, as the epoch advances ($y_o \to \infty$) the new integrals tend to a finite limit then all those particles having angular co-ordinate

$$\omega > \frac{c}{R_o H_o} \int_0^{\infty} \frac{dy}{y\sqrt{f(y)}} \tag{4.33}$$

in type E1 models can never be "seen" by an origin observer. A similar situation applies to type E2 models when the upper limit of the second integral in (4.32) in set equal to infinity.

Now, consider light quanta emitted from a fundamental particle in type E1 and type 0 models at time t=0. Then the equation

$$U(y) = R_o y[\omega(r_p) \pm \frac{c}{R_o H_o} \int_0^y \frac{dy'}{y'\sqrt{f(y')}}] \tag{4.34}$$

represents either a light front travelling away from the origin (positive sign) or a light front travelling towards the origin

(negative sign). Of course this is dependent on the integral being convergent.

Also, the equation to the observer's particle horizon follows from (4.31) and we have

$$U_{PH}(y) = \frac{cy}{H_o} \int_0^y \frac{dy'}{y'\sqrt{f(y')}} \qquad (4.35)$$

This equation also describes a light front emitted from the origin of co-ordinates at the singular creation event y = 0 so that the observer's particle horizon is evidently the boundary of his creation light cone. A fundamental particle is first "seen" when it crosses the observer's particle horizon which is (according to (4.34)) coincident with the observer crossing the particle's creation light cone. The fundamental particle first comes into view with a redshift of infinity since y = 0. The situation is illustrated in figure 4.22 where as before proper distances divided by R_o are plotted against y and epoch. The model is type E1 with $\sigma_o = 0.5$, $q_o = 0.75$. The fundamental particle A has an angular co-ordinate $\omega = 0.5$. The broken lines refer to A's creation light cone. The fundamental particle crosses the observer's particle horizon at the same epoch as the boundary of A's creation light cone reaches the origin.

The particle horizon is shown in figure 4.23 for the Einstein-de Sitter model ($\sigma_o = 0.5$, $q_o = 0.5$). The shape of the PH curve is

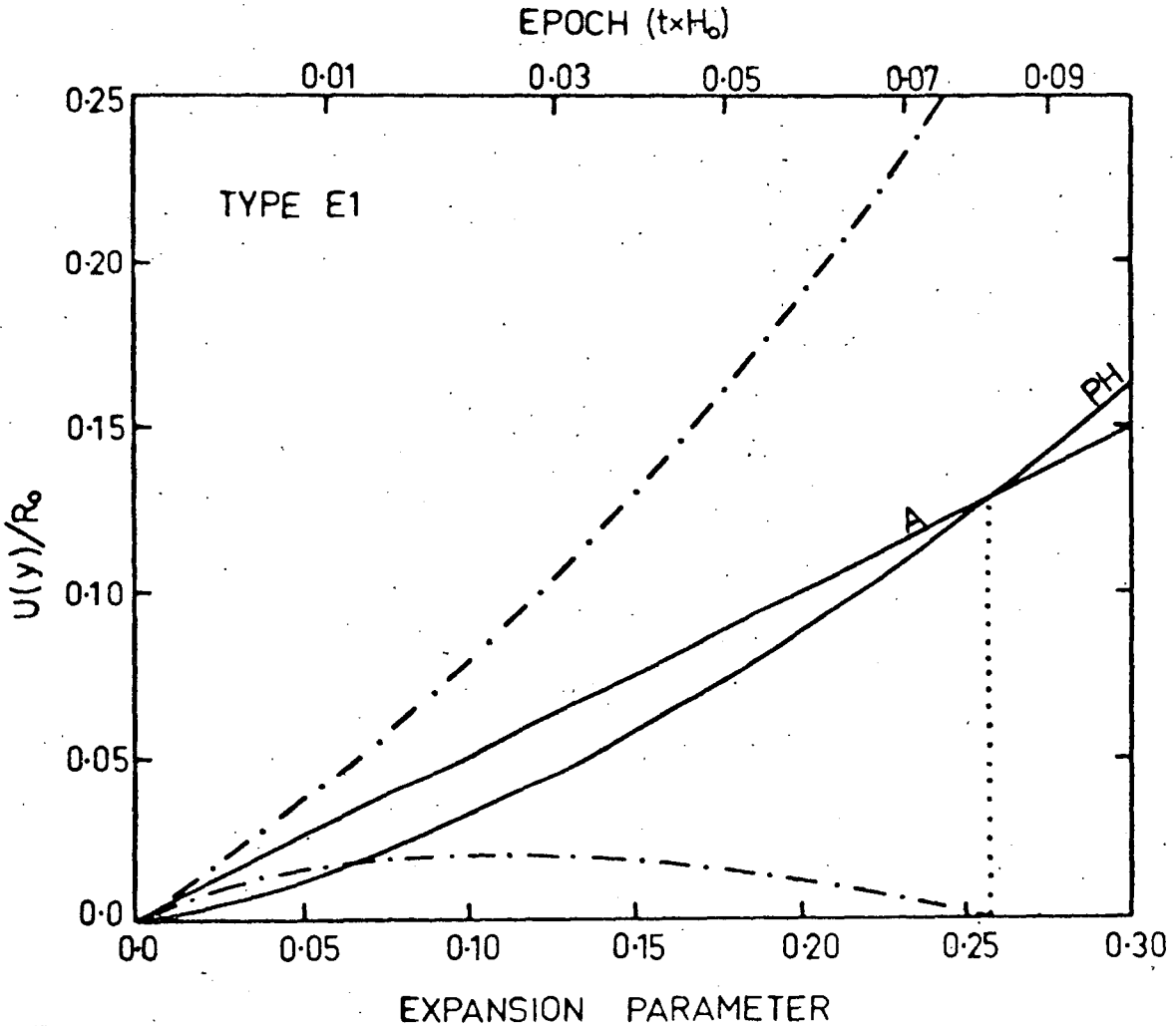

Figure 4.22 - Proper distances of particle horizons, fundamental particles and light fronts in a type E1 model defined by $\sigma_0 = 0.5$, $q_0 = 0.75$.

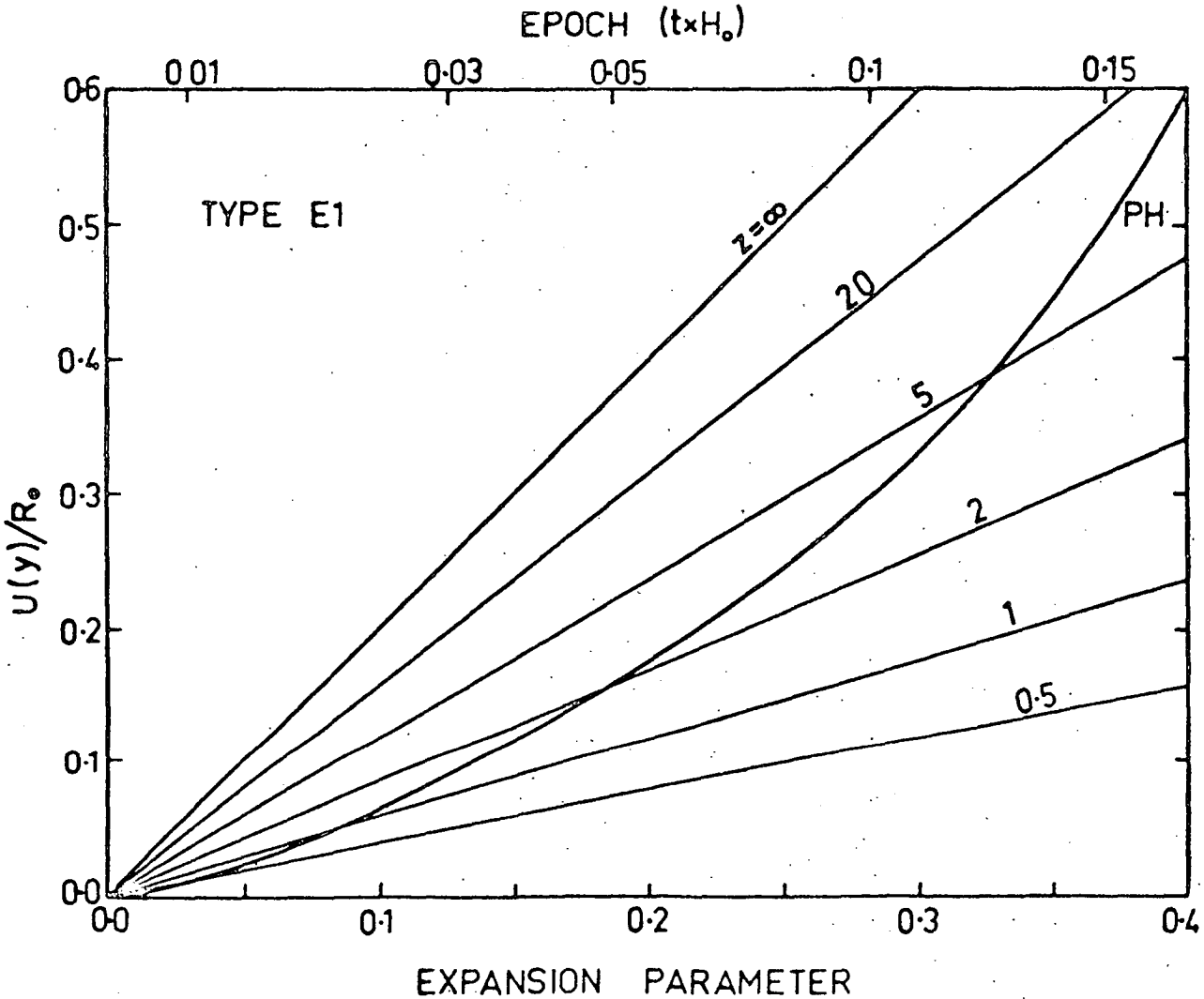

Figure 4.23 - Proper distances of the particle horizon and fundamental particles (defined by measured redshift values) in the Einstein-de Sitter model.

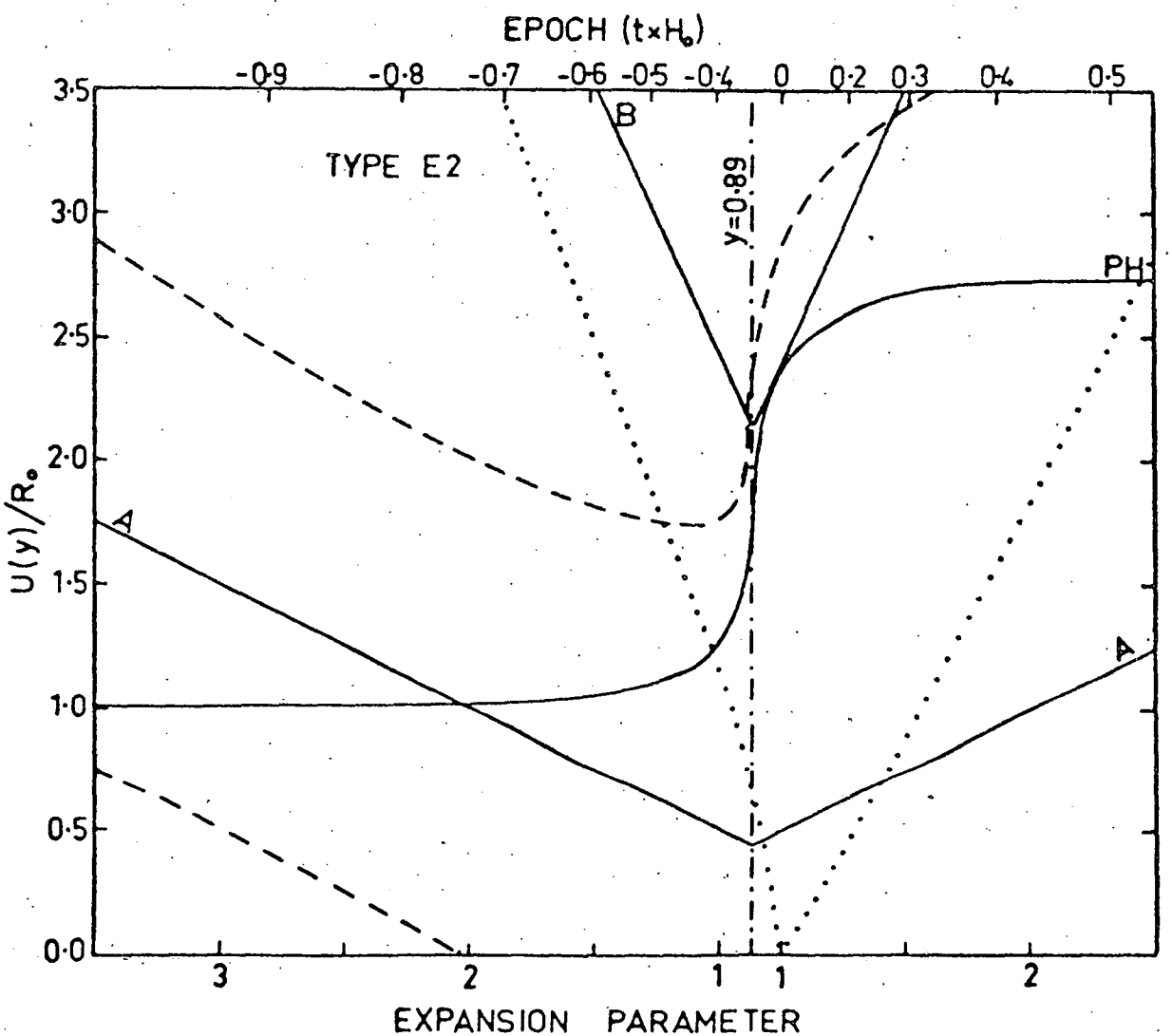

Figure 4.24 - Particle horizon, fundamental particles and light fronts in a type E2 model defined by $q_0 = 0.5$, $q_0 = -5.0$. The broken lines refer to light fronts from the particle A and the dotted lines represent light fronts from the particle B.

changed quite considerably for even a small change in q_o. Curves of $U(y)/R_o$ versus y are drawn for different fundamental particles having particular values of redshift as measured at the present epoch. The intersections of these lines with the curve representing the particle horizon indicate the epoch at which the particles are first "seen" by the origin observer.

The properties of particle horizons in type E2 models are illustrated in figure 4.24 for the model defined by $\sigma_o = 0.5$, $q_o = -5.0$. As before the particle A has angular co-ordinate $\omega = 0.5$. The fundamental particle is seen to cross the observer's particle horizon twice. This corresponds to a dual appearance of the particle with both events occurring with a redshift of $z = -1$ as measured by the origin observer. After the particle crosses the particle horizon its measured redshift increases to a value of $z_{max} = 1/y_{min} - 1$ which in this case is equal to 0.12 and then decreases to zero in the infinite future.

The particle B has an angular co-ordinate of $\omega = 2.383$ which is identical to the value of ω_{PH} at the present epoch. This particle comes into view only once and fundamental particles with $\omega > \omega_{PH}$ can never be detected.

The results of the numerical integration of equations (4.31) and (4.32) are shown in figure 4.25 where curves of constant ω_{PH} are

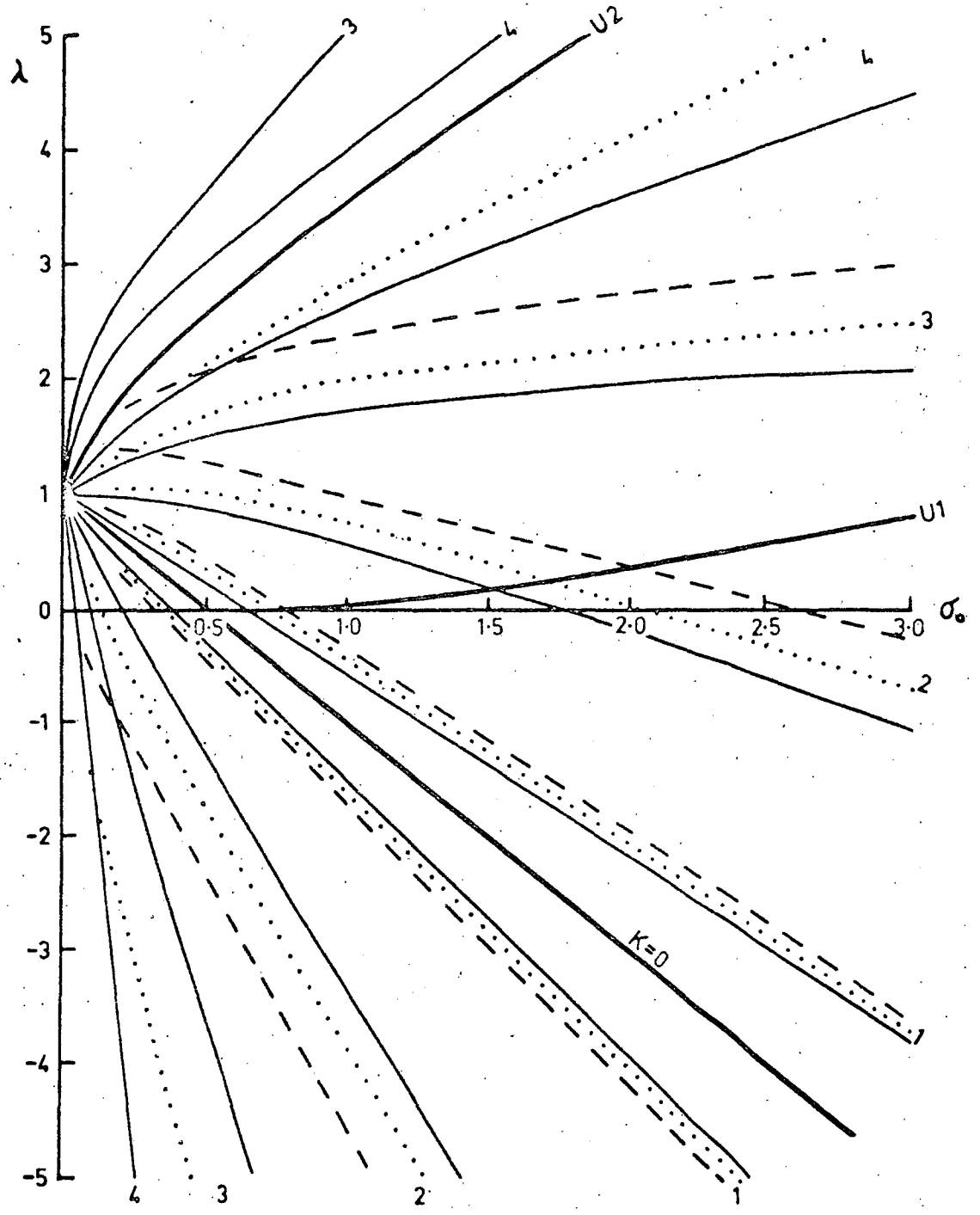

Figure 4.25 - The particle horizons in world-models illustrated by curves of ω_{PH} equal to a constant. The dotted lines correspond to $T_0 = 15°K$, and the broken lines to $T_0 = 20°K$.

drawn, for different values of T_o, in the (λ, σ_o) plane. The co-ordinate ω_{PH} tends to infinity for points near to the curve U2 defined by the radiation temperature. For a specific world-model, the effect of increasing the radiation intensity is a marked decrease in ω_{PH}, indicating a more rapidly evolving universe. The greatest departures from the value of ω_{PH} at $T_o = 0$ occur at relatively large values of ω_{PH}. A radiation field produces very little change in ω_{PH} for type E2 models, since the definition of y in these models does not extend to small values when the first term in equation (4.5) becomes important. The effects of the model parameters on particle horizons are evident from figure 4.25. For a particular radiation temperature, the equation to the line relating λ to σ_o is

$$\lambda = (1 + 3\varepsilon_o)\sigma_o - q_o \qquad (4.36)$$

where ε_o is given by equations (3.19) and (4.1). Applying this equation to figure 4.25 it is clear that, for a particular σ_o the result of increasing q_o is to decrease ω_{PH} in type E1 and type 0 models for which $k > 0$ while ω_{PH} is increased in type E2 and types E1 and 0 models with $k < 0$. The particle horizon is undefined on the line $k = 0$ and ω_{PH} must be calculated for each point (λ, σ_o) on this line.

4.9 The Small Redshift Approximation

It is possible to approximate the radial co-ordinate, r, by a power series provided the redshift z is much less than unity. The series is obtained here for universes containing black-body radiation and matter.

From (3.8) the angular co-ordinate of an event having expansion parameter y is

$$\omega = \frac{c}{R_o} \int_y^1 \frac{dy}{y\dot{y}} \tag{4.37}$$

Differentiating and using $dy/dz = -y^2$ it follows that

$$\frac{d\omega}{dz} = \frac{cy}{R_o\dot{y}} \tag{4.38}$$

and

$$\frac{d^2\omega}{dz^2} = -\frac{cy^2}{R_o\dot{y}}\left[1 - \frac{y\ddot{y}}{\dot{y}^2}\right] \tag{4.39}$$

and

$$\frac{d^3\omega}{dz^3} = \frac{cy^3}{R_o\dot{y}}\left[2 + \frac{3y^2\ddot{y}^2}{\dot{y}^4} - \frac{4y\ddot{y}}{\dot{y}^2} - \frac{y^2\dddot{y}}{\dot{y}^3}\right] \tag{4.40}$$

Now from equation (3.6)

$$\kappa p = -\frac{2\ddot{y}}{y} - \frac{\dot{y}^2}{y^2} - \frac{kc^2}{R_o^2 y^2} + \Lambda \tag{4.41}$$

where $\kappa = 8\pi G/c^2$

If the universe is filled with black-body radiation then

$$p = p_o y^{-4}, \quad \dot{p} = -p_o y^{-5}\dot{y}$$

and using these relations in equation (4.41)

$$\frac{y^2\dddot{y}}{\dot{y}^3} = \frac{\kappa p_o}{2\dot{y}^2} + \left(1 + \frac{kc^2}{R_o^2\dot{y}^2}\right) \tag{4.42}$$

Employing equations (3.19), (3.21), (4.14) and (4.16), the equations (4.38)-(4.40) become, at the present epoch

$$\frac{d\omega_o}{dz} = \frac{c}{R_o H_o} \tag{4.43}$$

$$\frac{d^2\omega_o}{dz^2} = \frac{-c}{R_o H_o}(1 + q_o) \tag{4.44}$$

$$\frac{d^3\omega_o}{dz^2} = \frac{c}{R_o H_o}(2 + 5q_o + 3q_o^2 - 3\sigma_o - 6\varepsilon_o\sigma_o) \tag{4.45}$$

Now the set of equations (3.11) for the radial co-ordinate may be written as

$$r = \omega - \frac{k\omega^3}{3!} + \frac{k^2\omega^5}{5!} - \frac{k^3\omega^7}{7!} + \ldots \tag{4.46}$$

Using Taylor's theorem to expand $\omega(z)$ around $z = 0$ we have

$$\omega(z) = z\,\frac{\partial\omega_o}{\partial z} + \frac{z^2}{2!}\,\frac{\partial^2\omega_o}{\partial z^2} + \frac{z^3}{3!}\,\frac{\partial^3\omega_o}{\partial z^3} + \ldots \tag{4.47}$$

and

$$\frac{k\omega^3(z)}{6} = \frac{k}{6}\left(\frac{\partial\omega_o}{\partial z}\right)^3 \tag{4.48}$$

since $\omega_o = 0$.

Combining equations (4.43) to (4.48) we have finally

$$r = \frac{cz}{R_o H_o}\left[1 - (1+q_o)z + (1+2q_o+q_o^2-2\sigma_o-3\varepsilon_o\sigma_o)\,\frac{z^2}{2} + \ldots\right] \tag{4.49}$$

The radiation field is therefore a third order effect in z. For $T_o = 3°K$ the pressure term is $3\varepsilon_o\sigma_o \simeq 2 \times 10^{-5}$ which is completely insignificant. Even for $T_o = 30°K$ the term is only about 0.2 and obviously all quantities describing the radiation field can be neglected for small values of z. Equation (4.49) is useful, however, since with the aid of equations (3.11) it is possible to quickly calculate such quantities as distance, velocity of recession and angular diameter of an object with a measured (small) redshift.

4.10 Conclusions

Relativistic world-models containing both matter and radiation are most easily classified by co-ordinates in the (λ, σ_o) plane. The boundaries of the different regions in this plane are determined by the temperature T_o of the Planckian radiation field. Depending on the values of λ, σ_o and T_o a relativistic world-model is specified as type E1, type E2 or type 0.

The analysis has shown that the deceleration parameter q approaches unity near the singularity at $y = 0$ independently of the radiation temperature. This result should be compared with the radiation free case in which $q \to 0.5$ as $y \to 0$. The age of the universe is decreased with increasing T_o and the effect is least for large values of the density parameter σ_o.

The properties of horizons in relativistic cosmologies can be described quite generally in terms of the expansion parameter and proper distance. The angular co-ordinate ω_{PH} defining the position of the particle horizon is markedly decreased with an increase in T_o for types E1 and 0 models while the radiation field has little effect in type E2 models. It is found that a fundamental particle may cross the observer's event and particle horizons twice in the course of evolution of the type E2 universe.

CHAPTER V

RADIO SOURCE PARAMETERS

In this chapter the properties of radio sources which require a description in cosmological terms are examined in some detail. The effects of different cosmological models on radio source parameters and observations are determined. Before any analysis is carried out which depends on the source population in the universe it is necessary to examine such matters as possible anisotropies in the spatial distribution of radio objects and the "spread" in source luminosities.

5.1 The Angular Distribution of Radio Sources

A number of radio source surveys have been examined statistically for any evidence of non-randomness of source positions. These analyses, apart from the recent 4C survey, were restricted by the limited resolution and sensitivity of the instruments to angular separations of greater than a few degrees.

Shakeshaft (1955), in an investigation based on the 2C survey at 81.5 MHz, found little evidence for clustering. Edge (1958), in an analysis of the 3C survey, concluded that for different ranges of flux densities (limiting flux 8×10^{-26} W m^{-2}Hz^{-1}) the source positions were randomly distributed in sample areas of 42.5 and 900 sq deg. Mills, Slee, and Hill (1960) concluded that for sources having $S \geq 6 \times 10^{-26}$ W m^{-2}Hz^{-1}, for $-90° \leq \delta \leq +10°$, there is no significant

departure from a random distribution, although small-scale clustering may occur in regions of the order of ½°. Results obtained with the 178 MHz Cambridge interferometer, operating as both an interferometer and a total power system, were used by Leslie (1961) in two methods of analysis, and these gave no evidence for clustering on a scale down to 2'.5 arc. Leslie also derived values for the maximum percentage of double or multiple systems that could occur without producing a detectable effect. Holden (1966), in an analysis based on the 4C survey, found the distribution of source positions for areas from 25 to 3600 sq deg to be uniform within the limits of statistical fluctuations. Further, Holden found no evidence of clustering for angular separations of ½° to 4°, although there was some evidence to suggest associations of sources having angular separations in the range 15' to 30'.

The Parkes 210 ft telescope has been used to complete two surveys in the declination zones 0° to +20° (Day et al. 1966) and 0° to -20° (Shimmins et al. 1966) at frequencies of 408, 1410, and 2650 MHz. The present investigation is based on these surveys at 1410 MHz. The sensitivity of the instrument at this frequency is 0.3×10^{-26} W m^{-2} Hz^{-1}, while the beamwidth is 13'.9 arc. Source surveys have also been made in the regions -20° to -60° (Bolton, Gardner, and Mackey, 1964) and -60° to -90° (Price and Milne, 1965) with an instrument sensitivity of approximately 0.8 flux units at 1410 MHz. These surveys were restricted to sources with flux densities

densities greater than 4 f.u. at 408 MHz that did not noticeably broaden the 48' beam of the telescope.

(i) The Probable Scale of Clustering

(1) Several authors (Mills 1960; van den Bergh 1961; Wills 1966) have shown that there is a significant correlation between the positions of radio sources and rich clusters of galaxies. The probability of collisions between galaxies will be greatly increased, and we might expect radio source associations with a scale of a few degrees. It can easily be shown, however, that even in clusters of galaxies the probability of encounters between galaxies is small, and the contribution of this process to the degree of clustering should be negligible.

(2) It is now well established that a radio source is generally larger than the associated optical galaxy and is often double, with the components situated on either side of the visible object. The most extensive investigations of the brightness distributions of radio sources are the long-baseline interferometer observations made at the California Institute of Technology (Moffet and Maltby 1962), using spacings out to 1557 wavelengths, and at Jodrell Bank (Allen et al. 1962), where by means of radio links spacings out to 61100 wavelengths were obtained. It was found that about 70 per cent of the sources are apparently double with an angular separation of about 1' arc. On

the basis of these observations we should expect association of extragalactic radio sources with a scale of a few minutes of arc.

Table 2

Results for 5° by 5° Zones

Number of sources in zone	0	1	2	3	4	5	6	7	8	9
Number of times observed	56	98	122	100	70	30	10	4	1	0
Number of times expected	45.5	108.2	128.7	102.1	60.7	28.9	11.4	3.9	1.16	0.31

(ii) Large-Scale Clustering

The distribution of source positions was investigated by dividing the sky into square areas and counting the number of squares containing 0, 1, 2, 3, etc. sources. The scales of clustering considered were for areas of 25, 100, 400, and 1600 sq deg. The sky was divided into regions 5°, 10°, 20°, and 40° wide in δ and the appropriate extent in α to produce the required areas. For areas of 400 and 1600 sq deg, where the number of zones was too small for a statistical investigation, the analysis was extended to $\delta = -80°$.

(a) 25 Sq Deg

There is no evidence for a non-random distribution of sources having $S \geq 0.3$. The results are shown in Table 2.

The mean of the distribution is 2.38, while the variance is 2.44. The observed results were compared with the theoretical Poisson distribution predicted for a random sky. A chi-square test gave a probability of 0.65 that the distribution is Poisson. The distribution of sources per zone as a function of α was also investigated, and a plot of the number of sources per zone against α showed a general tendency for the number of sources to decrease between 0800 and 1700 hr. It was found that the number of sources in the equal areas between 0800 and 1700 hr, and between 2000 and 0500 hr, was 485 and 587 respectively, i.e. an increase of approximately 25 per cent in the latter region.

(b) 100 Sq Deg

In this case there is a greater number of sources per zone, and three different flux ranges, $S \geq 0.3$, $S \geq 1.0$, and $S \geq 2.0$, were considered. The results are summarized in Table 3, which gives the calculated mean and variance and the probability P that the distribution is Poisson. It can be seen that there is no significant evidence for clustering on this scale.

Table 3

Results for 10° by 10° Zones

	Flux Range		
	$S \geq 0.3$	$S \geq 1.0$	$S \geq 2.0$
Mean	9.3	4.5	1.5
Variance	11.6	5.6	1.4
P	0.35	0.72	0.3

(c) 400 Sq Deg

The analysis for sources having $S \geq 0.3$ was restricted to declinations $+20° \geq \delta \geq -20°$, while for sources having $S \geq 1.0$ and $S \geq 2.0$ the analysis was extended to $\delta = -80°$. The results of the analysis are shown in Table 4.

It can be seen from this table that for zone areas of 400 sq deg there is no evidence for a non-random distribution of sources having $S \geq 0.3$ and $S \geq 2.0$. There is, however, significant evidence for clustering of sources having $S \geq 1.0$ in the region $+20° \geq \delta \geq -80°$. An analysis was made of sources having $S \geq 1.0$ in the region $+20° \geq \delta \geq -20°$ and the distribution was found to have a mean and variance of 17.8 and 30.7 respectively, while the probability that

Table 4

Results for 20° by 20° Zones

	Flux Range		
	$S \geq 0.3$	$S \geq 1.0$	$S \geq 2.0$
Mean	37.5	15.2	6.3
Variance	67.6	25.1	9.0
P	0.35	0.01	0.25

the distribution is Poisson was 0.60. In the region $-20° \geq \delta \geq -80°$ the distribution of sources was found to have a mean of 15.7, a variance of 37.2, and a probability of 0.20 that the distribution is random. The surveys in the declination zones $-20° \geq \delta \geq -60°$ and $-60° \geq \delta \geq -90°$ did not include sources that broadened the 48' beam of the telescope, whereas the surveys between +20° and -20° included a large number of extended sources, so that the apparent clustering on this scale can be explained in terms of source-selection effects in the separate surveys.

(d) 1600 Sq Deg

For sources having $S \geq 1.0$ and $S \geq 2.0$ the analysis has been extended to $\delta = -80°$. The number of zones of this size was

insufficient for a complete analysis to be made, but to allow for possible clustering on the boundaries of a zone each zone was shifted half a zone length in α. In both cases there were no obvious trends in the numbers of sources per zone to suggest any departure from a non-random distribution.

Table 5

Numbers of Pairs of Sources in Real and Random Skies

Flux Range	Type of Sky	Angular Separation 15'-30'	30'-1°	1°-2°	2°-3°	3°-4°
$S \geq 0.3$	Real	71	130	654	1103	1440
	Random	66.7	126	636	1077	1445
$S \geq 0.6$	Real	42	75	402	726	892
	Random	39.4	69.1	388	734	872
$S \geq 1.0$	Real	18	32	163	290	342
	Random	16.3	29.1	149	291	336
$S \geq 1.5$	Real	6	11	47	74	101
	Random	3.1	8.4	42.2	70.9	98.2
$S \geq 2.0$	Real	5	6	22	29	43
	Random	2.3	5.1	18.0	29.3	38.8

(iii) Small-Scale Clustering

An investigation of small-scale clustering was made for sources having flux densities greater than 0.3, 0.6, 1.0, 1.5, and 2.0 f.u., the total number of sources in each range being 1184, 949, 576, 305, and 191 respectively. The analysis did not include the regions of the galactic plane that were not covered in the Parkes surveys. The half-power beamwidth of the Parkes telescope at 1410 MHz is 13'.9 arc, so that the investigation of small-scale clustering is limited to a scale of 15' arc. The analysis of small-scale clustering is similar to that described by Holden (1966). The analysis uses a method of comparison between the distribution of its neighbours for each source in the real sky and the distribution obtained from a series of random skies. The positions of sources having $S \geq 0.3$ were compiled in an Elliott 503 computer, and for each source the number of sources falling within a specified angular separation, in α and δ, was calculated. Each pair of sources was included only once in the analysis, and the ranges of angular separation considered were 15' to 30', 30' to 1°, 1° to 2°, 2° to 3°, and 3° to 4° in α and δ. The analysis was then repeated for sources having $S \geq 0.6$, $S \geq 1.0$, $S \geq 1.5$, and $S \geq 2.0$.

A total of 60 random skies was compiled in the same computer. The number of sources within each flux range was made identical to that of the real sky. Any other parameters, such as those required for the exclusion of the galactic plane, simulated those of the real

sky. The effects of the finite resolution of the telescope were accounted for in the generation of the random skies. The results are summarized in Table 5. It can be seen from the values listed that there is, overall, no evidence for clustering of sources with angular separations 15' to 4°. Except for sources having $S \geq 1.5$ and $S \geq 2.0$ with an angular separation of 15' to 30', all departures from the random values can be accounted for by statistical fluctuations.

The minimum number of double sources occurring at the 10 per cent significance level was calculated from each random sky distribution and subtracted from the observed number of double sources in the real sky. This number was then expressed as a percentage of the total number of sources, giving the maximum percentage of clustering that could be present but undetected at the 10 per cent significance level. The maximum percentage of clustering for each flux range and for each angular separation is shown in Table 6.

The results given in Tables 5 and 6 show that there is no evidence for clustering of sources with angular separations 15' to 4°. Although there is a number of small-scale associations with intense sources, they represent only a small percentage of the total number of sources with the appropriate flux density. Thus, it is found that 4.5 per cent of sources having $S \geq 1.5$, and 5.5 per cent of sources having $S \geq 2.0$, lie within 15' to 30' of another such source.

Table 6

Maximum Percentage of Double Sources that could Occur at the 10% Significance Level

Flux Range	Angular Separation				
	15'-30'	30'-1°	1°-2°	2°-3°	3°-4°
$S \geq 0.3$	3%	3%	4%	6%	8%
$S \geq 0.6$	2	6	5	2	9
$S \geq 1.0$	9	4	12	7	10
$S \geq 1.5$	4	4	8	7	8
$S \geq 2.0$	5	2	3	2	11

5.2 The Luminosity Distribution

A determination of the luminosity distribution of radio galaxies is of crucial importance to the understanding of the physical processes involved in the evolution of these objects. A knowledge of this distribution is also necessary for the interpretation of radio source counts and related problems. The luminosity distribution will therefore provide some useful data for application in cosmological problems.

The distribution may be defined in terms of the spatial density $\rho(P)$ of sources of luminosity P in a given volume of space at a

particular epoch or, alternatively, the luminosity of all radio sources in a given range of flux density may be considered giving the luminosity distribution per unit flux density range, n(P). The luminosity of an individual source can only be derived once its luminosity distance is known and accurate determinations of radio luminosity are thus restricted to sources which have measured redshifts. However, using a relation between radio and optical magnitudes of galaxies, Longair and Scott (1965) have derived the luminosity distribution, n(P), of sources at 178 MHz. Their results are represented by the curve labelled n(P) in figure 5.1. The mean luminosity of sources is $P_o = 8 \times 10^{25}$ watts Hz^{-1} sr^{-1} at 178 MHz.

The main problem associated with the derivation of the distribution n(P) is to obtain a complete sample of radio sources. For a particular limiting flux density, S, it is clear that the sources having a large luminosity will in general be situated at greater distances and therefore be optically fainter than the less powerful sources. Hence, for sufficiently powerful sources, the radio galaxy will be too distant to be detected photographically and there will therefore be a limiting photographic magnitude beyond which identifications will not be possible. Obviously then, the analysis must be restricted to sources with flux densities greater than a certain minimum value depending on the maximum luminosity necessary to determine the n(P) distribution. It follows that it is not possible to determine with any accuracy the form of the distribution

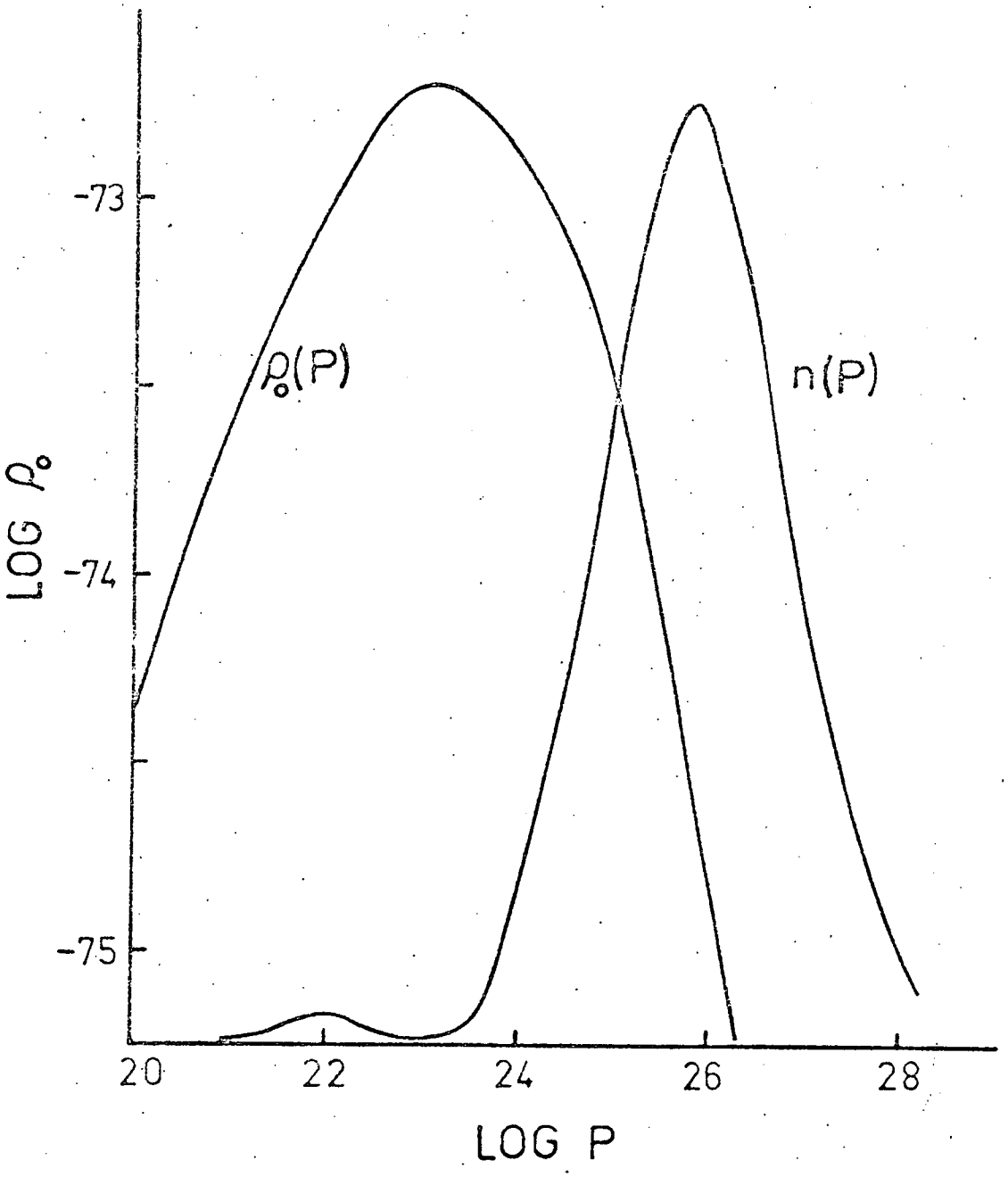

Figure 5.1 - The luminosity distribution n(P) and the derived distribution $\rho_o(P)$ for the spatial density of sources with luminosity P at 178 MHz.

at high luminosities. Longair and Scott have limited their analysis to sources having flux densities $S > 10 \times 10^{-26}$ f.u. at 178 MHz and this will lead to inaccuracies in the distribution for P greater than about 15×10^{26} W Hz^{-1} sr^{-1}.

The Parkes surveys provide a more complete sample of radio sources but, although a large number of identifications have been made, a large percentage of sources with relatively large flux densities remain unidentified. The derivation of luminosity distribution for the Parkes sources is therefore not feasible at present.

The n(P) distribution has only limited application and the distribution of $\rho(P)$ is of greater cosmological significance. We now assume that the distribution n(P) is Gaussian in $\log_e(P/P_o)$ with standard deviation σ. That is, the dispersion in n(P) may be represented by the equation

$$n(P/P_o) = n(1)e^{-x^2/2\sigma^2} \qquad (5.1)$$

where $x = \log (P/P_o)$.

Now, Davidson (1962) has shown that when S is large, to a first approximation, the number of sources of flux density exceeding S in any homogeneous isotropic universe is

$$N_o(S) = \frac{1}{3} S^{-1/2} \int_0^\infty \rho_o(m) P^{3/2} \, d \log m$$

$$= \frac{1}{3} n_o P_o^{3/2} S^{-3/2} \qquad (5.2)$$

where $m = P/P_o$ and $\rho_o(m)$ is the spatial density of sources at the present epoch and n_o is the weighted mean density of sources at the present epoch.

The complete log N/log S curve at 178 MHz has been derived by Gower (1966) using revised 3C data together with results from the 4C and North Polar surveys (Ryle and Neville, 1962). According to equation (5.2) the value of the product $n_o P_o^{3/2}$ may be estimated from the value of N at large flux densities where the effects of redshift are small and the statistical fluctuations also reasonably small. This method yields a value of

$$n_o P_o^{3/2} = 3.06_{10}{}^{-36} \qquad (5.3)$$

where n_o is expressed in sources m^{-3} and $P_o = 8 \times 10^{25}$ W Hz^{-1} sr^{-1}. It should be mentioned here that the log N/log S relation will be examined in greater detail in a later section.

Now by anology with the undispersed luminosity function the spatial distribution $\rho_o(P)$ at the present epoch may be written as

$$\rho_o(m) = \rho_o(1) m^{-1.5} e^{-x^2/2\sigma^2} \qquad (5.4)$$

where as before $m = P/P_o$. Integrating this equation and using (5.2) we find

$$N_o(S) = \frac{S^{-3/2}}{3} \int_0^\infty \rho_o(m) P^{3/2} d(\log m)$$

$$= \frac{\sqrt{2\pi}}{3} \sigma \rho_o(1) P_o^{3/2} S^{-3/2} \qquad (5.5)$$

so that

$$n_o = \sqrt{2\pi}\, \sigma \rho_o(1) \qquad (5.6)$$

which is similar to the equation derived by Davidson and Davies (1964).

Furthermore it is possible to estimate $\rho_o(m)$ for a particular m. A list of identified sources from the Parkes and 3C catalogues has been prepared and is presented in Table 7. This will be described in a later section. However, for our present purposes, there are found to be a total of 18 sources having luminosities between 10^{23} and 10^{24} W Hz^{-1} sr^{-1} at 178 MHz and which apparently lie within a distance corresponding to a redshift of 0.03. The mean luminosity of these sources is 8.2×10^{23} W Hz^{-1} sr^{-1} and their spatial density is 1.6×10^{-74} m^{-3}. This estimate agrees fairly well with the value of 4×10^{-74} m^{-3} given by Ginzburg and Syrovatskii (1964) for the sources

Cent. A, Virgo A and Fornax A which have an average luminosity of 8.1×10^{23} W Hz^{-1} sr^{-1} at 178 MHz. The sources probably all lie within the Local Group and their spatial density will be somewhat higher than the density on a larger cosmic scale. Using these values for ρ_o and P by substitution in equations (5.4) and (5.6) yields

$$\sigma = 2.05$$

and

$$\rho_o(1) = 1.85_{10}{}^{-75} \; m^{-3} \tag{5.7}$$

The value derived for σ is in close agreement for the value of $\sigma = 2.1$ obtained by fitting a Gaussian curve to the n(P) curve in figure 5.1. The values derived above for σ and $\rho_o(1)$ will be used in future for any theoretical model which requires a knowledge of the spatial distribution of sources.

The distribution $\rho_o(m)$ given by equation (5.4) is presented in figure 5.1. Also, since the luminosity distribution is assumed Gaussian in log m we note that according to (5.4)

$$d\eta_o = \rho_o(m) \; d(\log m)$$

$$= \rho_o(1) \; m^{-2.5} \; e^{-x^2/2\sigma^2} \; dm \tag{5.8}$$

is the number of sources per unit proper volume at the present epoch in the interval m, m + dm.

Table 7

Properties of Identified Radio Sources

Source	Type	S_{1410} (f.u.)	Alpha	Redshift	Distance (Mpc.)	Log L
0035-02	E	6.0	0.55	0.220	659.8	36.78
0051-03	E	2.1	0.75	0.210	629.9	36.15
0106+13	SO	14.2	0.85	0.063	189.6	35.91
0106+01	QSO	1.4	0.65	2.107	6319.5	37.89
0115+02	QSO	1.0	0.90	0.230	689.8	35.86
0122-00	QSO	1.0	-0.10	1.070	3209.3	37.89
0123-01	DB	4.5	0.90	0.019	57.0	34.36
0128+06	DB	1.4	1.00	0.022	66.0	33.98
0155-10	QSO	2.0	0.70	0.616	1847.6	37.05
0159-11	QSO	2.9	0.50	0.669	2006.5	37.40
0213-13	E	4.9	0.60	0.031	93.0	34.98
0214+10	QSO	1.3	0.70	0.408	1223.7	36.52
0237-23	QSO	7.2	-0.50	2.211	6631.5	39.57
0240-00	S	5.1	0.60	0.0038	11.4	33.17
0255+05	DB	5.9	0.75	0.023	69.0	34.69
0305+03	SO	7.1	0.45	0.030	90.0	35.25
0307+16	S	4.9	0.85	0.256	767.8	36.65
0320-37	FORN A	80.0	0.80	0.0056	16.8	34.57
0325+02	E	4.4	0.65	0.030	90.6	34.87
0349-14	QSO	2.8	1.00	0.546	1637.6	37.07
0349-27	E	4.1	0.80	0.066	198.0	35.42
0350-07	QSO	3.1	0.90	0.962	2885.3	37.57
0356+10	E	10.0	0.70	0.032	96.0	35.24
0403-13	QSO	3.3	0.85	0.571	1712.6	37.16
0405-12	QSO	2.7	0.90	0.574	1721.6	37.07
0518-45	PICT A	52.1	0.70	0.033	99.0	35.98
0521-36	N	14.7	0.50	0.055	165.0	36.04
0634-20	E	7.0	0.80	0.056	168.0	35.51
0736+01	QSO	2.7	0.40	0.191	572.9	36.46
0806-10	E	3.3	0.80	0.112	335.9	35.78
0812+02	QSO	1.9	0.70	0.402	1205.7	36.67
0819+06	E	2.3	1.10	0.081	244.4	35.36
0837-12	QSO	1.7	0.75	0.200	599.9	36.01
0838+13	QSO	2.6	0.70	0.684	2051.5	37.25
0850+14	QSO	2.4	1.20	1.109	3326.2	37.77
0855+14	N	2.4	0.70	0.053	159.0	35.05
0903+16	QSO	1.3	0.85	0.411	1232.7	36.48

Table 7 Continued

Source	Type	S_{1410} (f.u.)	Alpha	Redshift	Distance (Mpc.)	Log L
0915-11	HYD A	36.3	0.75	0.055	165.0	36.23
0922+14	QSO	0.7	1.20	0.896	2687.4	37.04
0932+02	QSO	0.7	0.65	0.659	1976.5	36.67
0947+07	E	7.3	0.85	0.103	308.9	36.04
0957+00	QSO	0.9	0.90	0.907	2720.4	36.99
1004+13	QSO	1.2	0.70	0.240	719.8	36.04
1116+12	QSO	1.8	0.80	2.118	6352.5	37.98
1131+21	E	0.7	0.90	0.066	198.0	34.63
1138+01	D	2.0	0.70	0.056	168.0	35.02
1142+19	NGC 3862	5.1	0.90	0.022	66.0	34.54
1216+06	E	15.3	0.60	0.0038	11.4	33.65
1217+02	QSO	0.7	0.60	0.240	719.8	35.88
1222+13	E	6.1	0.60	0.0038	11.4	33.25
1229-02	QSO	1.6	0.50	0.388	1163.7	36.71
1228+12	VIRG A	197.2	0.65	0.0038	11.4	34.72
1241+16	QSO	2.7	0.85	0.545	1634.6	37.03
1252+11	QSO	1.1	0.10	0.871	2612.4	37.57
1252-12	DB	6.6	0.55	0.014	42.0	34.46
1317-00	QSO	1.7	0.80	0.890	2669.4	37.25
1322-42	CENT A	300.0	0.80	0.0016	4.8	34.06
1358-11	E	1.9	0.60	0.025	75.0	34.38
1416+06	QSO	5.8	1.15	1.439	4316.0	38.34
1514+07	D	5.2	1.20	0.034	102.0	35.02
1559+02	DE	6.9	0.80	0.170	509.9	36.46
1648+05	HERC A	42.8	1.00	0.162	485.9	37.20
1717-00	D	48.7	0.75	0.031	93.0	35.87
1836+17	D	7.1	0.50	0.0034	10.2	33.32
2115-30	QSO	1.9	0.55	0.980	2939.3	37.48
2128-12	QSO	1.7	-0.20	0.501	1502.7	37.74
2134+004	QSO	3.1	-1.00	1.940	5818.7	39.71
2135-14	QSO	2.9	0.65	0.200	599.9	36.30
2146-13	QSO	1.5	0.90	1.800	5398.8	37.79
2212+03	DB	3.4	0.90	0.027	81.0	34.54
2221-02	N	5.1	0.80	0.058	174.0	35.40
2251+15	QSO	11.9	0.20	0.859	2576.4	38.49
2251+11	QSO	1.6	0.80	0.323	968.8	36.37
2300-18	N	1.5	0.50	0.129	386.9	35.77
2313+03	QSO	4.3	0.85	0.220	659.8	36.46
2322-12	E	1.9	1.20	0.084	251.9	35.37
2349-01	N	1.6	0.70	0.174	521.9	35.90

Table 7 Continued

Source	Type	S_{400} (f.u.)	Alpha	Redshift	Distance (Mpc.)	Log L
3C33	D	31.3	0.75	0.100	299.9	36.29
3C40	D	18.1	0.82	0.017	51.0	34.44
3C48	QSO	38.0	0.52	0.367	1100.7	37.81
3C47	QSO	12.9	0.89	0.425	1274.7	37.03
3C66	E	24.0	0.71	0.021	63.0	34.86
3C71	S	10.4	0.60	0.0039	11.7	33.18
3C78	D	12.9	0.45	0.029	87.0	35.24
3C83.1	E	11.3	0.57	0.018	54.0	34.59
3C84	E	29.2	0.62	0.018	54.0	34.93
3C196	S	38.3	0.73	0.018	54.0	34.91
3C195	D	10.4	0.71	0.107	320.9	35.91
3C219	D	24.4	0.80	0.053	159.0	35.57
3C261	U	3.7	0.93	0.614	1841.6	36.78
3C227	N	20.2	0.82	0.100	299.9	36.02
3C231	I	12.0	0.29	0.0010	3.0	32.56
3C218	D	137.0	0.93	0.053	159.0	36.22
3C334	QSO	6.4	0.78	0.550	1649.6	37.04
3C245	QSO	7.2	0.61	1.029	3086.3	37.85
3C254	QSO	10.6	0.93	0.734	2201.5	37.39
3C275	U	6.8	0.77	0.557	1670.6	37.09
3C234	N	16.6	0.85	0.187	560.9	36.46
3C264	D	15.7	0.78	0.021	63.0	34.60
3C270	S	38.2	0.50	0.0020	6.0	33.31
3C317	D	22.2	1.20	0.033	99.0	34.96
3C327	D	25.0	0.85	0.103	308.9	36.12
3C338	D	17.9	1.17	0.030	90.0	34.78
3C353	D	135.0	0.70	0.030	90.0	35.93
3C386	D	16.3	0.67	0.0030	9.0	33.05
3C383	D	14.8	0.40	0.090	269.9	36.37
3C405	D	4,600.0	0.80	0.057	171.0	37.91
3C430	E	19.0	0.76	0.017	51.0	34.52
3C442	DB	10.8	0.94	0.100	299.9	35.66
3C433	D	31.3	0.75	0.100	299.9	36.29
3C446	QSO	12.2	0.54	1.400	4199.0	38.45
3C445	N	15.7	0.74	0.057	171.0	35.51
3C465	D	22.7	0.81	0.029	87.0	35.01

5.3 Luminosity Distance and Flux Density

There is a problem associated with the concept of "distance" in space-times defined by the metric (3.4) since there is no unique definition for the distance of a source. It is possible to define a proper distance which was applied to the discussion of horizons in section 4.6, or distance by apparent angular size or the luminosity distance of a source of radiation. The latter quantity is the one usually employed to establish a distance between galaxies.

The luminosity distance, D, is defined in such a way that the intensity of a light source falls off inversely as the square of D. Consideration of emission and reception of light quanta (McVittie, 1965) leads to

$$D = \frac{R^2(t_o)}{R(t)} \frac{r}{1 + kr^2/4} \tag{5.9}$$

Now from equation (3.9) and using $R/R_o = y$ equation (5.9) yields

$$D = R_o y^{-1} T_k(\omega) \tag{5.10}$$

The chosen world-model determines the form of the function $T_k(\omega)$ since from equations (3.8), (3.12) and (4.4)

$$\omega = \frac{c}{R_o H_o} \int_y^1 \frac{1}{y' \sqrt{f(y')}} \tag{5.11}$$

for a source of redshift $z = y^{-1} - 1$.

The luminosity distance (in megaparsecs) is plotted against z for various cosmological models in figure 5.2. The radiation temperature T_o was taken equal to 3°K. The luminosity distance goes to zero at the antipole of co-ordinates in closed models and this is indicated in the diagram. Type E2 models which are also closed have a somewhat peculiar curve for log D versus log z and this is exemplified by the model $\sigma_o = 5.0$, $q_o = -5.0$.

Consider a source which has a luminosity $P(\nu')$ (W Hz^{-1} sr^{-1}) at frequency ν' in the interval $d\nu'$. This radiation will be detected at a frequency ν in an interval $d\nu$ and the flux density at the origin of co-ordinates will be given by

$$S(\nu)d\nu = \frac{P(\nu')d\nu'}{D^2} \tag{5.12}$$

Substituting for D from equation (5.10) and using $\nu = \nu' y$ then

$$S(\nu) = \frac{P(\nu y^{-1})}{R_o^2 y^{-1} T_k^2(\omega)} \tag{5.13}$$

The flux density from a certain type of source will depend primarily on the form of the luminosity distance curve. Obvious features are a minimum for the flux density in type E2 models and an infinite value of S for sources at the antipole of the origin of co-ordinates.

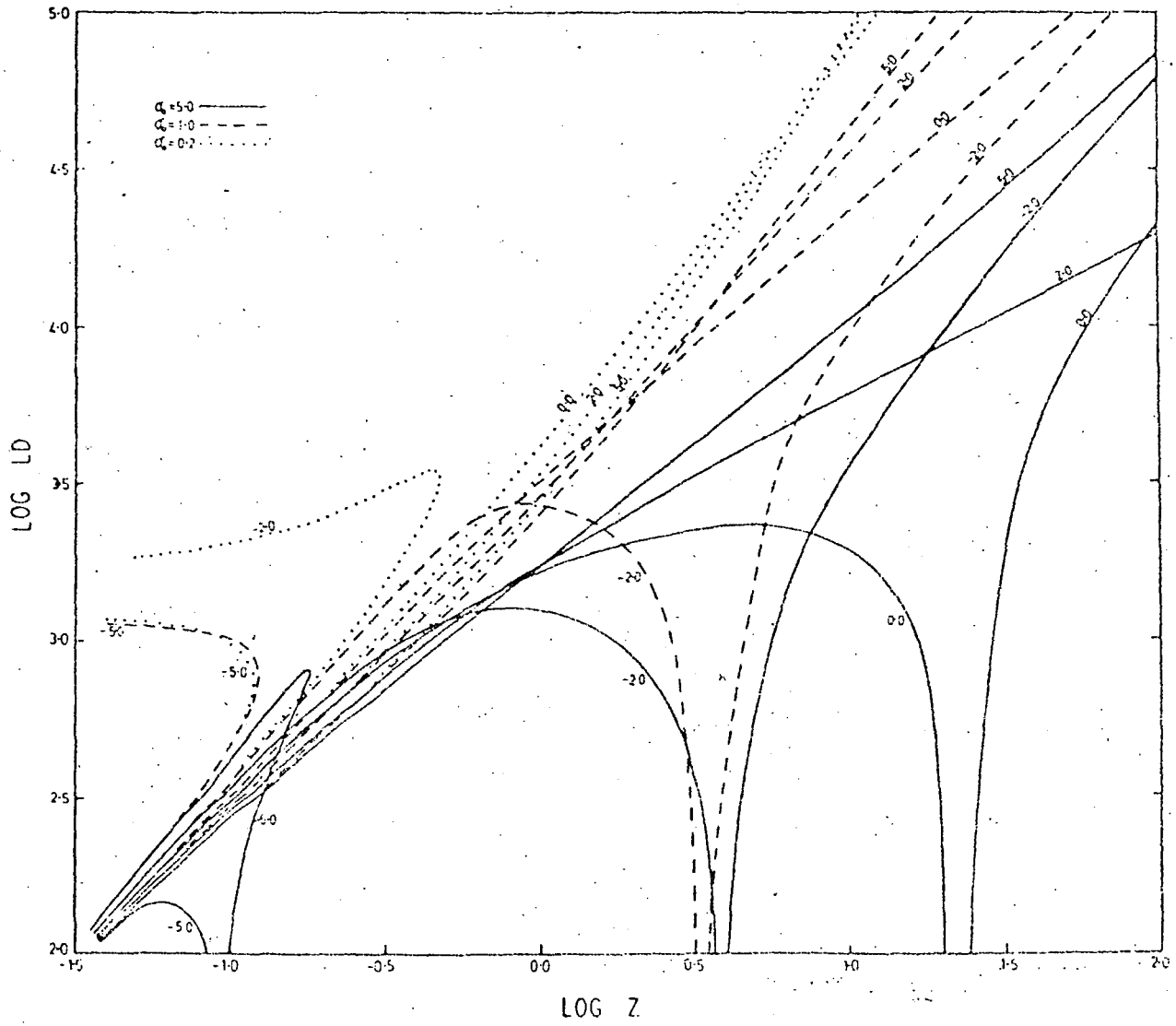

Figure 5.2 - The luminosity distance as a function of redshift and different world-models (T_o = 3°K). The distance is measured in megaparsecs.

5.4 Angular Diameters

Apart from the work of Ekers (1969), as far as the author is aware, there have been no systematic attempts at the measurement of angular diameters of large numbers of radio sources. Ekers observed 123 southern radio sources with a variable spacing interferometer and derived angular diameters for 57 of these. Of the latter sources only 2 have measured redshifts. Angular diameter measurements involve extreme difficulties. Interferometer techniques at large base lines are complex and interpretation of results from these instruments is made almost impossible due to the complex nature of the radio sources themselves. Very few radio galaxies have a simple brightness distribution and many consist of two or more separate components. There is also the problem as to whether or not radio sources form a single class of objects. The existence of quasars, as distinct from ordinary radio galaxies, infers that this situation is unlikely. Here, however, all extraneous effects are neglected and the analysis is restricted to the effects of the space-time geometry only on the angular diameters of radio sources.

A formula for the distance η of a source, according to its apparent angular size, has been derived by McVittie (1965) and may be written as

$$\eta = \frac{R_o}{1+z}\, T_k(\omega)$$

$$= R_o y T_k(\omega) \qquad (5.14)$$

If the linear dimension of a source is ℓ, then the apparent angular diameter will be

$$\Theta_P = \frac{\ell}{\eta} = \frac{\ell}{R_o y T_k(\omega)} \qquad (5.15)$$

The distance η has an interesting property, namely that it can attain a maximum value before the particle horizon is reached. Thereafter, η decreases monotonically for flat or open universes and has a zero value only at $z = \infty$. However, for closed universes $\eta = 0$ at the antipole ($\omega = \pi$) of the space-time and any source at this point will cover the whole horizon (provided $\omega_{PH} > \pi$ and gravitational defocussing of light rays is neglected).

Now from equation (5.14)

$$\frac{d\eta}{dz} = \frac{d\eta}{dy}\frac{\partial y}{\partial z} = -y^2 R_o\left[\frac{dT_k(\omega)}{dy} \cdot y + T_k(\omega)\right] \qquad (5.16)$$

But according to equation (5.11)

$$\frac{\partial \omega}{\partial y} = -\frac{c}{R_o H_o y \sqrt{f(y)}} \qquad (5.17)$$

and using this in (5.16)

$$\frac{d\eta}{dz} = - y^2 R_o \left[- \frac{dT_k(\omega)}{dw} \frac{c}{R_o H_o \sqrt{f(y)}} + T_k(\omega) \right] \tag{5.18}$$

Also from equation (3.11) it is clear that

$$\frac{dT_k(\omega)}{dw} = \sqrt{1 - kT^2} \tag{5.19}$$

and substituting this in (5.18)

$$\frac{d\eta}{dz} = \frac{y^2}{\sqrt{f(y)}} \left[\frac{c}{H_o} \sqrt{1 - kT_k^2(\omega)} - R_o \sqrt{f(y)} T_k(\omega) \right]$$

Hence the apparent angular diameter of a source attains a minimum value when

$$\frac{d\eta}{dz} = 0$$

That is, when

$$\frac{R_o^2 H_o^2}{c^2} f(y) T_k^2(\omega) + kT_k^2(\omega) - 1 = 0 \tag{5.20}$$

The last equation has been solved by numerical methods and the results are shown in figure 5.3 where the redshift z_m at which η attains its maximum value is plotted against σ_o for various q_o. The effect is one which is evidently manifest at fairly low values of z

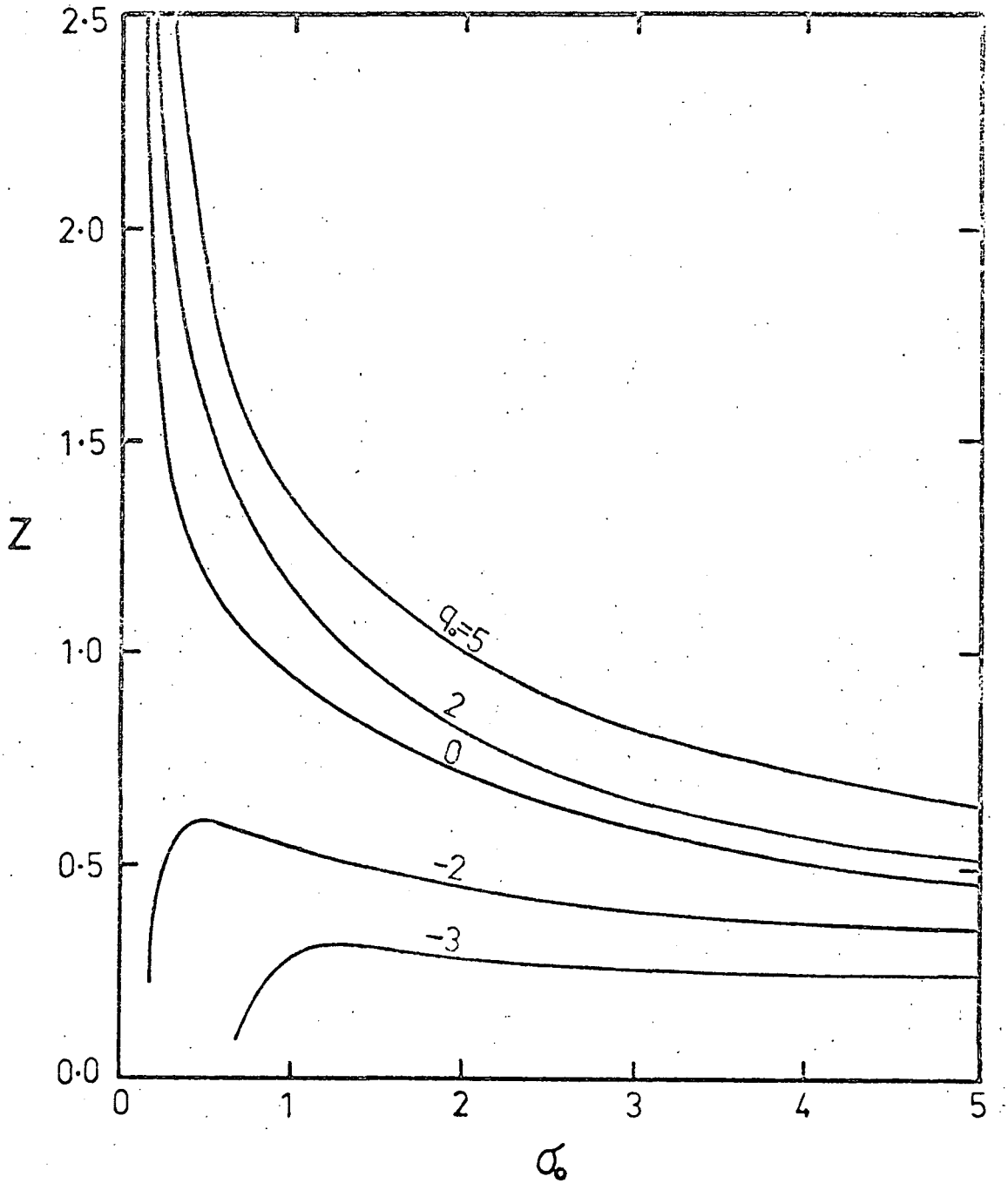

Figure 5.3 - The values of redshift at which the apparent angular diameter attains a minimum value as a function of σ_o for values of q_o.

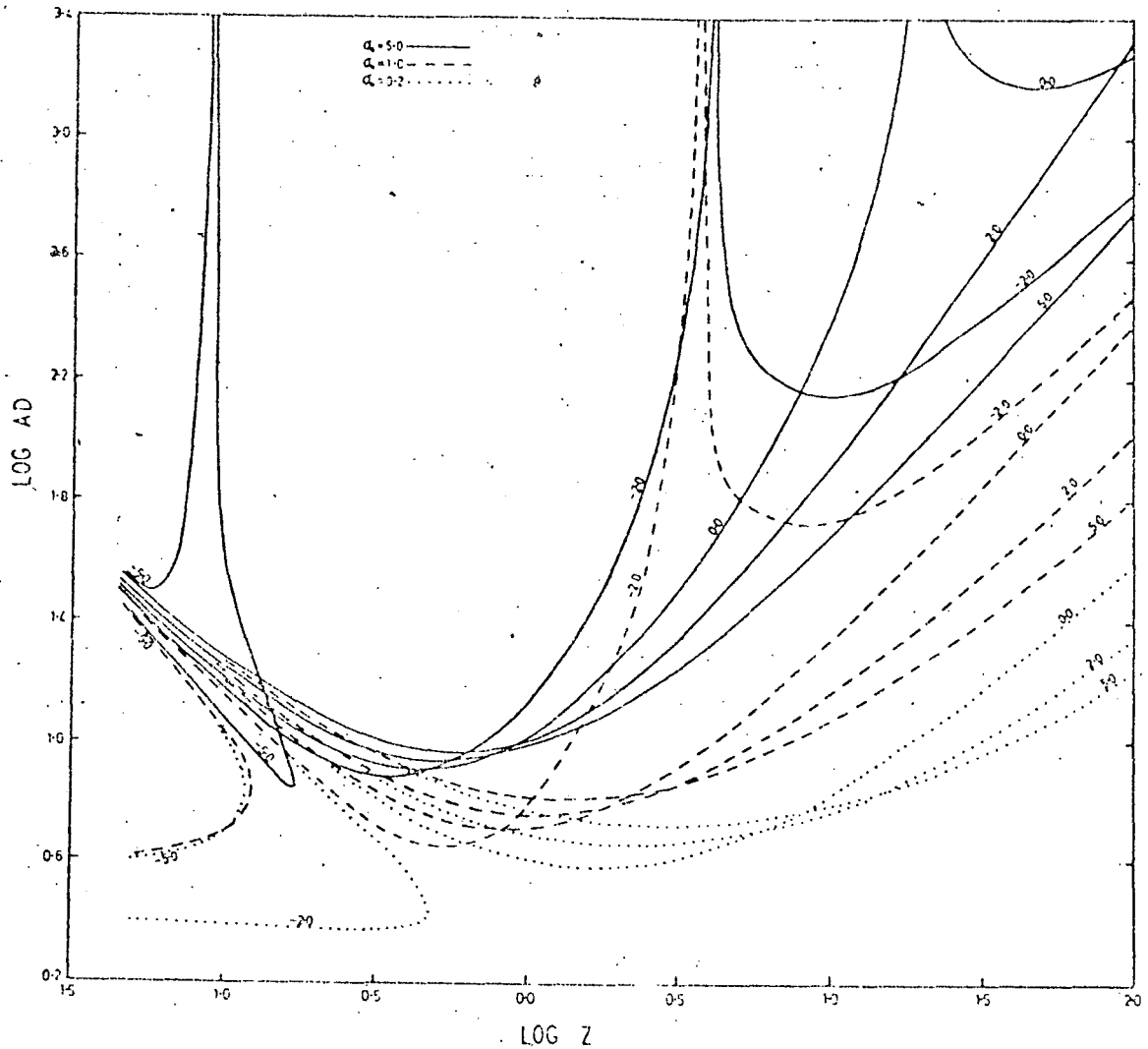

Figure 5.4 - The variation of apparent angular diameter (in seconds of arc) with redshift if the linear dimension of the source is 20 kpc.

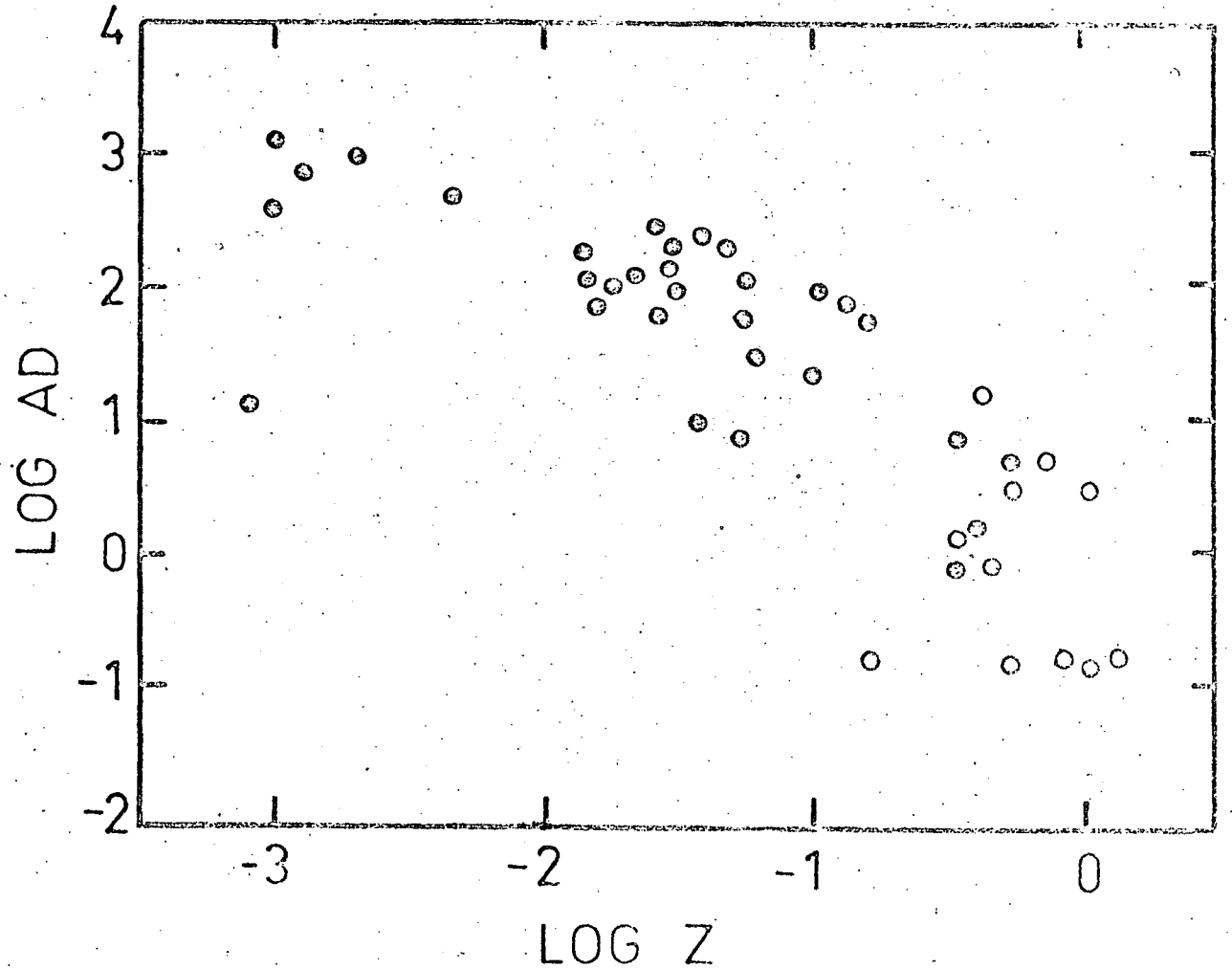

Figure 5.5 - The observed distribution of apparent angular diameters for ordinary radio galaxies and quasars (open circles).

and could therefore provide a valuable test for a cosmological model.

The actual variation of apparent angular diameter with redshift requires a knowledge of the source average linear diameter and unfortunately this is quite uncertain. The dimension ℓ in equation (5.15) has been assigned the value of 20 Kpc. which seems reasonable if ordinary galaxies are considered. Numerical computations for equation (5.15) have yielded the results illustrated in figure 5.4. The apparent angular diameter is well behaved for type E1 and type 0 models with curvature $k = 0$ or -1. If $k = +1$ then θ_p goes to infinity at the redshift corresponding to the antipole of the co-ordinate system. The variation of apparent angular diameter is even more complicated for type E2 models when z has a maximum value.

As mentioned earlier very little data is available on angular diameters of identified sources. However, Heeschen (1966) has published a list of about 50 sources with measured angular diameters. These angular diameters (in seconds of arc) have been plotted against redshift in figure 5.5. Although the number of sources is relatively small the distribution in figure 5.5 infers that there is no minimum in angular diameter for a redshift less than unity. Quasi-stellar sources are represented in the diagram by open circles. These objects appear to provide a natural extension of the angular diameter distribution at higher redshifts. When the observations represented in figure 5.5 are related to the theoretical results in figure 5.3 then

it can be asserted that the required cosmological model must have $q_o > -1$ for $\sigma_o > 0.3$ or $q_o > 1$ for $\sigma_o > 1$. The restrictions on q_o become quite stringent as σ_o increases. Thus at $\sigma_o = 2$ we must have $q_o > 4$.

The predictions of the steady-state model should be included in this analysis. The geometry in the steady-state model is the same as the de Sitter model in which $\sigma_o = 0$ and $q_o = -1$. The radiation-matter density is a constant (independent of epoch) non-zero quantity. Using these values for σ_o and q_o, equation (5.15) yields

$$\theta_p = \frac{\ell H_o}{c(1 - y)} \tag{5.21}$$

This equation clearly has no stationary value and consequently there will be no minimum in the angular diameter distribution. The observations are therefore consistent with a steady-state universe or an evolutionary universe in which the deceleration parameter will be positive for a reasonable value of the density parameter.

Before more precise conclusions can be drawn from the angular diameter distribution it is necessary to devise some method for the extension of measurements to greater redshifts. Williams (1963) and Slish (1963) have suggested that θ_p may be calculated from the frequency, ν_m, at which the radio source intensity spectrum has a maximum value. This method assumes that the low frequency turnover

in source spectra is due to synchrotron self-absorption. The spectra of radio sources will be described more fully in section 5.5.

The equations provided by Le Roux (1962) yield

$$P = \ell^2 \frac{\bar{\varepsilon}}{\psi} (1 - \ell^{-\psi\ell}) \tag{5.22}$$

for the synchrotron power output at frequency ν for an object of linear dimension ℓ. The emission per unit volume for electrons having an energy distribution spectrum $N(E) = KE^{-\gamma}$ is

$$\bar{\varepsilon} = \frac{\mu\alpha\ell^2 c}{2} \nu_o^{(\gamma+1)/2} \xi(\gamma) \nu^{(1-\gamma)/2} \frac{\bar{\gamma}}{2} [1 + 1/\tau(\gamma)] \tag{5.23}$$

and the optical thickness is

$$\psi\ell = \frac{\mu\alpha\ell^2 c}{16\pi m_o} \nu_o^{(\gamma+2)/2} (\gamma + 2)\ \xi(\gamma + 1)\ \frac{\bar{\chi}}{2} [1 + 1/\tau(\gamma + 1)] \tag{5.24}$$

where $\nu_o = \ell B/2\pi m_o$, $\tau(\gamma) = (3\gamma + 5)/2$ and

$$\bar{\chi} = \frac{1}{2} \int_0^{\pi} \sin\theta^{(\gamma+4)/2} d\theta, \quad \bar{\gamma} = \frac{1}{2} \int_0^{\pi} \sin\theta^{(\gamma+3)/2} d\theta$$

If the source becomes optically thick at a frequency $\nu = \nu_m$, then according to equation (5.22)

$$P(\nu_m) = \ell^2 \frac{\bar{\varepsilon}}{\psi} \tag{5.25}$$

Also, for a typical value of $\gamma = 3$, $\bar{X} = 0.62$ and $\bar{Y} = 2/3$ with the values of $\bar{X}$ and $\bar{Y}$ being fairly insensitive to changes in γ. Hence the last equation becomes, with aid of (5.23) and (5.24)

$$P(\nu_m) = \frac{\ell^2 8\pi m_o \nu_o^{-1/2} \nu_m^{5/2}}{\gamma + 2} \tag{5.26}$$

Now using the redshift relations, the flux density measured at a frequency $\nu_{mo} = \nu_m y$ by the origin observer will be

$$S(\nu_{mo})d\nu_{mo} = \frac{\ell^2 8\pi m_o \nu_o^{-1/2} \nu_m^{5/2} d\nu_m}{(\gamma + 2)4\pi D^2}$$

where D is the luminosity distance defined in equation (5.10). Employing equation (5.15), the last equation yields for the maximum flux density

$$S(\nu_{mo}) = \theta_p^2 \frac{2m_o}{\gamma+2} \nu_o^{-1/2} \nu_{mo}^{5/2} y^{1/2}$$

and re-arranging this equation the apparent angular diameter is

$$\theta_p^2 = (2m_o)^{-1}(2\alpha + 3)\nu_o^{1/2} S(\nu_{mo}) \nu_{mo}^{-5/2} y^{-1/2} \tag{5.27}$$

where $\alpha = (\gamma - 1)/2$ is the source spectral index (measured at frequencies greater than ν_{mo}). This equation differs by a factor of

two from that given by Williams. Also, both Slish and Williams suggest the high frequency spectrum be extrapolated to $\nu = \nu_{mo}$ and so, knowing α, determine $S(\nu_{mo})$. However, this procedure is open to the objection that for steep spectra the error introduced could be of the order of 100 per cent. Also, the source does not become optically thick at the frequency corresponding to maximum flux density. When the source is optically thick to synchrotron radiation the spectrum is of the form $S \propto \nu^{5/2}$. Hence the only accurate method of determining the apparent angular diameter is to measure the flux density at a frequency low enough to ensure a 2.5 power law spectrum.

According to equation (5.27), θ_p is a very weak function of redshift since $\theta p \propto (1 + z)^{1/4}$. It may therefore be possible with this method and sufficient accumulation of data to ascertain the value of z at which θ_p is a minimum providing of course that such a minimum does exist. Data of this type would provide valuable information for a cosmological model.

The main problem is the paucity of data on source spectra below 100 MHz. There are also other phenomena which may lead to a cut-off in source spectra at low frequencies. These include

(i) free-free absorption in ionized hydrogen either in the source itself or in the intervening medium. The relevant formulae are well known and in both cases the optical depth is greater than unity

below a frequency ν_m given by (e.g. Ginzburg and Syrovatskii, 1964)

$$\nu_m^2 = 0.16 \int \frac{n_e^2 d\ell}{T^{3/2}} \quad (c/s)^2 \qquad (5.28)$$

where n_e is the electron density, ℓ the thickness of the absorbing medium, T is the kinetic temperature of the gas and all quantities are measured in c.g.s. units. If emission regions are uniformly mixed with absorption regions the low frequency spectrum is $S\alpha\nu^{2-\alpha}$.

(ii) a cut-off at the low-energy end of the electron energy distribution responsible for the synchrotron radiation. The low energy cut-off is due to ionization and collision effects. In this case the low frequency spectrum is approximately $S\alpha\nu^{-1/4}$ so that although the effect can produce a change, it can hardly result in a maximum for the source spectrum.

(iii) the effect of a dispersive medium. The radio emission from ultra-relativistic electrons in dispersive media has been discussed by Razin (1960). If the medium refractive index is less than unity, then the power radiation spectrum from a single electron has two cut-off frequencies, one in accordance with ordinary synchrotron theory and another at a lower frequency

$$\nu_m = \frac{15 n_o}{H} \text{ MHz} \qquad (5.29)$$

where H is the magnetic field strength in units of 10^{-6} gauss. The low frequency spectrum in this case is quite a complicated function of frequency and energy.

Substitution of typical values for the quantities involved in the first two cut-off mechanisms indicates that the frequency at which the flux density is near its maximum value must be less than about 20 MHz. However the Rozin effect could produce a cut-off at frequencies greater than 100 MHz and so throw doubt on the validity of the interpretation of a high frequency turnover in the source spectrum as due to synchrotron self-absorption only. A large number of spectral observations would be necessary to determine the mechanism responsible for the spectrum cut-off. However, if a number of sources are found to have turnovers in their spectra due to synchrotron self-absorption then this data, combined with the direct measurements of angular diameter, could provide enough evidence for a definite conclusion on possible cosmological models.

5.5 Radio Source Spectra

The special physical conditions which pertain to radio galaxies have been the subject of extensive investigations. Radio sources are characterised by a non-thermal spectrum with intensity proportional

to $\nu^{-\alpha}$ where α is the spectral index. Any theory of radio sources must explain this basic power law and it is generally accepted that the radio emission is produced by "clouds" of relativistic electrons spiralling in magnetic fields.

One of the fundamental problems of radio galaxies is the mechanism of release of their vase energy. If the source of their radio emission is assumed to be the synchrotron process then the minimum total energy released by a radio galaxy is calculated to be of the 10^{60} ergs (e.g. Burbidge et al., 1963). A variety of processes have been suggested to explain energy releases of such magnitude. It now appears likely that in all cases the end result is an explosion ocurring in the nucleus of a galaxy. This produces an outward expansion of gas and magnetic fields along the axes of rotation. This situation is clearly evident in such objects as Centaurus A and 3C273. It is also illustrated (Lynds and Sandage, 1963) in the case of the irregular galaxy M82 which has a system of filaments directed in a cone about the minor axis. This effect is also seen in some Seyfert galaxies and finally there is also evidence for these types of explosions in our own Galaxy (Oort, 1964).

The energy source for strong radio sources and quasi-stellar sources is apparently gravitational in nature (e.g. Hoyle and Fowler, 1963; Hoyle et al., 1964; Piddington, 1966). A critical problem arises as to the process that gets gravitational energy out of an object.

Fragmentation, followed by multiple collisions between fragments might be invoked at small dimensions of the radio galaxy. However, the release of energy in many comparatively small-scale events does not fit the observational evidence well, since a typical radio source seems to be associated with the violent emission of one or more well directed jets.

Hoyle considers that angular-momentum transfer to an outer region may allow an inner region of an imploding object to condense to a radius close to the Schwarzschild limit. Unless the inner mass is spherically symmetric, radiation of gravitational waves occurs. This event may induce ordinary fissional instability as shown by Lyttleton (1953). The system breaks into two unequal pieces that recede from each other at a speed comparable to the original orbital speed.

Piddington considers the conversion of rotational kinetic energy into magnetic energy. The balance between gravitational and centrifugal forces is destroyed and contraction is found to continue to nuclear dimensions. A spherical stage is reached when explosions occur along the rotational axis and electrons up to cosmic ray energies are released. Piddington concludes that "ordinary" radio galaxies are formed if stars contract out of the plasma cloud while quasi-stellar sources result when star formation is inhibited with the whole galaxy shrinking to a nucleus. It is interesting to note that on the basis of these theories the difference between "ordinary" radio sources and

quasi-stellar sources is mainly in scale.

The average life-time of the radio emission stage may be estimated from total energy considerations and by the size and velocity of the expanding radio region. Maltby et al. (1963) have calculated an upper limit of 10^9 years as the lift-time for radio sources whereas Aizu et al. (1964) consider that the typical source life-time is in the range 10^6 to 10^7 years. It is also probable that an explosion of a galaxy is not limited once during the life-time, but may recur. Burbidge et al. have concluded that this indeed is the case for all galaxies. They suggest a radio source life-time of about 10^6 years or less. Explosions in each galaxy produce a radio source 1-10 times within the characteristic life-time of the universe (10^{10} years). In strong radio sources the process is considered to occur some 20-200 times.

The electron energy distribution in discrete radio sources is assumed to be of the form

$$N(E)dE = K\left(\frac{E}{E_o}\right)^{-\gamma} d\left(\frac{E}{E_o}\right) \qquad \text{for } E_1 \leq E \leq E_2 \qquad (5.30)$$

Such a distribution can be produced by the statistical Fermi-acceleration process and is observed directly in extra-terrestial cosmic ray particles. The power radiated per unit frequency interval at a frequency ν by a single electron moving in a uniform magnetic field can be written (e.g. Oort and Walraven, 1956; Kellermann, 1964) as

$$P(\nu, E, \theta) = CH_{\perp}\nu/\nu_c \int_{\nu/\nu_c}^{\infty} K_{5/3}(\eta)d\eta \qquad (5.31)$$

where $H_{\perp} = H \sin\theta$, $C = 2.34_{10}^{-22}$ c.g.s. units, $K_{5/3}$ is a modified Bessel function of the second kind and

$$\nu_c = L\, H_{\perp} E^2 = 1.61_{10}^{3} H_{\perp} E_{GeV}^2 \quad (c/s) \qquad (5.32)$$

The total power radiated by each electron is (e.g. Kellermann, 1964)

$$\frac{dE}{dt} = 3.8_{10}^{-6} H_{\perp}^2 E^2 \quad GeV/sec \qquad (5.33)$$

The total power emitted by an assembly of electrons of the form (5.30) having the same pitch angles will be

$$P(\nu, \theta) = \frac{1}{2} CKL^{(\gamma-1)/2} H_{\perp}^{(\gamma+1)/2} \nu^{(1-\gamma)/2} \int_{\nu/\nu_1}^{\nu/\nu_2} (\nu/\nu_c)^{(\gamma-1)/2} \times \int_{\nu/\nu_c}^{\infty} K_{5/3}(\eta)d\eta d(\nu/\nu_c) \qquad (5.34)$$

For most values of γ, the major contribution to this integral occurs when $\nu/\nu_c \simeq 1$. Thus, when $\nu/\nu_1 \gg 1$ and $\nu/\nu_2 \ll 1$ the integral is essentially constant and the limits of integration can be extended from zero to infinity. The result is

$$P(\nu) \propto \nu^{-\alpha} \qquad (5.35)$$

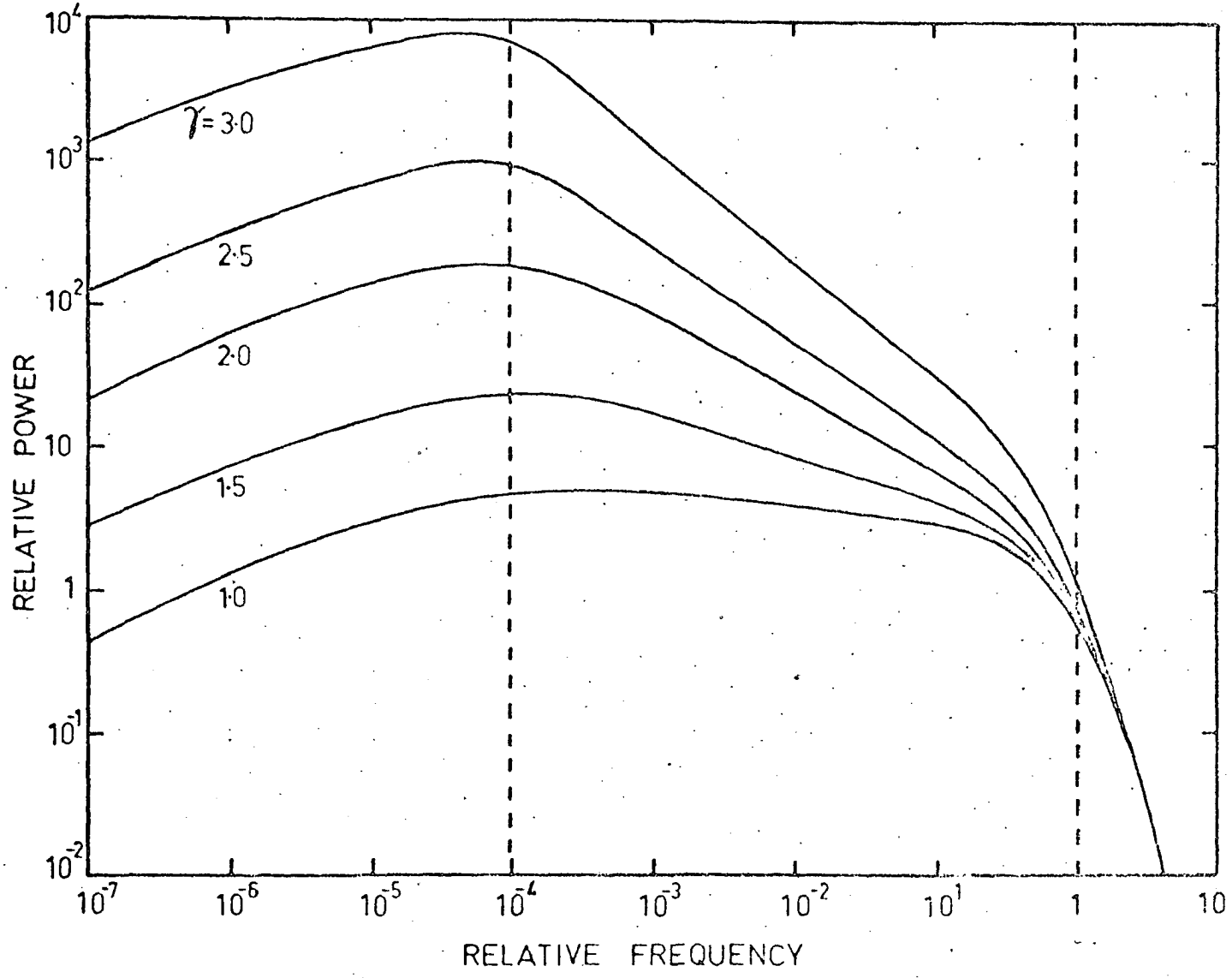

Figure 5.6 - Theoretical radiation spectra for an electron distribution of the form $N(E) = KE^{-\gamma}$ for various values of γ (Kellermann, 1964). The dotted lines represent the critical frequencies corresponding to the upper and lower cut-off

where $\alpha = (\gamma-1)/2$ is called the spectral index. The radiation spectra for an electron distribution of the form (5.30) are shown in figure 5.6.

Now reference to equations (5.34) and (5.35) show that the flux density measured at the origin will obviously be of the form

$$S = C\,\nu^{-\alpha} \tag{5.36}$$

where C is a slowly varying function of α. Alternatively we have

$$\log S = A - \alpha \log \nu \tag{5.37}$$

where A is a constant. When the logarithm of the flux density is plotted against the logarithm of the frequency it is found that the spectra of most radio sources do, in fact, conform to the simple law (5.37). It is of some interest to examine the "spread" in the index α for effect which may have a cosmological significance.

Several authors have studied the distribution of spectral indices with somewhat varying results. Whitfield (1958), in a study of 85 radio sources, concluded that the mean spectral index of identified extragalactic sources is about 0.9 while that of unidentified sources that are further than 10° from the galactic plane is about 1.2. Whitfield also points out that there appears to be a gradual

diminution of the mean spectral index from about 0.8 for the strongest sources to 1.3 for the weakest sources. A similar trend was found by Kellermann and Harris (1960) for a total of 739 sources listed both in the two catalogues of Mills, Slee and Hill (1958, 1960) and in the California Institute of Technology 960 MHz data. Taking the spectral index of Hydra A to be 0.96 they found a mean spectral index of 0.89 with 50 per cent of the sources lying within 0.2 of the median value.

Using data obtained from a series of surveys at different frequencies Conway et al. (1963) reported a medium value of 0.71 for α with 50 per cent of the sources having spectral indices between 0.61 and 0.81.

In an investigation based on data of greater accuracy Kellermann (1964) refuted the conclusions of Whitfield and his own earlier results when he found the spectral index to be independent of the flux density for sources having $S > 14$ f.u. at 178 MHz. Kellermann derived a distribution of spectral indices which was approximately Gaussian with a median value of 0.76 and a standard deviation of 0.14.

Most of these analyses for the spectral index distribution have relied upon data obtained from surveys made with different instruments and different observational techniques. The series of surveys made with the Parkes radio telescope have the important advantage that the same instrument has been used to observe sources at three frequencies.

A finding survey was carried out at 408 MHz and flux densities were measured at 408, 1410 and 2650 MHz. Here, for the purposes of deriving an average spectral index the surveys of Mills et al. (1958, 1960, 1961) at 85.5 MHz have been used in conjunction with the Parkes results. All sources having a flux density greater than 4 f.u. at 408 MHz were considered and any source fulfilling this requirement and also having a measured flux for at least three frequencies was included in the analysis. This method provides a complete sample of sources and gives an average value for α over a wide frequency range. Errors in the flux density measurements were due to variation in calibration signal, unknown polarization, noise fluctuations and confusion effects. The total r.m.s. error was (Day et al., 1966): 5% ± 0.86 f.u. at 408, 5% ± 0.14 f.u. at 1410, 6% ± 0.06 f.u. at 2650 and 10% ± 2.5 f.u. at 85.5 MHz. Each flux was weighted according to the inverse square of its r.m.s. error. A total of 980 sources were analysed using an Elliott 503 computer and the final result was the value of

$$\alpha = 0.84 \tag{5.38}$$

for the mean spectral index. The variance of this result was 0.063.

Now radio sources in an evolutionary universe must undergo aging processes which could produce changes in spectral index. For example, high energy electrons responsible for the radio emission should lose energy by the synchrotron mechanism. This would lead to

a steepening of a source spectrum as the epoch advances. On the basis of this type of argument several authors (Ko, 1966; Long et al., 1966) have suggested that a dependence of the mean spectral index on flux density would provide useful information concerning the way in which the intrinsic nature of a radio source varies with epoch. It has been inferred that if there is any correlation between spectral index and flux density, then it will strongly support the case for an evolutionary universe. The average spectral index is expected to be independent of flux density in a steady-state universe.

Many processes can produce a time varying spectrum and these have been discussed by Kellermann (1964, 1966) and Kardashev (1962). It is thought that electron losses in radio galaxies are due mainly to synchrotron radiation. If this is the case, then the electron energy distribution and consequently the radio spectrum will be non-stationary. Integrating equation (5.33) we find that the time taken for an electron with initial energy E_o to decay to half its original value is

$$t_{1/2} = \frac{8.85}{H_\perp^2 E_o} \times 10^{-3} \text{ years} \qquad (5.39)$$

where as before E_o is measured in GeV. These energy losses are responsible for a "break" in the radiation spectrum at a frequency ν_c given by

$$\nu_c = \frac{10^3}{H_\perp^3 t^2 \text{ years}} \text{ MHz} \qquad (5.40)$$

At frequencies greater than ν_c the spectral index changes to a value of $\alpha + 0.5$. Electron losses by the inverse Compton effect, like the synchrotron losses, are proportional to E^2 and will therefore influence the radiation spectrum in the same way. These processes can only lead to a steepening in the source spectrum and, after sufficient time has elapsed, the critical frequency, ν_c, will fall below the observable frequency range and the spectral index will have a constant value equal to $\alpha + 0.5$.

The stronger radio sources are expected to have relatively intense magnetic fields and an electron population will lose energy primarily by synchrotron radiation whereas, in the weaker sources the electrons will probably lose energy by some other process. These general arguments are supported by figure 5.7 in which the spectral indices of identified sources are plotted as a function of their total radiated power. The data for figure 5.7 have been derived from flux densities and spectral indices of optically identified sources listed in the 3C and Parkes catalogues. Now according to equation (5.12) the flux density is related to the emitted power by

$$S(\nu)d\nu = \frac{P(\nu_e)d\nu_e}{4\pi D^2} \qquad (5.41)$$

where D is the luminosity distance. Integrating between a lower cut-

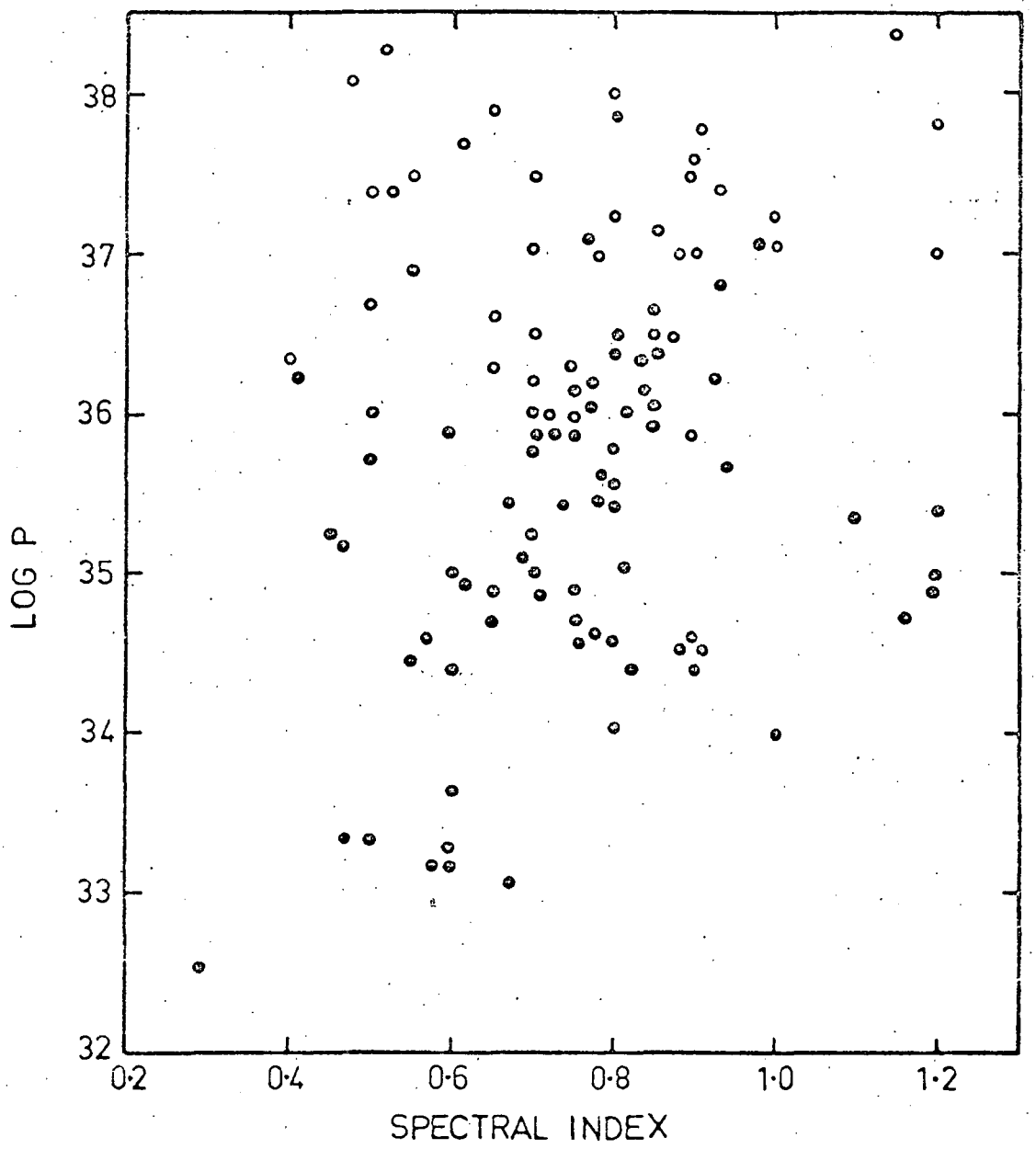

Figure 5.7 - Spectral indices of identified sources as a function of their total radiated power P(watts $(c/s)^{-1}$). The dots refer to "ordinary" radio galaxies and the circles to quasars.

off frequency ν_1 and upper cut-off frequency ν_2 of the emission spectrum and employing equation (5.36) we have

$$4\pi D^2 \int_{\nu_1'}^{\nu_2'} c\nu^{-\alpha} d\nu = \int_{\nu_1}^{\nu_2} P(\nu_e) d\nu_e \tag{5.42}$$

where $\nu_1 = (1 + z)\nu_1'$, $\nu_2 = (1 + z)\nu_2'$. It follows that the total emitted power is

$$P_e = 4\pi D^2 (1 + z)^{\alpha - 1} S_t \tag{5.43}$$

where
$$S_t = \int_{\nu_1'}^{\nu_2'} c\nu^{-\alpha} d\nu = \frac{c}{1 - \alpha} [\nu_2^{1-\alpha} - \nu_1^{1-\alpha}] \tag{5.44}$$

In this analysis the critical emission frequencies were chosen to be $\nu_1 = 10^7$ c/s and $\nu_2 = 10^{10}$ c/s. Also, a Taylor expansion for the luminosity distance defined in (5.10) yields

$$D = \frac{c}{H_o} z(1 + \tfrac{1}{2} z) \tag{5.45}$$

for $q_o = 0$ and values of redshift $z << 1$. This formula for distance will of course be inaccurate at large redshifts but it serves to give an approximation to the problem. Using equations (5.43)-(5.45) the radio luminosities of 3C and Parkes sources were calculated and the results are listed in Table 7. Matthews et al. (1964) have also calculated some source luminosities but they did not include in their equations the bracketed term of equation (5.43). This would lead to

an error in their quoted luminosities depending on the spectral index. However, the uncertainty in the cut-off frequencies ν_1 and ν_2 would probably mask any errors due to redshift effects.

Inspection of figure 5.7 indicates that there is only a very weak correlation between power radiated and spectral index. In fact the correlation coefficient is only 0.017 with a standard error of 0.03 implying that the two quantities are practically independent. These results are different to those of Kellermann (1964) who finds a (fairly weak) relation in the sense that weaker sources have flat spectra.

Any analysis of spectral index and flux density will contain an obvious selection effect. This is the progressive increase in the percentage of detectable sources of large absolute power with decreasing flux density. Now, from equation (5.10) and (5.43) the total emitted power for sources in a steady-state universe will be

$$P_m = \frac{4\pi c^2}{H_o^2} z^2 (1 + z)^{1+\alpha} S_t \qquad (5.46)$$

while for evolutionary universes

$$P_m = 4\pi R_o^2 T_k^2(\omega) (1 + z)^{1+\alpha} S_t \qquad (5.47)$$

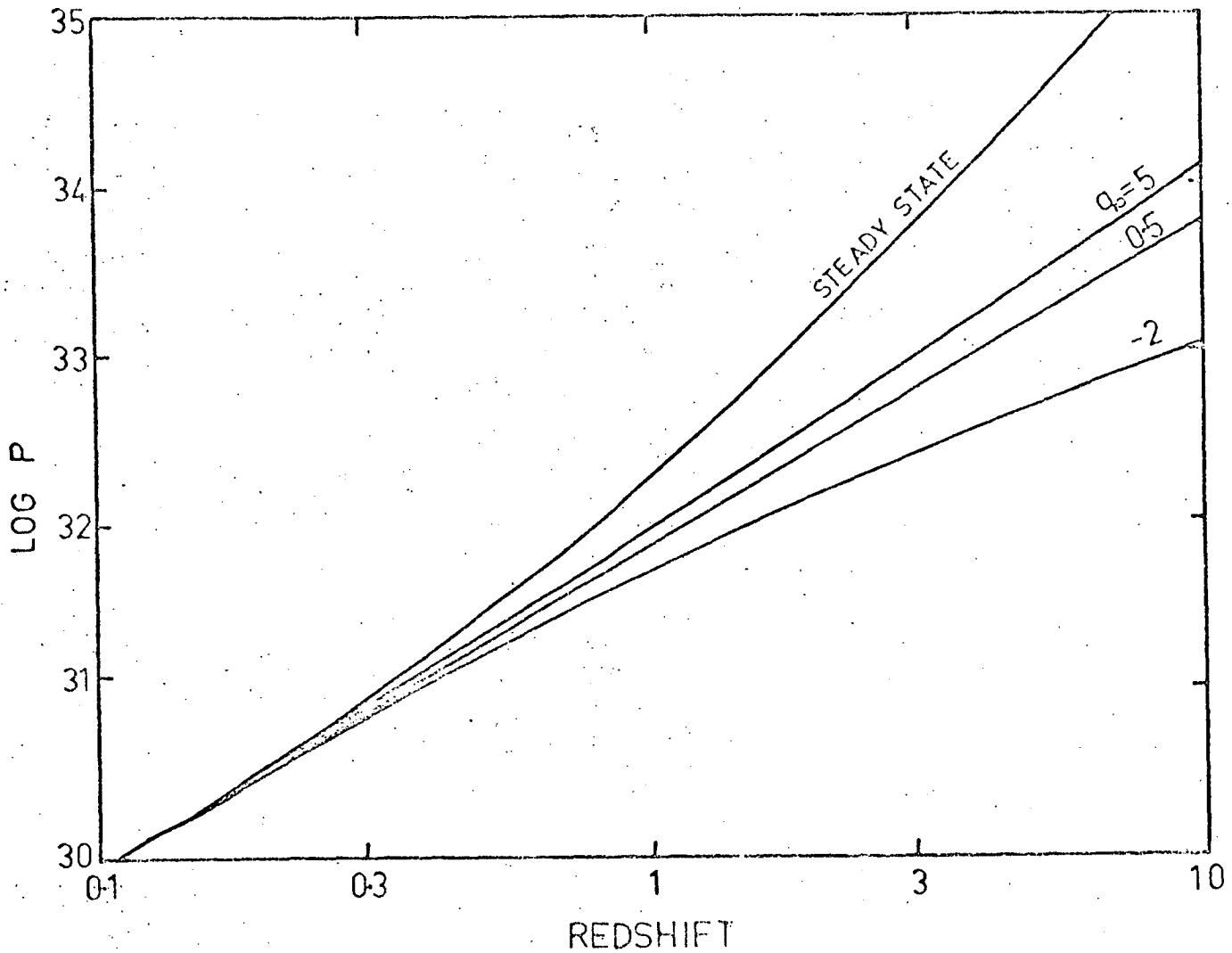

Figure 5.8 - The average minimum luminosity of detectable sources as a function of redshift. The evolutionary models have $\sigma_o = 0.5$ and a series of values for q_o.

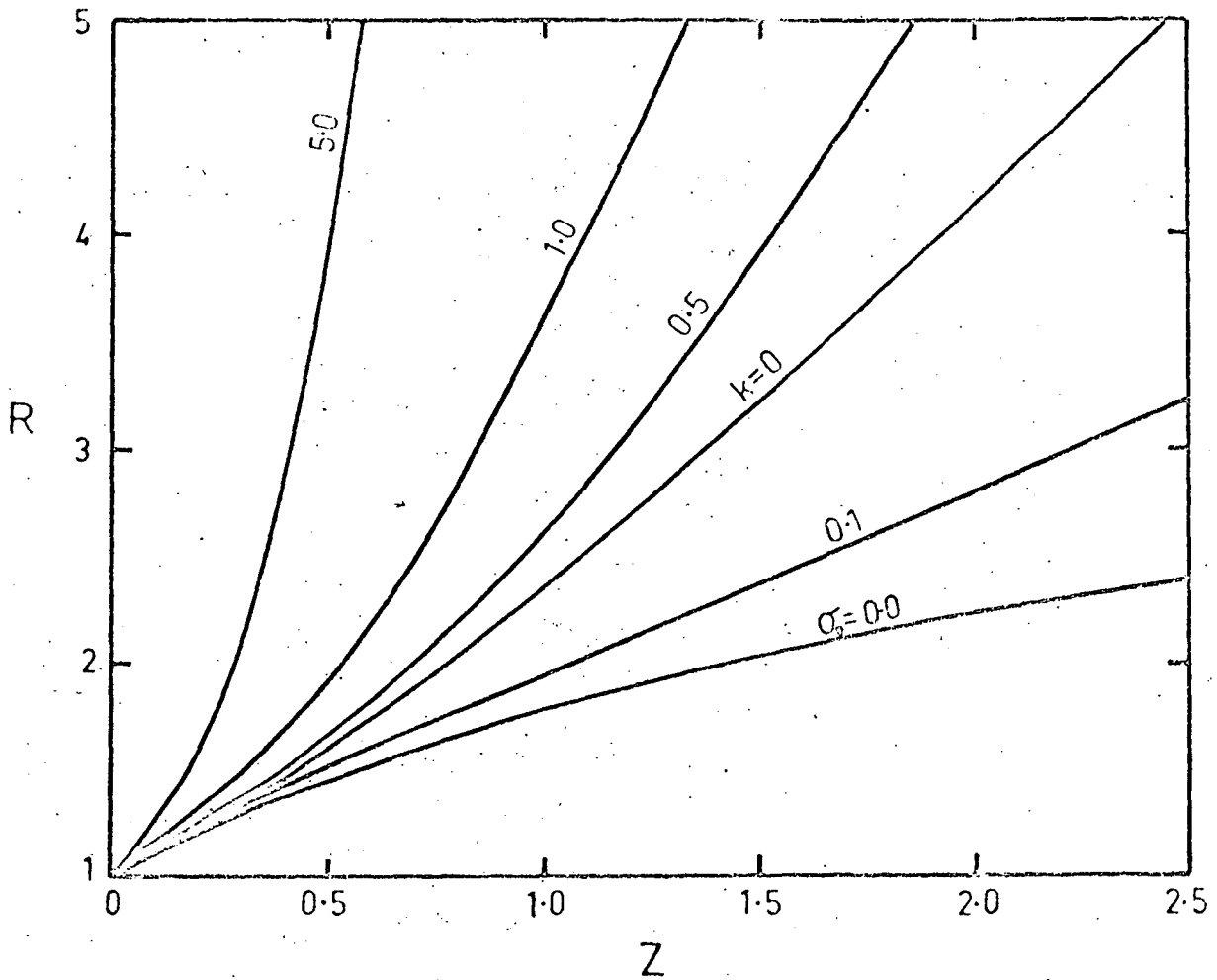

Figure 5.9 - the ratio of the average minimum of source luminosity detectable in a steady-state model to that detectable in evolutionary cosmologies. The models have $q_o = 0$ and a series of values for σ_o.

The average spectral index for Parkes radio sources has been calculated to be $\alpha = 0.84$, and assuming the sensitivity of the telescope to be 3 f.u. at 408 MHz, equations (5.46) and (5.47) may be used to plot the average minimum luminosity of detectable sources as a function of redshift. This has been done in figure 5.8 for the steady-state universe and evolutionary universes with defining parameter $\sigma_o = 0.5$ and a series of values for q_o. The average minimum luminosity, P_m, increases rapidly in the steady-state model for redshifts greater than one while P_m also increases but at a slower rate for open and flat evolutionary universes. In closed world-models P_m attains a maximum value. The ratio of the average minimum of source luminosity detectable in a steady-state model to that detectable in evolutionary cosmologies is derived directly from equations (5.46) and (5.47). The result is

$$R = (P_m)_S/(P_m)_E = z^2 \frac{c^2}{T_k^2(\omega) R_o^2 H_o^2}$$

and using equation (3.21) this becomes

$$R = z\,/T_k^2(\omega) \qquad (5.48)$$

$$= |q_o + 1 - 3(1 + \varepsilon_o)\sigma_o| z^2/T_k^2(\omega) \qquad k \neq 0$$

Plots of R versus z are presented in figure 5.9 for $q_o = 0$, $T_o = 3°K$ and a series of values for σ_o. The properties of this ratio are evident from the diagram and do not require further comment.

We now examine in some detail the effect of decreasing the flux density $S(\nu)$ on the number of observable sources which have a luminosity $P(\nu)$. Suppose initially, that in evolutionary universes radio sources do not have luminosities that are functions of epoch and further there is no spatial evolution in source density, i.e. the number of sources per unit co-ordinate volume remains constant. Then the luminosity distribution at an epoch corresponding to an expansion parameter y will be

$$\rho(P) = y^{-3}\rho_o(P) \tag{5.49}$$

where ρ_o is the number of sources with power P in unit proper volume at the present epoch. Employing equation (5.4), the total number of sources with power P in proper volume dV will therefore be

$$dN(P) = \rho(P)dV$$

$$= \rho_o(P_o)(P_o/P)^{3/2}e^{-x^2/2\sigma^2}y^{-3}dV \tag{5.50}$$

Now it is obvious from the metric (3.4) that the volume element is

$$dV = R^3(t)\,\frac{r^2\,\sin\Theta d\Theta d\phi dr}{(1 + kr^2/4)^3}$$

Integrating over 4π steradians and using equations (3.8) and (3.9) we have

$$dV = 4\pi R_o^3 y^3 T_k^2(\omega)\, d\omega \tag{5.51}$$

and substituting in (5.50), we have for evolutionary universes

$$dN(P) = R_o^3 T_k^2(\omega)\rho_o(P_o)\,(P_o/P)^{3/2} e^{-x^2/2\sigma^2} d\omega \tag{5.52}$$

as the number of sources per steradian in the angular co-ordinate interval $d\omega$.

The flux density as measured by the origin observer is related to the emitted power by

$$S(\nu_r)\, d\nu_r = \frac{P(\nu')\, d\nu'}{D^2}$$

where as before D is the luminosity distance and P has units $\omega\ (c/s)^{-1}\ sr^{-1}$. Substituting $\nu' = \nu_\sim y^{-1}$ and using equation (5.35) we obtain

$$S(\nu_r) = \frac{P(\nu)\,(\nu/\nu_r)^{\alpha} y^{1+\alpha}}{R_o^2 T_k^2(\omega)} \tag{5.53}$$

$$= GPy^{(1+\alpha)} T_k^{-2}(\omega) \tag{5.54}$$

where $G = (\nu/\nu_r)^{\alpha}/R_o^2$ and P is the luminosity at frequency ν. Now differentiating the last equation

$$\frac{dS}{dy} = S\left[-\frac{2T_k'(\omega)}{T_k(\omega)}\ \frac{\partial\omega}{\partial y} + (1+\alpha)/y\right] \qquad (5.55)$$

where $T_k'(\omega) = \dfrac{\partial T_k(\omega)}{\partial\omega}$

Substituting this last equation into (5.52) we have for the number of sources per steradian of luminosity P observed in the flux interval dS at S

$$\frac{dN(P)}{dS} = R_o^3\rho_o(P_o)(P_o/P)^{3/2}e^{-x^2/2\sigma^2}T_k^2(\omega)\ \frac{\partial\omega}{\partial y}\,S^{-1}\left[(1+\alpha)/y - \frac{2T_k'(\omega)}{T_k(\omega)}\ \frac{\partial\omega}{\partial y}\right]^{-1} \qquad (5.56)$$

and as before $\dfrac{\partial\omega}{\partial y} = -\dfrac{c}{R_o H_o y\sqrt{f(y)}}$

The solutions to equation (5.56) are shown in figures 5.10 and 5.11 for $\sigma_o = 0.5$ and a series of values of q_o. The observational frequency was chosen to be $\nu_r = 408$ MHz while the luminosity distribution was identical to that derived in section 5.2. The distribution is defined for a frequency $\nu = 178$ MHz. Curves of log (dN/dS) versus log (P/P_o) are given for three different values of the flux density S. Although the maxima in these curves move to lower luminosity as S decreases the result is still a progressive increase in the percentage of sources of high luminosity. In a particular flux density range, the number of sources is greatest in a closed world model and for a particular σ_o the number decreases with

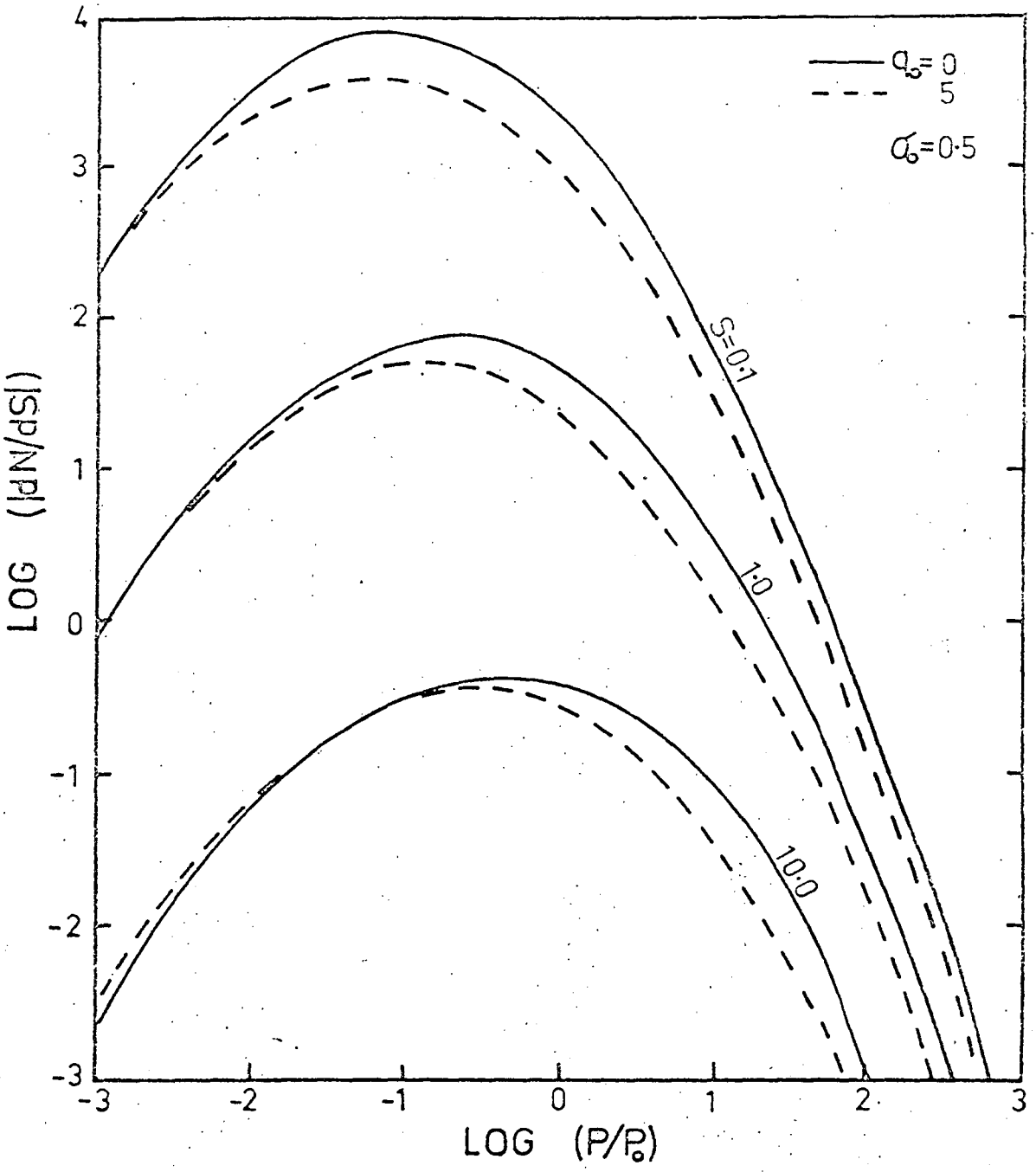

Figure 5.10 - The number of sources with power P_{178} observed in the interval dS at S for two open models with σ_o = 0.5, q_o = 0, 5.

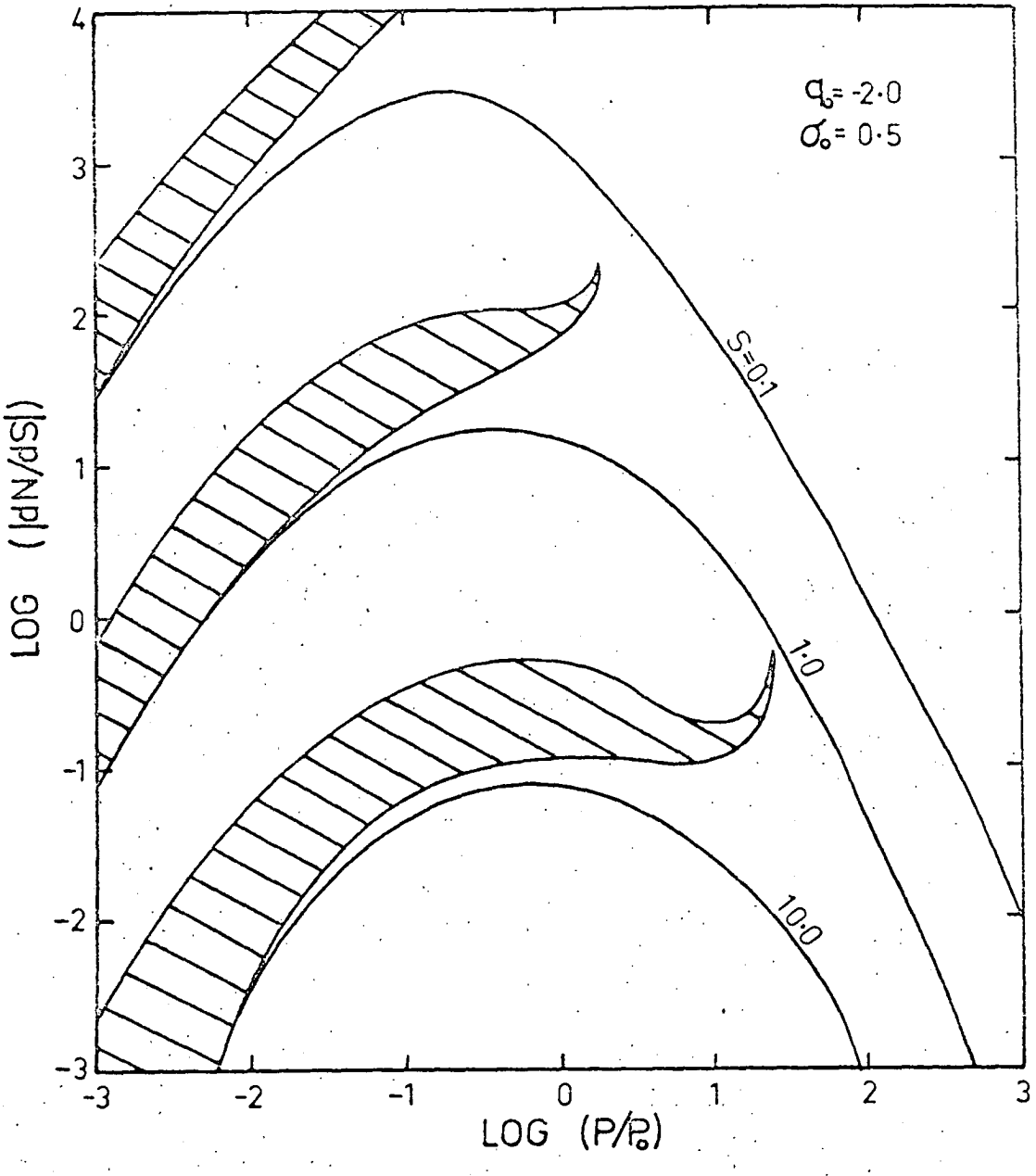

Figure 5.11 - The number of sources with power P_{178} observed in the interval dS at S. The cosmological model is closed with σ_o = 0.5, q_o = -2.0.

increasing q_o.

In the steady-state model the source luminosity distribution must be independent of epoch. Hence the number of sources in an element of proper volume will be

$$dN(P) = \rho_o(P_o)(P_o/P)^{3/2} e^{-x^2/2\sigma^2} dV$$

and using (5.51) with $\sigma_o = 0$, $q_o = -1$ for the steady-state we have

$$dN(P) = -\rho_o(P_o)(P_o/P)^{3/2} e^{-x^2/2\sigma^2} \left(\frac{c}{H_o}\right)^3 (1 - y)^2 y^{-1} dy \tag{5.57}$$

is the number of sources per steradian in interval dy.

Also, for the steady-state universe, the flux density is related to the emitted power by

$$S(\nu_r) = P(\nu)(\nu/\nu_r)^{\alpha} \frac{H_o^2}{c^2} \left(\frac{1}{y} - 1\right)^{-2} y^{(1+\alpha)} \tag{5.58}$$

from which it follows that

$$\frac{dS}{dy} = S\left[\frac{2}{2(1 - y)} + (1 + \alpha)/y\right] \tag{5.59}$$

Hence from the last two equations, we have for the steady-state models

$$\left| \frac{dN(P)}{dS} \right| = \rho_o(P_o)(P_o/P)^{3/2} e^{-x^2/2\sigma^2} \left(\frac{c}{H_o} \right)^3 (1 - y)^3 S^{-1}$$

$$\times [2 + (1 + \alpha)(1 - y)]^{-1} \qquad (5.60)$$

is the number of sources with power P observed in the interval dS at S. The plots of log $|dN/dS|$ against log (P/P_o) lie just below the curves for $q_o = 5$ in figure 5.10.

We return now to the problem of a possible correlation between spectral index and flux density. The source spectra should evolve with epoch due to electron energy losses by synchrotron radiation. This effect is expected to be greatest for the more powerful sources in which the magnetic field strengths should exceed average values. Furthermore, the percentage number of high luminosity sources in any sample increases as observations proceed to lower flux densities. On the basis of this evidence a dependence of average spectral index on flux density would not be unexpected. Ko (1966) has made a limited investigation of the spectral index distribution for sources listed in the Parkes catalogues between declinations -20° to -90° (Bolton et al., 1964; Price and Milne, 1965). He considered three different flux ranges and found the median spectral index to be essentially independent of flux density.

Sources listed in the complete Parkes catalogue (Ekers, 1969) were examined for any evidence indicating a relation between spectral

index and flux density. The catalogue comprises a total of 1780 sources in a declination zone +20° to -90° and the source data are somewhat improved over that presented in the previous catalogues. Six different flux ranges were considered at 408 MHz; $S \geq 10$, $5 \leq S < 10$, $4 \leq S < 5$, $3 \leq S < 4$, $2 \leq S < 3$, $S < 2$. The number of sources and their mean spectral index was calculated for each flux density range. Also as described earlier, the source spectral index may increase (by synchrotron losses) by a value of 0.5 for frequencies greater than the critical frequency ν_r defined in equation (5.40). In order to investigate this effect the change in α over the frequency range 408-2650 MHz was examined for each source. The total number of sources with spectral indices increasing by a value between 0.4 and 0.6 was determined for each flux range. The results are presented in Table 8.

Table 8

Spectral Index Distribution for Radio Sources

Flux Range	No. of Sources	$\bar{\alpha}$	No. with $\alpha \to \alpha+0.5$	Percentage
$10 \leq S$	83	0.84	3	3.5
$5 \leq S < 10$	232	0.78	8	3.4
$4 \leq S < 5$	178	0.83	10	5.6
$3 \leq S < 4$	342	0.89	21	6.2
$2 \leq S < 3$	426	0.84	32	7.5
$S < 2$	363	0.70	7	2.0

A total of 1624 sources were included in the analysis for Table 8 and the sample is obviously large enough for reliable statistical conclusions. There is clearly no correlation between $\bar{\alpha}$ and flux density for $S \geq 2$. The result for $S < 2$ lies well outside a 95% confidence limit and appears significant. However, the low value obtained for $\bar{\alpha}$ in this case is almost certainly due to observational selection effects. The finding survey at 408 MHz was made with an instrument sensitivity of only 4 f.u. in the declination zone -20° to -60° and 2.5 f.u. in the other zones. It may therefore be concluded that there is no correlation between flux density and spectral index. This result is not surprising since we have no indication of a correlation between source luminosity and spectral index.

Furthermore, there is no evidence for a functional dependence of spectral index on redshift for the identified sources for which redshifts have been determined. This is illustrated in figure 5.12 for radio sources listed in Table 7. The spectral index is seen to be independent of redshift for both ordinary radio galaxies and quasars.

The remaining results in Table 8 reveal that the percentage number of curved spectra (of the type $\alpha \rightarrow \alpha + 0.5$) increases with decreasing flux density. This effect may be explained in terms of electron energy losses for radio sources in either a steady-state or an evolutionary universe.

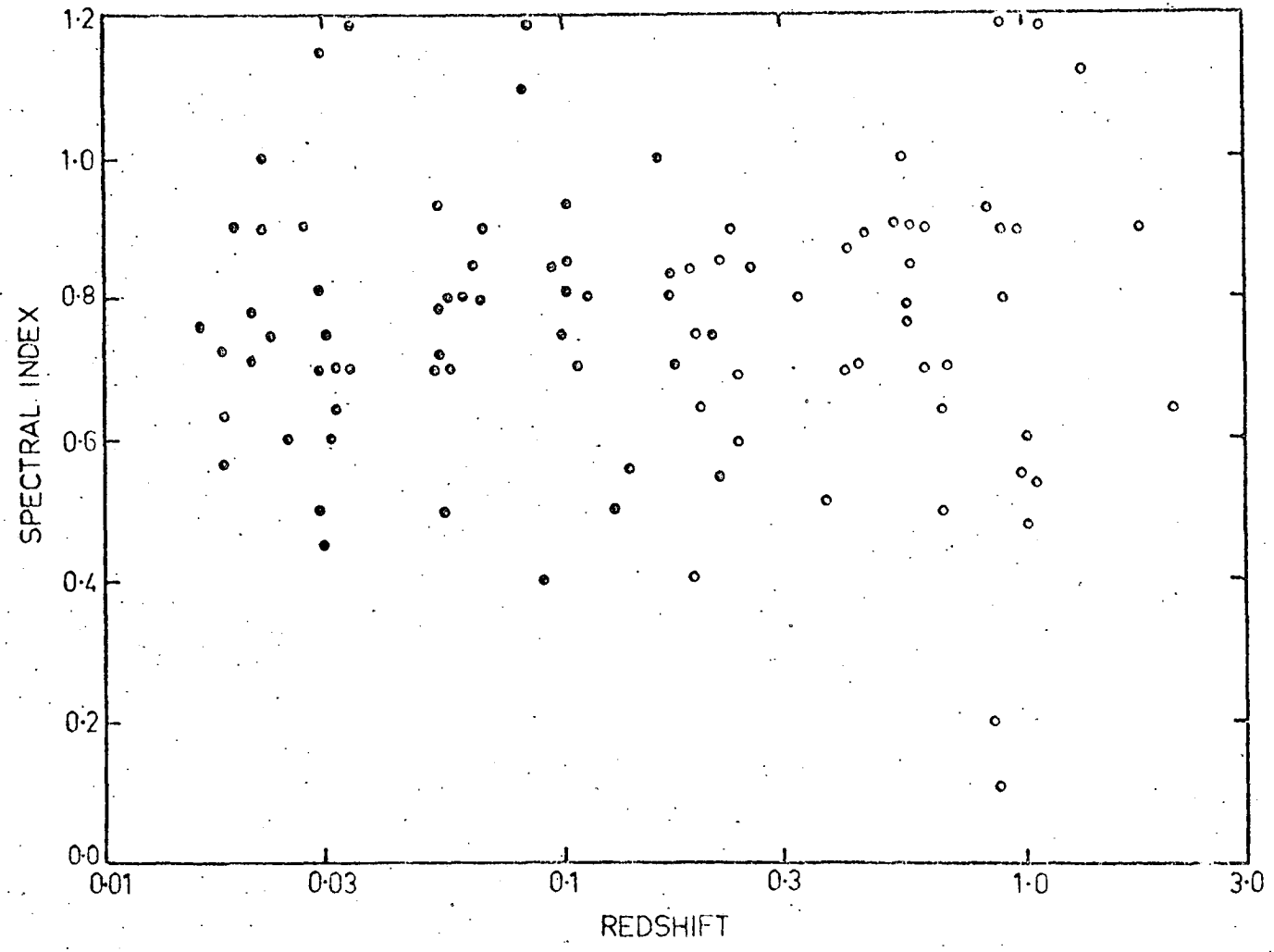

Figure 5.12 - The spectral index-redshift relation for ordinary radio galaxies and quasars (open circles).

The shape of a source emission spectrum depends on the rate of injection of relativistic electrons. According to equation (5.40), the entire emission spectrum for frequencies greater than

$$\bar{\nu}_c = \frac{1000}{H^3 T^2} \tag{5.61}$$

has a spectral index $\bar{\alpha} + 0.5$ provided $t >> T$ where T is the average period in years between bursts. The quantities defined in equation (5.61) relate to the average source spectrum. We have already seen that the typical lifetime of a radio galaxy is in the range 10^6 to 10^7 years. The period T may be expected to be of the same order of magnitude.

The average value of T must be constant independent of epoch in the steady-state models. The corresponding average cut-off frequency will be redshifted by expansion of co-ordinates. The analysis in Table 8 has assumed a cut-off frequency $\bar{\nu}_{co}$ close to 1410 MHz. In this case the source emission spectrum will have an average cut-off frequency

$$\bar{\nu}_c' = \bar{\nu}_{co}(1 + z) \tag{5.62}$$

Hence in a steady-state universe the number of sources with curved spectra will reach a maximum at the flux density corresponding to $\bar{\nu}_c' = \bar{\nu}_c$. There is no evidence for such a maximum in Table 8 but this

certainly does not provide an argument against the steady-state model. Substituting in equation (5.61) a typical field strength $H = 5 \times 10^{-6}$ oersted it follows that the source cut-off frequency lies in the range 8×10^4 to 8×10^6 MHz for $10^6 < T < 10^7$. These values for $\tilde{\nu}_c$ would imply a very low value of flux density before a large percentage of sources with curved spectra could be detected in the frequency range of interest here. On the other hand a value for T much greater than 10^7 years would produce a very marked increase in this percentage as the flux density is decreased. The results in Table 8 are therefore consistent with a period of electron injection of the order of 10^6 years.

In evolutionary universes the rate of occurrence of the disruptive events responsible for radio emission is expected to decrease with advancing epoch, that is the period T decreases with increasing redshift. This would modulate the effect described above for steady-state models. The net result is a weakening of the functional dependence of the number of curved spectra with flux density. The amount of weakening will depend on the relation between T and redshift. As in the case of the steady-state, the results in Table 8 are not inconsistent with the predictions of the evolutionary model.

In conclusion, we may assert that the spectral index-flux density results given in Table 8 do not provide evidence for steady-

state or evolutionary cosmologies. The average spectral index may be considered to be practically independent of epoch. The results indicate that the period of electron injection in radio galaxies is probably less than 10^7 years. An analysis of the spectral index-flux density relation could produce useful results if a higher frequency range was considered.

5.6 Number-Flux Relations

In this section equations are derived which relate numbers of observable radio sources to flux densities. These equations will provide valuable information for selection of a cosmological model.

First, the total number of sources observable in a flux interval dS at S may be derived. If luminosity and source density evolution are assumed to be absent, then from equation (5.54)

$$\frac{dm}{dy} = T^2 y^{-(1+\alpha)} S\left[\frac{2T'}{T}\frac{\partial \omega}{\partial y} - (1+\alpha)/y\right]/GP_o \qquad (5.63)$$

for evolutionary universes with $m = P/P_o$ as before. Using this result and equations (5.8) and (5.56) it follows that the total number of sources observed in the interval dS and in unit solid angle is

$$\left| \frac{dN_t}{dS} \right| = \int_{-\infty}^{\infty} \frac{dN(m)}{dS} d(\log m) = \int_{0}^{\infty} \frac{dN(m)}{dS} \frac{1}{m} dm$$

$$= -\rho_o(P_o) \left(\frac{\nu}{\nu_r}\right)^{3\alpha/2} P_o^{3/2} S^{-5/2} \times$$

$$\int_0^1 e^{-x^2/2\sigma^2} \frac{\partial \omega}{\partial y} T_k^{-1}(\omega) y^{3(1+\alpha)/2} dy \qquad (5.64)$$

or writing the last equation in a simplified form

$$\left| \frac{dN_t}{dS} \right| = -K(\nu_r, S) \int_0^1 F(y) dy \qquad (5.65)$$

Suppose, now, that the number of sources per unit co-ordinate volume varies smoothly with epoch. The number of sources per unit proper volume at the epoch corresponding to an expansion parameter y may be written as

$$\rho(P, y) = \rho_o(P_o) (P_o/P)^{3/2} e^{-x^2/2\sigma^2} y^{-(3+n)} \qquad (5.66)$$

In this case equation (5.65) becomes

$$\left| \frac{dN_t}{dS} \right| = -K(\nu_r, S) \int_{y_o}^1 F(y) y^{-n} dy \qquad (5.67)$$

where y_o is, as yet, an undetermined lower limit of integration.

If the average source luminosity is a function of epoch then the luminosity of a particular radio galaxy may be written as

$$P = P' y^{-\beta} \tag{5.68}$$

where P' is the luminosity at the present epoch and β is a constant expected to be positive. The spatial luminosity distribution at the epoch corresponding to y will then be

$$\rho(P, y) = \rho_o(P_o)(P_o/P)^{3/2} e^{-x^2/\sigma^2} y^{-3\beta/2} \tag{5.69}$$

The equation for the number of sources in flux interval dS then becomes

$$\left| \frac{dN_t}{dS} \right| = -K(\nu_r, S) \int_{y_o}^{1} F(y) y^{-3\beta/2} dy \tag{5.70}$$

for evolutionary universes in which source luminosities vary smoothly with epoch.

The steady-state universe does not allow spatial or luminosity variations for radio sources. According to equation (5.59)

$$\frac{dm}{dy} = -\frac{S}{P_o} \left(\frac{\nu_r}{\nu} \right)^{\alpha} \frac{c^2}{H_o^2} \left(\frac{1}{y} - 1 \right)^2 y^{-(1+\alpha)} \left[\frac{2}{y(1 - y)} \right.$$

$$\left. + (1 + \alpha)/y \right] \tag{5.71}$$

Hence substituting in equation (5.60) we have

$$\left| \frac{dN_t}{dS} \right| = \int_{-\infty}^{\infty} \left| \frac{dN(m)}{dS} \right| d(\log m)$$

$$= K(\nu_r, S) \int_0^1 e^{-x^2/2\sigma^2} y^{(5+\alpha)/2} dy \qquad (5.72)$$

where $K(\nu_r, S)$ is defined in equation (5.65).

The theoretical models should now be compared with the observational results. In figure 5.13 the ratio $|dN_t/dS|$ is plotted against flux density for all radio sources listed in the Parkes catalogues at a frequency of 408 MHz. The theoretical prediction for models without source luminosity and density evolution are examined first. The appropriate equations are (5.65) for evolutionary models and (5.72) for the steady-state models. The luminosity distribution for sources at the present epoch is defined as usual through equations (5.4) and (5.7). The theoretical curves are superimposed on figure 5.13. The evolutionary models are defined by $\sigma_o = 0.5$ and a series of values for q_o while the black-body radiation temperature is given the value of 3°K as usual. The average spectral index is assumed to be independent of epoch as implied by the results in Table 8.

Inspection of figure 5.13 shows that neither a steady-state nor an ordinary evolutionary model can account for the observed curve of $|dN_t/dS|$ versus S. Consequently we are forced to consider spatial and luminosity evolution for radio galaxies.

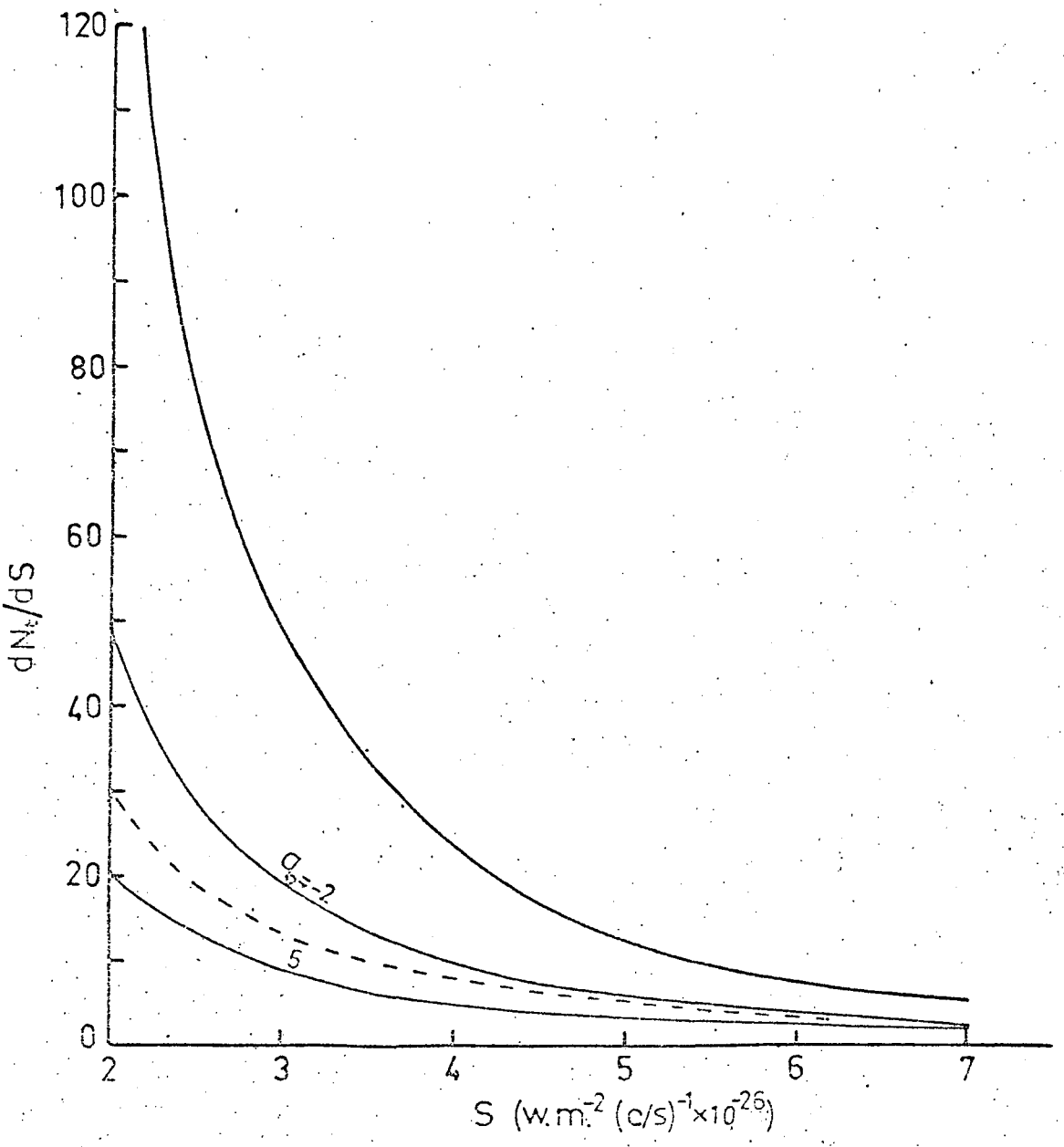

Figure 5.13 - The observed number of sources in the flux interval dS at S and in unit solid angle for sources listed in the Parkes catalogues at a frequency of 408 MHz. Theoretical curves are shown for evolutionary universes with $\sigma_o = 0.5$ and $q_o = -2$ and 5 and for the steady-state model (broken line).

First, suppose that the number of sources in unit co-ordinate volume is proportional to y^{-n} where $n > 0$. The quantity $|dN_t/dS|$ as a function of S is now given by equation (5.67). Once the cosmological model has been chosen there remain two parameters, y_o and n, which may be determined by fitting the theoretical curve to the observational points. A computer program was evolved to calculate the parameters y_o and n for a least squares fit condition. The program minimised the function

$$F(\sigma_o, q_o, y_o, n) = \sum_i [R(S_i) - R_o(S_i)]^2$$

where R is the theoretical value and R_o the observed value of the ratio $|dN_t/dS|$ at flux density S_i. The parameters σ_o and q_o were chosen and the function $F(y_o, n)$ minimised with respect to y_o and n. The results are summarised in Table 9. The values for F_n are the minimum values of F for each model which have been normalised to the minimum value of F for the model $\sigma_o = 5$, $q_o = 2$. That is F_n provides a measure of the relative goodness of fit. The best fit theoretical curves require values for y_o and n which in general increase with decreasing σ_o. There is a tendency also for F_n to increase with decreasing σ_o but the effect is very weak. A stronger relationship between F_n and the parameters defining the cosmological model may be expected if the limiting flux density of the survey could be reduced. The limiting flux of the recent 5C surveys (Ryle, 1968) is close to 0.01 f.u. at 408 MHz. It is probable therefore that greater information on cosmological models may be derived from an examination of the 5C source counts. This is done

in the following section.

If radio source luminosity varies according to the law $P(y) = P(1)y^{-\beta}$ then the ratio $|dN_t/dS|$ is given by equation (5.70). It is evident that minimisation with respect to y_o and β will yield the same value of y_o and a value for β equal to two-thirds of the value of n derived for the case of spatial evolution. The results for β are listed in Table 9.

Table 9

Cosmological Parameters from Parkes Source Counts

σ_o	q_o	y_o	n	β	F_n
5	5	0.141	3.680	2.454	1.2
	2	0.103	3.211	2.142	1.0
	0	0.167	3.078	2.053	1.2
	-2	0.254	3.325	2.218	1.6
2	5	0.243	4.006	2.672	1.2
	2	0.199	3.815	2.545	1.1
	0	0.219	3.668	2.447	1.1
	-2	0.488	4.556	3.039	2.3
1	5	0.267	4.571	3.049	1.3
	2	0.312	4.579	3.054	1.2
	0	0.367	4.512	3.009	1.2
	-2	0.537	4.521	3.016	3.3

5.7 The Log N - Log S Relation

It is well known that in Euclidean universes

$$N = \frac{1}{3} \rho P^{3/2} S^{-3/2} \qquad (5.73)$$

where N is the number of radio sources per steradian with flux densities exceeding S, P is the mean luminosity and ρ is the number of sources per unit proper volume. According to equation (5.73) the log N - log S relation for sources of the same intrinsic power in a Euclidean universe will be a straight line of slope equal to -1.5. The precise form of the log N - log S curve depends on the assumed cosmology and on the dispersion in radio source luminosity. A theoretical analysis will therefore provide useful evidence for a cosmological model.

The form of the number-flux relation has been investigated in some detail by many authors (e.g. Ryle and Clarke, 1961; Oort, 1961, 1964; Sciama, 1963; Scott, 1963; Davidson and Davies, 1964; Gower, 1966; Longair, 1966). All these analyses have assumed a functional dependence between source luminosity or spatial density with epoch and none have allowed for the possible effects of the space-time geometry on the log N - log S curve.

Here, we assume initially that the number of sources per unit co-ordinate volume is constant and that all sources have the same luminosity P_o independent of epoch. In this way it is possible to separate out the geometrical effects and to establish a log N - log S curve for a particular cosmological model. As a further simplification

the radiation density and pressure terms are assumed to be negligible. Under these conditions the number of sources in unit solid angle (as measured by the origin observer) out to an angular co-ordinate ω is

$$N = \int \rho dV = \int_0^{\omega} \rho_o y^{-3} dV$$

$$= \rho_o R_o^3 \int_0^{\omega} T_k^2(\omega) d\omega \qquad (5.74)$$

where ρ_o is the present spatial density of radio galaxies. Recalling that $T_k(\omega) = \sin \omega$ for $k = 1$ and $T_k(\omega) = \sinh(\omega)$ for $k = -1$ the last equation may be written in a more simplified form

$$N(\omega) = \frac{\rho_o R_o^3}{2} k[\omega - 0.5T_k(2\omega)] \quad \text{for } k \neq 0$$

and $$N(\omega) = \rho_o \frac{R_o^3 \omega^3}{3} \quad \text{for } k = 0 \qquad (5.75)$$

The received flux density as a function of y (or ω) is easily derived from equation (5.13) and $N(\omega)$ will be the number of sources detected with flux densities exceeding S. If the source luminosity is taken as the weighted mean value of 8×10^{25} watts $(c/s)^{-1}$ str^{-1} at 178 MHz then from equation (5.3) the number of sources per unit proper volume at the present epoch is $\rho_o = 4.24_{10}{}^{-75}$ m^{-3}. Substituting these values in equation (5.75), the log N - log S curve may be computed for different world models defined through the parameters σ_o and q_o. The results are presented in figure 5.14. The form of

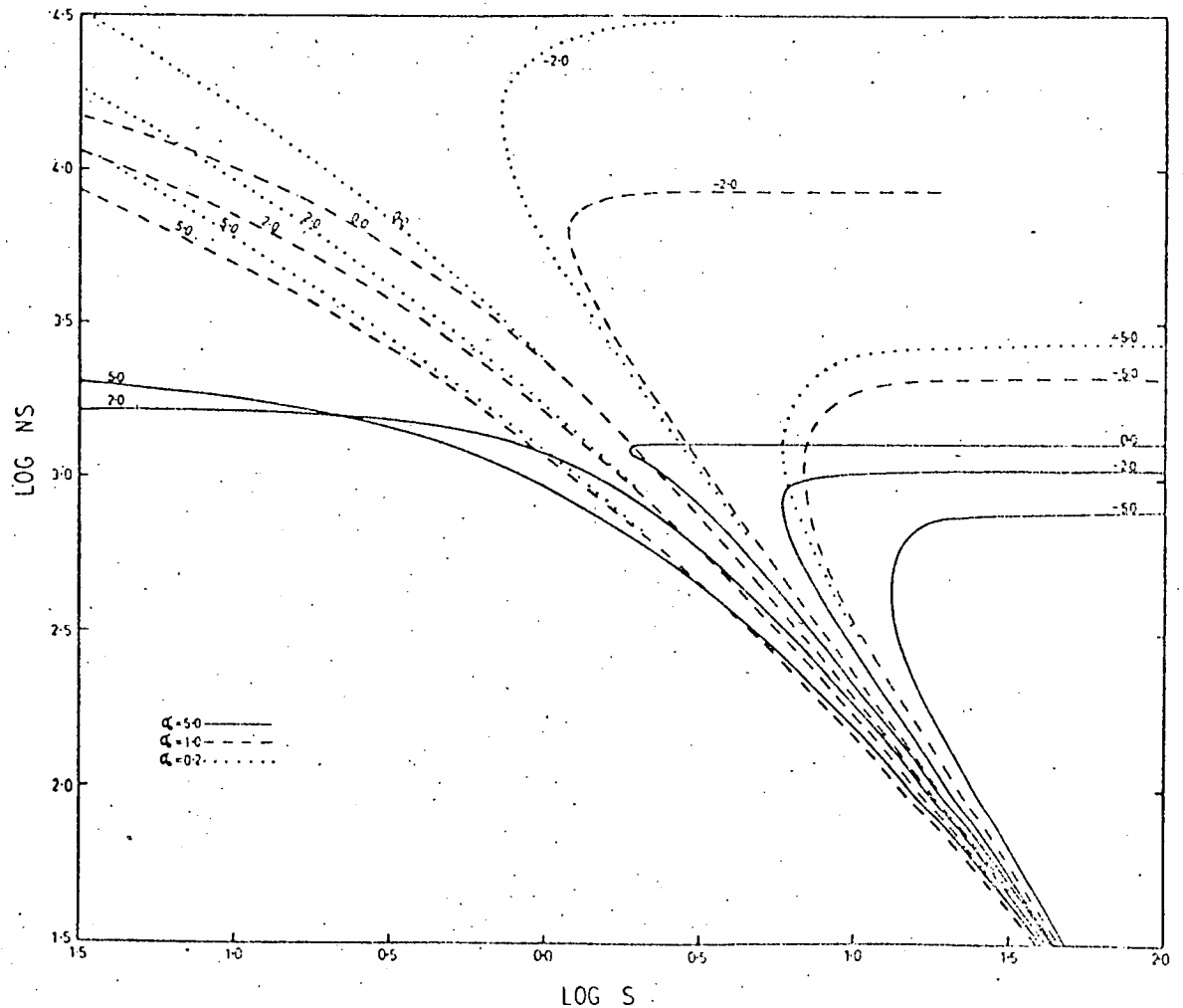

Figure 5.14 - Log N - log S curves at 178 MHz for evolutionary universes in which source luminosity and spatial density are independent of epoch.

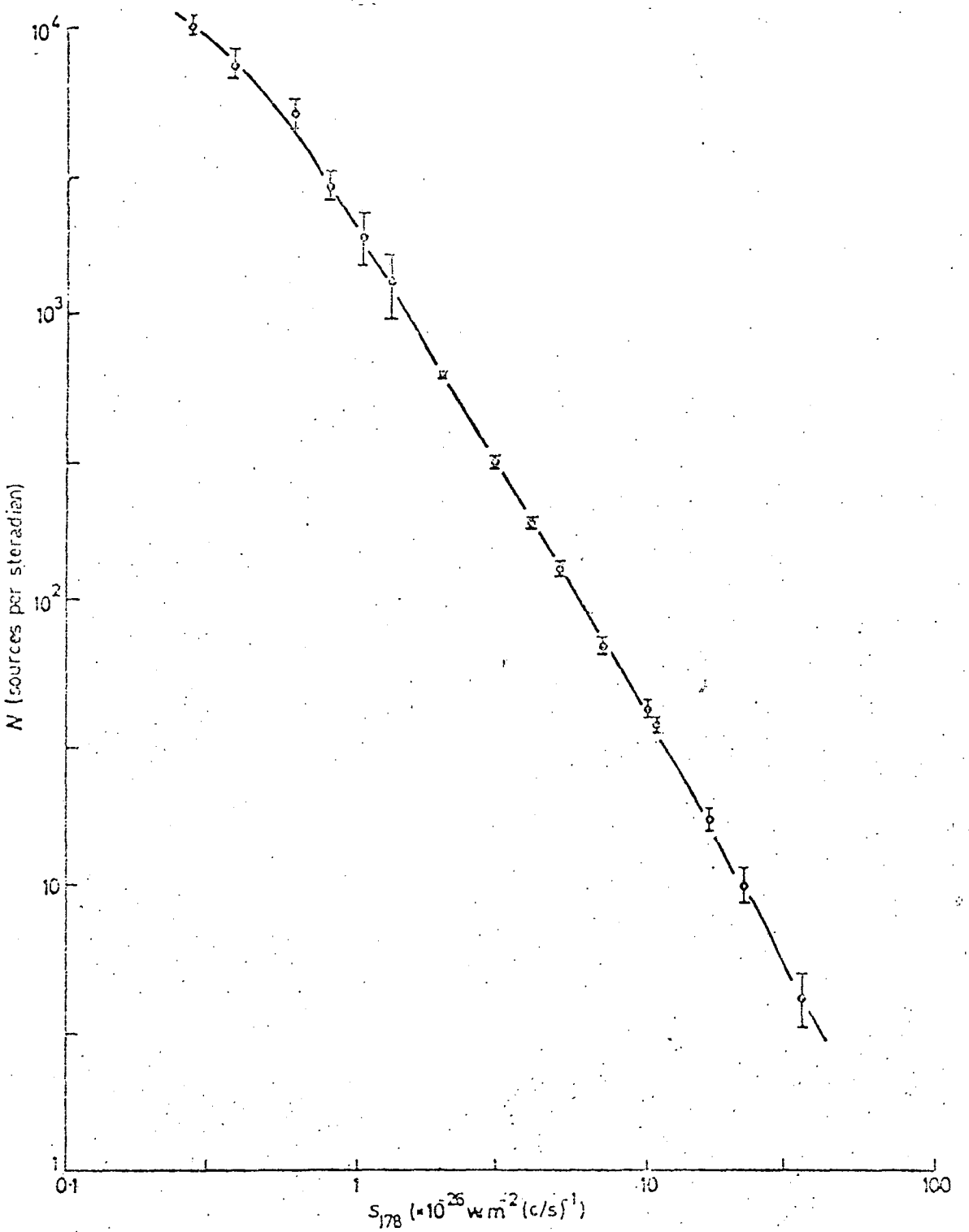

Figure 5.15 - The experimental log N - log S relation derived from the 4C catalogue and the North Polar Survey (Gower, 1966).

the log N - log S curve is seen to be a strong function of the cosmological model at relatively low values of flux density. The theoretical curves should be compared with the observed log N - log S curve presented in figure 5.15 for radio sources at 178 MHz. The experimental results used to derive this curve have already been described in section 5.2. The comparison indicates that it is rather difficult to reconcile the theoretical and experimental results for this particular model for radio source luminosities and spatial density. It is obvious, however, that the choice of a world-model will strongly modulate any theoretical curve, particularly at low flux densities. Gower (1966) considers that the variation of source spatial density could be determined from the source counts if all radio sources were of a single power. But this apparently is not the case since, according to figure 5.14, large deviations from the expected straight line relation of slope equal to -1.5 in steady-state and Euchlidean universes may be produced by an appropriate cosmological model.

The problem is now to derive some equations for the log N - log S curve which allow for the geometry of space-time. The observational curve has a slope of about -1.8 and a cut-off at a flux density near to one flux unit. Both these features must be accounted for by any theoretical model. Gower (1966) has considered density evolution in Einstein-de Sitter world models in order to account (approximately) for the observed log N - log S curve. Similarly, Longair (1966) has

investigated the radio source counts by allowing for both luminosity and density evolution in an Einstein-de Sitter universe. He also used the log N - log S curve to derive a more precise luminosity distribution for local radio sources.

Here, we first of all examine the effects of introducing a luminosity dispersion of the form (5.4). Consider a three-dimensional volume element dV at the epoch corresponding to expansion parameter y. The number of sources in this volume which are measured by the origin observer to have flux densities greater than S is determined by equation (5.54). All those sources in dV with luminosities greater than

$$P' = S \times T_k^2(\omega) y^{-\alpha}/G \tag{5.76}$$

will have detected flux densities greater than S. Hence the number of observed sources (in dV) per steradian with flux densities exceeding S will be

$$dN(S, y) = \int_{m'}^{\infty} d\eta(m)\, dV \tag{5.77}$$

where $\eta(m)$ is defined from equation (5.8), $m' = P'/P_o$ and $m = P/P_o$. Substituting for dV and integrating between the two extreme values for y we have

$$N(S) = -\rho_o(P_o) R_o^3 \int_0^1 \int_{m'}^{\infty} m^{-5/2} e^{-x^2/2\sigma^2} dm \; T_k^2(\omega) \frac{\partial \omega}{\partial y} \; dy \tag{5.78}$$

where according to equations (4.3) and (5.8)

$$dn(m) = \rho_o(P_o) m^{-5/2} e^{-x^2/2\sigma^2} dm \; y^{-3} \tag{5.79}$$

Equation (5.78) provides an equation for the log N - log S curve for evolutionary universes in which radio sources have a luminosity dispersion defined by equation (5.4).

In steady-state models $n(m)$ is independent of epoch and hence

$$dn(m) = \rho_o(P_o) m^{-5/2} e^{-x^2} dm \tag{5.80}$$

Using the expression for dV defined in equation (5.57) the equation to the log N - log S curve in a steady-state universe is

$$N(S) = -\rho_o(P_o) \left(\frac{c}{H_o} \right)^3 \int_0^1 \int_{m'}^{\infty} m^{-5/2} e^{-x^2/2\sigma^2} dm (1 - y)^2 y^{-1} dy \tag{5.81}$$

where according to equation (5.58)

$$m' = \frac{S}{P_o} \left(\frac{\nu_r}{\nu} \right)^{\alpha} \frac{c^2}{H_o^2} \left(\frac{1}{y} - 1 \right)^2 y^{-(1+\alpha)} \tag{5.82}$$

The degree of dispersion in the source luminosity function is determined by the standard deviation σ and its effect on the log N - log S curve may be determined through equations (5.78) and (5.82). For purposes of illustration an Einstein-de Sitter universe has been assumed in the evolutionary case. Clearly, for a chosen world-model, the slope of the log N - log S curve will be modulated by the term

$$f(m') = \int_{m'}^{\infty} m^{-5/2} e^{-x^2/2\sigma^2} dm \qquad (5.83)$$

and, for finite values of σ the magnitude of the slope will be less than that in the undispersed case. This situation is illustrated in figure 5.16 where the log N - log S curve (at 178 MHz) is provided for the Einstein-de Sitter universe in which the radio source luminosity has a standard deviation of three. The curve is normalised to fit the observations at S = 30 f.u. and obviously the slope of this line is considerably less than required. The same general conclusions apply to the log N - log S curve in steady-state models as indicated by the broken line in figure 5.16. The inability of these models to account for the observed log N - log S curve forces us to consider those models which admit radio source luminosity and density evolution.

Using the same arguments described in section 5.6 the number of sources with flux densities exceeding S will be

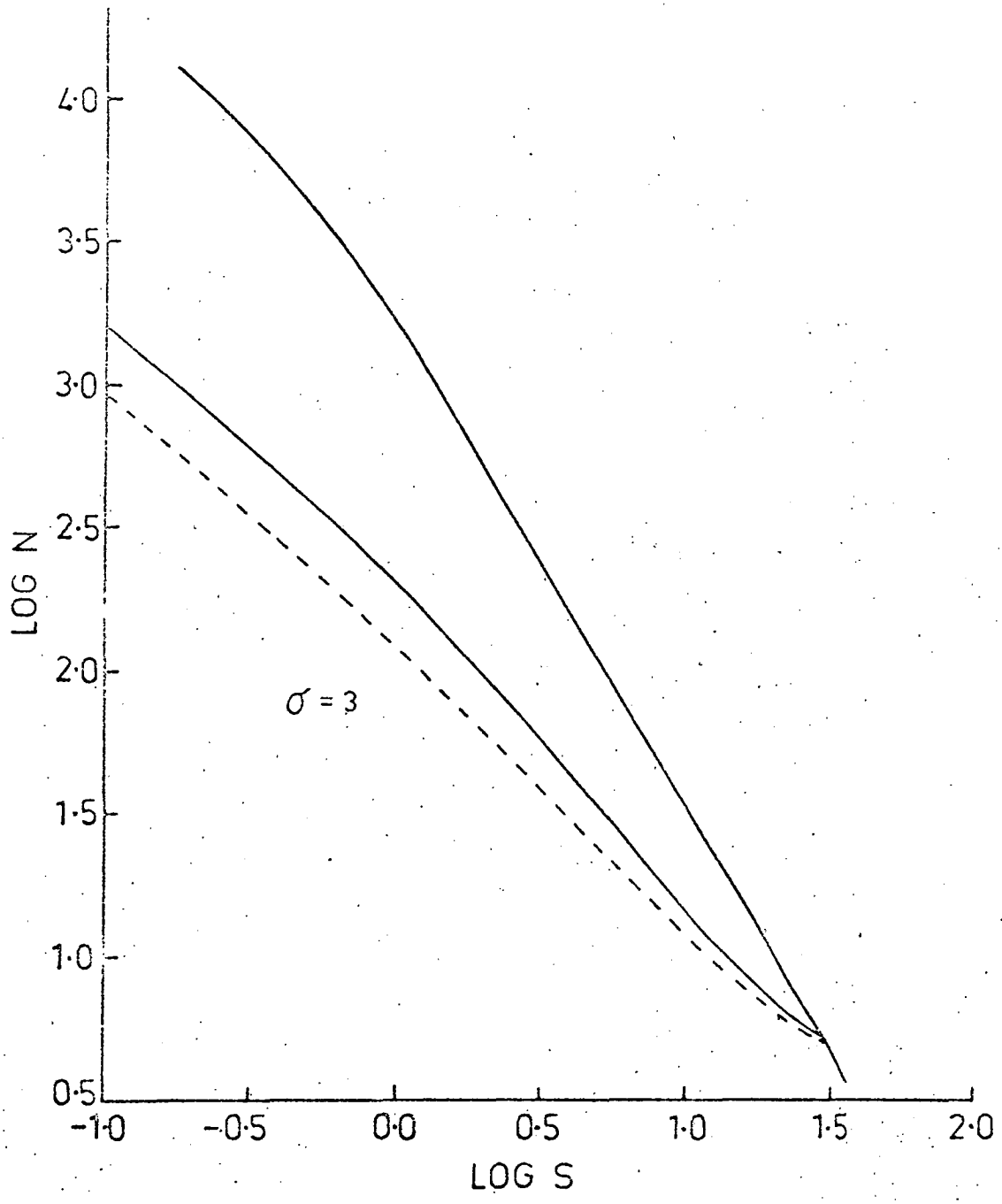

Figure 5.16 - Theoretical log N - log S curves at 178 MHz for Einstein-de Sitter and steady-state universes in which the standard deviation is $\sigma = 3$ and the source population in co-ordinate volume is independent of epoch.

$$N(S) = -\rho_o(P_o)R_o^3 \int_{y_o}^{1} \int_{m'}^{\infty} m^{-5/2} e^{-x^2/2\sigma^2} dm\, T_k^2(\omega) \frac{\partial \omega}{\partial y} y^{-n} dy \qquad (5.84)$$

for models in which the number of sources in unit co-ordinate volume is proportional to y^{-n}. Similarly,

$$N(S) = -\rho_o(P_o)R_o^3 \int_{y_o}^{1} \int_{m'}^{\infty} m^{-5/2} e^{-x^2/2\sigma^2} dm\, T_k^2(\omega) \frac{\partial \omega}{\partial y} y^{-3\beta/2} dy \qquad (5.85)$$

for models in which source luminosity is proportional to $y^{-\beta}$.

Recent work has extended the number-flux density relation to very small flux densities (Pooley and Ryle, 1968; Ryle, 1968). The new observations were made with the Cambridge One-Mile Telescope at a higher frequency (408 MHz) than that of the 4C survey. The improved log N - log S relation is shown in figure 5.17. The slope of the line drawn is approximately constant at -1.85 for $S_{408} > 4$ f.u., and at lower flux densities changes progressively to about -0.8 in a range of 10^3 in S.

A computer program was developed to fit the theoretical curves given by equations (5.84) and (5.85) to the experimental points of figure 5.17. The program implemented a revised version of the function minimisation procedure described by Nelder and Mead (1965). Although this procedure has no strong theoretical basis, it provides the most useful general method that does not require the partial derivatives as well as the function values. Here a minimum value must be obtained

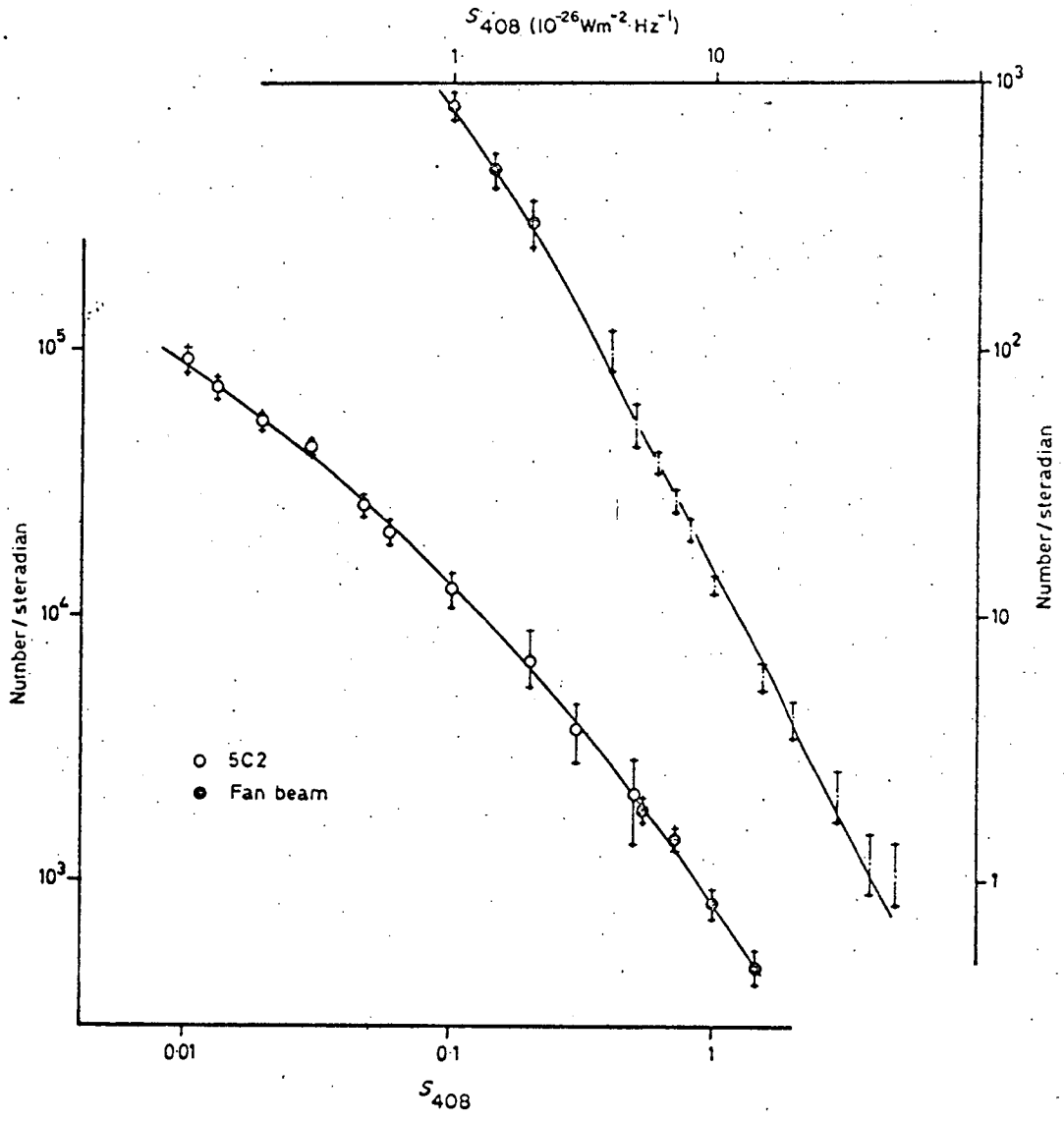

Figure 5.17 - The log N - log S relation for $S_{408} \geq 0.01 \times 10^{-26}$ f.u (Pooley and Ryle, 1968).

for the function

$$F(\sigma_o, q_o, y_o, n) = \sum_i [N(S_i) - N_o(S_i)]^2 \omega_i$$

where $N(S_i)$ is the theoretical source count given by equation (5.84) and $N_o(S_i)$ is the observed source count for sources having flux densities greater than S_i. Each source count was given a weight ω_i according to the inverse square of its r.m.s. uncertainty. The results of the analysis are listed in Table 10 for different cosmological models defined by σ_o and q_o with $T_o = 3°K$. For each σ_o, the value of q_o is listed which provides the best fit condition. The values F_n are the normalised values of the minima of $F(y_o, n)$ and provide a measure of the relative goodness of fit. The minima of F are found to be quite unique and well defined. There is a general increase in the values of y_o and the indices n and β with decreasing σ_o. Moreover F_n increases with decreasing σ_o indicating that the best fit condition occurs for large values of σ_o and relatively large positive values for the deceleration parameter q_o. Reference to the discussion in section 4.3 shows that the best fit condition is provided by those models which are closed and in a state of rapid expansion. Furthermore, these models do not require extremely strong evolutionary functions for source luminosity and density. If the value of y_o corresponds to the epoch of galaxy formation then the evidence from the source counts indicates that this event must occur at a very late stage of cosmic evolution for models having small values of σ_o. The restriction on y_o (and therefore on the maximum redshift at galaxy formation) is much less severe in models

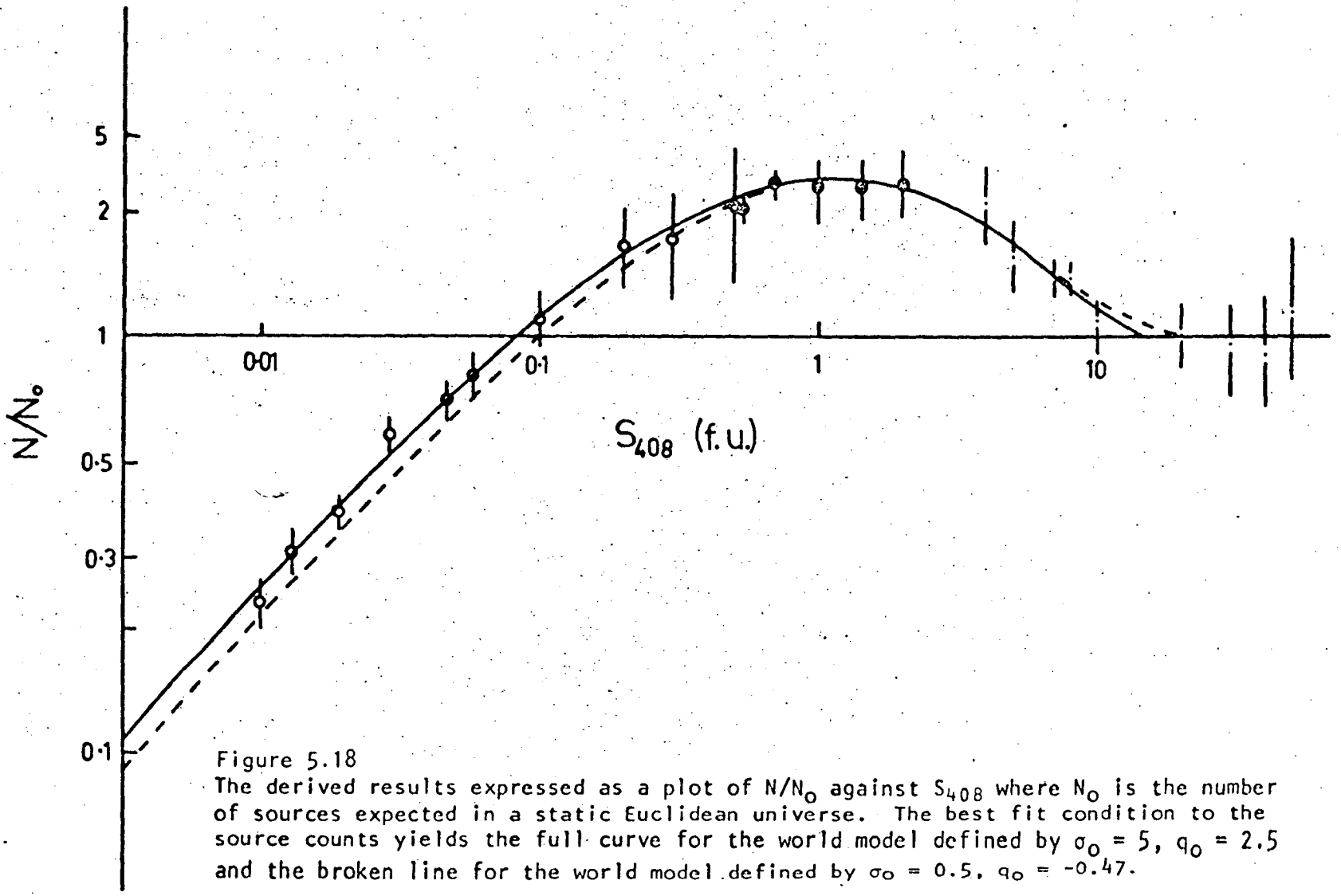

Figure 5.18
The derived results expressed as a plot of N/N_0 against S_{408} where N_0 is the number of sources expected in a static Euclidean universe. The best fit condition to the source counts yields the full curve for the world model defined by $\sigma_0 = 5$, $q_0 = 2.5$ and the broken line for the world model defined by $\sigma_0 = 0.5$, $q_0 = -0.47$.

having large σ_o.

The quality of the fit to the experimental results is shown in figure 5.18. The expected number of sources, N_o, with flux densities greater than S has been calculated for a homogeneous isotropic universe and after normalisation to $N_o = 6.2$ per steradian at $S_{408} = 15$ f.u. Plots of log (N/N_o) against log S are provided for two world models defined by the parameters $\sigma_o = 5$, $q_o = 2.53$ and $\sigma_o = 0.5$, $q_o = -0.47$. Clearly a very good fit is obtained by the first model whereas the second gives an excessive number at high flux densities and a number which is low at small values of S.

Table 10

Cosmological Parameters from 5C Source Counts

σ_o	q_o	y_o	z_{max}	n	β	F_n
5	2.53	0.112	7.9	3.21	2.14	1.0
3	1.98	0.215	3.7	3.73	2.49	1.1
2	0.93	0.249	3.0	4.26	2.84	1.5
1	0.36	0.364	1.8	4.59	3.06	2.1
0.5	-0.47	0.397	1.5	4.97	3.31	2.8

It is worthwhile to recapitulate here the arguments which have led to the results just described. First the luminosity distribution, n(P), has taken to be Gaussian in log P/P_o and this is apparently a

close approximation to the real situation. Next, the local spatial distribution $\rho_o(P)$ was derived from the observations. The average spectral index was assumed to be independent of epoch as suggested by the observations while luminosity and spatial evolution were assumed to vary smoothly with the expansion parameter y. All radio sources were considered to evolve as a single class of objects and the parameters y_o, n and β were determined for the best fit condition for a series of values for σ_o.

These results are in some disagreement with the conclusions of Longair (1966) who states that a large number of cosmological models may be fitted if all sources are allowed to evolve. However the luminosities of the sources which contribute most significantly to the source counts at a particular flux density are determined by the lower-limit of integration, m', in equation (5.83). We recall that

$$m' = S \times T_k^2(\omega) y^{-\alpha} / G\ P_o$$

and inspection of this equation in relation to equations (5.84) and (5.85) shows that the greatest contribution to the source counts at lower flux densities is provided by the relatively powerful sources with $m > m' > 1$. Thus it is irrelevant whether or not radio sources evolve as a single class of objects. The same general results will be obtained as those described above if only powerful sources evolve.

There may be some evidence for an excessive number of quasars at cosmological distances (Sandage, 1968) and this will produce appropriate changes in the source counts at low flux densities. It is therefore tempting to explain the source counts in terms of the evolution of quasi-stellar sources as suggested by Longair (1966).

Some mention should be given here of the implications of the source counts to the steady-state cosmology. Hoyle (1967) considers that the slope of the log N - log S curve may be accounted for by quasi-stellar sources which have a particular luminosity distribution. In this analysis the luminosity distribution has been derived for all radio sources and the observed log N - log S relation is accounted for by subsequent theory. Moreover, we have found that the introduction of a finite dispersion for source luminosities decreases the magnitude of the slope of the curve log N versus log S instead of increasing it as required by the observations. There is some evidence that the log N - log S curve for quasars has a slope of about -2.2 (Veron, 1966). This could account for the source counts in a steady-state cosmology only if the average spectral index of quasars is considerably greater than that of ordinary radio galaxies. However, there is no evidence at all for such a result. It is possible to retain the steady-state theory by invoking irregularities in the distribution of sources on the scale of the observable universe itself. This requires a special position for the Galaxy in order to account for the isotropy and, as pointed out by Ryle (1968), the

probability of such a situation is $\simeq 10^{-6}$. The easiest and most satisfactory explanation of the source counts is that radio galaxies evolve with advancing epoch as should be expected to some extent in an evolutionary cosmology.

The calculated upper limits of the redshift for each model is listed in Table 10. It is interesting to note that the observed distribution of quasi-stellar sources appears to exhibit an abrupt cut-off at z = 2.2 (Longair and Scheuer, 1967). Other authors (e.g. Eggen et al., 1962; Weymann, 1967) have suggested that galaxy formation occurs at epochs corresponding to z = 4.8. The results in Table 10 do not disagree with any of these estimates but indicate that the best fit to the source counts is secured by models having relatively large values of z_{max}. On the basis of present available evidence it is not possible to determine whether z_{max} corresponds to a cut-off in source emission or to the epoch of galaxy formation. This point will be discussed further in subsequent analyses.

5.8 Conclusions

The analyses in this chapter have been concerned with observable quantities associated with radio sources. Special attention has been given to the application of source data to the solution of the cosmological problem. The investigation into possible clustering of radio sources has indicated that source positions are random down to

a scale of 15' of arc. An analysis of the spectral indices for sources listed in the Parkes catalogues yielded a mean index of $\alpha = 0.84$ which was found to be practically independent of source redshift or luminosity. A luminosity distribution has been derived for local radio galaxies. The distribution at 178 MHz is found to be almost Gaussian in $\log_e(P/P_o)$ with a standard deviation $\sigma = 2.05$.

Assuming that source luminosity or density in co-ordinate volume varies smoothly with the expansion parameter, it is possible to analyse the source counts for different cosmological models. The best fit condition is attained by those models having large values for the density parameter σ_o and deceleration parameter q_o. Reference to section 4.3 shows that these models are closed and oscillating. The evolution in source luminosity or density becomes less severe with increasing σ_o. Large positive values for q_o are in good agreement with the value of $q_o = 1.65 \pm 0.3$ proposed by Sandage (1968). The source count results are also supported by the results of the analysis of the distribution of source angular diameter with redshift. Hence the evidence presented in this chapter points to a dense and rapidly oscillating universe.

CHAPTER VI

RADIO WAVES IN THE INTERGALACTIC MEDIUM

6.1 The Universal Plasma

Various cosmological theories predict a mean density for the universe which, according to Oort (1958), is about two orders of magnitude greater than the mean density of matter in galaxies averaged over all space. Similar results have been found by other workers (Sandage, 1961; Hoyle and Narlikar, 1962; Sciama, 1964) from analyses based on steady-state and evolutionary cosmologies. They find a mean value for the density of matter in the universe of approximately 2×10^{-29} g cm^{-3}, whereas the mean density of matter in the galaxies is about 5×10^{-31} g cm^{-3}. If it is assumed that there are no aggregations of matter in the universe other than the types of galaxies already known, then there is a problem of the specification of the intergalactic material. For the lack of any other evidence, the bulk of the matter density is attributed to uncondensed intergalactic hydrogen. There are several experimental results that support the argument for an intergalactic medium of ionized hydrogen, although it should be noted that there is no direct evidence for an ionized medium and the only information obtained so far concerns atomic hydrogen. Goldstein (1963) made measurements of the 21 cm line emission in the direction of the north celestial pole, and concluded that the intergalactic atomic hydrogen density is $n_H < 2.1 \times 10^{-25}$ cm^{-3}. According to the measurements by

Davies (1964), on the absorption spectrum of Cygnus A, n_H is less than 9×10^{-8} cm^{-3} for an Einstein-de Sitter universe. Gunn and Peterson (1965) examined the redshifted Lyman α-line of the quasi-stellar source 3C 9 for any evidence of photon scattering by intergalactic hydrogen. They found the spatial density of atomic hydrogen to be almost negligible for several cosmological models. On the basis of these results, it will be assumed in the following work that all the matter in the universe exists as ionized hydrogen.

The thermal history of the universal plasma is of fundamental importance to any analysis of the background radiation. Several authors have considered the question of the temperature of the intergalactic gas, and a brief account will be given summarizing these investigations. A useful upper limit to the temperature at the present epoch can be calculated from the requirement that the background intensity cannot exceed the observed flux in the X-ray region of the spectrum. This method was employed by Field and Henry (1964) to derive an upper limit of 4×10^6 °K in the steady-state model and 3×10^6 °K in evolutionary models. These results proved the hot (10^9 °K) universe proposed by Gold and Hoyle (1959) to be invalid. Kahn and Woltjer (1959) obtained a temperature of 5×10^5 °K for the ionized hydrogen in the local group by assuming that the gravitational self-attraction was balanced by the kinetic pressure nkT. The temperature of the intergalactic gas was estimated by Field (1965) to be 5×10^4 °K on the basis of theoretical investigations

of thermal instabilities leading to the formation of galactic clusters. Sciama (1964) proposed that the temperature of the intergalactic gas would be about 10^5 °K if an equilibrium state exists in which heating of the gas by cosmic ray ionization is balanced by cooling due to bremsstrahlung and recombination radiation.

Gould and Ramsay (1966) have examined the question of the temperature of the intergalactic gas in terms of a quasi-equilibrium state in which a thermal balance is attained in a time less than the characteristic time of expansion of the universe. They consider that heating of the gas is a result of ionization by a universal cosmic ray flux and the dissipation of hydrodynamic turbulance while cooling is due to inelastic electron collisions with H, H_e, and H_e^- and by free-free emission and recombination radiation. Gould and Ramsay adopt a universal flux mainly because of the simplicity that this assumption introduces into the equations. They assume the same cosmic ray spectrum calculated by Pollack and Fazio (1963) and they find a probable equilibrium temperature in the range 10^4 to 5×10^4 °K, depending on the density and a possible non-equilibrium temperature greater than 2×10^5 °K.

On the basis of these investigations, we shall take, as a very reasonable assumption, a temperature at the present epoch in the range 10^4 to 10^6 °K, regardless of the density of the intergalactic material.

6.2 Low Frequency Absorption in Isotropic World Models

It is well known that discrete radio sources can have low frequency turnovers in their spectra owing to a combination of thermal absorption, synchrotron self-absorption, and/or absorption in the HII region. There is a further possible cause of a low frequency turnover and this is free-free absorption in intergalactic space, which is described in the last section as filled with ionized hydrogen. The aim of this present section is to show the effects of intergalactic free-free absorption on the spectra of radio sources as a function of their redshift.

When free-free absorption by ionized hydrogen occurs in the intergalactic medium, the received flux can be written as

$$S'(\nu_o) = S(\nu_o)e^{-\tau(\nu_o)} \qquad (6.1)$$

where S is the unattenuated value and $\tau(\nu_o)$ is the optical depth for the radiation received at frequency ν_o. We require to calculate the absorption factor $e^{-\tau(\nu_o)}$ as a function of redshift for various world models.

Now the ordinary absorption coefficient in ionized hydrogen is

$$K(\nu) = A\, g\{1 - e^{-h\nu/kT}\}T^{-1/2}N^2\nu^{-3} \qquad (6.2)$$

where N is the electron density, T is the kinetic temperature, A is a constant and g is the Gaunt factor which is a slowly varying function of frequency and temperature. In the following work, the function g will be approximated by use of the numerical results of Karzas and Latter (1961), which indicate that g is between 0.8 and 1.0 for a temperature range of 10^4 to 10^{10} °K.

The absorption coefficient in evolutionary models at the epoch defined by the parameter y follows from equation (6.2) and it may be written in the form

$$K(\nu, y) = Ag(y)\{1 - e^{-h\nu_o/kTy}\}y^{-3}T^{-1/2}N_o^2\nu_o^{-3} \qquad (6.3)$$

where the subscripts correspond to values at the present epoch and $T \equiv T(y)$ is the gas temperature.

Hence by analogy with the ordinary equation for free-free absorption

$$\delta\tau(\nu_o) = K(\nu, y)\delta U \qquad (6.4)$$

where δU is the element of proper distance. But according to equations (3.8) and (4.23)

$$\delta U = R(t)\delta\omega = c\delta t \qquad (6.5)$$

Therefore

$$\tau(\nu_o) = c \int_{t_o}^{t} K(\nu, y)dt$$

and using equation (4.4) this becomes

$$\tau(\nu_o) = \frac{c}{H_o} \int_1^y \frac{K(\nu, y)}{\sqrt{f(y)}} dy \qquad (6.6)$$

According to equation (6.3) the absorption properties of the intergalactic medium will be fairly strong functions of the thermal history of the universe. The variation of the kinetic temperature with epoch will be examined in closer detail in the next chapter. Here, we shall consider only some simple models for the thermal history of the intergalactic material and compare the low-frequency absorption effects in different world-models.

As a very close approximation, all the matter in the universe may be considered to exist as ionized hydrogen. In this case equation (3.19) gives the number of electrons per unit proper volume at the present epoch as

$$N_o = \frac{3H_o^2\sigma_o}{4\pi G m_H} \qquad (6.7)$$

where m_H is the mass of a hydrogen atom. Hence N_o is essentially determined by the density parameter σ_o. For typical values of σ_o

N_o is of the order of 10^{-5} cm^{-3}. Two thermal histories are considered for evolutionary universes.

(a) Adiabatic Expansion

If, as suggested by equation (3.7), the expansion of the universe is adiabatic then the temperature of the intergalactic plasma can be written as

$$T = T_o[N(y)/N_o]^{\gamma-1}$$

Since $N = N_o y^{-3}$ and $\gamma = 5/3$ for ionized hydrogen we have

$$T = T_o y^{-2} \tag{6.8}$$

for evolutionary universes which expand adiabatically. Substituting for T in equations (6.3) and (6.6) the optical depth for frequencies $\nu_o << kT/h$ is

$$\tau(\nu_o) = \frac{BN_o^2}{T_o^{3/2}\nu_o^2} \frac{c}{H_o} \int_y^1 \frac{g(y)y^{-1}dy}{\sqrt{f(y)}} \tag{6.9}$$

where $B = Ah/k \simeq 0.4$ c.g.s. units and $Y = (1 + z)^{-1}$ is determined by the source redshift.

(b) Constant Temperature Expansion

Layzer (1963, 1966) has advanced the concept of a constant temperature universe in which local non-uniformities in the distribution of matter give rise to a negative gravitational contribution to the internal energy density. The expansion of the metagalaxy tends to decrease the kinetic contribution to the internal energy, and to increase the gravitational contribution. Layzer suggests that when account is taken of energy losses by radiation, the temperature of the gas remains approximately constant with time. If this is the case then according to equations (6.3) and (6.6) the optical depth is

$$\tau(\nu_o) = \frac{BN_o^2}{T_o^{3/2}\nu_o^2} \frac{c}{H_o} \int_1^{\infty} \frac{g(y)y^{-4}}{\sqrt{f(y)}}\, dy \qquad (6.10)$$

for constant temperature universes.

The absorption factor $e^{-\tau(\nu_o)}$ is plotted against frequency in figure 6.1 for cosmological models having $\sigma_o = 0.5$ and sources with a redshift of one. Low frequency absorption of radio waves is apparently not a strong function of the deceleration parameter, q_o, either in an adiabatic or constant temperature expansion. The absorption factor in the Einstein-de Sitter world model is shown as a function of redshift in figure 6.2. In this case free-free absorption of radio waves is only a weak function of redshift for an

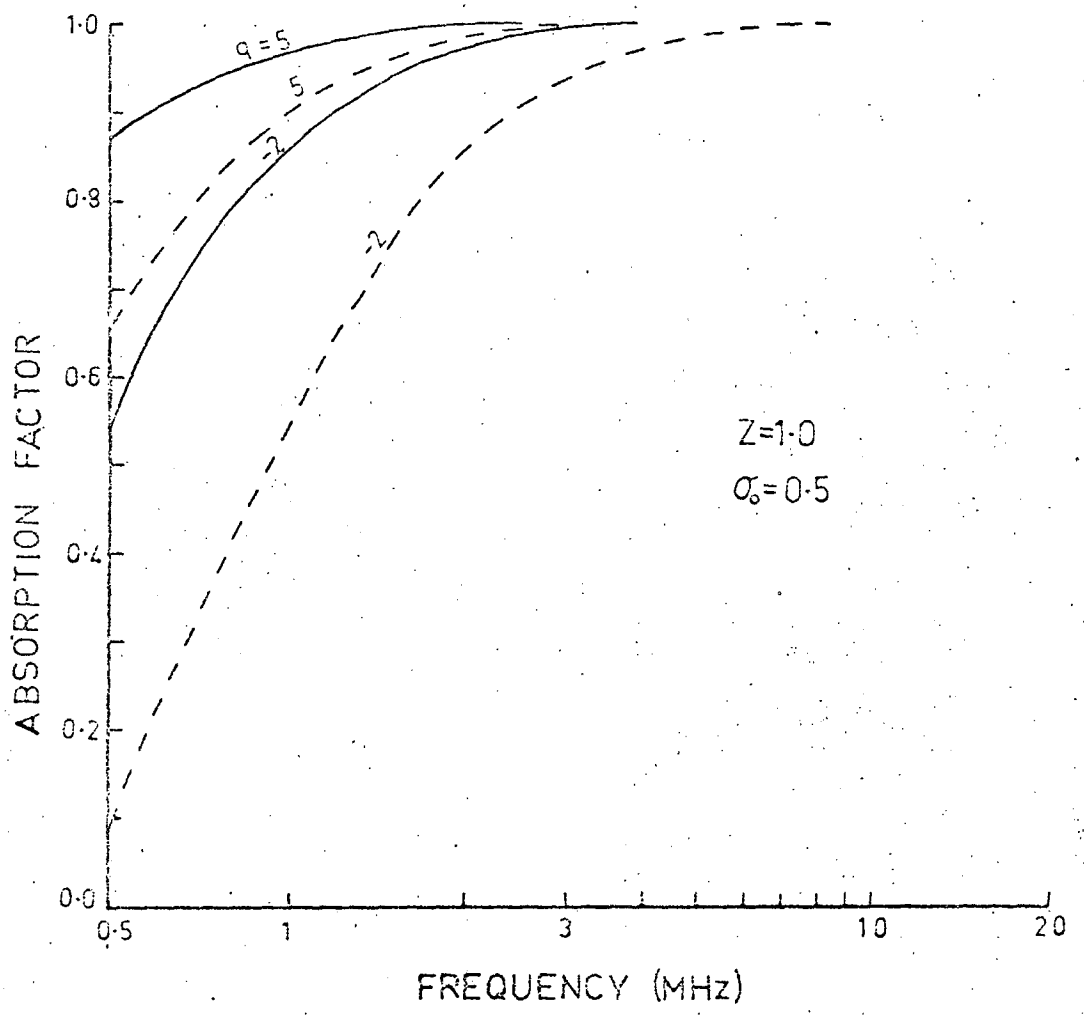

Figure 6.1 - Low frequency absorption in the intergalactic medium indicated by plots of the absorption factor, exp $(-\tau)$, against frequency for world-models having $\sigma_o = 0.5$ and radio sources with redshift of unity.

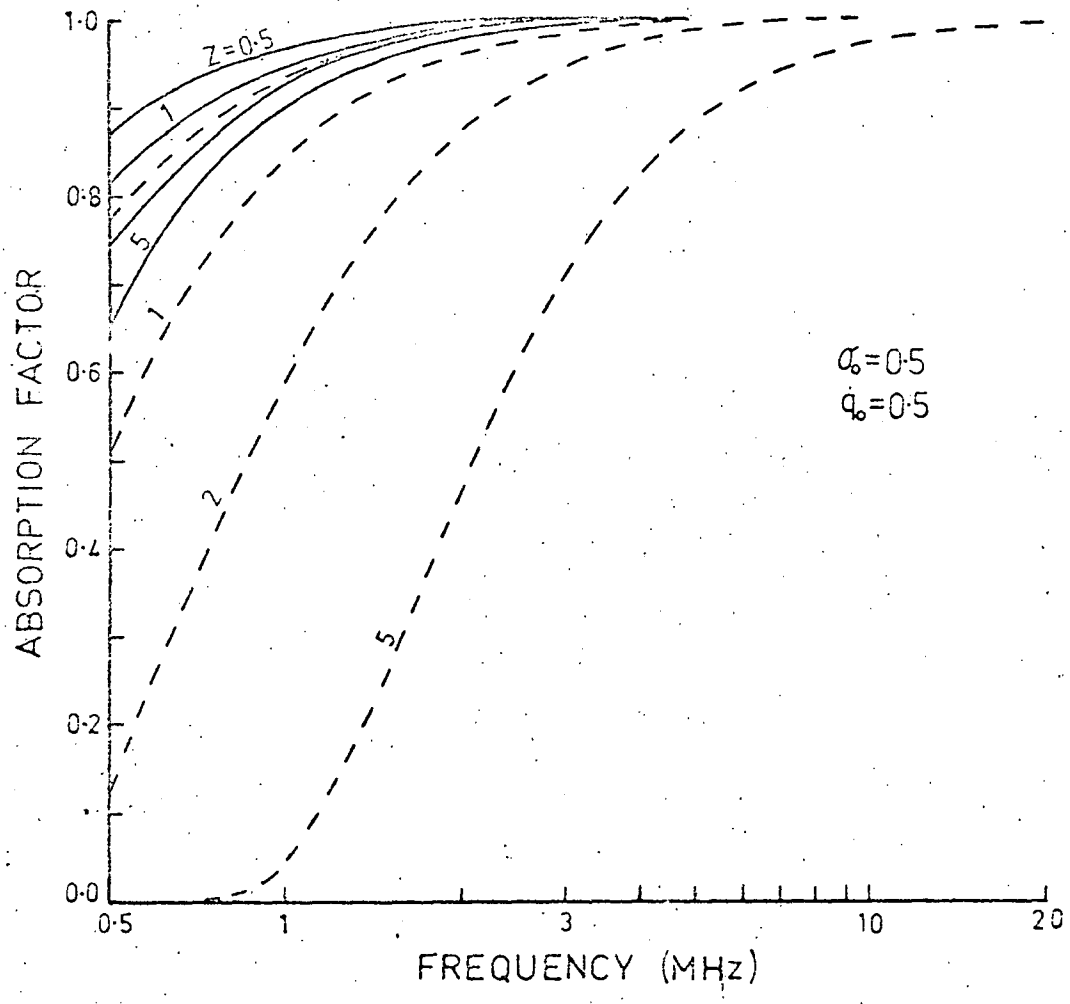

Figure 6.2 - The absorption factor in an Einstein-de Sitter universe for sources with different redshifts.

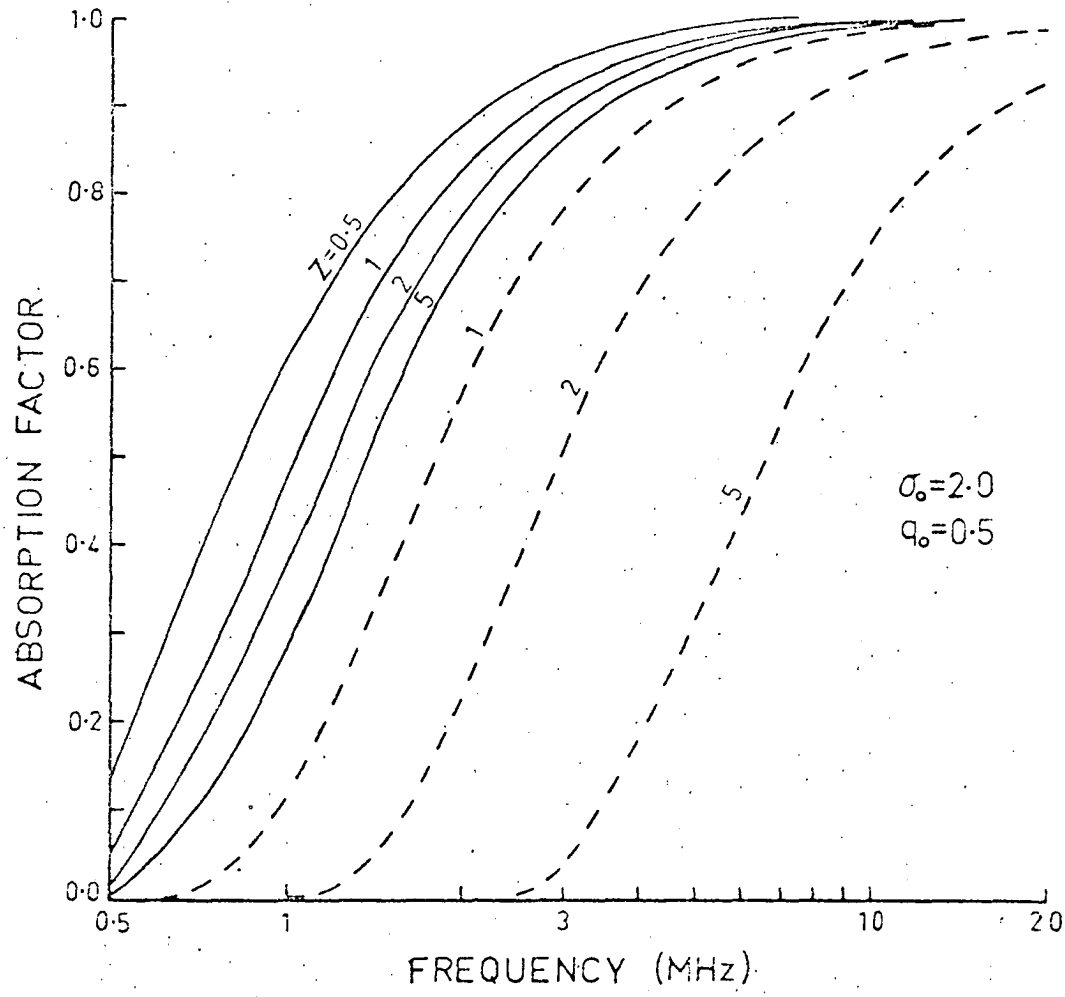

Figure 6.3 - The absorption factor for world-models defined by $\sigma_o = 2$ and $q_o = 0.5$.

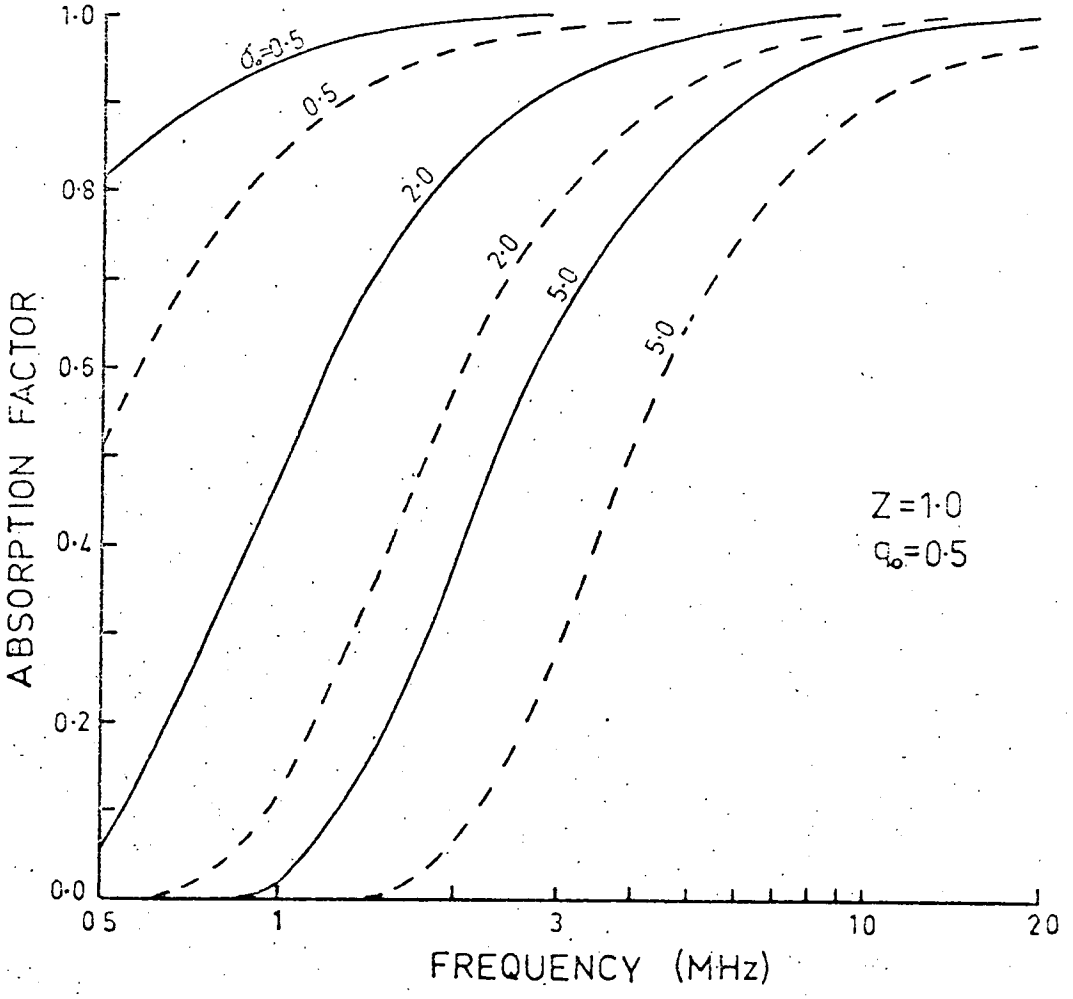

Figure 6.4 - The absorption factor for world-models with deceleration parameter q_o = 0.5 and radio sources having unit redshift.

adiabatic expansion while it is a much stronger function of redshift in the constant temperature model. The last diagram is repeated in figure 6.3 for $\sigma_o = 2.0$. The absorption factor is now seen to decrease substantially for frequencies less than 20 MHz. Absorption is strongly dependent on σ_o and this is simply due to the N_o^2 term in equations (6.9) and (6.10). The variation of the absorption factor with σ_o is shown in figure 6.4 for world models having $q_o = 0.5$ and for sources with redshifts of unity.

(c) Steady-State Models

In steady-state universes the density and temperature of the universal plasma must be independent of epoch. Substituting $\sigma_o = 0$, $q_o = -1$ in equation (6.6) we have

$$\tau(\nu_o) = \frac{BN_o^2}{T_o^{3/2}\nu_o^2}\frac{c}{H_o}\int_y^1 g(y)y\,dy \qquad (6.11)$$

and since in this case g is constant then

$$\tau(\nu_o) = \frac{BgN_o^2}{T_o^{3/2}\nu_o^2} \times 0.5[1 - (1+z)^{-2}] \qquad (6.12)$$

Hence in a steady-state universe the optical depth does not go to infinity with redshift but reaches a maximum value. The electron density in the steady-state universe as originally proposed by Hoyle (1948) will be given by

$$N_o = 3H_o^2/8\pi G m_H = 1.1_{10}{}^{-5} \text{ cm}^{-3} \qquad (6.13)$$

It follows that the absorption factor in steady-state models will be insignificant for frequencies greater than about 1 MHz. The same situation applies even if the electron density is twice the value given in equation (6.13) as suggested by a later version of the steady-state theory (Hoyle and Narlikar, 1962).

An exercise which could provide some useful information on cosmological parameters would be a search for a correlation between the cut-off frequency in source spectra and their redshift. Unfortunately the available low frequency data is very limited. Surveys of discrete radio sources have been made at 26.3 MHz (Erikson and Cronyn, 1965), 38 MHz (Williams et al., 1966), and in the range 20-40 MHz (Bazelean et al., 1965). Only a few flux measurements of radio galaxies have been made at frequencies less than 20 MHz (e.g. Ellis and Hamilton, 1966).

Erikson and Cronyn have plotted the ratio of measured flux at 26.3 MHz to the extrapolated high frequency spectrum against distance. Data was available for a total of only 23 sources which had distance determinations out to approximately 1000 Mpc ($z \simeq 1$). Some of these data were unreliable but there was some slight evidence for a decrease in the ratio for increasing distance. However, the analysis of free-free absorption given in this chapter indicates that a correlation

analysis between cut-off frequency and redshift should be carried out at frequencies less than about 10 MHz, if any useful results are to be obtained.

6.3 Conclusions

The results obtained in this chapter are rather tentative since they depend rather critically on uncertain parameters such as the density and temperature of the intergalactic ionized hydrogen. The source count analyses of Chapter V have indicated the possibility of relatively large electron densities. The electron temperature and its variation with epoch will be considered in some detail in the following chapter.

In this chapter, adiabatic and constant temperature universes have been considered and it has been shown that a significant amount of intergalactic free-free absorption may occur in radio spectra below about 20 MHz. The effect on the low frequency spectra of discrete radio sources depends on the particular cosmological model and the source redshift as well as the parameters mentioned above. It is apparent from the calculations that the low frequency cut-off in source spectra is not necessarily due solely to synchrotron self-absorption or thermal absorption in the source itself.

CHAPTER VII

THE BACKGROUND RADIATION IN ISOTROPIC WORLD MODELS

In this chapter, a general equation for the extragalactic background intensity is derived for the general case of an isotropic homogeneous universe. The extragalactic radio background depends fairly critically on the thermal history of the universe and numerical results will be obtained for different possible models.

The radio background is considered here to be the sum of contributions from two sources: (1) emission by ordinary radio galaxies and (2) free-free emission from intergalactic ionized hydrogen. Account will also be taken of the free-free absorption that must occur at low frequencies if significant amounts of ionized hydrogen actually exist in the space between galaxies.

7.1 Equation for the Background Radiation

Consider the 3-space specified by the co-ordinate (r, Θ, ϕ). According to equation (3.4), these three mutually perpendicular co-ordinates define a volume element

$$dv = \frac{R^3(t) r^2}{(1 + kr^2/4)^3} \, dr \, d\Omega \qquad (7.1)$$

where $d\Omega$ is the solid angle subtended by the element, as measured by the origin observer.

Further, let us suppose that the emission coefficient (watts $(c/s)^{-1}sr^{-1}$ per unit proper volume) is $j(\nu, t)$. The total flux received at the origin at time t_o will be $dS(\nu_o)d\nu_o$ (watts m^{-2}) given by

$$dS(\nu_o)d\nu_o = \frac{j(\nu, t)}{D^2(t)}\, d\nu\, d\nu \tag{7.2}$$

where as usual D is the luminosity distance defined by equation (5.9). Using $d\nu = d\nu_o R_o/R$ we obtain for the received flux density at frequency ν_o

$$dS(\nu_o) = \frac{j(\nu, t)R^4(t)}{R_o^3(1 + kr^2/4)}\, dr\, d\Omega \tag{7.3}$$

Now the equation to the null-geodesic is

$$\frac{dr}{1 + kr^2/4} = -\frac{cdt}{R(t)} \tag{7.4}$$

and substituting in (7.3) we have

$$S(\nu_o) = -c\left(\int_{t_o}^{t} j(\nu, t)(R/R_o)^3 dt\right) d\Omega \tag{7.5}$$

If the absorption coefficient of ionized hydrogen in intergalactic space is denoted by $K(\nu, t)$, then the last equation must be modified appropriately. Hence changing equation (7.5) from an integration over epoch to an integration over expansion parameter y the intensity of the background radiation in evolving world models must be

$$I(\nu_o) = c \int_{y_o}^{1} j(\nu_o y^{-1}, y) y^3 \exp\left(- c \int_{y}^{1} K(\nu_o y'^{-1}, y) \frac{\partial t'}{\partial y'} dy'\right) \frac{\partial t}{\partial y} dy \qquad (7.6)$$

where the exponential term is analogous to optical depth. The partial derivative, $\partial t/\partial y$, is given as a function of y (and the particular cosmological model) through equation (4.4). Hence, if the parameters q_o, σ_o and T_o are specified then the world model is defined, and together with an estimate of the function $j(\nu, y)$ the expected extragalactic background intensity may be calculated by the numerical integration of equation (7.6).

It should be noted that in the steady-state model the emission and absorption coefficients should be independent of epoch and the equation to the background intensity becomes

$$I(\nu_o) = \frac{c}{H_o} \int_0^1 j(\nu_o y^{-1}) y^2 \exp\left(-\frac{c}{H_o} \int_y^1 K(\nu_o y'^{-1}) y'^{-1} dy'\right) dy \tag{7.7}$$

since in this case $\partial y/\partial t = H_o y$.

The lower limit y_o of equation (7.6) will depend on the y corresponding to the observer's particle horizon. In evolutionary cosmologies the limit is usually zero and the geometry of the model assists the convergence of the integral. In oscillating models the limit is undefined, unless the universe is treated as existing for a finite time (the time for one oscillation). The type E2 models which have large negative values for q_o collapse from an infinitely rarefied state to a state of finite density corresponding to an expansion parameter value of $y = y_{min} > 0$. At this stage, the universe reverses its motion and expands monotonically into an empty de Sitter model. The limit of integration in this case will be $y_o = \infty$ and (7.6) must be integrated through a singularity at y_{min} where $dy/dt = 0$. In this case the derived background intensity will diverge to infinity unless a cutoff is introduced for the emission coefficient at a particular value of y. The integral of equation (7.7) for the background radiation in steady-state cosmologies has a lower limit $y_o = 0$ and the geometry of the metric aids the convergence of the integral, although not as strongly as in most of the evolutionary models. We shall find later however that the emission coefficient will increase with redshift at a much faster rate in evolutionary cosmologies than in the steady-state model.

7.2 The Emission Coefficient

(a) Radio Sources

The contribution from radio galaxies to the background intensity will depend on their luminosity distribution and the variation of their spatial density and luminosity with epoch. All these quantities have been discussed in earlier chapters. As far as the background radiation is concerned these properties of radio galaxies are assumed to be defined by equation (5.4) and the values of y_o, n and β which were derived from the radio source counts in Chapter V.

Now, it is well known that radio sources may exhibit low frequency turnovers in their spectra due to a variety of possible causes including thermal absorption, synchrotron, self-absorption in the source itself, and a cut-off in the electron energy distribution. These effects have been described briefly in section 5.4. Here, the low frequency spectral behaviour of radio galaxies is approximated by assuming that the power emitted is of the form

$$P(\nu) = C(\nu^{-\alpha+2}/\nu_c^2)[1 - \exp\{-(\nu_c/\nu)^2\}] \qquad (7.8)$$

where ν_c is the critical frequency corresponding to unit optical depth in the source. Obviously for frequencies $\nu >> \nu_c$ the source luminosity is of the form given in equation (5.35). Using $\nu = \nu_o y^{-1}$,

the emitted power at the epoch corresponding to y is

$$P(\nu_o y^{-1}) = P_{178}\left(\frac{\nu_o}{178}\right)^{-\alpha}\left(\frac{\nu_o}{\nu_c}\right)^{2} y^{\alpha-2}\left[1 - \exp\left\{-\left(\frac{\nu_c y}{\nu_o}\right)^{2}\right\}\right] \tag{7.9}$$

with the radiation being detected at frequency ν_o. The last equation applies only to those sources whose luminosity is not a function of epoch. Hence we first consider the emission coefficient for radio sources having spatial densities which evolve smoothly with epoch. The contribution to $j(\nu, y)$ will be

$$dj_r = n(m')\, P(\nu_o y^{-1})\, dm' \tag{7.10}$$

where n is the number of sources in the range m', $m' + dm'$ and $m' = P(\nu_o y^{-1})/P_o$. But, clearly $n(m') \equiv n(m)$ where now $m = P_{178}/P_o$ as before. Hence integrating (7.10) and using (5.8) we have

$$j_r(\nu, y) = \rho_o P_o \int_0^{\infty} m^{-2.5} e^{-x^2/2\sigma^2} \frac{P(\nu_o y^{-1})}{P_o} y^{-(3+n)}\, dm \tag{7.11}$$

where as before n determines the variation of the number of sources in unit co-ordinate volume. Now using equation (7.9) the last equation becomes

$$j_r(\nu, y) = \rho_o P_o \left(\frac{\nu_o}{178}\right)^{-\alpha} \left(\frac{\nu_o}{\nu_c}\right)^2 y^{\alpha-5-n} \left[1 - \exp\left\{-\left(\frac{\nu_o y}{\nu_o}\right)^2\right\}\right]$$

$$\times \int_0^\infty m^{-1.5} e^{-x^2/2\sigma^2} \, dm \qquad (7.12)$$

for universes in which the spatial density of sources evolves with epoch. Rewriting this equation in a simplified form

$$j_r(\nu, y) = F(\nu_o) y^{\alpha-5-n} \left[1 - \exp\left\{-\left(\frac{\nu_c y}{\nu_o}\right)^2\right\}\right] \qquad (7.13)$$

If the luminosity of radio galaxies varies according to the law $P(y) = P(1)y^{-\beta}$ as described in section 5.6, then it is clear that the contribution to the emission coefficient from these sources will be

$$j_r(\nu, y) = F(\nu_o) y^{\alpha-5-\beta} \left[1 - \exp\left\{-\left(\frac{\nu_c y}{\nu_o}\right)^2\right\}\right] \qquad (7.14)$$

(b) Free-Free Emission

According to Allen (1965), the free-free emission per unit volume and unit frequency range for ionized hydrogen of density N and temperature T is

$$\varepsilon(\nu) = B \, g \, N^2 T^{-1/2} \exp(-h\nu/kT) \qquad (7.15)$$

where $B = 6.8 \times 10^{-39}$ MKS units and g is the Gaunt factor.

Substituting $N = N_o y^{-3}$ we obtain for evolutionary universes

$$\varepsilon(\nu, y) = B\, g(y)\, \exp(-h\nu_o/kTy)\, y^{-6} N_o^2 T^{-1/2} \qquad (7.16)$$

where as before $T \equiv T(y)$ is as yet an unknown function of the expansion parameter y.

Similarly, for the steady-state models

$$\varepsilon(\nu) = B\, g(y)\, \exp(-h\nu_o/kT_o y) N_o^2 T_o^{-1/2} \qquad (7.17)$$

The last two equations indicate that the background radiation due to free-free emission will be considerably greater in evolutionary cosmologies than in steady-state models unless the temperature T is a steep function of y.

The total emission coefficient may now be written in the general form

$$j(\nu, y) = j_r(\nu, y) + \varepsilon(\nu, y) \qquad (7.18)$$

7.3 The Observed Background Intensity

It is the purpose of this chapter to examine the predicted background spectrum as a function of possible thermal histories of

the universe. Account will be taken of the results obtained in Chapter V for radio source luminosity and spatial evolution. As far as the author is aware, only one account has been given of the background radiation in the low frequency region of the radio spectrum. Kaufman (1965), who restricted her analysis to the Einstein-de Sitter universe, derived theoretical background spectra with the assumption that the ionized gas behaved isothermally back to infinite densities. Kaufman assumed that the observed background spectrum was due entirely to extragalactic sources of radiation, and by fitting theoretical curves to the experimental spectrum in the frequency range 5-100 MHz, and to the spectral point at 4080 MHz (Penzias and Wilson, 1965), she was able to determine limits for intergalactic hydrogen density. However, we shall find that, on the basis of the available evidence it is unlikely that the extragalactic component could contribute much more than 10 per cent. to the observed background intensity. Here, a more systematic approach will be made to the problem of the extragalactic background intensity. Some models will be considered only briefly while more attention will be given to those models which are consistent with the results derived from the source counts.

The experimental background spectrum has been plotted in figure 7.1. The spectral points are taken from the measurements of many observers and are plotted for directions near to the galactic poles, corresponding to minimum disk effects such as non-thermal emission or low frequency absorption. The experimental points at

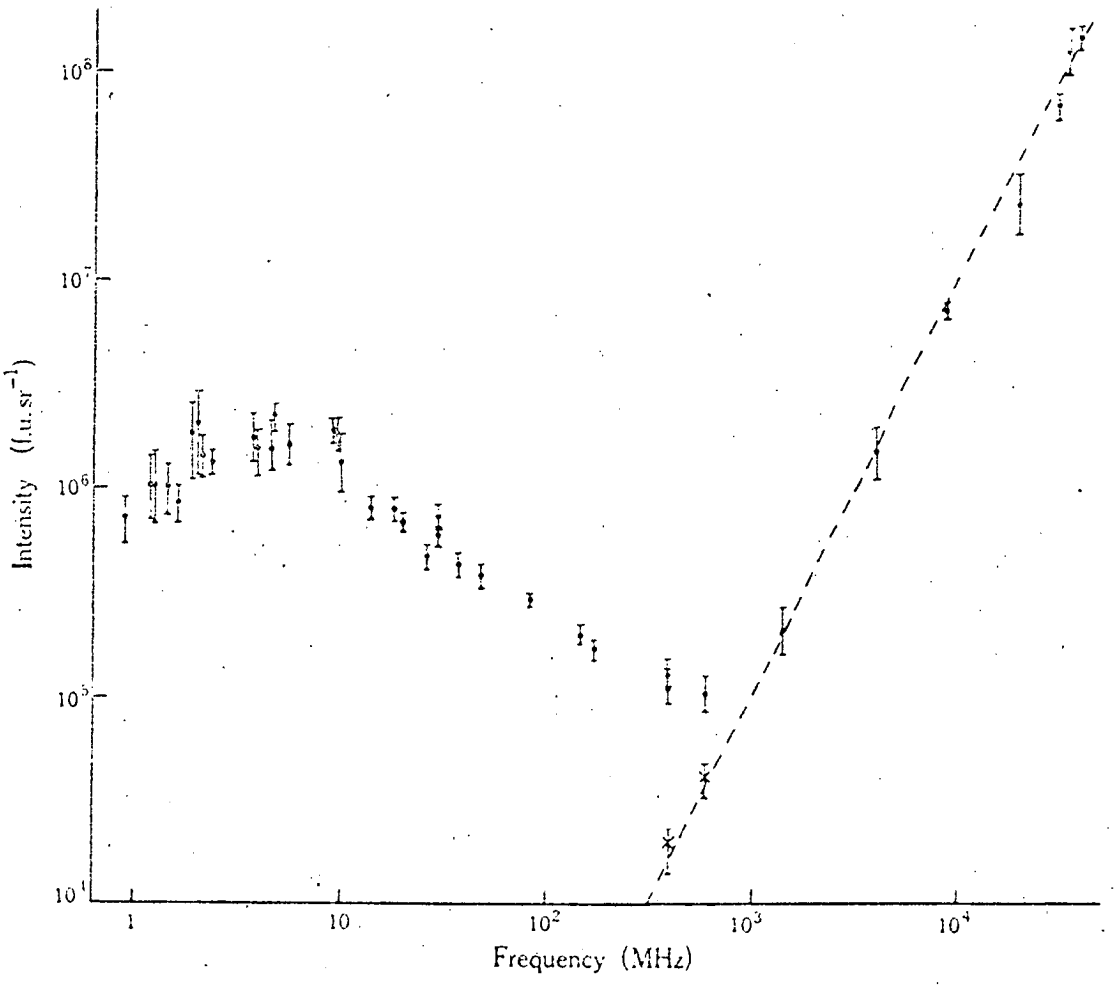

Figure 7.1 - Observed total background spectrum for direction near to the galactic poles.

frequencies greater than 1000 MHz, which approximate closely to a 3°K black-body spectrum, are also included. The spectral points in figure 7.1 have been obtained from the following measurements:

Observer	Frequency (MHz)
Ellis (1957)	0.9, 1.43, 2.13, 3.8, 4.4, 5.65, 9.13, 10.05
Walshe, Haddock, and Schulte (1963)	1.225, 2.0
Ellis (1964)	1.65, 2.4, 4.8, 4.6
Yates and Wielebinski (1965)	14.1
Yates and Wielebinski (1966)	14.1, 20, 30, 48.5, 85
Shain and Higgins (1954)	18.3
Turtle et al. (1962)	26.3, 38, 178, 400
Mathewson, Broten, and Cole (1965)	30
Yates (personal communication)	85
Mills (1959)	85.5
Howell and Shakeshaft (1967)	408, 610
Penzias and Wilson (1966)	1430
Howell and Shakeshaft (1966)	1450
Penzias and Wilson (1965)	4080
Roll and Wilkinson (1966)	9380
Welch et al. (1967)	2×10^4
Thaddens and Clauser (1966)	1.15×10^5

7.4 Steady-State Models

Although the radio source counts have thrown considerable doubt on the validity of the steady-state theory the expected background intensity in these models is briefly discussed in this section. In steady-state cosmologies, the density and temperature of the universal plasma must remain constant, independent of epoch. Assuming 100 per cent ionization, the electron density for the model originally proposed by Hoyle (1948) will be given by

$$N_o = 3H_o^2/8\pi G m_H = 1.1_{10}{}^{-5} \text{ cm}^{-3} \qquad (7.19)$$

In another version of the steady-state theory, Hoyle and Narlikar (1962) suggested that, as a consequence of the existence of the creation field C^μ, the observed homogeneity and isotropic state is an asymptotic state for all initial conditions. It follows from the theory that a perturbation $C_i^i \neq 0$, introduced into the C field, will cause the expansion factor y(t) to converge to an exponential form while the matter density, ρ, approaches $3H_o^2/4\pi G$. Hence we have an alternative electron density in a steady-state model which is twice the value predicted by ordinary theory. The free-free emission and optical depth for a particular y will be correspondingly four times the values calculated on the basis of equation (7.19). The expected background intensity may be derived for both cases with the aid of equations (7.7), (7.9), (7.17) and (7.18). The numerical results are shown in figures 7.2 and 7.3 for electron densities of $1.1_{10}{}^{-5}$ and $2.2_{10}{}^{-5}$ cm^{-3} respectively and various kinetic temperatures for the intergalactic gas. Comparing figures 7.2 and 7.3 with figure 7.1 we see that the expected background intensity in steady-state universes is approximately 9 per cent of the observed intensity at 10 MHz and this value is reduced to almost 1 per cent at 1000 MHz. At even higher frequencies the contribution to the background intensity in the steady-state models is insignificant and if it is shown conclusively that the 3°K black-body radiation is indeed extragalactic in origin, then it is difficult to imagine how any modification of the

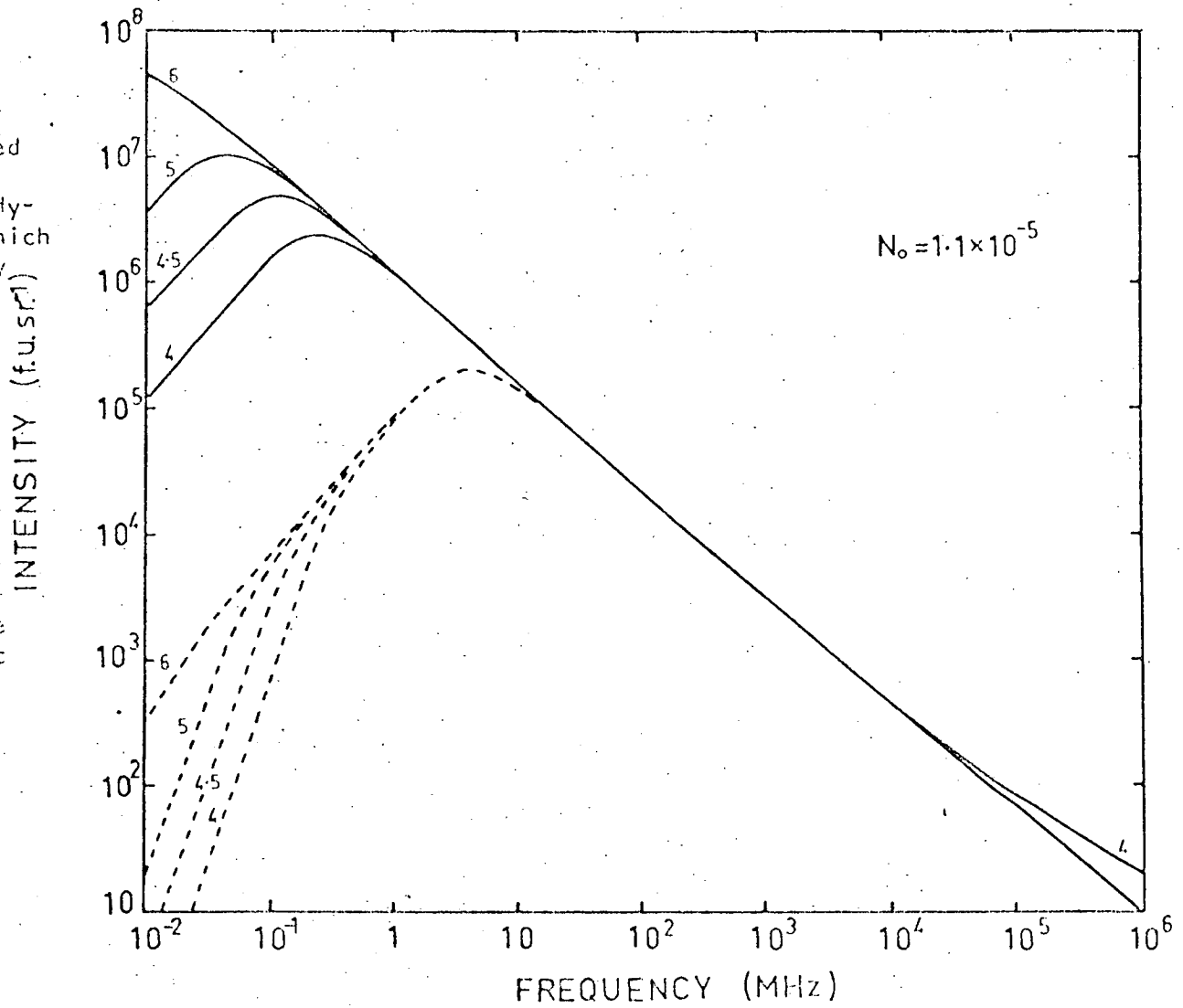

Figure 7.2 - Expected extragalactic radio spectrum for a steady-state universe in which the electron density is $1.1 \times 10^{-5} cm^{-3}$. The dashed curves indicate the possible low frequency spectra if the source average spectrum has a 5 MHz cut-off. The numbers on the curves are the logarithms of the constant temperature of the intergalactic gas.

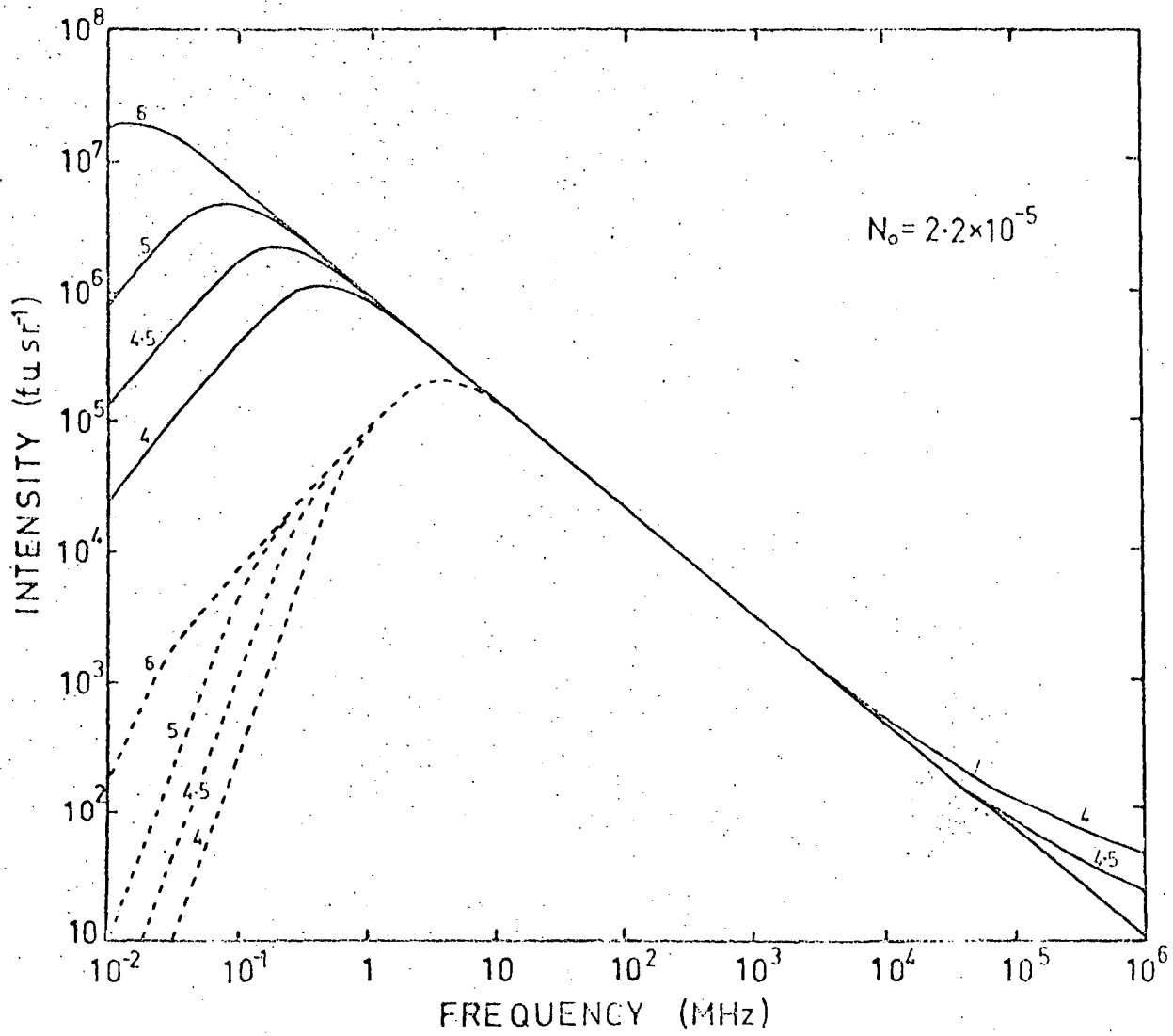

Figure 7.3 - Expected extragalactic radio spectrum for a steady-state universe in which the electron density is $2.2 \times 10^{-5} cm^{-3}$.

steady-state theory can fit the observed data.

7.5 Constant Temperature Model

The cosmological energy equation, which can be written as

$$\frac{d\varepsilon y^3}{dt} + \frac{p dy^3}{dt} = 0 \qquad (7.20)$$

where ε is the mean energy density, is easily derived from the Einstein field equations for a homogeneous, unbounded, isotropic medium. Equation (7.20) is usually accepted as the form of the first law of thermodynamics which describes a universe undergoing adiabatic expansion. However, certain conceptual difficulties arise in the interpretation of this equation since it is implied that an expanding volume element does work on the surrounding gas, although symmetry considerations show that there cannot be a net flow of energy across a co-moving surface. Layzer (1963, 1966) believes equation (7.20) to be of a completely kinematical origin. Briefly, Layzer argues from the theory of particle dynamics in a homogeneous unbounded system and he finds two coupled equations for the mean kinetic energy per unit mass and the mean potential energy per unit mass. One equation is analogous to equation (7.20), while the other is the cosmogonic virial theorem. The total energy is negative, and if the effects of radiation are small then the kinetic and potential energies are approximately constant and as a consequence the kinetic temperature of the

distribution must also remain constant.

The theory for a constant temperature universe as described by Layzer is valid only in the absence of heat sources, and in the numerical calculations for the background intensity it was assumed that the gas temperature remained constant throughout the entire history of the universe. This assumption will not significantly affect the high frequency spectrum, but the intensity at low frequencies may be under-estimated. The numerical results in figure 7.4 are based on an Einstein-de Sitter universe in which the electron density is $1.1_{10}{}^{-5}$ cm^{-3} for 100 per cent ionization. In this model the free-free emission was calculated with the use of equation (7.16) after substituting $T = T_o$ = constant. Comparison with figure 7.1 shows that the predicted intensity of the constant temperature model will exceed the total background intensity up to frequencies of 10^4 MHz, while at frequencies higher than this but less than about 10^5 MHz it is considerably less than the observed intensity. We also note that radiation in the microwave region has a spectral index of about 1.2 which is almost independent of either temperature or the degree of ionization. The value differs significantly from the spectral index of 2 for a Planck function, and we must conclude that the constant temperature model in its present form does not produce a satisfactory representation of the observations.

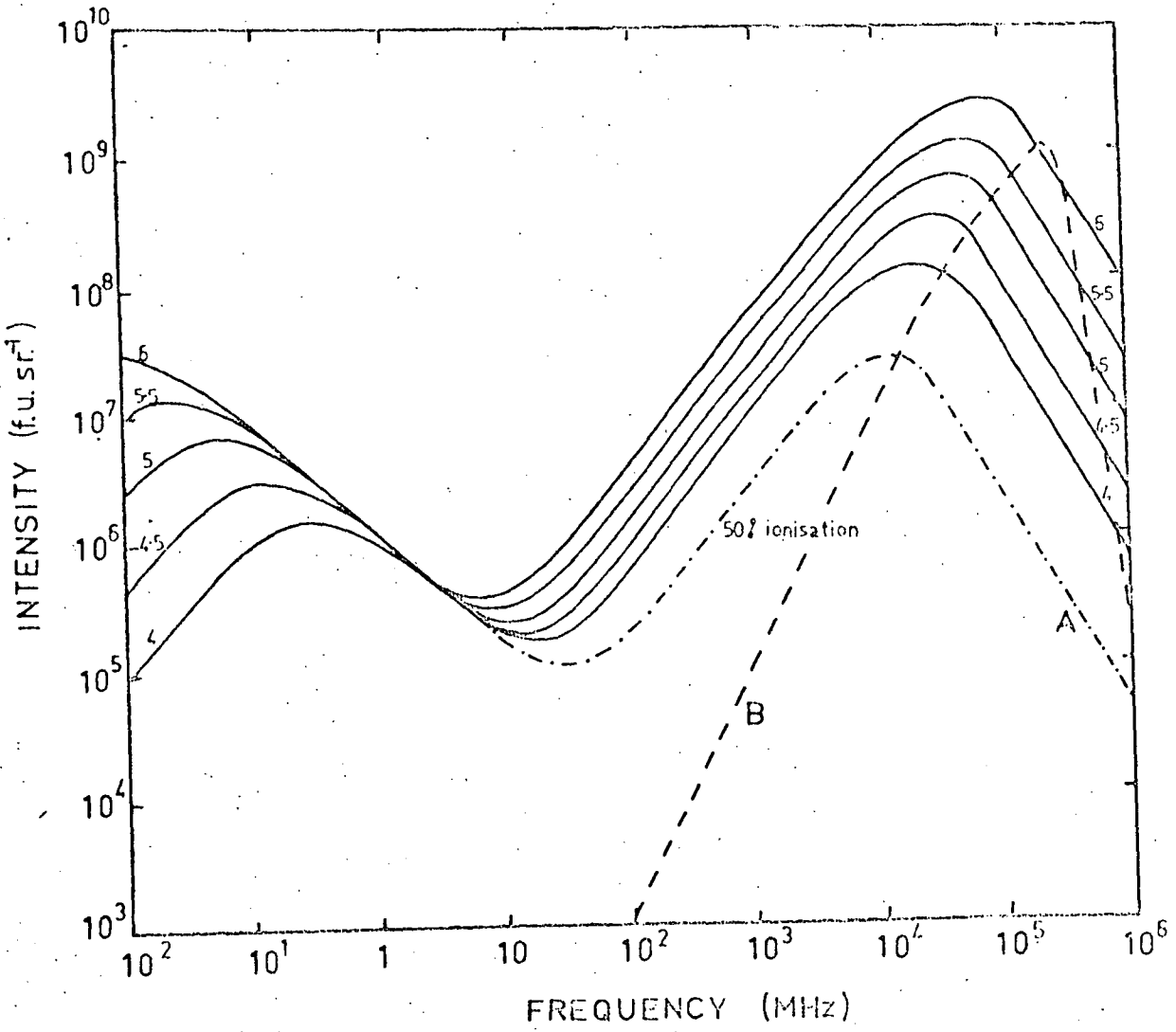

Figure 7.4 - Derived extragalactic background spectra for a constant temperature Einstein-de Sitter universe. The full curves correspond to a gas that is completely ionized, while the dashed curve represents the 3°K black-body spectrum.

7.6 The Thermal History of the Intergalactic Gas

Before consideration is given to the evaluation of the background intensity in further models it is proposed to examine in closer detail the possible thermal histories of the intergalactic gas. In evolving world models the thermal behaviour of the gas can be strongly influenced by heating and cooling mechanisms that destroy the adiabatic nature of the expansion.

Ginzburg and Ozernoi (1966) have considered the kinetic temperature of the intergalactic gas in the Einstein-de Sitter model. They include in their analysis heating effects due to plasma oscillations excited by anisotropic cosmic rays and heat generation from ionization by "sub-cosmic rays". They also account for cooling due to free-free transitions, recombination radiation, and the expansion of the metagalaxy. In this analysis each of these processes shall be considered in a more general way and a differential equation describing the temperature of the intergalactic gas shall be derived.

(a) Radiation Cooling

The rate of energy loss per unit volume through free-free emissions will be given by integrating equation (7.16) over all frequencies. The result is

$$\frac{\partial E_{ff}}{\partial t} = -\int_0^\infty \varepsilon(\nu)d\nu$$

$$\simeq -1.4_{10}{}^{-27}T^{1/2}N^2 = -\alpha T^{1/2}N^2 \text{ erg cm}^{-3} \text{ sec}^{-1} \qquad (7.21)$$

The energy losses due to recombination radiation may be written (Kaplan and Pikelner, 1963) as

$$\frac{\partial E_{fb}}{\partial t} \simeq -5.4_{10}{}^{-22}T^{-1/2}N^2 = -\beta T^{-1/2}N^2 \text{ erg cm}^{-3} \text{ sec}^{-1} \qquad (7.22)$$

(b) Heating by Ionization Losses

It seems reasonable that metagalactic space should be filled with a flux of cosmic rays. As described earlier, radio galaxies are the sources of highly disruptive events which must inject streams of hot gas and a large number of relativistic and sub-cosmic particles into metagalactic space. Thus the galactic explosions responsible for radio emission will be also indirectly responsible for heating of the intergalactic gas. Now the spatial density of strong radio sources is about 10^{-78} cm^{-3} while their energy content in cosmic rays is close to 10^{59} ergs. It has been shown that the duration of the radio emitting phase is about 3×10^6 years. Hence the cosmic ray injection power is 10^{46} ergs/sec and, if this injection power is available for the characteristic time of evolution of the universe, H_o^{-1}, then the cosmic

ray energy density will be

$$\eta \simeq 3 \times 10^{-16} \text{ erg cm}^{-3}$$

This value must be regarded as rather tentative. Ginzburg and Syrovatskii (1964) suggest a cosmic ray energy density of about 10^{-15} erg cm^{-3} while Burbidge (1962) obtains a value of $\eta \simeq 3 \times 10^{-14}$ erg cm^{-3}.

The energy released per unit time by a non-relativistic particle as it moves through ionized hydrogen is (Ginzburg and Syrovatskii, 1964)

$$\frac{dE}{dt} = 7.62_{10}{}^{-9}\left(\frac{2m_pc^2}{E_k^2}\right)^{1/2}\{\ell n \frac{E_k}{m_pc^2} - \ell n\, N^{1/2} + 38.7\}N$$

Hence the heating due to sub-cosmic rays becomes

$$\frac{dE_i}{dt} = \left(-\frac{dE}{dt}\right)N_p = 6.7_{10}{}^{-22}\frac{\eta' N}{E_k^{3/2}}\{\ell n \frac{E_k}{m_pc^2} - \ell n\, N^{1/2} + 38.7\} \qquad (7.23)$$

where N_p is the concentration of fast non-relativistic protons of energy E_k and η' is their energy density. It would hardly be reasonable for η' to exceed η and as a rough estimate we take $\eta' \simeq \eta$. To a first approximation the last equation can then be written

$$\frac{dE_i}{dt} \simeq 8.0_{10}{}^{-14}\,\eta\, N \text{ erg cm}^{-3} \text{ sec}^{-1} \qquad (7.24)$$

(c) Heating by Cosmic Rays

Ginzburg and Ozernoi (1966) suggest that the injection of relativistic particles is followed by an efficient build-up of plasma and other waves in the intergalactic plasma. The energy density of these waves will be $\eta_o \simeq \eta + \eta'$. These oscillations are subsequently converted into heat and the time required for the thermalising process is extremely short $\simeq 10^4$ years. The heat generated by exploding galaxies at the present epoch is therefore

$$\frac{dE_p}{dt} \simeq \rho_o \bar{P}$$

where ρ_o is the spatial density of sources and $\bar{P}$ is the power of the high energy particles expelled into the surrounding space. This may then be rewritten as

$$\frac{dE_p}{dt} \simeq 3 \times 10^{-18} \eta \qquad (7.25)$$

The effect of these heating and cooling mechanisms on the temperature of the intergalactic gas may now be calculated from the equation for the first law of thermodynamics. Consider unit mass of gas, then we may write

$$\left(\frac{dE_t}{dt} \right)_{\rho^{-1}} = \frac{dQ}{dt} = \frac{dU}{dt} + \frac{pdV}{dt}$$

$$\left(\frac{\partial E_t}{\partial t}\right)_\rho^{-1} = c_V \frac{dT}{dt} + \frac{p d\rho^{-1}}{dt} \tag{7.26}$$

But from the usual laws of thermodynamics

$$c_V = \frac{R}{M(\gamma - 1)}, \quad P = \frac{\rho RT}{M} \tag{7.27}$$

where $\gamma = c_p/c_V = 5/3$, R is the universal gas constant and M is the molecular weight. All these equations are applicable to co-moving co-ordinate systems and hence substituting (7.27) in (7.26) we get

$$\frac{\partial E_t}{\partial t} = a\rho \frac{dT}{dt} + b\rho^2 \frac{d\rho^{-1}T}{dt} \tag{7.28}$$

where $E_t = E_{ff} + E_{fb} + E_p + E_i$, $a = R/(M(\gamma - 1))$, $b = R/M$. Changing to differentiation with respect to expansion parameter y we have

$$\frac{\partial t}{\partial y}\frac{\partial E_t}{\partial t} = \rho_o y^{-3}\left(a \frac{dT}{dy} + b\rho_o y^{-3} T \frac{d\rho^{-1}}{dy}\right)$$

or using equation (4.4) this becomes

$$\frac{dT}{dy} = \frac{\rho_o^{-1} y^3}{aH_o\sqrt{f(y)}} \frac{\partial E_t}{\partial y} - 3T(\gamma - 1)y^{-1} \tag{7.29}$$

In equations (7.21) and (7.22) we must substitute $N = N_o y^{-3}$. The ionization losses are proportional to $\eta E^{-3/2} N$ and the energy of high energy particles varies as y^{-1} in expanding cosmologies.

Furthermore, the results of Chapter V indicate evolution in source spatial density or luminosity so that the cosmic ray density is proportional to $y^{-(3+n)}$ or $y^{-(3+\beta)}$. Hence at the epoch corresponding to y

$$\frac{\partial E_i}{\partial t} = 8.0_{10}{}^{-14} n N_o y^{-(9/2+n)} \tag{7.30}$$

Similarly, heating by plasma oscillations and shock waves is

$$\frac{\partial E_p}{\partial t} = 3.0_{10}{}^{-18} n y^{-(3+n)}$$

Using these relations, the differential equation defining the gas temperature is given by

$$\frac{dT}{dy} = \frac{1}{\rho_o a H_o \sqrt{f(y)}} \left[8.0_{10}{}^{-14} n N_o y^{-(3/2+n)} + 3.0_{10}{}^{-18} n y^{-n} - \alpha N_o^2 T^{1/2} y^{-3} - \beta N_o^2 y^{-3} T^{-1/2}\right] - 3T(\gamma - 1) y^{-1} \tag{7.31}$$

This differential equation may now be solved by numerical methods in different situations.

7.7 "Adiabatic" Cooling

If it is assumed that the universe has cooled adiabatically throughout its history, then according to the laws of thermodynamics $T = T_o y^{-2}$. In an Einstein-de Sitter universe it follows, with the aid of equations (4.4) and (6.3), that the limit of the optical depth is

$$\lim_{y \to 0} \left(\int_y^1 K(\nu_o, y) \frac{\partial t}{\partial y} \, dy \right) = 2\bar{g} \, K(\nu_o, 1)$$

where $\bar{g}$ is some suitable mean of the Gaunt factor. Hence the optical depth converges to a finite limit while, according to equations (7.7) and (7.16), the free-free emission diverges to infinity. It follows that equation (7.7) cannot be integrated back to the infinite past, and a cut-off in emission must be introduced at a particular y if the background intensity is to remain finite.

Now the differential equation controlling the thermal properties of the gas has been derived in the last section. Heating and cooling processes will destroy the adiabatic nature of the expansion. Also, the average source luminosity and density in co-ordinate volume are assumed to be constant so that n = 0 in equation (7.31). In this case, cooling by free-free and free-bound transitions dominate other heating or cooling mechanisms. Inspection of equation (7.31) shows that $T \to \text{const.} \times y^{-3}$ as $y \to 0$. The differential equation has been

solved by numerical methods.for a series of values T_o in the range 10^4 to 10^7 °K and for cosmic ray energy densities in the range 10^{-14} to 10^{-16} erg cm^{-3}. The possible solutions are illustrated in figure 7.5 where T is plotted as a function of y.

Unless a cut-off in emission is introduced for some arbitrary y, these thermal histories will lead to background intensities far in excess of the observed brightnesses. Indeed the free-free emission must diverge to infinity but at a slower rate than for a simple adiabatic expansion. There are further difficulties associated with adiabatic expansions which will be mentioned briefly in section 7.8 below. An "adiabatic" expansion of this type cannot at any epoch attain a state of thermal equilibrium and this condition restricts the age of the universe.

In the derivation of the background radiation for the adiabatic model a cosmic ray energy density of 10^{-15} erg cm^{-3} was assumed and equation (7.7) was integrated back to the epoch corresponding to a gas temperature of 10^9 °K. At temperatures much greater than this pair creation and annihilation processes would produce a thermal equilibrium distribution between particles and radiation. The type of expansion considered here is impossible under these initial conditions. The results are shown in figure 7.6 and comparison with figure 7.1 indicates that the same general conclusions apply for this model as for the two models of the steady-state theory.

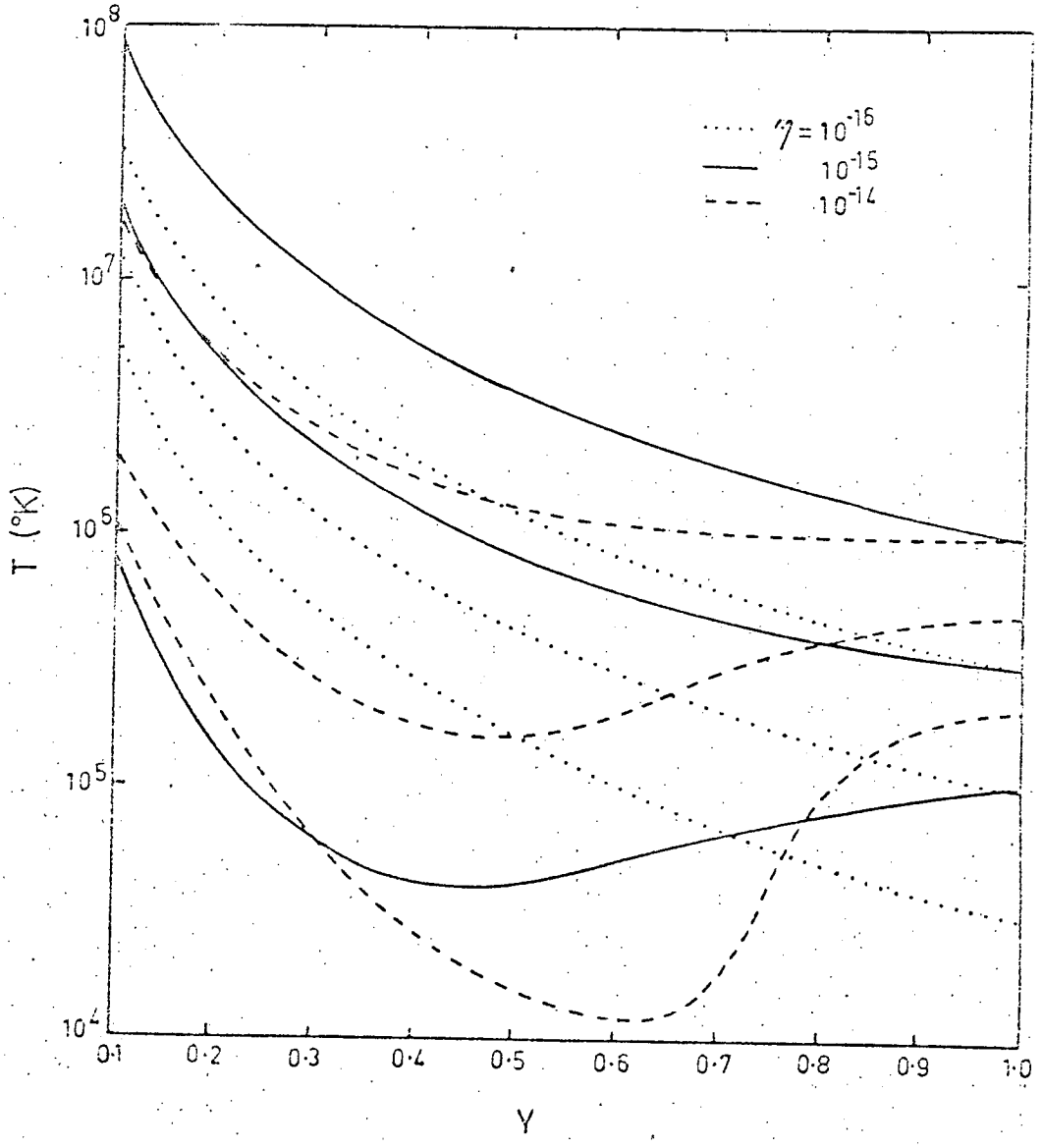

Figure 7.5 - Plots of the temperature T as a function of the expansion parameter y showing possible thermal histories in an adiabatically cooling universe.

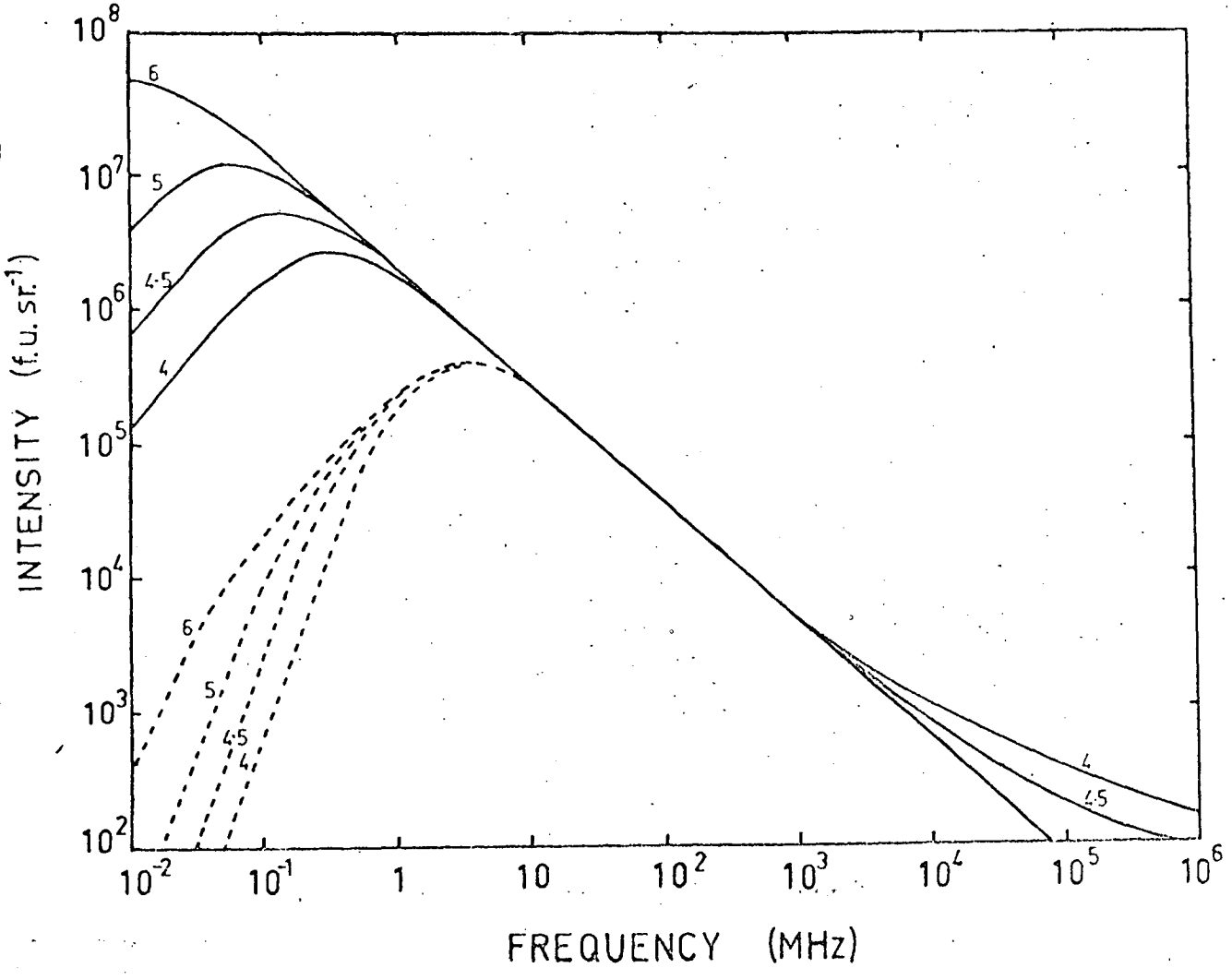

Figure 7.6 - Expected extragalactic background spectra for an adiabatically cooling Einstein-de Sitter universe. The dashed curves indicate the possible low frequency spectra if the source average spectrum has a 5 MHz cut-off. The numbers on the curves are the logarithms of the temperature of the intergalactic gas at the present epoch.

7.8 Black-Body Radiation

The apparent detection of "relic" black-body radiation at 3.5°K by Penzias and Wilson (1965) has some important consequences, for it not only deals a severe blow to the steady-state theory, but it also implies that the universal plasma could not be as hot as a result of initial conditions. In evolutionary universes at early epochs, when the temperature was presumably high and the Thomson scattering depth large, energy exchanges between electrons and photons would ensure a Planck function. We would therefore find, at the present epoch, a gas which is cooler than the black-body radiation and this, of course, is a direct contradiction to the observations. According to Dicke et al. (1965), the gas remains in thermal equilibrium with the radiation until the onset of hydrogen recombination at approximately 4000°K, when the matter consequently cools faster than the radiation. Peebles (1965) believes that this stage of the expansion corresponds to the formation of galaxies. The subsequent release of nuclear energy with the conversion of gravitational energy into heat could be sufficient to increase the temperature of the remaining intergalactic gas as the epoch advances.

According to the calculations of Peebles (1966) on the primeval element abundances issuing from the "big bang", the mass abundance of helium is a function of the mean mass density in the universe and the present temperature of the fireball. For a density range 7×10^{-31}

to 2×10^{-29} g cm^{-3}, the computed helium abundance is 27-30 per cent by mass. The helium content of the universe is not known exactly, but earlier abundance observations have indicated an upper limit of about 25 per cent. However, very recent measurements by Palmer at the United States National Radio Astronomy Observatory have shown that this value is probably an under-estimate. If the 3°K fireball radiation and a low helium abundance is confirmed by future measurements, then the evolutionary universes based on general relativity must have an extremely low density or the fundamental concepts of general relativity theory itself must be invalid. In this work, for the lack of any further evidence, the implications of the helium abundance shall be ignored and the expected background intensity will be derived on the basis of ordinary relativistic cosmology.

Weymann (1966) has examined the possible distortion of the Planck function due to inverse Compton scattering and free-free emission. He did not consider in detail the thermal history of the universal plasma after galaxy formation, but assumed an isothermal expansion at a temperature of 3×10^6 °K. In view of recent evidence presented in Chapter VI, it appears that this estimate for the gas temperature is too high and the consequences of a lower temperature will be an increase in free-free emission and a decrease in emissivity due to electron scattering. It should be noted that Weymann's analysis neglects the contribution of radio sources to the background intensity - a contribution that is certainly significant at frequencies less than

10^3 MHz. In the present analysis, an estimation is made of the temperature path of the gas, so enabling a more accurate calculation for the distortion of the black-body curve, and further the analysis is restricted to relatively low frequencies where the effects of Compton scattering are negligible.

If the microwave spectrum is interpreted as due to fireball radiation, then we can draw some tentative conclusions concerning the temperature of the plasma. Since the gas is tied to the radiation field, it must cool according to the law $T = T_o y^{-1}$, at least until recombination commences. The gas will dissociate from the radiation field at a temperature close to 10^4 °K ($y = 3 \times 10^{-4}$). Formation of gravitationally bound gas clouds follows and thereafter galaxies condense out through gravitational contraction. The time scale for collapse under self gravitation is of the order of $(\rho G)^{-1/2}$, where ρ is the initial matter density and G is the gravitational constant, unless collapse is prevented by non-gravitational forces. If the present matter density is about 10^{-29} gm cm^{-3} then the expansion parameter at the onset of galaxy formation is $y \approx 3 \times 10^{-4}$ and $\rho \approx 3 \times 10^{-19}$ gm cm^{-3}. This then implies a time scale of about 5×10^4 years for galaxy formation. After consideration of rotation and internal pressures Hoyle et al. (1965) suggest a time scale of about 10^5 years. The expansion parameter at completion of galaxy formation would then be of the order of 10^{-3} in the more slowly evolving models and 10^{-2} in the rapidly evolving world models.

The analysis of the source counts has placed lower limits on the value of y corresponding to the onset of radio emission. This limit varies from about 0.1 in the rapidly expanding models to about 0.35 in models which expand more slowly. There is a clear discrepancy between the epoch at which galaxy formation is expected to reach completion and the epoch at the initiation of radio emission. These events will occur at commensurate epochs in rapidly evolving cosmologies if the time scale for the formation of radio sources out of the universal plasma is of the order of 10^7 years. This figure does not seem unreasonable in view of the accepted lifetime of 10^6 to 10^7 years for radio sources. On the other hand models which are slowly expanding require a time of about 3×10^8 years before the commencement of radio emission. This condition is unlikely to be met under the present theories for radio sources. However, according to Peebles (1965), the condensation of galaxies may be retarded by the radiation drag on the electrons. The amount of retardation will depend on the magnitude of the plasma density fluctuations. The results derived from the source counts indicate that the condensation process did not take place until quite late when N was less than about 10^{-2} cm^{-3}.

Heating of the intergalactic gas is considered to commence at the epoch defined by the values of y_o in Table 10. If the heating is due to cosmic rays and exploding galaxies an estimate can be made for the temperature path of the gas. The cosmic ray energy density is assumed to vary with source concentration as given by n, or source

luminosity as given by β. The temperature of the gas is again controlled by the differential equation (7.31). The boundary conditions are defined by the value of y_o and the initial temperature $T_i = T_o y^{-1}$. The exact value for T_i may be in some doubt but the temperature path of the gas will depend most critically on y_o while being practically independent of T_i, provided $T_i < 10^4$ °K.

The temperature path of the gas has been calculated for two models taken from Table 10: (a) $\sigma_o = 5$, $q_o = 2.5$ and (b) $\sigma_o = 1$, $q_o = 0.36$. The derived values for y_o were 0.11 and 0.36 respectively. The results are presented in figure 7.7 where $\eta = 10^{-15}$ and figure 7.8 where $\eta = 10^{-16}$ erg cm^{-3}. Initially the temperature increases until the radiative losses by free-free emission are equal to the rate of heating by cosmic rays and plasma oscillation. The maximum temperature attained depends quite critically on the cosmic ray energy density and this is a quantity which is open to considerable conjecture. If we accept that $\eta \simeq 10^{-15}$ erg cm^{-3} as proposed by Ginzburg and Ozernoi, then the present temperature of the plasma is 4×10^5 °K in model (a) and 2×10^6 °K in model (b) for source density evolution. Luminosity evolution implies temperatures at the present epoch of 10^5 °K and 7×10^5 °K respectively. Clearly models with small values of y_o will provide temperatures which are in general agreement with those derived by other methods as discussed in section 6.1. The conclusions here must be regarded as very tentative since they depend so critically on the cosmic ray energy density and its variation with epoch.

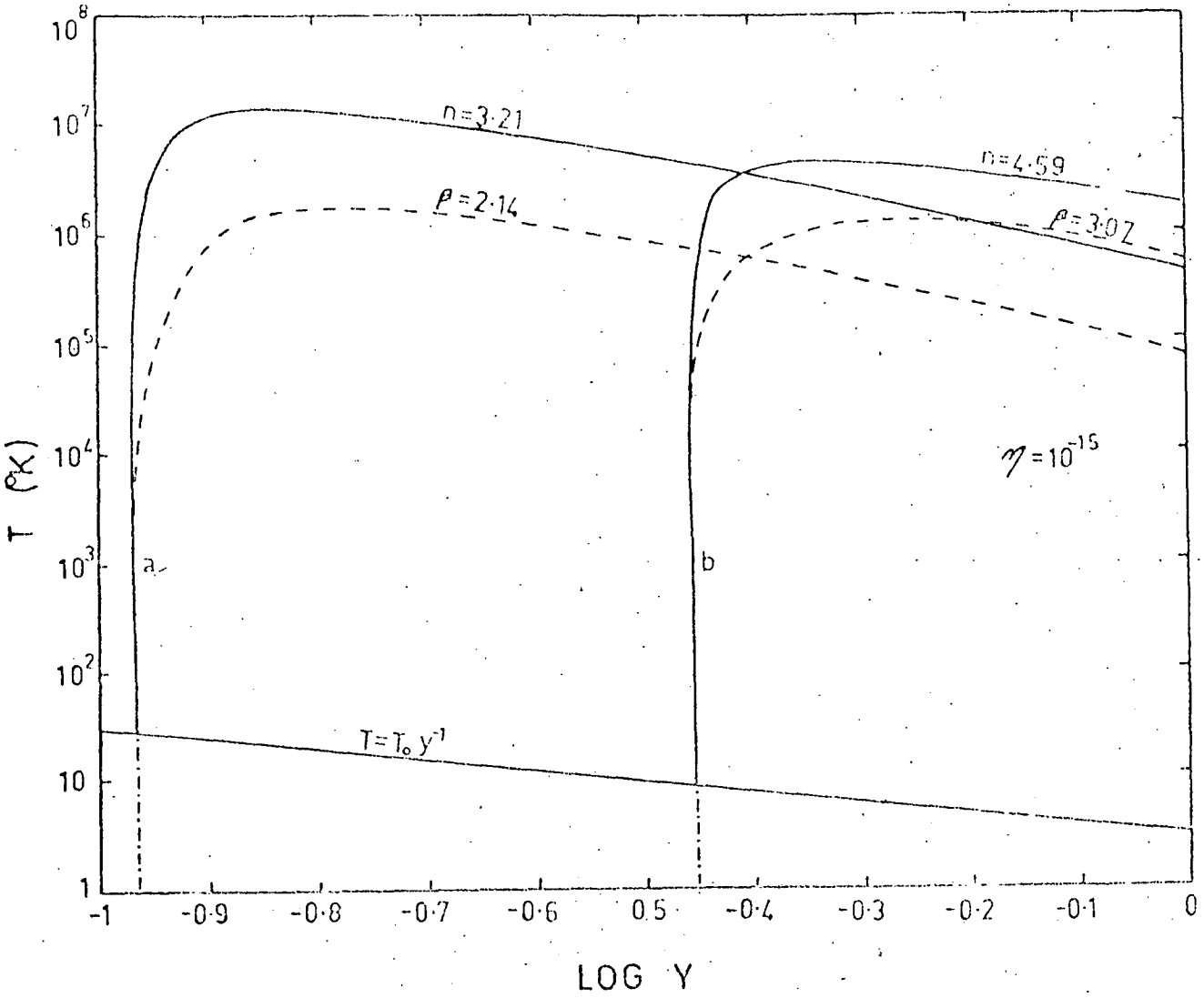

Figure 7.7 - The temperature of the intergalactic gas as a function of the expansion parameter for two extreme world-models (a) $\sigma_o = 5$, $q_o = 2.53$ and (b) $\sigma_o = 1$, $q_o = 0.36$. The cosmic ray energy density at the present epoch is 10^{-15}erg cm^{-3}.

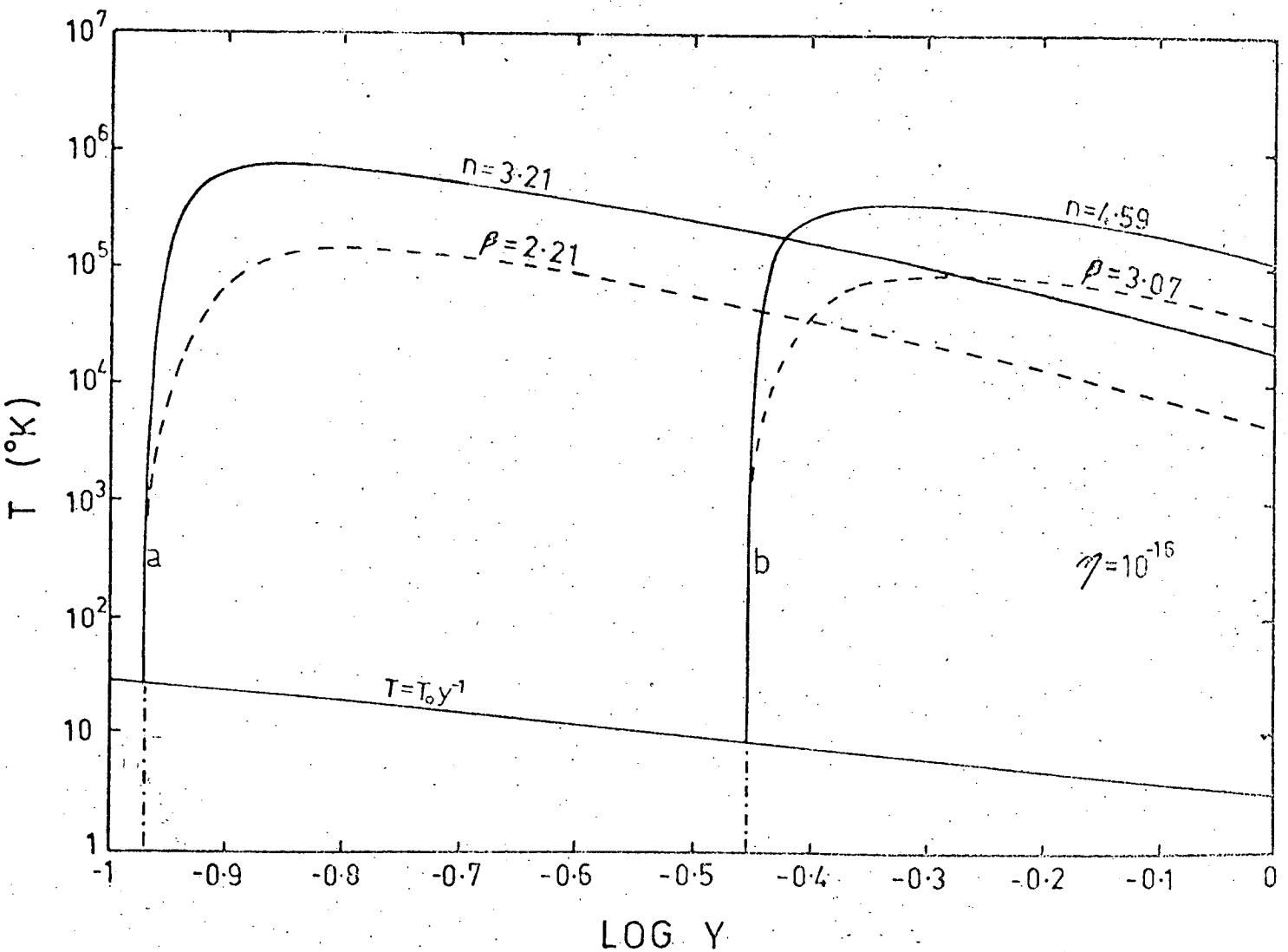

Figure 7.8 - The temperature of the intergalactic gas as a function of the expansion

7.9 The Background Spectrum

In this section the extragalactic radio background spectrum is derived by using the values for the required parameters which have been calculated in the earlier work. The postulates involved in this derivation are listed as follows:

1. The universe is described by evolutionary cosmologies.
2. A 3°K black-body radiation field exists at the present epoch.
3. The background intensity is due to ordinary emission from radio galaxies, free-free emission and fireball radiation.
4. The values of y_o, n and β required in equation (7.6) are given by the results of the source counts.
5. The temperature of the intergalactic gas is governed by equation (7.31).

As before, two extreme models are considered: (a) $\sigma_o = 5$, $q_o = 2.5$, and (b) $\sigma_o = 1.0$, $q_o = 0.36$. The parameters y_o, n and β are respectively 0.11, 3.21, 2.14 in the first case and 0.36, 4.59, 3.06 in the second. The integrated spectrum is shown in figure 7.9 and the shaded area represents the range in background intensities consistent with all the results derived so far. The theoretical low frequency spectra are omitted from the diagram for clarity. The proposed range of background intensities finds confirmation in the spectral points given by Howell and Shakeshaft (1967) at 408 and 610

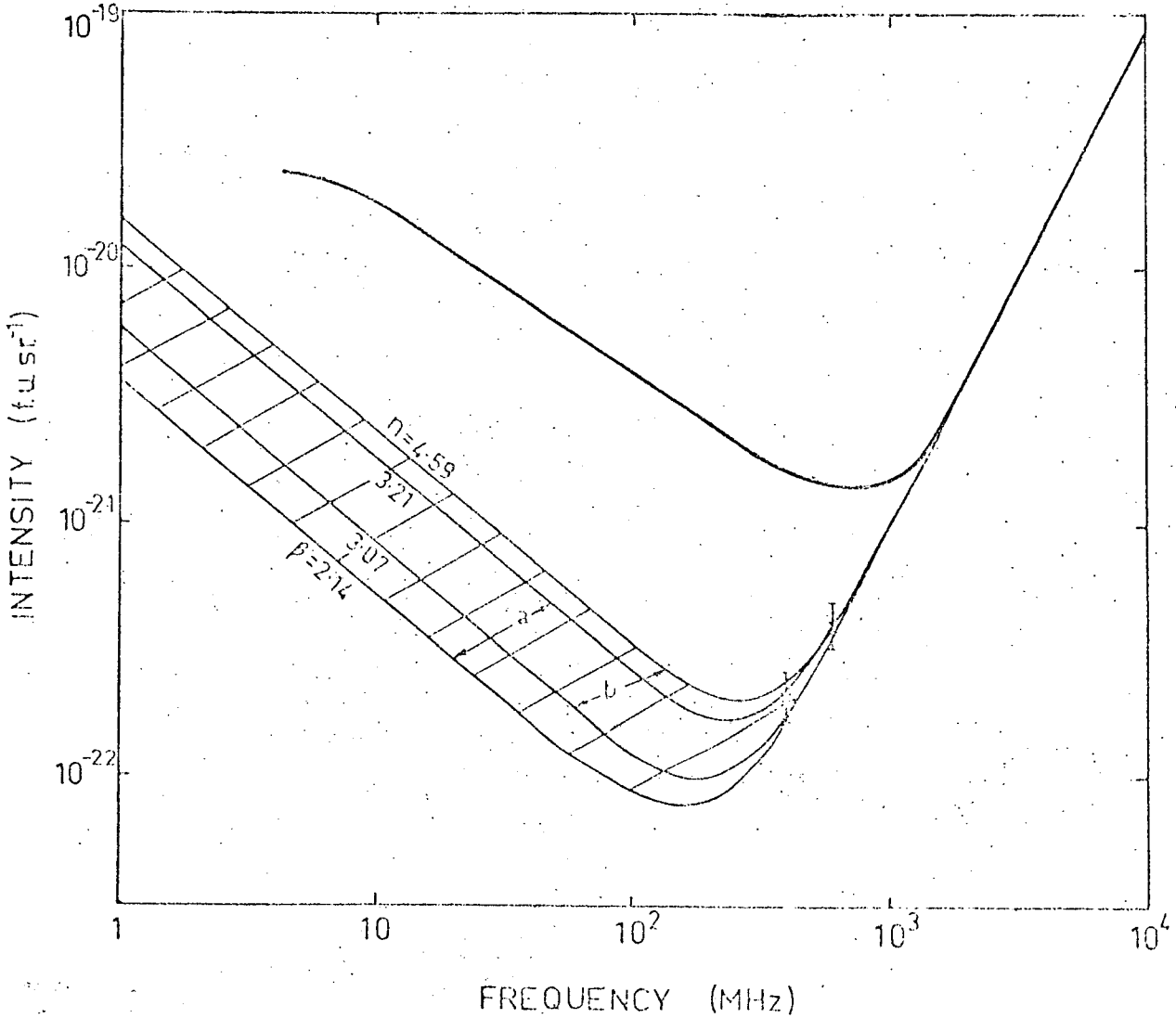

Figure 7.9 - The derived background intensity for two extreme cosmological models (a) and (b) in which source luminosity and density evolution is present.

MHz. The small deviations from the black-body curve at these frequencies is seen to be due to emission from radio galaxies. The contribution to the background intensity from free-free emission is insignificant at these frequencies and is in fact less than about 10^{-23} f.u. sr^{-1} for frequencies below 10^{6} MHz.

The extragalactic component contributes between 4.1 and 12.9 per cent of the total observed background intensity at 100 MHz. Also the analysis of the variation of sky brightness with frequency and galactic co-ordinates has yielded an estimate for the extragalactic component of about 10 per cent (Hamilton, 1969). Although there is some doubt as to the precise value for the extragalactic intensity the value of 10 per cent must be regarded as a close lower limit while an extreme upper limit would be about 20 per cent. If the extragalactic component is, in fact, greater than or near 10 per cent of the total sky brightness, then the theoretical results indicate that spatial evolution must be the dominant process producing change in the radio source population. Absorption measurements on the Magellanic Clouds by Shain (1958) yielded an estimate of 10 per cent for the extragalactic component. Again this result agrees fairly well with the theoretically derived intensities.

The variation of the background intensity with cosmological model is shown in Table II where the ratio of calculated to observed brightness at 100 MHz is listed for both spatial and luminosity evolution.

Table 11

Radio Background Parameters in Relativistic World-Models

σ_o	q_o	I/I_{100}		ν_c(MHz)
		n	β	
5	2.53	10.5	4.1	0.35
3	1.98	11.1	4.2	0.23
2	0.93	11.8	4.4	0.006
1	0.36	12.9	4.8	0.003
0.5	-0.47	14.9	5.8	0.001

Clearly the extragalactic intensity is least in those models which are most rapidly expanding and which also provide the best fit to the radio source counts. The precise value of the background intensity is not however a strong function of cosmological model. Also included in Table 11 are the frequencies ν_c at which the low frequency background intensity attains a maximum value for source density evolution. Inspection of the values for ν_c indicate that at frequencies less than 1 MHz, we could expect an increase in the observed background intensity, if galactic absorption is small and there is no low frequency cut-off in source spectra. The latter condition is unlikely to be met in view of the well-known mechanisms which lead to a decrease in source flux density at long wavelengths.

However, if an increase in observed background intensity is evident at a frequency less than 1 MHz, then absorption in the plane of the Galaxy must be considerably less than previous estimates, which have been based on the assumption of linear spectra in the halo and disk regions (Ellis and Hamilton, 1966).

7.10 The Soft X-ray Background Flux

Two groups (Bowyer et al., 1968; Henry et al., 1968) have recently obtained measurements of the diffuse X-radiation at photon energies near 0.27 keV. The flux is considered to originate outside the galaxy. Further measurements between 0.2 and 4 keV have been made by Baxter et al. (1969). Although the observational data is so far very limited it is of some interest to calculate the expected soft X-ray flux based on our postulated cosmological models. Here we use the same two extreme models employed to calculate the radio frequency background. The models are defined by (a) $\sigma_o = 5.0$, $q_o = 2.5$, (b) $\sigma_o = 1$, $q_o = 0.36$. Integrating equation (7.6) with the aid of (7.16) and (7.31) yields the two sets of theoretical curves drawn in figure 7.10. The observed fluxes may easily be accounted for by some model defined within the postulated range. Intergalactic free-free emission is the predominate radiation mechanism at these photon emergies. Quantum effects become important at high energies ($h\nu > kT$) and the exponential term in equation (7.16) produces a cut-off in the spectrum at a photon energy which depends on the particular

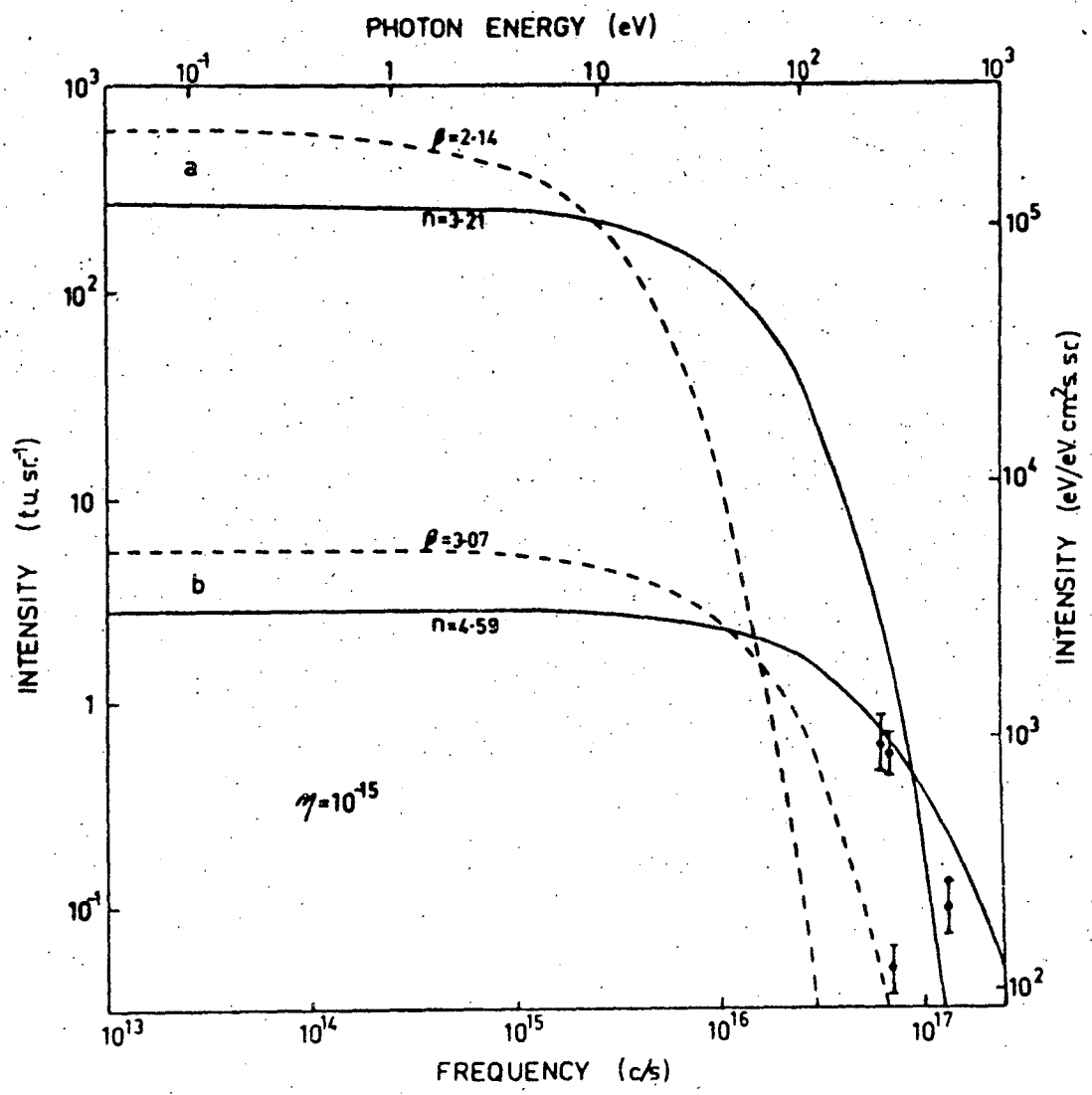

Figure 7.10 - The soft X-ray background flux for the two extreme world-models (a) and (b). The full curves correspond to source density and the broken curves correspond to source luminosity evolution.

model.

There is some argument as to the validity of the high intensity flux measurements (Bowyer and Field, 1969). However, in this analysis a high flux value is suggested by the results for the preferred models (that is, those models which are rapidly evolving with the occurrence of source density evolution). The apparent disagreements in the measurements of the soft X-ray intensities could well be due to the existence of a very steep spectrum as shown in figure 7.10. The present data is obviously insufficient to fit a precise theoretical model. Furthermore, it is not possible to place any great reliance on derived spectra since the intensity due to free-free emission at these energies is such a strong function of kinetic temperature and electron density. The temperature path of the gas depends, in turn, on the cosmic-ray energy density and this is another quantity which is subject to considerable speculation. More definitive measurements of the soft X-ray flux would provide useful information about these astrophysical quantities. It is quite impossible, however, to give an estimate for the gas temperature from the measurements at one photon energy as suggested by some authors.

7.11 Conclusions

The background intensity for evolutionary universes in which intergalactic free-free absorption exists is given by the integral equation (7.6). This equation requires a knowledge of the temperature path of the intergalactic gas for its solution and several "thermal" models have been considered. Using the derived luminosity distribution from section 5.2, the expected extragalactic background spectrum was calculated for the steady-state, "adiabatic", and constant temperature universes. It is found that the theoretical spectra for these models do not explain any feature of the observed spectrum.

The radio background was calculated for two extreme world-models defined in Table 10. In these models the expansion parameter at galaxy formation is given by y_o, which is also the lower limit of integration in equation (7.6). Furthermore the background intensity depends on the derived parameters n and β, which determine the evolution in source density and luminosity respectively. All these parameters are used in equation (7.31) which governs the thermal history of the universe. Results for the two extreme world-models show that, for any model specified in Table 10, the extragalactic component contributes between 10.5 and 12.9 per cent of the observed background intensity at 100 MHz for source density evolution and between 4.1 and 5.8 per cent for source luminosity evolution. The former estimates are in good agreement with the observational evidence

and independent estimates for the extragalactic component.

Integrating the free-free emission from intergalactic ionized hydrogen, for the world-models considered above, yields soft X-ray intensities which are near to the observed fluxes.

CHAPTER VIII

THE X-RAY BACKGROUND IN ISOTROPIC WORLD-MODELS

In this chapter an attempt is made to describe the diffuse X-ray background in terms of Compton radiation from cosmic ray electrons in intergalactic space. Similarities between the X-ray and radio source spectra suggest that fast electrons escape more or less freely from radio galaxies. It is assumed that the time scale of electron injection is small when compared with the characteristic time of evolution of the universe. The electrons are considered to lose energy through Compton scattering (due to the presence of the universal black-body radiation at 3°K) and by expansion of the co-ordinate system.

8.1 Introduction

The diffuse X-ray background depends for its explanation on an efficient mechanism for the conversion of cosmic ray electron energies into X-ray quanta. It is generally believed that inverse Compton scattering (i.e. the production of high energy photons from the collisions of fast electrons with thermal photons) is responsible for the X-ray radiation. The question of the origin of these scattering processes has been investigated in some detail by different authors. Gould (1965) and Felten and Morrison (1966) have examined the

possibility that the Compton interaction of relativistic electrons in the halo with black-body photons or the stellar radiation field could produce the observed isotropic background. However, the halo model predicts a flux which is two orders of magnitude less than that required by the observations and the shape of the derived spectrum does not provide a good match to the experimental spectrum. Further, there is no evidence of strong anisotropy in the X-ray background and there are therefore convincing reasons why we must exclude the halo model as a possible explanation of the observed flux.

Difficulties are also encountered if it is assumed that the X-ray background is the sum of contributions from the halos of all external galaxies. Felton and Morrison have shown that, unless the X-ray or gamma-ray emission in the average galaxy is much greater than our own, the integrated radiation from external galaxies will be several orders of magnitude less than the observed X-ray background.

Gould and Burbidge (1966) have suggested that the diffuse flux is the result of radiation from discrete X-ray sources in external galaxies but, if our galaxy is typical, it appears (Oda, 1966) that the expected flux will be only one per cent of the observed value. Bergamini et al. (1967) have proposed that the X-ray background is due to the inverse Compton interaction of fast electrons with the universal black-body radiation in strong radio galaxies. They find an equation for the ratio of the expected radio and X-ray background intensities

and allow for an evolution in radio source population. Further, they assume that the radio background at 178 MHz is about 25 per cent of the observed intensity, and with a few other reasonable assumptions they conclude that the X-ray background can be interpreted as due to emission from strong extended galaxies if the magnetic field strength is of the order of 1 μG. However, their assumption of the extra-galactic radio background intensity appears to be excessive if we accept the results of Chapter VII. Consequently the required field strength is less than is acceptable from radio frequency observations and equipartition arguments.

We are led finally to consideration of the possible origin of the diffuse X-ray flux in intergalactic space through the interaction of cosmic ray electrons with the 3°K black-body radiation. The difficulty in this model is the provision of a reliable estimate for the rate of injection of relativistic electrons from galaxies. The problem has been dealt with briefly by Felten and Morrison, and they consider a model in which electrons are supplied by explosive events in strong radio sources. If the total energy content of relativistic particles in these objects is about 10^{58} ergs and 1 per cent of this figure is in fast electrons which are lost to intergalactic space in a time of approximately 10^6 years, then the calculated X-ray intensity is two orders of magnitude less than required by the observations. However, Burbidge (1962) suggests that the usual assumption of equipartition between particle and magnetic field energies is hardly

tenable for sources subject to frequent disruptive events. This argument is used by Felten and Morrison who point out that electrons, sufficient to produce the observed X-ray background, can be injected into space by galaxies in which a non-equipartition condition exists.

The analysis provided by Felten and Morrison does not include the effects of the space-time geometry, and they also assume an electron energy spectrum which is constant independent of epoch. In this work, allowance will be made for a non-Euclidean geometry and the electron spectrum will be essentially dynamic through its dependence on epoch.

The experimental X-ray background which must be compared with theoretical models is plotted in figure 8.1 from results supplied by Gould (1967) and recent measurements by Henry et al. (1968) at low energies. The spectrum of the diffuse flux in the range 1 keV to 1 MeV has been derived from data furnished by balloon, rocket, satellite and space-probe experiments. The evidence so far indicates that the X-ray background is isotropic, at least to the limits of accuracy ($\sim$ 10 per cent) of the observations. Here, we do not enter into a detailed description of each set of data; the experimental results are presented in figure 1 without further comment. The data may be fitted by a power law of the form

$$I(\epsilon) = K\epsilon^{-(m+1)} \qquad (8.1)$$

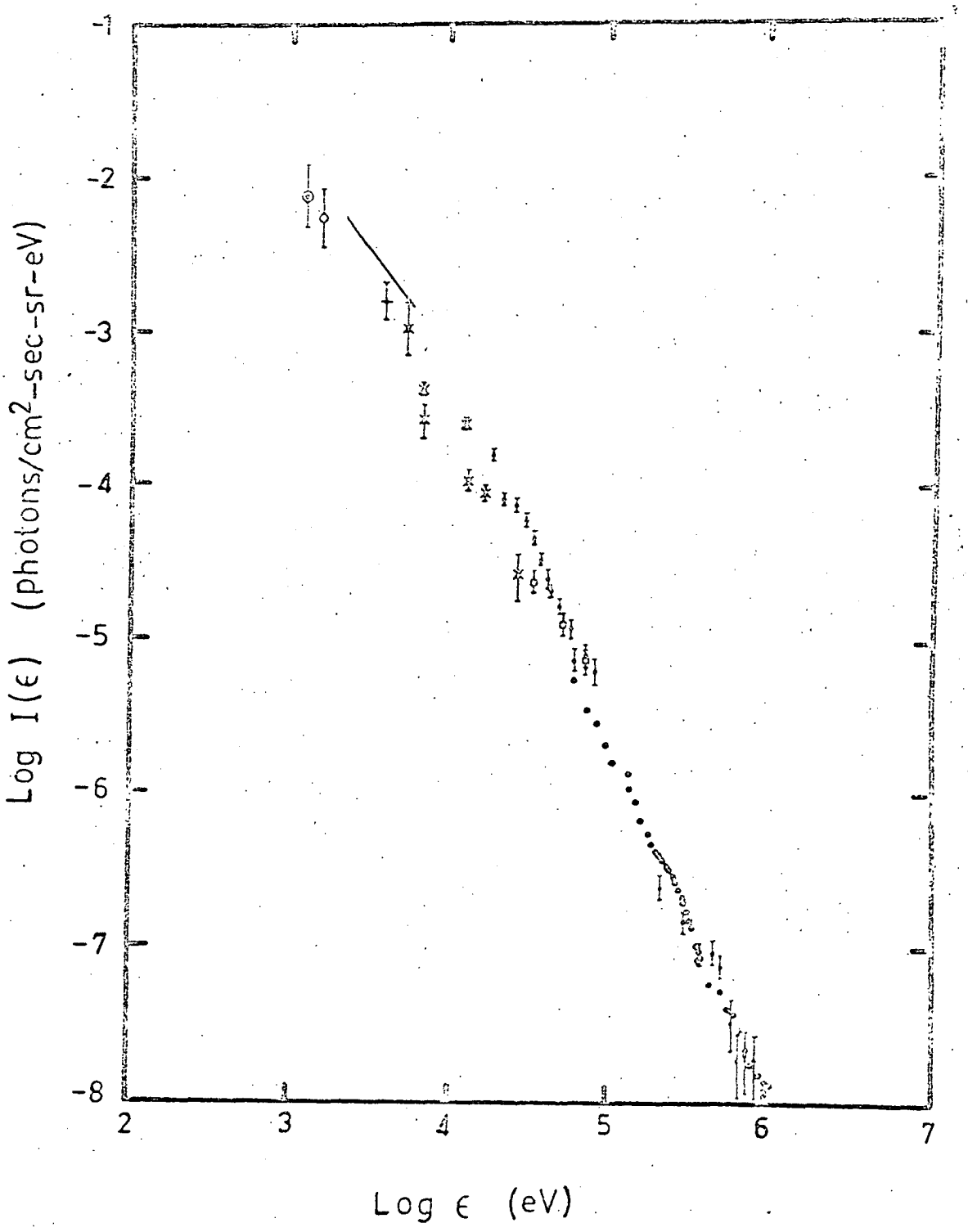

Figure 8.1 - Spectrum of the diffuse background of cosmic X-rays.

where ϵ is the photon energy and m is the index for the energy-intensity spectrum obtained by multiplying the photon numbers by ϵ. A least squares fit over the whole observational range (1 keV to 1 MeV) yields a value of $m = 1.25 \pm 0.18$, while fitting over the steeper part of the spectrum yields $m = 1.42 \pm 0.12$. The value obtained for m is important, not only for the definition of the energy distribution of the cosmic ray electrons responsible for the X-ray flux, but in providing a clue as to the possible origin of these fast electrons.

8.2 Electron Energy Losses in Metagalactic Space

In this section, the actual injection processes of the relativistic electrons are ignored and our attention is confined to the problem of electron energy losses in intergalactic and metagalactic space. The cosmic ray electrons may dissipate their energy by the inverse Compton effect, synchrotron and bremsstrahlung radiation, expansion of the co-ordinate system, and by the ionization of atomic hydrogen. The spatial density of intergalactic atomic hydrogen is extremely small and measurements indicate (Goldstein, 1963; Davies, 1964) a maximum value of about 10^{-7} cm^{-3}, while some evidence (Gunn and Peterson, 1965) suggests a value as low as 10^{-9} cm^{-3}. Therefore we may immediately dispense with ionization losses since they are approximately proportional to the concentration of atomic hydrogen and are accordingly exceedingly small. The density of intergalactic

ionized hydrogen, at the present epoch, may be taken to be about 10^{-5} cm^{-3} and, when compression of the plasma is allowed for, this implies that the characteristic time for energy losses by bremsstrahlung radiation is much greater than the characteristic time, H_0^{-1}, of evolution of the universe. Also, this analysis is concerned with the latter stages of the expansion of the universe when galaxy formation has been completed and the plasma density is fairly small. In this case, bremsstrahlung losses will be insignificant and can be neglected in the following calculations.

Now before we can progress to a discussion of the remaining types of energy losses, it is necessary to define the space-time metric. The interval ds between two events in the 4-dimensional continuum is defined as usual by the Robertson-Walker metric:

$$ds^2 = dt^2 - \frac{R^2(t)}{c^2}\left\{\frac{dr^2 + r^2(d^2 + \sin^2\Theta d\phi^2)}{(1 + kr^2/4)^2}\right\} \qquad (8.2)$$

where (r, Θ, ϕ) are 3-dimensional co-moving radial co-ordinates, t is the universal time, R is the radius of curvature which is a function of t only, and k is the curvature constant having values +1, 0, -1 depending on whether the space-time is closed, flat or open. It is now possible to consider the electron energy losses in more detail.

(a) Energy Losses by Expansion

The problem of propagation of cosmic rays through intergalactic space has been examined in some detail by Ginzburg and Syrovatskii (1964). They find that these fast electrons essentially pervade the whole of metagalactic space in a time which is short compared with the characteqistic time of evolution of the universe. In these circumstances "redshift" losses by expansion will be relevant and the loss may be written as

$$\frac{dE}{dt} = - \frac{V}{R} E = - \frac{\dot{R}}{R} E \qquad (8.3)$$

and using $y = R/R_o$ this becomes

$$\frac{dE}{dt} = - \frac{\dot{y}}{y} E$$

Substituting $dt = (\partial t/\partial y)dy$, this may be rewritten in the simple form

$$\frac{dE}{dy} = \frac{E}{y} \qquad (8.4)$$

which defines the energy of an electron as a function of the expansion parameter y only.

(b) Inverse Compton Losses

The inverse Compton process involves the production of a high energy photon from the collision of a relativistic electron with a low energy photon. The properties of the generated power depend on the energy and velocity distributions of electrons and photons. The problem has been treated in some detail by Feenberg and Primakoff (1948), and they derive a rather complicated formula for the total power dissipated by a single fast electron. However, for an isotropic distribution of relativistic electrons interacting with thermal photons, the formula reduces to the simple equation

$$\frac{dE}{dt} = -\frac{4}{3}\sigma_t c\rho\left(\frac{E}{m_o c^2}\right)^2 \qquad (8.5)$$

where σ_t is the total Thomson cross-section and ρ is the photon energy density. The temperature of the universal black-body radiation at the present epoch is close to 3°K, and this corresponds to an energy density $\rho = 0.38$ eV cm^{-3}. Also, as the universe expands, the cosmological redshift serves to adiabatically cool the black-body radiation while preserving a Planck function. In the absence of interaction with matter, the temperature is proportional to y^{-1} and the photon energy density at an epoch defined by y may be written as

$$\rho = \sigma T^4 = \rho_o y^{-4} \qquad (8.6)$$

where σ is the Boltzmann constant. Therefore, from equation (8.5), the energy loss by photon scattering is

$$\frac{dE}{dy} = - \frac{BE^2}{y^4} \frac{\partial t}{\partial y} \qquad (8.7)$$

where $B = \frac{4}{3} c\sigma_t \frac{\rho_o}{(m_o c^2)^2}$ and $\partial t/\partial y$ is obtained from equation (4.4). It is clear from equation (8.7) that the inverse Compton loss is a strong function of the expansion parameter and will be most important at early epochs.

(c) Synchrotron Losses

Arguments based on energy equipartition between magnetic field and matter (Ginzburg and Syrovatskii, 1961) yield a value of $H \simeq 0.5$ μgauss for the intergalactic magnetic field strength. It is natural to assume that the energy density $H^2/8\pi$ varies in the same way as the gas energy density. In evolutionary cosmologies, $\rho = \rho_p y^{-3}$ and if the relative velocities of galaxies are approximately constant then $H = H_p y^{-3/2}$ where H_p and ρ_p are the present values for the magnetic field strength and matter density. Now the synchrotron loss of a single electron moving in a magnetic field with perpendicular component $H_\perp$ can be written (Oort and Walraven, 1956) as

$$\frac{dE}{dt} = - \frac{2}{3} \frac{e^4 c}{(m_o c^2)^4} H_\perp^2 E^2 \qquad (8.8)$$

Converting the energy loss to a function of the expansion parameter y and assuming that the magnetic field is isotropic on the average ($H_\perp^2 = \frac{2}{3} H^2$) we have

$$\frac{dE}{dy} = - \frac{\sigma_t}{6\pi} cH_p^2 \left(\frac{E}{m_o c^2} \right)^2 y^{-3} \frac{\partial t}{\partial y} \qquad (8.9)$$

The ratio of the total power generated by photon scattering to that generated by synchrotron emission is, by equations (8.7) and (8.9),

$$\frac{P_c}{P_s} = \rho_o (H_p^2/8\pi)^{-1} y^{-1} \simeq 60 y^{-1} \qquad (8.10)$$

if the magnetic field strength $H_p \simeq 0.5$ μgauss. Synchrotron emission in metagalactic space is therefore seen to be small compared with the emission by inverse Compton scattering and will be neglected in this analysis.

8.3 The Electron Energy Spectrum

It is the purpose of this section to obtain an equation for the quasi-equilibrium electron energy spectrum at any epoch. There are only two remaining energy losses which must be considered in the following analysis and these are the losses by Compton scattering and expansion of co-ordinates. Under these conditions, the differential equation describing the electron energy as a function of the expansion

parameter will be

$$\frac{dE}{dy} = -\left(\frac{E}{y} + \frac{BE^2}{y^4}\frac{\partial t}{\partial y}\right) \tag{8.11}$$

The solution to this equation with boundary conditions at injection of $E = E_o$ and $y = y_o$ is

$$E(y) = \frac{E_o y_o}{y}\left[1 + BE_o y_o \int_{y_o}^{y} \frac{1}{y'^5}\frac{\partial t'}{\partial y'}dy'\right]^{-1} \tag{8.12}$$

which again demonstrates the dependence of electron energy on the chosen world-model.

We now turn our attention to the problem of the electron energy spectrum in metagalactic space. An assembly of electrons with a number density $N(E,y)dEdy$ will have an energy distribution determined by the equation

$$\frac{\partial N(E, y)}{y} + \frac{\partial}{\partial E}\left[\frac{dE}{dy}N(E, y)\right] = 0 \tag{8.13}$$

which is the continuity equation for electrons in (E, y) space without a source function and N is the number of electrons in an arbitrary region of the ordinary 3-space. Equation (8.13) has been solved for initial conditions $N(E, y_o)dE = KE^{-\gamma}dE$ corresponding to an instantaneous injection spectrum at $y = y_o$. The solution is

$$N(E, y) = KE^{-\gamma}\left(\frac{y_o}{y}\right)^{\gamma-1}\left[1 - BEy\int_{y_o}^{y}\frac{1}{y'^5}\frac{\partial t'}{\partial y'}dy'\right]^{\gamma-2}$$

(8.14)

Suppose now that from suitable galaxies electrons are injected at a constant rate $qE^{-\gamma}$. The number of electrons, with energy E, escaping from a single galaxy in time dt_o will be $qE^{-\gamma}dt_o$, and it follows from equation (8.14) that the energy spectrum is

$$N(E, y) = V(y)qE^{-\gamma}\int_{t_{om}}^{t}\rho(y_o)\left(\frac{y_o}{y}\right)^{\gamma-1}\left[1 - BEy\int_{y_o}^{y}\frac{1}{y'^5}\right.$$
$$\left.\times\frac{\partial t'}{\partial y'}dy'\right]^{\gamma-2}dt_o \qquad (8.15)$$

where V is the volume of the region under consideration and ρ is the spatial density of sources. It is assumed here that the galaxies emitting fast electrons form a single class of objects with the quantity ρ representing their weighted mean density. In this way the difficulties involved in accounting for source luminosity dispersion will be circumvented. As before the source population is assumed to vary smoothly with epoch so that $\mu = \mu_o y^{-x}$ where $x = 3 + n$. Hence, converting equation (8.15) to a function of the expansion parameter y and defining N^* as the number of electrons per unit proper volume, we have, finally

$$N^*(E, y) = \mu_o q E^{-\gamma} \int_{y_{om}}^{y} y_o^{-x} \left(\frac{y_o}{y} \right)^{\gamma-1} \left[1 - BEy \int_{y_o}^{y} \frac{1}{y'^5} \right.$$

$$\left. \times \frac{\partial t'}{\partial y'} dy' \right]^{\gamma-2} \frac{\partial t_o}{\partial y_o} dy_o \qquad (8.16)$$

The minimum value of y_{om} for the lower limit of integration is determined not only by E and y but also by the properties of the injection spectrum. This will be discussed in more detail in the next section. It is sufficient here to point out that y_{om} must satisfy the relation

$$BEy \int_{y_{om}}^{y} \frac{1}{y'^5} \frac{\partial t'}{\partial y'} dy' \leq 1 \qquad (8.17)$$

It is also clear from equation (8.16) that the exponent x may be replaced by $x = 3 + \beta$ in the case of source luminosity evolution.

8.4 Equation for the X-ray Background Intensity

In this section an expression is derived for the X-ray emission per unit proper volume which will lead to the equation for the X-ray background intensity through the general equation for the background radiation in isotropic world-models. The total power generated by a single electron by photon scattering can be written, for the epoch y, as

$$P(E, y) = \frac{4}{3} c \sigma_t \rho_o y^{-4} \left(\frac{E}{m_o c^2} \right)^2 \qquad (8.18)$$

which follows immediately from equations (8.5) and (8.6). The spectral distribution of the radiation involves difficult integrations over electron energies, photon energies and the scattering angles of the Compton interactions. However, the spectral power must possess the property

$$P(E, y) = \int_0^\infty P(E, y, \nu)d\nu \tag{8.19}$$

and since we are concerned here with a continuum of cosmic ray electron energies ranging over several orders of magnitude, the problem may be simplified by collapsing the emission spectrum into a δ-function at its peak or characteristic frequency. Thus, we may write

$$P(E, y, \nu) = P(E, y)\delta(\nu - \nu_c) \tag{8.20}$$

where ν_c is the characteristic emission frequency for electrons of energy E at an epoch corresponding to y.

Now it is easily verifiable (e.g. Ginzburg and Syrovatskii, 1964) that, in a local inertial frame and for an isotropic distribution of electron velocities, the average energy of a recoil photon following a Compton interaction with a relativistic electron is

$$\bar{\varepsilon}' = \frac{4}{3}\left(\frac{E}{m_o c^2}\right)^2 \bar{\varepsilon} \tag{8.21}$$

where $\bar{\varepsilon}$ is the mean photon energy. The properties of black-body radiation produce $\bar{\varepsilon} = 2.7\ kT$ and therefore equation (8.21) yields

$$\bar{\varepsilon}' = 3.6\ \left(\frac{E}{m_o c^2}\right)^2 kT \tag{8.22}$$

Then, allowing for the adiabatic expansion of the photon gas, the characteristic frequency is

$$\nu_c = 3.6\ \left(\frac{E}{m_o c^2}\right)^2 \frac{kT_o}{h}\, y^{-1} \tag{8.23}$$

where T_o is the temperature of the black-body radiation at the present epoch. Furthermore, the received frequency, ν_{co}, is independent of the epoch of emission and depends solely on the electron energy. This follows from the redshift $\nu_c = \nu_{co} y^{-1}$ which exactly compensates the relation $T = T_o y^{-1}$ for the photon temperature. The X-ray emission per unit proper volume may now be written in the form

$$\begin{aligned} j(\nu, y) &= \int_{m_o c^2}^{\infty} P(E, y, \nu) N^*(E, y)\, dE \\ &= \int P(E, y)\, \delta(\nu - \nu_c) N^*(E, y)\, \frac{\partial E}{\partial \nu_c}\, d\nu_c \end{aligned} \tag{8.24}$$

and from equation (8.23) and the properties of the δ-function the emission coefficient is

$$j(\nu, y) = P(E_\nu, y) N^*(E_\nu, y)\, \frac{h(m_o c^2)^2}{7.2 E_\nu k T_o y^{-1}} \tag{8.25}$$

where the emission frequency, ν, is equal to the frequency, ν_o, measured by the origin observer and equation (8.22) yields

$$E_\nu = m_o c^2 \frac{h\nu_o}{\sqrt{3.6kT_o}} \tag{8.26}$$

Combining equations (8.18), (8.25) and (8.26), we find

$$j(\nu_o, y) = \frac{2}{3} \sigma_t c \rho_o y^{-3} \left(\frac{h}{3.6kT_o} \right)^{3/2} m_o c^2 \nu_o^{1/2} N^*(E_\nu, y) \tag{8.27}$$

Recalling that $N(E, y)$ is the number of electrons, with energy E, per unit proper volume, per unit energy, we replace in equation (8.16) $q = q'(m_o c^2)^{\gamma-1}$, and from equation (8.27) the formula for the emission coefficient is

$$j(\nu_o, y) = \frac{2}{3} \sigma_t c \rho_o y^{-3} \left(\frac{h}{3.6kT_o} \right)^{(3-\gamma)/2} \nu_o^{(1-\gamma)/2} \mu_o q' \times \int_{y_{om}}^{y} f(y_o) \frac{\partial t_o}{\partial y_o} dy_o \tag{8.28}$$

where q' has units $\sec^{-1}$ and

$$f(y_o) = y_o^{-x} \left(\frac{y_o}{y} \right)^{\gamma-1} \left[1 - BE_\nu y \int_{y_o}^{y} \frac{1}{y'^5} \frac{\partial t'}{\partial y'} dy' \right]^{\gamma-2} \tag{8.29}$$

with the electron energy, E_ν, being determined through equation (8.26). The general equation for the extragalactic background intensity follows

from (7.6) and may be written as

$$I_\nu = \frac{c}{4\pi} \int_{y_{min}}^{1} j(\nu y^{-1}, y) y^3 \frac{\partial t}{\partial y} dy \qquad (8.30)$$

where absorption in the intergalactic medium is negligible. So, finally, equations (8.28) and (8.30) yield the rather complicated equation for the X-ray background intensity

$$I(\nu_o) = A_1 A_2^{3-\gamma} \nu_o^{(1-\gamma)/2} \mu_o q' \int_{y_{min}}^{1} \frac{\partial t}{\partial y} \int_{y_{om}}^{y} f(y_o) \frac{\partial t_o}{\partial y_o} dy_o \, dy \qquad (8.31)$$

where $A_1 = \dfrac{\sigma_t c^2 \rho_o}{6\pi}$ and $A_2 = \left(\dfrac{h}{3.6kT_o} \right)^{1/2}$ are constants determined by the properties of the black-body radiation. Equation (8.31) involves an integration over three variables and it is necessary to introduce some simplifying assumptions before this can be accomplished by numerical techniques. If, as must be the case, there is a maximum electron energy E_m for the injection spectrum, then the lower limit, y_{om}, of the inner integral of equation (8.31) will depend not only on y and E but also on the value of E_m. This introduces severe complications into the equations since y_{om} is then the solution to the equation

$$\frac{E}{E_m} = \frac{y_{om}}{y} \left[1 + B E_m y_{om} \int_{y_{om}}^{y} \frac{1}{y'^5} \frac{\partial t'}{\partial y'} dy' \right]^{-1} \qquad (8.32)$$

In order to avoid these extra difficulties, we have assumed a linear injection spectrum defined over all energies, and in the ensuing computations the maximum initial energy will be infinite. The value of y_{om} will then be determined by substituting E_m equal to infinity in equation (8.32) which then yields

$$\int_{y_{om}}^{y} \frac{1}{y'^5} \frac{\partial t'}{\partial y'} dy' = \frac{1}{ByE} \qquad (8.33)$$

It follows from equations (8.32) and (8.33) that, for $E_m >> E$, the errors introduced into the calculations by assuming an infinite energy range will not be significant. At high photon energies, the X-ray intensity may be over-estimated, but at relatively low energies the calculations should approximate to the real situation. The lower cut-off frequency of the X-ray background will correspond with the low energy cut-off for the electron spectrum which, in the absence of ionization losses, is close to the electron rest mass energy. The actual energy at which this cut-off occurs does not concern us here since we can arbitrarily limit our derived spectrum by the low frequency limit of the observations and this will not affect the equations.

The experimental radio and X-ray background spectra are drawn schematically in figure 8.2. The solid lines indicate measured regions of spectrum, while the broken lines are extrapolations of theoretical predictions. The positions of the high and low frequency cut-offs for

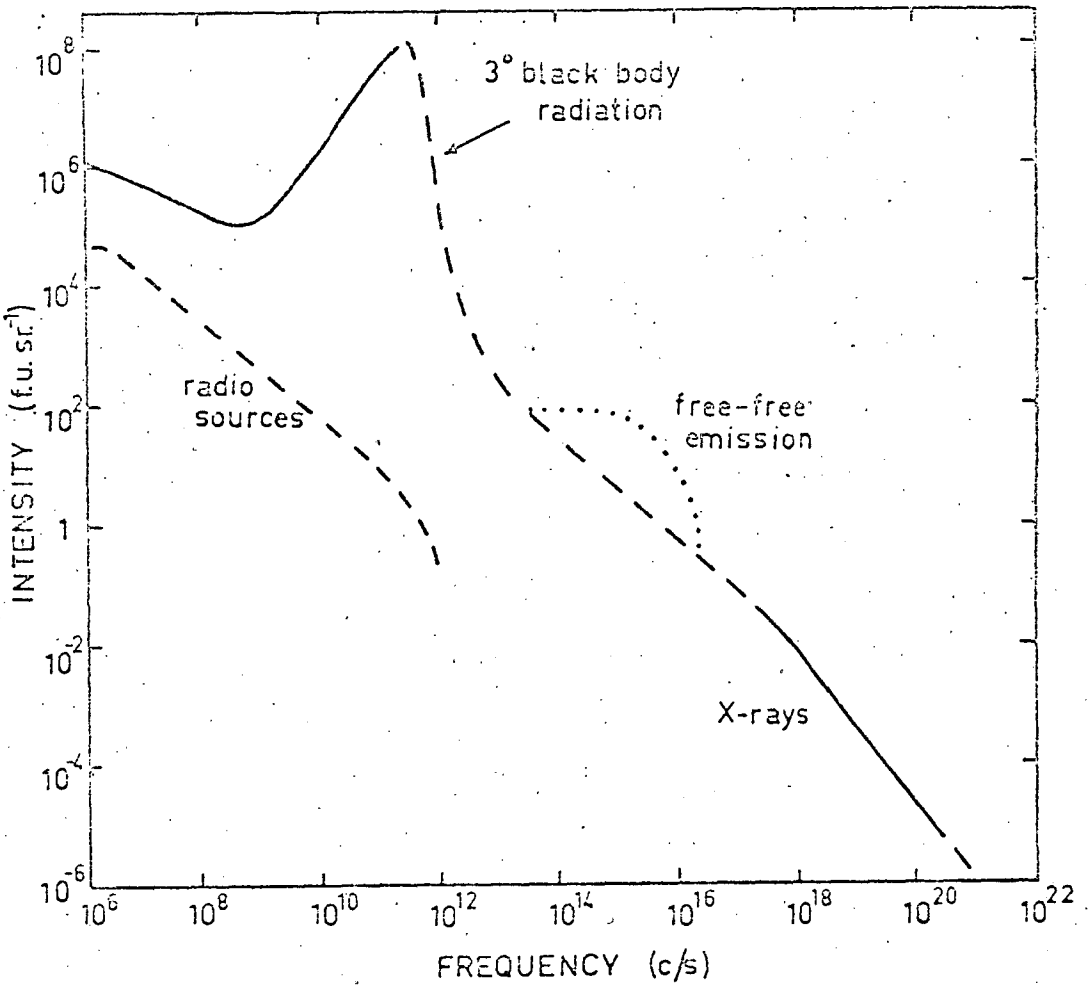

Figure 8.2 - Qualitative features of the measured and estimated background intensities for the observable region of the electromagnetic spectrum. The solid line indicates measured regions of the spectrum and the broken lines are theoretical predictions.

both spectra will depend on the exact form of the appropriate electron energy spectrum and are sketched only roughly in the diagram.

The spectral index analysis of the sources listed in the Parkes catalogues implies a mean spectral index of $\alpha = 0.84$ with a variance on this value of approximately 0.06. Therefore according to the relation $\gamma = 2\alpha + 1$, the differential energy spectrum for the electrons responsible for the radio emissions must have an index $\gamma_r = 2.68$. On the other hand, the X-ray spectrum (figure 8.1) implies an electron population having $\gamma_x \simeq 3.8$, which differs from γ_r by a value close to unity. Furthermore, the numerical computations in the following section show that inverse Compton and expansive energy lossescan account for a change of unity in γ.

It is therefore asserted that X-ray photons are produced in intergalactic space by the interaction of fast electrons with thermal photons and that the electron population has an original energy spectrum close to the average spectrum in radio sources. It is unlikely, of course, that the energy spectrum would remain completely unaltered with the escape of electrons from the radio source into intergalactic space. In all probability, there will be a tendency for an excess of high energy electrons to be produced by the injection process which will lead to a flattening of the initial electron spectrum. Comparison of the radio and X-ray background spectra indicate that the change in index produced by this effect is less than

the uncertainties involved in defining the slope of the X-ray spectrum. Hence we propose a model in which explosive and disruptive events in radio galaxies are the source of relativistic electrons which escape more or less unimpeded into the surrounding space. The initial electron energy distribution may therefore be assumed, for present purposes, to have a spectral index of $\gamma_x = 2.68$.

Also included in figure 8.2 is the possible effect on the background intensity of free-free emission from intergalactic ionized hydrogen. This has been discussed in section 7.6 and the exact form of the spectrum is open to considerable conjecture. If the soft X-ray flux is indeed of the order of that reported by Henry et al. (1968), then the contribution to the background intensity due to bremsstrahlung emission will dominate the contributions from other processes, and it follows that the predictions of the present analysis can only find direct application at photon energies greater than about 100 eV.

8.5 Theoretical X-ray Spectra

(a) Model Definition

The numerical integration of equation (8.31) will prove too difficult if we revert to the usual differential equation (4.4) for the expansion factor. It is possible to analyse several world-models

which have simple expansion functions. These may be listed as follows

Model	R/R_o	$dy/(H_o dt)$
Dirac	$(t/t_o)^{1/3}$	y^{-2}
Einstein-de Sitter	$(t/t_o)^{2/3}$	$y^{-0.5}$
Milne	t/t_o	1
Page	$(t/t_o)^2$	$y^{0.5}$
de Sitter	$e^{H_o(t-t_o)}$	y

So, in the interests of a fast calculation procedure, the conditions defining models have been simplified by assuming that, in general,

$$\frac{dy}{dt} = H_o y^n \qquad (8.34)$$

where the value of n now determines the evolutionary path of the model. If $n > 1$, then the universe is in a state of continuous contraction which is hardly permissible since all available evidence indicates an expanding model. The analysis is therefore restricted to values of n less than unity. This means that models examined by this method will always be in a state of expansion and other models such as those of the oscillating type cannot have definition. The method is still instructive, however, and by suitable choice of the parameter n, equation (8.34) can closely simulate the expansive period of an oscillating universe.

It is now a simple matter to transform equation (8.29) into the function

$$f(y_o) = y_o^{-x}\left(\frac{y_o}{y}\right)^{\gamma-1}\left[1 - \frac{BE_\nu y}{n'}\left(y_o^{-n'} - y^{-n'}\right)\right]^{\gamma-2} \quad (8.35)$$

where $n' = n + 4$. The equation (8.31) now degenerates into an integration over two variables which may be evaluated by numerical methods. The lower limit for the inner integral (corresponding to infinite initial electron energy) is, by equation (8.33),

$$y_{om} = \left[\frac{n'}{BEy} + y^{-n'}\right]^{-1/n'} \quad (8.36)$$

The three equations (8.31), (8.35) and (8.36) are sufficient for the derivation of theoretical spectra as functions of n and y_{min}.

(b) Derived Spectra

As before, we examine the X-ray intensity in terms of the cosmological models defined in Table 10. The values of y_{min} corresponding to the epoch at which the electron injection phase begins are the same as the listed values of y_o in Table 10. Now, as described above, equation (8.31) can be numerically integrated provided the expansion parameter is redefined through equation (8.34). This requires fitting the curve given by (8.34) to the points in the (y, t) plane appropriate to each world-model. In other words, for

each pair of values (σ_o, q_o) the value of n must be calculated which provides the best fit to the true expansion curve over the range of integration $y_{min} \leq y \leq 1$. This can be carried out quite easily.

For reasons described earlier, we take $\gamma = 2.68$ for the index of the initial electron energy spectrum. The theoretical spectra have been normalised to fit the observed intensity at a photon energy of 1 MeV and for each model this procedure gives a value for the product $\mu_o \times q'$. The net result of electron energy losses by Compton scattering is a steepening of the X-ray spectrum at high photon energies. A "break" occurs at a photon energy E_b which depends on y_{min} and the rate of expansion of the universe (Payne, 1969). However, for the models considered here we find that $E_b < 100$ eV since the Compton losses dominate the loss due to expansion of co-ordinates. At energies much greater than E_b, the spectral index increases by 0.5 implying a change of unity in γ for the energy distribution of the electrons responsible for the X-radiation.

The results are summarised in Table 12 which includes, for both extreme models, the normalisation constant $\mu_o \times q'$ equal to the total number of high energy electrons injected per unit time and per unit proper volume. In the third column, "d" denotes density evolution and "ℓ" luminosity evolution.

Table 12

Derived Quantities for the X-ray Background in Two Extreme World-Models

σ_o	q_o	Evolution	$\mu_o x q'$ ($x10^{-26} m^{-3}$)	$\eta_e x10^{-17}$ erg cm^{-3}
5	2.53	d	7.36	4.1
5	2.53	ℓ	16.4	9.2
1	0.36	d	3.39	2.66
1	0.36	ℓ	8.54	6.7

We consider, first, the predictions and consequences of the normalisation constants listed in Table 12. Recalling that q' is the number of electrons injected per unit time, the total power, P, output in the form of cosmic ray electrons will be

$$P = \int_{E_1}^{E_2} q' (m_o c^2)^{\gamma-1} E^{1-\gamma} \, dE \qquad (8.37)$$

where E_1 and E_2 are the minimum and maximum energies of the injected electrons. As a close approximation we may take $E_2 = \infty$. The value of E_1 is somewhat uncertain so let us suppose that E_1 corresponds to the "break" in the X-ray spectrum. The exact position of this break will be discussed later but it apparently lies in the range 10-60 keV. Equation (8.37) becomes

$$P = q' \frac{m_o c^2}{\gamma - 2} \left(\frac{E_1}{m_o c^2} \right)^{2-\gamma} \qquad (8.38)$$

Also the cosmic ray energy density is given by

$$n_e \simeq P \times \mu_o \times T$$

where T is the elapsed time after commencement of electron injection. Substituting for P in this equation yields

$$n_e \simeq \mu_o \times q' \times 1.2 \times 10^{-6} \times \left(\frac{E}{m_o c^2} \right)^{-0.68} \times T$$

for $\alpha = 0.84$. The time T may be calculated for each model by employing equation (4.21) with the lower limit of integration equal to y_{min}. Using (8.26) this equation can be written

$$n_e \simeq \mu_o \times q' \times 1.2 \times 10^{-6} \times \left(\frac{E_b}{3.6kT_o} \right)^{-0.34} \times T \qquad (8.39)$$

where E_b is photon energy at the break in the spectrum. The calculated values for n_e are listed in the last column of Table 12 for $E_b = 10$ keV. The energy density of the electron components of cosmic rays is seen to be of the order of 10^{-17} erg cm^{-3}. Now, in galaxies (both normal and radio galaxies) the energy density of the electron component is generally taken to be 0.01 in order of magnitude of the density of the energy of all the cosmic rays (e.g. Burbidge, 1959). The same ratio can therefore be expected in

the cosmic rays ejected into metagalactic space from the galaxies. This means the total cosmic ray energy density, η, is of the order of 10^{-15} erg cm^{-3} at the present epoch. This estimate is the same as the preferred value given by Ginzburg and Ozernoi (1966). It should be pointed out that estimates for η range from about 10^{-14} to 10^{-17} erg cm^{-3} (e.g. Ginzburg and Syrovatskii, 1967; Schmidt, 1967) but a value of 10^{-15} erg cm^{-3} appears to be most commonly accepted. If the break in the spectrum occurs as high as E_b = 60 keV, then the derived cosmic ray energy densities will be approximately half the derived values for E_b = 10 keV. According to equation (8.26) the metagalactic electron spectrum must have a low energy cut-off between 1.65 and 4 GeV. This is not at all unreasonable since in all probability only the highly energetic electrons will escape into intergalactic space.

The theoretical spectra will have a spectral index of $\alpha = 1.34$ at photon energies greater than E_b and provides an excellent fit to the observed hard X-ray spectrum. As far as the observations are concerned there seems little doubt that a break in the spectrum does actually exist but there is some argument about its exact position. The data given in figure 8.1 indicates a cut-off at about 10 keV; however other observations have not confirmed this. Gorenstein et al. (1968) have measured the cosmic X-ray flux in the range 1-13 keV. They report that there is little, if any, change in the degree of spectral hardness between 1 and 60 keV and propose a spectral index in this range of 0.7 ± 0.2. Contradictory evidence is given by

Boldt et al. (1969). They find a break in the spectrum near 20 keV with an apparent change of unity in the spectral index.

Hamilton and Francey (1969) have attempted to explain these differences in terms of different electron distributions in directions towards the north and south galactic poles. There is some evidence that, in north galactic regions, the electron spectrum is flatter and the synchrotron emissivity greater than in the southern regions. It is suggested by these authors that there are analogous differences in the soft X-ray flux and a galactic origin is proposed which can account for 20-50 per cent of the soft (less than 10 keV) X-ray flux. However, the model should account for at least 90 per cent of the X-ray intensity otherwise the spectral indices cannot be correlated in the manner suggested. Furthermore, if the flux is almost entirely of galactic origin then a fairly large anisotropy must be expected. The degree of the anistropy will of course depend on the size of the halo and the electron distribution within it but the X-ray is apparently isotropic within 10 per cent. The ratio of synchrotron intensity to Compton intensity may be written (Felten and Morrison, 1966) as

$$\frac{I_S}{I_C} = \frac{H^2/8\pi}{\rho} \left(\frac{2 \times 10^4 \times T_o}{H} \right)^{(3-\gamma)/2}$$

where H is the average galactic field strength, T_o is the black-body temperature and all quantities are in c.g.s. units. The analysis of

Hamilton and Francey requires H ≈ 1 μgauss with a corresponding increase in the number of high energy electrons to account for the low frequency radio intensities. They also take $\alpha = 0.61$ which implies an electron distribution with $\gamma = 2.32$. Now according to the last equation, the derived Compton intensity is quite sensitive to field strength and if the X-ray flux is entirely galactic in origin then H ≈ 0.4 μgauss.

The precise value for the galactic magnetic field strength remains in some doubt. Earlier estimates based on cosmic ray confinement and other energy considerations have yielded (e.g. Woltjer, 1965; Ginzburg and Syrovatskii, 1964) values of about 5×10^{-6} μgauss for the field in the halo. However more recent measurements (Radhakrishnan, 1969) based on the dispersion of pulsar radiation and Faraday rotation have given H < 1 μgauss in the disk, implying a very weak field in the halo. This in turn means that cosmic rays with energy density of the order of 10^{-12} erg cm^{-3} cannot be contained within the halo. Clearly, the problem of the magnetic field intensity must be clarified before a galactic origin for the soft X-ray flux can be accepted.

8.6 Conclusions

The analysis has shown that inverse Compton radiation in intergalactic space may account for the diffuse X-ray flux provided the cosmic ray energy density is of the order of 10^{-15} erg cm^{-3} at the present epoch. Compton losses lead to a spectral index of $\alpha = 1.34$ for the theoretical X-ray background and this provides a very good fit to the observed spectrum. The analysis applies only to flux measurements at photon energies greater than the energy E_b which corresponds to the break in the X-ray spectrum. Unfortunately, due to the acute shortage of data, the exact position of this break remains unconfirmed. However the break apparently lies in the range 10-60 keV and this corresponds to a low energy cut-off in the metagalactic electron distribution of 1.6-4 GeV.

CHAPTER IX

A GENERAL VECTOR-FIELD COSMOLOGY

9.1 Introduction

In the original steady-state theory Hoyle (1948) introduced into Einstein's field equations a vector

$$C^{\mu} = 3H_o(0,0,0,1) \tag{9.1}$$

This led to a metric for space-time which was identical to the de Sitter metric obtained by defining $\sigma_o = 0$, $q_o = -1$. If $R = R_o$ at $t = t_o$, then the steady-state theory yields

$$R = R_o \exp[-H_o(t-t_o)], \qquad \rho = 3H_o^2/4\pi G \tag{9.2}$$

so that the matter density is a constant, non-zero quantity. The steady-state theory is the basis of the perfect cosmological principle which states that apart from local irregularities, the universe presents the same aspect from any place at any time.

The steady-state universe admits a particular creation field and this produces a unique and exact description of the nature of the universe. In view of the mounting evidence against this theory, it is of some interest to examine the general case of a C-field cosmology.

9.2 Theory for Universes of Arbitrary Curvature

As the mathematical basis of the analysis we take the Roberston-Walker line element,

$$ds^2 = dt^2 - \frac{R^2(t)}{c^2}\left\{\frac{dx^2 + dy^2 + dz^2}{(1 + kr^2/4)^2}\right\} \qquad (9.3)$$

where x,y,z are three-dimensional comoving coordinates with $r^2 = x^2 + y^2 + z^2$.

We now introduce at each point, P, of the space-time continuum a vector A_μ directed along the unique geodesic connecting the origin observer 0 to P. The vector is therefore a function of the cosmic time, t, only,and accordingly we define

$$A_\mu = \Phi(t)(0,0,0,1) \qquad (9.4)$$

where the general point of the space-time continuum is

$$x^\mu = (x,y,z,t) \qquad (9.5)$$

It should be noted here that Hoyle has examined the case of $\Phi(t)$ equal to a positive constant in flat spaces.

The tensor field corresponding to A_μ is given by the covariant derivative of this vector and according to equation (2.13) this may be written in the form

$$A_{\mu\nu} \equiv \nabla_\nu A_\mu = \frac{\partial A_\mu}{\partial x^\nu} - \Gamma^\sigma_{\mu\nu} A_\sigma \tag{9.6}$$

where $\Gamma^\sigma_{\mu\nu}$ denotes the Christoffel symbol of the second kind. As usual, the contravariant tensor will be related to the covariant tensor, $A_{\mu\nu}$, through the equation

$$A^{\mu\nu} = g^{\mu\alpha}\, g^{\nu\beta}\, A_{\alpha\beta} \tag{9.7}$$

Where the functions $g^{\mu\alpha}$ are contravariant components of the metrical tensor.

Equations (9.3),(9.6) and (9.7) now yield

$$A^{ij} = -c^2(1 + kr^2/4)\,(\dot{R}/R^3)\,\Phi(t)\,\delta_{ij} \qquad i,j = 1,2,3 \tag{9.8}$$
$$A^{44} = \dot{\Phi}(t)$$

where as before δ_{ij} is the Kronecker delta.

Following Hoyle, we now introduce the tensor $A^{\mu\nu}$ into Einstein's field equations and from (2.40) it follows that

$$-\kappa c^2 T^{\mu\nu} = G^{\mu\nu} - \frac{1}{2} g^{\mu\nu} G^\rho_\rho + A^{\mu\nu} \tag{9.9}$$

the cosmological constant being incorporated into the tensor $A^{\mu\nu}$.

Using equations (2.51) and (9.7), the set of ten equations (9.9) yield the solutions

$$-\kappa c^2 T^{ij} = \left[\frac{2\ddot{R}}{R} + \frac{\dot{R}^2}{R^2} + \frac{kc^2}{R} - \frac{\dot{R}}{R}\Phi(t)\right] \frac{c^2}{R^2}(1+ kr^2/4)\delta_{ij} \qquad (9.10)$$

$$-\kappa c^2 T^{44} = -3\left(\frac{\dot{R}^2}{R^2} + \frac{kc^2}{R^2}\right) + \dot{\Phi}(t) \qquad (9.11)$$

Considering only the smoothed out problem in which matter is assumed to behave as a perfect fluid, the energy tensor may be written in the form

$$T^{\mu\nu} = \left(\rho + \frac{P}{c^2}\right) u^\mu u^\nu - g^{\mu\nu}\frac{P}{c^2} \qquad (9.12)$$

where the symbols have their usual meanings. In the cosmological case, introduction of comoving coordinates imply $u^1 = u^2 = u^3 = 0$, and $u^4 = 1$. Hence equations (9.10) and (9.11) reduce to

$$-\kappa P = \frac{2\ddot{R}}{R} + \frac{\dot{R}^2}{R^2} + \frac{kc^2}{R^2} - \frac{\dot{R}}{R}\Phi(t) \qquad (9.13)$$

$$\kappa c^2 \rho = 3\left(\frac{\dot{R}^2}{R^2} + \frac{kc^2}{R^2}\right) - \dot{\Phi}(t) \qquad (9.14)$$

These equations should be compared with the ordinary equations (3.5) and (3.6). It should be noted that (9.13) and (9.14) could be derived directly from the equations (2.51).

Now taking the vectorial divergence of (9.12), we obtain

$$-\kappa c^2 \nabla_\nu T^{\mu\nu} = \nabla_\nu A^{\mu\nu} \qquad (9.15)$$

since the divergence of the tensor $G^{\mu\nu} - \frac{1}{2} g^{\mu\nu} G^\rho_\rho$ is identically equal

to zero. Using equations (9.8) and (2.16) for the vectorial divergence, it follows that

$$\nabla_\nu A^{i\nu} = 0 \tag{9.16}$$
$$\nabla_\nu A^{4\nu} = 3[-\frac{\dot{R}^2}{R^2}\Phi(t) + \frac{\dot{R}}{R}\dot{\Phi}(t)] + \ddot{\Phi}(t)$$

Calculating $\nabla_\nu T^{4\nu}$ from equation (9.12), and employing equations (9.15) and (9.16), we finally derive

$$\kappa c^2[\frac{3\dot{R}}{R}(\rho + \frac{P}{c^2}) + \frac{\partial\rho}{\partial t}] = \frac{3\dot{R}}{R}[\frac{\dot{R}}{R}\Phi(t) - \dot{\Phi}(t)] - \ddot{\Phi}(t) \tag{9.17}$$

Since $\nabla_\nu A^{4\nu} \neq 0$, it follows from equations (9.12) and (9.15) that matter is either being created or annihilated, depending on the sign of $\Phi(t)$. Also the matter after creation or before annihilation must possess zero-momentum in the system of coordinates, since $\nabla_\nu A^{i\nu} = 0$ for $i = 1,2,3$.

Equations (9.13), (9.14) and (9.17) are sufficient to solve the expansion properties of the universe, provided, of course, that initial or boundary conditions are determined. A solution to these equations also requires a knowledge of the function $\Phi(t)$.

If the contribution to the cosmic pressure from ordinary matter is negligible, then equation (9.17) yields

$$\frac{\partial\rho_m}{\partial t} = \frac{1}{\kappa c^2}[\frac{3\dot{R}}{R}(\frac{\dot{R}}{R}\Phi(t) - \dot{\Phi}(t)) - \ddot{\Phi}(t)] - \frac{3\dot{R}}{R}\rho_m \tag{9.18}$$

for the rate of change of matter density with epoch. Now, $\partial\rho_m/\partial t$ will be the sum of the rate of change of ρ_m due to expansion of coordinates and the Φ field. Hence we may write

$$\left(\frac{\partial\rho_m}{\partial t}\right)_{\Phi} = \frac{\partial\rho_m}{\partial t} - \left(\frac{\partial\rho_m}{\partial t}\right)_{exp} \tag{9.19}$$

and since instantaneously $\rho_m = \rho_{mo}(R/R_o)^{-3}$, then

$$\left(\frac{\partial\rho_m}{\partial t}\right)_{exp} = -\frac{3\dot{R}}{R}\rho_m \tag{9.20}$$

Substituting equations (9.18) and (9.20) into (9.19), we have

$$\left(\frac{\partial\rho_m}{\partial t}\right)_{\Phi} = \frac{1}{\kappa c^2}\left[\frac{3\dot{R}}{R}\left(\frac{\dot{R}}{R}\Phi(t) - \dot{\Phi}(t)\right) - \ddot{\Phi}(t)\right] \tag{9.21}$$

for the rate of change of matter density due to the Φ field.

9.3 A Conjectural Model

Suppose we assume that $\Phi(t)$ is constant and of the form

$$\Phi(t) = mH_o \tag{9.22}$$

where m is a dimensionless constant. At the present epoch, equations (9.13) and (9.14) yield the equations

$$\begin{aligned} m &= 2[\sigma_o(1 + \varepsilon_o) - q_o] \\ \frac{kc^2}{R_o^2H_o^2} &= 2\sigma_o - 1 \end{aligned} \tag{9.23}$$

which should be compared with equations (3.20) and (3.21). We note that the first of equations (9.23) implies that the possibility of a large positive q_o is enhanced by a negative value for m, corresponding to matter annihilation. The steady-state model may be defined by specifying $k = 0$, $q_o = -1$ and $\varepsilon_o = 0$. The equations (9.23) then yield $\sigma_o = 0.5$, $m = 3$, and consequently from equation (9.21) $(\partial\rho_m/\partial t)_\Phi = 9H_o(\dot{R}/R)^2/8\pi G$. Then using equations (9.19) and (9.14) in turn we find that the matter density and the ratio $\dot{y}/y$ are both constant. The steady-state universe may be defined more generally by assuming $\Phi(t) = 3\dot{R}/R$.

Substituting (9.22) in (9.21), we have

$$\left(\frac{\partial\rho_m}{\partial t}\right)_\Phi = 3\left(\frac{\dot{R}}{R}\right)^2 \frac{mH_o}{\kappa c^2} \tag{9.24}$$

Hence, at the present epoch,

$$\left(\frac{\partial\rho_m}{\partial t}\right)_\Phi = \frac{3mH_o^3}{8\pi G} \tag{9.25}$$

$$\simeq 5.9_{10}{}^{-47} \text{ gm cm}^{-3}\text{sec}^{-1}$$

Also, the source count analysis has shown that the number of radio sources per unit coordinate volume must vary as y^{-n} where n is in the range 3.5 to 4.5. The most obvious and most acceptable explanation of this result is that a proportion of radio galaxies become extinct radio emitters in a time short compared with H_o^{-1}. Now the same result is obtained if some galaxies actually disappear

out of existence. It is well known (e.g. Harrison et al, 1965) that a spherically symmetric distribution of matter can collapse under gravitational forces to a stage where its radius is less than the critical Schwarzschild radius $r = 2\,GM/c^2$. After this event, collapse can no longer be halted and no radiant energy can flow in or out. The dynamical history of such a configuration - despite its own constant energy - contains all the 3-geometries with mass-energy less than the total mass-energy as sensed externally. Here, then, is a mechanism suggestive of the annihilation of matter. However, the phenomenon of gravitational collapse cannot affect the cosmological equations since the extrinsic 3-geometry is constant independent of time. But, if the matter present in galaxies does actually (by some as yet unknown process) disappear out of existence - as determined by the absence of a gravitational field - then it is possible to derive a rough estimate for the rate of annihilation of matter from the source count results. The number of sources per unit proper volume at the epoch defined by y is

$$n = n_o y^{-(3+n)}$$

where n_o is the galactic density at the present time. Differentiating and converting to the equivalent mass density, the rate of disappearance of matter is given by

$$\left(\frac{d\rho_m}{dt}\right)_\Phi = -n\rho_m y^{-n-1}\,\dot{y} \qquad (9.26)$$

$$= -n\rho_{mo}H_o$$

at the present epoch. Taking $n = 4$ and $\rho_{mo} = 5 \times 10^{-31}$gm cm^{-3} for the local mass density of galaxies, the rate of annihilation of matter is about $6.4_{10}{}^{-48}$gm cm^{-3}sec^{-1}. If m is of the order of unity as

indicated by the first of equations (9.23), then this estimate is surprisingly close to the estimate given in equation (9.25). These calculations are quite sketchy and if $\Phi(t)$ is not identically zero then it is not possible to reach any sort of conclusion until the function $\Phi(t)$ is somehow determined. In view of the present difficulties in specifying world-model parameters, it seems likely that $\Phi(t)$ will be derived from basic physical theory rather than from cosmological considerations.

9.4 Conclusions

If, at every point of the space-time continuum, a vector field exists of the form $A_\mu = \Phi(t)(0,0,0,1)$, then the evolution of the universe is described completely by equations (9.13), (9.14) and (9.18). The steady-state theory deals with a particular case of matter creation. It is suggested here that the possibility of large scale annihilation of matter should not be disregarded. The proposal that source counts (indicating possible source density evolution) and a large positive value for q_o lend support to the theory ofmmatter annihilation is speculative. The analysis has only provided an outline of the problems involved with the introduction of a vector field into Einstein's equations. Obviously a complete analysis of metagalactic evolution is required for different functions $\Phi(t)$. However, there are difficulties inherent to the basic cosmological theory and further data is required before an absolutely convincing case can be made for a particular world-model. Thus, there seems little point, at this stage,

of extending the analyses to include vector fields of the form A_μ, but the implications of such a field should be kept in mind.

CHAPTER X

CONCLUSIONS

The development of world-models suitable for the large scale description of the evolutionary properties of the universe begins with an analysis of the observable quantities associated with radio sources. The distribution of source angular diameters with redshift and the variation of source average spectral index with redshift or luminosity both contribute to a solution of the cosmological problem.

Assuming that source luminosity or density in co-ordinate volume varies smoothly with expansion parameter it is possible to analyse the source counts as a function of cosmological model. This has been done for the source counts of the recent 5C surveys. Function minimisation techniques indicate that the best fit condition is attained by those models having relatively large values for the density parameter σ_o and the deceleration parameter q_o. Reference for section 4.3 shows that these models are closed and oscillating. The analysis also provides important information on the variation of source luminosity or density with epoch and the redshift (or epoch) corresponding to galaxy formation.

The low frequency spectra of discrete radio sources will be affected by intergalactic absorption to an extent depending on the temperature path of the gas, the source redshift and the particular cosmological model which may apply. If σ_o is somewhat greater than unity as suggested by the source counts then a significant amount of intergalactic absorption will be exhibited in source spectra at frequencies less than about 20 MHz.

The radio background has been calculated for two extreme cosmological models consistent with the source counts. It is found that, at 100 MHz, the extragalactic component amounts to approximately 11 per cent of the total background intensity for source density evolution and 5 per cent for source luminosity evolution. Taking account of other independent evidence it seems that the smooth variation of source density (in co-ordinate volume) with epoch is the dominant evolutionary process. The integrated free-free emission from intergalactic ionized hydrogen yields, for the world-models derived from the source counts, soft X-ray spectra which are reasonably consistent with the measured fluxes.

The diffuse X-ray background can be described in terms of inverse Compton interactions of metagalactic cosmic ray electrons with 3°K black-body photons. Initially the electron energy spectrum has an index $\gamma = 2.68$ which is identical to the proposed average index for cosmic rays in radio galaxies. As usual the analysis was

restricted to the cosmological models derived from the source counts. The theoretical background spectrum has a spectral index of $\alpha = 1.34$ (corresponding to a change of unity in γ) and this is close to the spectral index obtained from a least squares fit to the measured intensities. Normalisation requires a cosmic ray energy density of the order of 10^{-15} erg cm^{-3} at the present epoch and again this value is consistent with other estimates.

Finally, a brief analysis has been given of the consequences of the existence of a vector field in universes of arbitrary curvature. The results suggest that the possibility of large scale annihilation of matter should not be disregarded.

REFERENCES

Chapters II and III

Einstein, A. (1916). - Ann. Phys. 49, 769.

Einstein, A. (1917). - "Kosmolgische Betrachtungen zur allgemeinen Relativitätstheorie," Sitzungsberichte der Preussischen Akad. d. Wissenschaften.

Fock, V. (1959). - "The Theory of Space-time and Gravitation." (Pergamon Press: London.)

Kustaanheimo, P. (1953). - Proc. Edinb. Math. Soc. Ser. 2, 9, 17.

Landau, L., and Lifshitz, E. (1961). - "The Classical Theory of Fields." (Pergamon Press: London.)

McVittie, G.C. (1965). - "General Relativity and Cosmology." (Chapman and Hall: London.)

Robertson, H.P. (1935). - Astrophys. J. 82, 284.

Synge, J.L. (1960). - "Relativity: The General Theory." (North-Holland Publishing Company: Amsterdam.)

Tolman, R.C. (1934). - "Relativity, Thermodynamics and Cosmology." (University Press: Oxford.)

Walker, A.G. (1936). - Proc. Lond. Math. Soc. (2) 42, 90.

Weyl, H. (1918). - "Space-Time-Matter." (Dover Publications: New York.)

Chapter IV

Alpher, R.A., and Herman, R.C. (1949). - Phys. Rev. 75, 1089.

Bondi, H. (1961). - "Cosmology." (University Press: Cambridge.)

Davidson, W. (1962). - Mon. Not. R. astr. Soc. 124, 79.

Jacobs, K.C. (1967). - Nature 215, 1156.

McIntosh, C.B.G. (1967). - Nature 215, 36.

Penzias, A.A., and Wilson, R.W. (1965). - Astrophys. J. 142, 420.

Rindler, W. (1957). - Mon. Not. R. astr. Soc. 116, 662.

Robertson, H.P. (1933). - Rev. Mod. Phys. 5, 62.

Shivanandan, K., Houck, J.R., and Harwit, M.O. (1968). - Phys. Rev. Lett. 21, 1460.

Stabell, R., and Refsdal, S. (1966). - Mon. Not. R. astr. Soc. 132, 379.

Tolman, R.C. (1934). - "Relativity, Thermodynamics and Cosmology." (University Press: Oxford.)

Chapter V

Aizu, K., Fujimoto, Y., Hasegawa, H., Kawabata, K., and Taketani, M. (1964). - Prog. theor. Phys., Suppl. No. 31, 35.

Allen, L.R., Anderson, B., Conway, R.G., Palmer, H.P., Reddish, V.C., and Dowson, B. (1962). - Mon. Not. R. astr. Soc. 124, 477.

van den Bergh, S. (1961). - Publs. astr. Soc. Pacif. 73, 46.

Bolton, J.G., Gardner, F.F., and Mackey, M.M. (1964). - Aust. J. Phys. 17, 340.

Bolton, J.G., Shimmins, A.J., Eckers, R.D., and Cole, D.J. (1966). - Aust. J. Phys. 19, 35.

Burbidge, G.R., Burbidge, E.M., and Sandage, A.R. (1963). - Rev. Mod. Phys. 35, 947.

Conway, R.G., Kellermann, K.I., and Long, R.J. (1963). - Mon. Not. R. astr. Soc. 125, 261.

Davidson, W. (1962). - Mon. Not. R. astr. Soc. 123, 425.

Davidson, W. and Davies, M. (1964). - Mon. Not. R. astr. Soc. 127, 241.

Day, G.A., Shimmins, A.J., Eckers, R.D., and Cole, D.J. (1966). - Aust. J. Phys. 19, 35.

Eckers, R.D. (1969). - Aust. J. Phys., Suppl. No. 6.

Edge, D.O. (1958). - A survey of radio stars at 159 Mc/s, Ph.D. thesis, University of Cambridge.

Eggen, O., Lynden-Bell, D., and Sandage, A.R. (1962). - Astrophys. J. 136, 748.

Ginzburg, V.L., and Syrovatskii, S.I. (1964). - "The Origin of Cosmic Rays." (Pergamon Press: Oxford.)

Gower, J.F.R. (1966). - Mon. Not. R. astr. Soc. 133, 151.

Heeschen, D.S. (1966). - Astrophys. J. 146, 517.

Holden, D.J. (1966). - Mon. Not. R. astr. Soc. 133, 225.

Hoyle, F., and Fowler, W.A. (1963). - Nature 197, 533.

Hoyle, F., and Fowler, W.A. (1964). - Quasi Stellar Sources and Gravitational Collapse. (University of Chicago Press: Chicago.)

Hoyle, F., Fowler, W.A., Burbidge, E.M., and Burbidge, G.R. (1964). - Astrophys. J. 139, 909.

Kardashev, N.S. (1962). - Soviet Astr. 6, 317.

Kellermann, K.I., and Harris, D.E. (1960). - Obs. Calif. Inst. Tech. Radio Observatory No. 7.

Kellermann, K.I. (1964). - Astrophys. J. 140, 983.

Kellermann, K.I. (1966). - Astrophys. J. 146, 621.

Ko, H.C. (1966). - Astrophys. J. 145, 936.

Le Roux, E. (1960). - Annls. Astrophys. 23, 1010.

Le Roux, E. (1962). - Annls. Astrophys. 24, 11.

Leslie, P.R.R. (1961). - Mon. Not. R. astr. Soc. 122, 28.

Long, R.J., Smith, M.A., Stewart, P., and Williams, P.J.S. (1966). - Mon. Not. R. astr. Soc. 134, 371.

Longair, M.S., and Scott, P.F. (1965). - Mon. Not. R. astr. Soc. 130, 379.

Longair, M.S. (1966). - Mon. Not. R. astr. Soc. 133, 421.

Longair, M.S., and Scheuer, P.A.G. (1967). - Nature 215, 919.

Lynds, C.R., and Sandage, A.R. (1963). - Astrophys. J. 137, 1005.

Lyttleton, R.A. (1953). - "The Stability of Rotating Liquid Masses." (Cambridge University Press: Cambridge.)

McVittie, G.C. (1965). - "General Relativity and Cosmology." (Chapman and Hall: London.)

Maltby, P., Matthews, T.A., and Moffet, A.T. (1963). - Astrophys. J. 137, 153.

Matthews, T.A., Morgan, W.W., and Schmidt, M. (1964). - Astrophys. J. 140, 35.

Mills, B.Y., Slee, O.B., and Hill, E.R. (1958). - Aust. J. Phys. 11, 360.

Mills, B.Y. (1960). - Aust. J. Phys. 13, 550.

Mills, B.Y., Slee, O.B., and Hill, E.R. (1960). - Aust. J. Phys. 13, 676.

Mills, B.Y., Slee, O.B., and Hill, E.R. (1961). - Aust. J. Phys. 14, 497.

Moffet, A.T., and Maltby, P. (1962). - Astrophys. J., Suppl. Ser. 1, No. 67.

Nelder, J.A., and Mead, R. (1965). - Comput. J. 7, 308.

Oort, J.H., and Walraven, T. (1956). - Bull. astr. Insts. Neth. 12, 285.

Oort, J.H. (1961). - O.E.C.D., Paris Symposium, p. 35.

Oort, J.H. (1964). - General Assembly I.A.U., Hamburg.

Piddington, J.H. (1966). - Mon. Not. R. astr. Soc. 133, 164.

Pooley, G.G., and Ryle, M. (1968). - Mon. Not. R. astr. Soc. 139, 515.

Price, R.M., and Milne, D.K. (1965). - Aust. J. Phys. 18, 329.

Razin, V.A. (1960). - Radiofizika 3, 921.

Ryle, M., and Clarke, R.W. (1961). - Mon. Not. R. astr. Soc. 122, 349.

Ryle, M., and Neville, A.C. (1962). - Mon. Not. R. astr. Soc. 125, 39.

Ryle, M. (1968). - Ann. Rev. Astr. and Astrophys. 6, 249.

Sandage, A. (1968). - Private communication.

Sciama, D.W. (1963). - Mon. Not. R. astr. Soc. 126, 195.

Scott, P.F. (1963). - Mon. Not. R. astr. Soc. 127, 37.

Shain, C.A. (1960). - Proc. Symp. I.A.U. No. 9 (Paris, 1958).

Shakeshaft, J.R. (1955). - Phil. Mag. 45, 1136.

Shimmins, A.J., Day, G.A., Ekers, R.D., and Cole, D.J. (1966). - Aust. J. Phys. 19, 837.

Slish, V.I. (1963). - Nature 199, 682.

Véron, P. (1966). - Nature 211, 274.

Weymann, R. (1967). - Astrophys. J. 147, 887.

Whitfield, G.R. (1958). - Proc. Symp. I.A.U. No. 9 (Paris, 1958).

Williams, P.J.S. (1963). - Nature 200, 56.

Wills, D. (1966). - Observatory 86, 140.

Chapter VI

Bazelyan, L.L., Braude, S. Ya., Waisberg, V.V., Krymkin, V.V., Men, A.V., and Sodin, L.G. (1965). - Astr. Zh. 42, 618.

Davies, R.D. (1964). - Mon. Not. R. astr. Soc. 128, 133.

Ellis, G.R.A., and Hamilton, P.A. (1966). - Astrophys. J. 143, 227.

Erickson, W.C., and Cronyn, W.M. (1965). - Astrophys. J. 142, 1156.

Field, G.B., and Henry, R.C. (1964). - Astrophys. J. 142, 1002.

Field, G.B. (1965). - Astrophys. J. 142, 531.

Gold, T., and Hoyle, F. (1959). - Proc. Symp. I.A.U. No. 9 (Paris, 1958) 583.

Goldstein, S.J. (1963). - Astrophys. J. 138, 151.

Gould, R.J., and Ramsay, W. (1966). - Astrophys. J. 144, 587.

Gunn, J.E., and Peterson, B.A. (1965). - Astrophys. J. 142, 1633.

Hoyle, F. (1948). - Mon. Not. R. astr. Soc. 108, 372.

Hoyle, F., and Narlikar, J.V. (1962). - Proc. R. Soc. 270, 334.

Kahn, F.D., and Woltjer, L. (1959). - Astrophys. J. 130, 705.

Karzas, W.J., and Latter, R. (1961). - Astrophys. J., Suppl. Ser. 6, 167.

Layzer, D. (1963). - Astrophys. J. 138, 735.

Layzer, D. (1966). - Astrophys. J. 145, 349.

Oort, J.H. (1958). - Proc. Conf. on Structure and Evolution of the Universe, 163.

Pollack, J.B., and Fazio, G.G. (1963). - Phys. Rev. 131, 2684.

Sandage, A.R. (1961). - Astrophy. J. 133, 355.

Sciama, D.W. (1964). - Q. Jl. R. astr. Soc. 5, 196.

Williams, P.J.S., Kenderdine, S., and Baldwin, J.E. (1966). - Mem. R. astr. Soc. 68, 163.

Chapter VII

Allen, C.W. (1965). - "Astrophysical Quantities." (Athlone Press: London.)

Baxter, A.J., Wilson, B.G., and Green, D.W. (1969). - Astrophys. J. 155, L145.

Bowyer, C.S., Field, G.B., and Mack, J.E. (1968). - Nature 217, 32.

Bowyer, C.S., and Field, G.B. (1969). - Nature 223, 573.

Burbidge, G.R. (1962). - Prog. theor. Phys., Kyoto 27, 999.

Dicke, R.H., Peebles, P.J.E., Roll, P.G., and Wilkinson, D.T. (1965). - Astrophys. J. 142, 414.

Ellis, G.R.A. (1957). - J. geophys. Res. 62, 229.

Ellis, G.R.A. (1964). - Nature 204, 171.

Ellis, G.R.A., and Hamilton, P.A. (1966). - Astrophys. J. 146, 78.

Ginzburg, V.L., and Syrovatskii, S.I. (1964). - "The Origin of Cosmic Rays." (Pergamon Press: Oxford.)

Ginzburg, V.L., and Ozernoi, L.M. (1966). - Soviet Astr. 9, 726.

Hamilton, P.A. (1969). - Private communication.

Henry, R.C., Fritz, G., Meekins, J.R., Friedmann, H., and Bryam, E.T. (1968). - Astrophys. J. 153, L11.

Howell, T.F., and Shakeshaft, J.R. (1966). - Nature 210, 1318.

Howell, T.F., and Shakeshaft, J.R. (1967). - Nature 216, 753.

Hoyle, F. (1948). - Mon. Not. R. astr. Soc. 108, 372.

Hoyle, F., and Narlikar, J.V. (1962). - Proc. R. Soc. 270, 334.

Kaplan, S.A., and Pikelner, S.B. (1963). - "The Interstellar Medium." Fizmatgiz.

Kaufman, M. (1965). - Nature 207, 736.

Layzer, D. (1963). - Astrophys. J. 138, 735.

Layzer, D. (1966). - Astrophys. J. 145, 349.

Mathewson, D.S., Broten, N.W., and Cole, D.J. (1965). - Aust. J. Phys. 18, 665.

Mills, B.Y. (1959). - Publs. astr. Soc. Pacif. 71, 267.

Peebles, P.J.E. (1965). - Astrophys. J. 142, 1317.

Peebles, P.J.E. (1966). - Phys. Rev. Lett. 16, 410.

Penzias, A.A., and Wilson, R.W. (1965). - Astrophys. J. 142, 419.

Penzias, A.A., and Wilson, R.W. (1966). - American Astr. Soc. Meeting, Los Angeles (unpublished).

Roll, P.G., and Wilkinson, D.T. (1966). - Phys. Rev. Lett. 16, 405.

Shain, C.A., and Higgins, C.S. (1954). - Aust. J. Phys. 7, 130.

Thaddens, P., and Clauser, J.F. (1966). - Phys. Rev. Lett. 16, 819.

Turtle, A.J., Pagh, J.F., Kenderdine, S., and Pauliny-Toth, I.I.K. (1962). - Mon. Not. R. astr. Soc. 124, 297.

Walshe, D., Haddock, F.T., and Schulte, H.F. (1963). - Univ. Mich. Radio Astronomy Observatory Rep.

Welch, W.J., Keachie, S., Thornton, D.D., and Wrixon, G. (1967). - Phys. Rev. Lett. 18, 1068.

Weymann, R. (1966). - Astrophys. J. 145, 560.

Yates, K.W., and Wielebinski, R. (1965). - Nature 208, 64.

Yates, K.W., and Wielebinski, R. (1966). - Aust. J. Phys. 19, 389.

Chapter VIII

Bergamini, R., Londvillo, P., and Setti, G. (1967). - Nuovo Cim. B52 (N2), 495.

Boldt, E.A., Desai, U.D., Holt, S.S., and Serlemitsos, P.J. (1969). - Publication of NASA/Goddard Space Flight Center Greenbelt, Maryland, X-611-69-248.

Burbidge, G.R. (1959). - Proc. Symp. I.A.U. No. 9 (Paris, 1958), 541.

Burbidge, G.R. (1962). - Prog. theor. Phys., Kyoto 27, 999.

Davies, R.D. (1964). - Mon. Not. R. astr. Soc. 128, 133.

Feenberg, E., and Primakoff, H. (1948). - Phys. Rev. 73, 449.

Felten, J.E., and Morrison, P. (1966). - Astrophys. J. 146, 686.

Ginzburg, V.L., and Syrovatskii, S.I. (1961). - Prog. theor. Phys., Kyoto Suppl. No. 20.

Ginzburg, V.L., and Ozernoi, L.M. (1966). - Soviet Astr. 9, 726.

Ginzburg, V.L., and Syrovatskii, S.I. (1967). - Proc. Symp. I.A.U. No. 31.

Ginzburg, V.L. (1968). - Astrophys and Space Sci. 1, 125.

Goldstein, G.J. (1963). - Astrophys. J. 138, 978.

Gorenstein, P., Kellogg, E.M., and Gursky, H. (1968). - Astrophys. J. 156, 315.

Gould, R.J. (1965). - Phys. Rev. Lett. 15, 511.

Gould, R.J., and Burbidge, G.R. (1966). - In "Handbuch der Physik." Vol. 46, p. 2. (Springer-Verlag: Berlin.)

Gould, R.J. (1967). - Am. J. Phys. 35, 376.

Gunn, J.E., and Peterson, B.A. (1965). - Astrophys. J. 142, 1633.

Hamilton, P.A., and Francey, R.J. (1969). - Nature (to be published).

Henry, R.C., Fritz, G., Meekins, J.R., Friedmann, H., and Bryam, E.T. (1968). - Astrophys. J. 153, L11.

Oda, M. (1966). - Proc. Cosmic Ray Conf. (London), p. 68.

Oort, J.H., and Walraven, T. (1956). - Bull. astr. Insts. Neth. 12, 285.

Payne, A.D. (1969). - Aust. J. Phys. 22, 521.

Radhakrishnan, V. (1969). - Publs. astr. Soc. Aust. (to be published).

Schmidt, M. (1967). - Proc. Symp. I.A.U. No. 31 and Astrophys. J. 149, L39.

Woltjer, L. (1965). - Stars and Stellar Systems, Vol. V, 531.

Chapter IX

Harrison, B.K., Thorne, K.S., Wakano, M., and Wheeler, J.A. (1965). - "Gravitation Theory and Gravitational Collapse," (University of Chicago Press: Chicago.)

Hoyle, F. (1948). - Mon. Not. R. astr. Soc. 108, 372.

CORRIGENDA

Replace equations (2.50) and (2.51) on pages 21 and 22 by the following:

$$G_{1212} = \frac{e^{\mu}}{c^2} r^2 \left[\frac{1}{2}\mu'' + \frac{\mu'}{2r} - \frac{1}{4}\frac{e^{\mu-\nu}}{c^2}\dot{\mu}^2 \right]$$

$$G_{1242} = \frac{e^{\mu}}{c^2} r^2 \left[\frac{1}{2}\dot{\mu}' - \frac{1}{4}\dot{\mu}\nu' \right]$$

$$G_{3134} = \sin^2\theta\, G_{1242}$$

$$G_{3131} = \sin^2\theta\, G_{1212}$$

$$G_{4114} = e^{\nu} r^2 \left[\frac{1}{2}\nu'\left(\frac{1}{2}\mu' + \frac{1}{r}\right) - \frac{e^{\mu-\nu}}{c^2}\left(\frac{1}{2}\ddot{\mu} + \frac{1}{4}\dot{\mu}^2 - \frac{1}{4}\dot{\mu}\dot{\nu}\right)\right]$$

$$G_{4224} = G_{4114}$$

$$G_{4334} = \sin^2\theta\, G_{4114}$$

The non-vanishing components of the curvature tensor are from equation (2.23)

$$G_{11} = \mu'' + \frac{1}{2}\nu'' - \frac{1}{4}\mu'\nu' + \frac{1}{4}\nu'^2 + \frac{\mu'}{r} - \frac{e^{\mu-\nu}}{c^2}\left(\frac{1}{2}\ddot{\mu} + \frac{3}{4}\dot{\mu}^2 - \frac{1}{4}\dot{\mu}\dot{\nu}\right)$$

$$G_{22} = r^2\left[\left(\frac{1}{2}\mu'' + \frac{1}{4}\mu'^2 + \frac{1}{4}\mu'\nu' + \frac{3\mu' + \nu'}{2r} + \frac{1}{r^2}\right) - \frac{e^{\mu-\nu}}{c^2}\left(\frac{1}{2}\ddot{\mu} + \frac{3}{4}\dot{\mu}^2 - \frac{1}{4}\dot{\mu}\dot{\nu}\right)\right] - 1$$

$$G_{33} = \sin^2\theta\, G_{22}$$

$$G_{44} = -\frac{e^{\mu-\nu}}{c^2}\left(\frac{1}{2}\nu'' + \frac{1}{4}\mu'\nu' + \frac{1}{4}\nu'^2 + \frac{\nu'}{r}\right) + \left(\frac{3}{2}\ddot{\mu} + \frac{3}{4}\dot{\mu}^2 - \frac{3}{4}\dot{\mu}\dot{\nu}\right)$$

$$G_{14} = \dot{\mu}' - \frac{1}{2}\dot{\mu}\dot{\nu} = G_{41}$$